Optimal Transport Techniques for Atmospheric Dynamics

Théo Philippe LAVIER

Submitted for the degree of
Doctor of Philosophy

Heriot-Watt University

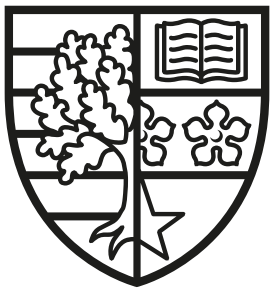

Department of Mathematics,
School of Mathematical and Computer Sciences.

February, 2026

Abstract

This thesis develops a comprehensive theoretical and numerical framework for the semi-geostrophic equations of atmospheric dynamics, grounded in the theory of semi-discrete optimal transport. First, we present a novel, mesh-free, 3D numerical scheme for the incompressible semi-geostrophic equations. This method is structurally energy-conserving, enabling robust, long-term simulations, as demonstrated by the first fully 3D simulation of a twin cyclone using a semi-discrete optimal transport approach. Second, we establish a major theoretical result: the global-in-time existence of weak solutions for the compressible semi-geostrophic equations with compactly supported, measure-valued initial data. This significantly generalizes previous results by leveraging a particle discretization strategy and a dual formulation of the underlying energy minimization problem. Finally, we provide a rigorous justification for the framework's applicability to physically relevant settings by verifying the necessary geometric conditions for rectangular domains, which are not covered by standard c-convexity assumptions. As a first step towards simulating the compressible system, the final chapter derives a 2D slice model and its particle-based discretization, establishing the foundation for future 2D and 3D compressible simulations. Together, these contributions provide a unified and powerful approach for the analysis and simulation of large-scale atmospheric flows.

There's no such thing as neutral education. Education either functions as an instrument to bring about conformity or freedom.

Paulo Freire, *Pedagogy of the Oppressed*

Acknowledgements

Beatrice and David – Thank you for investing so much of your time and energy into me. These past four years, the most challenging yet rewarding of my life, were shaped immeasurably by y'all. I'll forever recall our meetings with a unique blend of excitement and, a touch of pre-meeting jitters! My apologies if my late-night work habits ever disrupted your peace. It's been an immense privilege and a true honour to collaborate with mathematicians as brilliant and knowledgeable as you, and more importantly, with people as genuinely kind. I hope our paths continue to cross, both professionally and personally, for many years.

Charlie, Lucia and Alex – My unofficial supervisors, you each played an absolutely crucial role in shaping my PhD journey. Whether it was through our focused collaborations, the indispensable gin and tonics, or gracing us with your dinner party prowess. My experience was richer for each of you. I hope to see you all often.

Sofie – From countless bus rides and maths discussions to board game battles and TV binges, these past years wouldn't have been half as enjoyable without you. Through the toughest stretches of this PhD, I felt incredibly lucky to have a friend like you helping to carry me across the finish line. And it was an equal honour, to be there for you when you needed support. You always made me feel valued, and I'll miss you terribly. I will always remember our time together with immense fondness.

India, Nina, Mike, and Alice – Thank you for bearing with me when I was difficult and for making living in Edinburgh so enjoyable. Coming home was as exciting as going to work, and I'll always cherish our random adventures, beach days, spa days, shopping trips, dinners, and TV binges.

Liam, Łukasz, Berni, Hannah, Elise, Daphne, Jenni, Sophie, Samir, Martina, Elliot, Xell – I wouldn't have had nearly as much fun as I did without all of you. It was a real pleasure having dinner parties, board game nights, and movie nights together. I'll miss our time together greatly.

Ryan, Billy, Mary, and Tom – My officemates, you made each and every day in the office special. I greatly enjoyed getting wraps, discussing maths, and going on walks with you all.

Emma – Thank you for being an amazing boss. Being a TA for you was incredibly fun and helped me gain perspective when I needed it most.

To all members of the department – You're the best maths department a student could ask for. I thoroughly enjoyed discussing maths, life, politics, and food with you all over lunch these

past three years.

To my friends from university and childhood across the world – Your support and encouragement have played a significant role in my journey, and I am forever grateful.

To my primary school teachers – Thank you for encouraging me and pushing me to work harder at maths, even when I struggled with counting and adding coins.

I would also like to thank my internal and external examiners for taking the time to read this thesis and for being part of my PhD journey.

Last but certainly not least, I want to thank my parents and sister. They have supported me from the very beginning, and I truly could not have completed this PhD without them.

Funding Acknowledgement

Thank you to The Maxwell Institute Graduate School in Modelling, Analysis, and Computation, a Centre for Doctoral Training funded by the EPSRC (grant EP/S023291/1), the Scottish Funding Council, Heriot-Watt University and the University of Edinburgh.

Inclusion of Published Works Form

Declaration

This thesis contains one or more multi-author published works. I hereby declare that the contributions of each author to these publications is as follows:

Citation details	Bourne, D. P., Egan, C. P., Lavier, T., & Pelloni, B. (2025). Semi-discrete optimal transport techniques for the compressible semi-geostrophic equations. *arXiv preprint arXiv:2504.20807*. Submitted to SIAM Analysis
Bourne, D. P.	Conceptualization, proofs, examples, editing, writing. Equal contribution.
Egan, C. P.	Conceptualization, proofs, examples, editing, writing. Equal contribution.
Lavier, T.	Conceptualization, proofs, examples, editing, writing. Equal contribution.
Pelloni, B.	Conceptualization, proofs, examples, editing, writing. Equal contribution.

Table of Contents

Chapter 1

Introduction

1.1 History of Mathematical Meteorology

Being able to predict the weather has long been a matter of the utmost importance for human civilization. Whether it is determining sunshine or rain for an upcoming festival, guiding agricultural practices, or informing military decisions, forecasting weather conditions across both short and long timescales has been a topic of study since the beginning of recorded history. For much of that history, understanding weather patterns relied primarily on intuition, local experience, and communal knowledge. However, the advent of radar, satellites, and computers has transformed our relationship with these mercurial atmospheric phenomena, enabling us to make informed and precise predictions. The modern study of meteorology began in the mid-19th century, marked by systematic data collection and the establishment of structured observation networks enabled by the invention of the electric telegraph. With the 1854 founding of the UK's Meteorological Department by Admiral Robert FitzRoy and the ideas of Vilhelm Bjerknes, meteorology as we know it took shape.

In 1904, Vilhelm Bjerknes [7] articulated his vision of weather prediction based on underlying mathematical and physical principles. He layed out a program to forecast weather using the Navier–Stokes equations for a rotating fluid, the continuity of mass equation, and atmospheric thermodynamics. His vision framed weather forecasting as an initial value problem, however actually carrying out this vision posed enormous challenges, as early 20th-century scientists had no practical means to solve the system of equations in full. Even setting up the problem was daunting: vast amounts of data were needed for the initial state, and solving the full equations by hand or graphical methods was impossible.

One of the earliest attempts to predict weather by calculation was made by Lewis Fry Richardson during World War I [58]. Richardson essentially tried to step forward the full system of atmospheric equations, which we now call the *primitive equations*, by hand calculation. The

result, unfortunately, was physically implausible because the full set of equations allowed fast-moving sound waves and certain gravity-inertia waves to dominate the solution with "noise" and spurious oscillations. Richardson's pioneering trial made it clear that some form of filtering or simplification was necessary. To predict the slow (relative to sound waves) evolution of weather systems one would need to filter out the rapid oscillations. This insight, combined with the sheer computational impracticality of the primitive equations, provided a strong motivation for developing reduced forms of the Navier–Stokes equations for large-scale atmospheric modelling.

By the late 1940s, with electronic computers on the horizon, meteorologists revisited the problem of numerical weather prediction armed with new tools and the lessons of Richardson's failure. Jule Charney [15], Arnt Eliassen [30], and others spearheaded an effort to find a simplified set of equations that would capture the essential slow dynamics of the atmosphere while filtering out the troublesome fast modes. The result was the formulation of the *quasi-geostrophic* (QG) equations. The QG system is derived by assuming that large-scale motions are nearly in *geostrophic balance*, i.e. the Coriolis force and horizontal pressure gradient are nearly in equilibrium. In this regime, which is typical of mid-latitude weather systems, the acceleration of air parcels is relatively small compared to the forces acting on them. Charney established that geostrophic balance was a reasonable assumption via a scale analysis of the Navier–Stokes equations in 1948 [13]. He showed that for synoptic-scale flows, with horizontal lengths on the order of thousands of kilometres and wind speeds of a few tens of meters per second, the ratio of inertial force to Coriolis force is very small. This implies that the flow is very nearly steady in the rotating frame, and thus to a first approximation one can set the local acceleration terms to zero. This is known as the *geostrophic approximation*. The QG equations omit sound waves and fast inertial waves because hydrostatic balance is assumed. Hydrostatic balance eliminates vertical accelerations due to the balance between pressure and gravity and the lack of vertical acceleration means that sound waves cannot propagate. This greatly reduces the influence of fast gravity-inertia waves, leaving a system that describes the slow, balanced evolution of pressure and flow. These equations govern the changes in the *geopotential* due to advection and slowly varying motions, and diagnostic relations can be used to infer vertical motion from horizontal temperature and pressure fields.

Not only did QG theory provide a theoretical framework for understanding atmospheric waves and instabilities, for example, Charney's and Eady's classic theories of baroclinic instability [14, 28] were built on the QG model, but it also enabled the first practical numerical

weather forecasts. In 1950, Charney, together with Ragnar Fjørtoft and John von Neumann [16], performed a historic numerical weather prediction experiment that proved the concept of using these simplified equations. They integrated a barotropic, single-layer QG model on the ENIAC computer for a 24-hour forecast of the 500-mb height field over North America. Unlike Richardson's hand-calculated attempt, this forecast was recognizably accurate: the predicted pressure pattern after one day bore a strong resemblance to the observed pattern, demonstrating that the filtered model was capturing the real evolution of the weather. This success was a proof of concept that large-scale weather could be predicted by numerical integration, as long as one uses an appropriate simplified model. QG models quickly became the backbone of mid 20th-century dynamic meteorology: they were used in research to understand jet streams, storm tracks, cyclones, and frontogenesis, and even as the basis for early operational forecasting models in the 1950s and 1960s. The QG equations were attractive not only because they filtered out fast acoustic modes, but also because they can be described in terms of a single conserved quantity, *potential vorticity*, with the rest of the flow deduced from the potential vorticity via underlying physical relationships.

There exists a well-developed mathematical theory for the QG equations, primarily because they form a system of conservation laws. This structure allows for the application of classical analytical techniques, enabling robust proofs of existence, uniqueness, and regularity of solutions. Moreover, this theoretical framework facilitates rigorous estimates of the convergence properties of numerical approximations.

It is important to stress the assumptions and limits behind the QG equations, which are derived under the assumption that the atmosphere is stably stratified, i.e. density decreases monotonically as you rise in the atmosphere, and in *hydrostatic balance*, i.e. vertical accelerations are negligible compared to gravity, which is well justified for large-scale motion. However, the QG system fails when the flow is not sufficiently near geostrophic balance, or when the time/space scales of interest approach those of convection, gravity-wave propagation, or equatorial motion. Phenomena like small mesoscale convective systems, tropical cyclones, or equatorial waves fall outside QG theory. These restrictions meant that, while QG was excellent for midlatitude cyclones and planetary waves, it could not address every atmospheric scenario and refined models that relax the strict assumptions of QG while still keeping the problem manageable were needed. Furthermore, QG requires that the rotation coefficient of the system is constant, this is not physical and is a limitation removed in the system that this thesis is

chiefly interested in.

One of the first people to push beyond the quasi-geostrophic paradigm was Arnt Eliassen, the Norwegian meteorologist who had worked closely with Charney. He developed what is known as the *geostrophic momentum approximation*, which forms the basis of the *semi-geostrophic* (SG) equations. In essence, Eliassen's SG model [30] kept the spirit of the QG approach assuming the atmosphere is largely governed by rotation and stratification, but allowed a bigger role for momentum advection in the flow. Eliassen's formulation acknowledged that in some intense large-scale phenomena, such as narrow jet-stream perturbations or developing frontal zones, the departures from geostrophic balance, though still small in an absolute sense, are not negligible second-order effects as QG would assume. In those situations, the atmosphere can develop sharp gradients, for example, a frontal surface with large temperature contrasts over a short distance, or strong accelerations along a jet streak. The SG equations include certain nonlinear terms that QG omits, most notably, they use the *geostrophic wind* to advect momentum, an approximation that allows for a more robust handling of momentum conservation while still filtering out fast waves. By using the geostrophic wind in the advection terms of the momentum equations, Eliassen's model permitted a larger ageostrophic circulation to develop than QG would allow. This made the SG model more capable of simulating phenomena like the distortion of weather fronts and the accompanying vertical circulations that are crucial for frontogenesis.

Early computers and limited data made the implementation of SG challenging, so for a while QG remained the preferred tool for operational forecasting. Nevertheless, Eliassen's contribution was significant as a forward-looking theoretical development. It laid a foundation for later scientists to analyze and simulate the life cycle of fronts and other balanced disturbances that QG theory handles imperfectly. In fact, the SG equations turned out to be especially powerful in studying atmospheric frontogenesis, the process by which weather fronts sharpen, because the SG model can represent the increasing asymmetry and the intense ageostrophic secondary circulations, the rising and sinking motions, that attend a developing front.

Despite its potential, Eliassen's SG formulation initially remained underutilized until it was independently rediscovered by Bretherton and Hoskins in the 1970s [42]. Their work recognized that SG theory offered an effective mathematical framework for accurately capturing the sharp discontinuities observed in atmospheric flows, particularly those marking weather fronts, where the QG approximation proved insufficient [42, 43]. Building upon these foundations, Cullen

at the UK Met Office championed SG theory as a practical means of improving numerical weather prediction models, particularly in resolving frontal dynamics. Cullen and collaborators made substantial progress in understanding the SG equations, systematically exploring their mathematical structure and identifying critical energy- and structure-preserving properties [25]. A key contribution by Cullen was his *convexity principle*, guided by his physical intuition, conjecturing that physically relevant solutions to the SG equations must satisfy the condition that the *modified pressure* is convex. This convexity condition is crucial for ensuring the stability and predictability of solutions.

1.1.1 Modern Semi-Geostrophic Theory

As part of his work Hoskin's introduced a coordinate transformation (see Eq. (1.20)). A significant conceptual breakthrough emerged in 1998 when Brenier and Benamou established an unexpected yet profound connection between Hoskins' coordinate transformation and the theory of optimal transport [5]. Guided by Cullen's convexity principle they interpreted the gradient of the modified pressure as an optimal transport map. By interpreting the SG equations as an optimal transport problem, Brenier and Benamou provided powerful new analytical tools and insights, opening the door to rigorous results on the existence and regularity of solutions. This remarkable insight was rapidly expanded and refined by a number of mathematicians whose collective contributions provided a robust theoretical foundation and deeper understanding of the geometric and variational structure underlying SG flows [3, 12, 32–36, 38]. Their work not only advanced mathematical theory but also laid essential groundwork for practical computational methodologies.

Ultimately, this fruitful synergy between meteorology and optimal transport theory culminated in the work of Egan et al. [29] and Benamou et al. [6]. Leveraging the optimal transport formulation, they developed innovative particle-based computational methods capable of simulating large-scale atmospheric dynamics with remarkable resolution and fidelity, specifically capturing sharp fronts and complex discontinuities characteristic of real-world atmospheric phenomena.

The present thesis continues and extends their pioneering efforts. Here, we generalize the existing numerical semi-discrete optimal transport methods from two to three spatial dimensions, extending the rigorous mathematical analysis from the incompressible to the compressible SG equations. Additionally, we leverage these theoretical advances to build novel numerical

simulations of compressible atmospheric flows, and deepen our understanding of the intrinsic geometry that defines the optimal transport formulation of the SG equations.

For a comprehensive and rigorous introduction to the mathematical and physical background of large-scale atmospheric phenomena and the semi-geostrophic equations, the reader is referred to the authoritative monograph by Cullen [19] as well as [44].

Viewed in a broader mathematical context, the deep link established by Brenier and Benamou between SG theory and optimal transport might appear natural rather than surprising. Indeed, it was precisely Brenier's fluid-dynamics perspective that initially inspired his celebrated polar factorization theorem, enabling the proof of existence for an optimal transport map in the quadratic cost case, one of the landmark results of modern mathematics [10]. In retrospect, the interplay between optimal transport and fluid dynamics emerges as fundamentally interconnected, underscoring the profound unity between these fields.

1.2 History of Monge and Optimal Transport

Optimal transport, much like meteorology, has a colourful history. Popular lore claims that Gaspard Monge was asked by Napoleon for the optimal manner in which his troops could dig defensive trenches and build artillery ramparts with the displaced dirt. However, this story is most certainly apocryphal as Monge first introduced the optimal transport problem in his 1781 memoir when Napoleon was only 11 years old and enrolled in school in Autun. The true origin of optimal transport begins with Monge's time at the prestigious École du Génie at Mézières, a military engineering school. While there Monge designed military fortifications such that an enemy could neither see nor fire upon a protected position, regardless of the enemy's line of sight. In order to do this Monge reformulated the problem as one of intersecting surfaces and lines in three dimensions. This work eventually earned him the title as the "Father of Descriptive Geometry". Monge's formative experiences at Mézières shaped the trajectory of his intellectual interests. Immersed in an environment of military engineers, Monge turned his powerful geometric insight toward problems of direct practical importance. One such class of problems was the movement of earth for construction. Building fortifications, canals, roads, or reservoirs often required excavating soil in one place, déblais, or "cuts", and depositing it in another, remblais, or "fills". The efficiency of these projects depended on minimizing the labour of transporting huge volumes of material.

In, *Mémoire sur la théorie des déblais et des remblais* [56], Monge was explicitly motivated

by military applications and fortress construction. In this treatise Monge posed, in rigorous terms, what is now recognized as the first statement of the optimal transport problem: given two volumes of soil, one to be excavated and one to be filled, find the way to move the soil that minimizes the total transportation cost. Monge assumed the *cost* of moving an elemental parcel of soil is proportional to the distance it is carried, essentially formulating a variational problem to minimize the work of transport with respect to the ℓ^1-norm. He described the soil as composed of infinitely many "molecules of earth" that need to be relocated from their initial positions to new target positions. The mathematical challenge was to determine a mapping from the initial volume to the final volume that minimizes the integrated distance. Monge intuited that the optimal mapping has a certain geometric structure: in his words, the transporting paths should be such that they do not intersect each other. In modern optimal transport theory, this property corresponds to the solution being *c-cyclically monotonic*. Monge would later go on to be one of the co-founders of the École Polytechnique. But within his native Burgundy, Monge's legacy can be seen as part of a continuum: Navier's and Darcy's, also native Burgundians, later achievements in fluid mechanics and hydraulics echoed Monge's paradigm of applying analytical thinking to solve practical engineering issues. And it is the work of the Monge and Navier in particular that we will carry forward in this thesis.

1.3 Outline of the Thesis

The thesis is structured around the application and theoretical development of semi-discrete optimal transport techniques for solving the SG equations. In Chapter 2 we present a mesh-free, three-dimensional numerical scheme for the incompressible SG equations, significantly generalising prior two-dimensional implementations. We show this approach conserves energy enabling robust and efficient numerical simulations exemplified by a benchmark cyclone problem, the first fully three-dimensional simulation of its kind. Building on these numerical developments, in Chapter 3 we rigorously establish the existence of global-in-time weak solutions of the compressible SG equations with compactly supported measure-valued initial data. Our analysis employs a particle discretisation strategy coupled with optimal transport theory, generalising previous results of [24] and providing a solid theoretical foundation for numerical approximations. In Chapter 4 we investigate conditions related to the domain geometry and seed and weight configurations that yield the necessary regularity of integrals defined over Laguerre cells, enhancing our understanding of stability and regularity properties within semi-discrete opti-

mal transport frameworks. In Chapter 5, we develop a novel semi-discrete optimal transport scheme tailored specifically to the compressible SG equations. Finally, in the Conclusion we will summarise the results of this thesis and briefly present some open problems.

1.4 Notation

We adopt the following standard notation:

- We make extensive use of the following constants: $g > 0$ is the acceleration due to gravity; $f_{\text{cor}} > 0$ is the Coriolis parameter, which we assume constant for the thesis; $\theta_0 > 0$ and $p_0 > 0$ are reference potential temperature and pressure, respectively; $\gamma = c_p/c_v > 1$ is the adiabatic index; $R_d = c_p - c_v > 0$ is the specific gas constant for dry air, with $c_p > 0$ and $c_v > 0$ being the specific heats at constant pressure and volume, respectively; and $\kappa = c_v(R_d/p_0)^{\gamma-1} > 0$.

- $\mathcal{X} \subset \mathbb{R}^d$ denotes the fluid or physical domain with $d = 2$ or 3. This is also referred to as the source space. We assume that $\mathcal{X}$ is nonempty, connected, compact, and that it coincides with the closure of its interior.

- $\mathcal{Y} \subset \mathbb{R}^d$ denotes the geostrophic domain, also referred to as the target space.

- $\mathcal{C}_c^\infty(\mathcal{Y} \times \mathbb{R})$ denotes the space of real-valued infinitely-differentiable and compactly supported test functions on $\mathcal{Y} \times \mathbb{R}$.

- $\mathcal{C}_b(\mathbb{R}^d)$ denotes the space of real-valued continuous and bounded test functions on $\mathbb{R}^d$.

- $\mathcal{H}^d$ denotes the d-dimensional Hausdorff measure.

  Let S be a subset of R^d and let $d \geq 0$ be a dimension. Consider all possible countable covers of the set S by sets $\{U_i\}$ where the diameter of each set, $\text{diam}(U_i)$, is less than some small number $\delta > 0$. For a given δ, we have

$$\mathcal{H}_\delta^d(S) = \inf\left\{\sum_{i=1}^{\infty}(\text{diam}(U_i))^d : S \subseteq \bigcup_{i=1}^{\infty} U_i,\ \text{diam}(U_i) < \delta\right\}. \tag{1.1}$$

  Then the d-dimensional Hausdorff measure, denoted $\mathcal{H}^d(S)$, is given by

$$\mathcal{H}^d(S) = \lim_{\delta \to 0} \mathcal{H}_\delta^d(S). \tag{1.2}$$

- For a Borel set $A \subset \mathcal{X}$, $\mathbb{1}_A : \mathcal{X} \to \{0, 1\}$ denotes the characteristic function of the set A. That is

$$\mathbb{1}_A(\mathbf{x}) = \begin{cases} 1 & \text{if} \quad \mathbf{x} \in A, \\ 0 & \text{otherwise.} \end{cases}$$

- $\mathscr{P}(A)$ denotes the set of Borel probability measures on $A \subseteq \mathbb{R}^d$.

  Let A be a topological space and $\mathcal{B}(A)$ be the Borel σ-algebra on A. A Borel probability measure on A is a function $\mu : \mathcal{B}(A) \to [0, 1]$ that satisfies the following two properties:

  1. Normalization. The measure of the entire space is one, i.e. $\mu(A) = 1$.
  2. Countable or σ-additivity. For any countable sequence of disjoint sets $A_1, A_2, \ldots \in \mathcal{B}(A)$, the measure of their union is equal to the sum of their individual measures, i.e.

$$\mu\left(\bigcup_{i=1}^{\infty} A_i\right) = \sum_{i=1}^{\infty} \mu(A_i). \tag{1.3}$$

- $\mathscr{P}_{\mathrm{ac}}(A)$ denotes the set of Borel probability measures on $A \subseteq \mathbb{R}^d$ that are absolutely continuous with respect to the Lebesgue measure.

- Given a Borel map $S : A \to B$ and a measure $\mu \in \mathscr{P}(A)$, the pushforward of μ by S is the measure $S_{\#}\mu \in \mathscr{P}(B)$ defined by $S_{\#}\mu(U) = \mu(S^{-1}(U))$ for all Borel sets $U \subseteq B$.

- $\mathscr{P}_{\mathrm{c}}(\mathcal{Y})$ denotes the set of Borel probability measures on $\mathcal{Y}$ with compact support.

- We will abuse notation slightly and use the same symbol to denote the probability density function and the measure, i.e.

$$\int_A \mu(\mathbf{x}) \, \mathrm{d}\mathbf{x} = \int_A \mathrm{d}\mu(\mathbf{x}). \tag{1.4}$$

- In what follows the subscript t on a dependent variable denotes evaluation at time t. For example $\mu_t(\mathbf{x})$ it the measure μ at time t.

1.5 Optimal Transport Theory

The optimal transport problem, as originally formulated by Monge, assumes one has a *source measure*, $\sigma \in \mathscr{P}(X)$, on a *source space*, $X \subseteq \mathbb{R}^d$, and a *target measure*, $\alpha \in \mathscr{P}(Y)$, on a *target space*, $Y \subseteq \mathbb{R}^d$, and seeks a mapping T that pushes σ forward to α, i.e. $T_{\#}\sigma = \alpha$, while minimizing the total transport cost. Written in modern mathematical terms this is as follows

$$\mathcal{T}_c = \inf_{\substack{T:X\to Y \\ T_{\#}\sigma=\alpha}} \int_X c(\mathbf{x}, T(\mathbf{x}))\, \mathrm{d}\sigma(\mathbf{x}), \tag{MP}$$

where $\mathcal{T}_c$ is the optimal transport cost of moving σ to α according to the cost, $c : X \times Y \to \mathbb{R}$. The minimizing map T is the *optimal transport map*. Unfortunately for us, this optimization problem has a highly non-linear constraint, $T_{\#}\sigma = \alpha$, i.e. that the target measure α is the *push-forward* of the source measure σ under the transport map T. In Monge's classical example, the cost was the ground distance travelled, $c(\mathbf{x}, \mathbf{y}) = \|\mathbf{x} - \mathbf{y}\|$. This formulation is geometrically natural but notoriously challenging, in no small part due to the push-forward constraint. Note that the push-forward constraint is equivalent to the conservation of mass.

Example 1.5.1. Consider, for simplicity, a fully discrete optimal transport problem where the source measure is a Dirac mass located at the origin, and the target measure is given by two equal Dirac masses at separate points,

$$\sigma = \delta_0 \quad \text{and} \quad \alpha = \frac{1}{2}\delta_{-1} + \frac{1}{2}\delta_1. \tag{1.5}$$

Although this represents a perfectly well-posed and intuitive scenario for transporting one unit mass from a single pile into two separate, equally sized piles, no optimal transport *map* exists, regardless of the cost function, precisely because the act of splitting mass from one point to multiple destinations would constitute a one-to-many mapping, which violates the definition of a map.

Indeed, Monge's original problem lacked general existence results and remained open until the pioneering work of Kantorovich in 1942 [45]. Kantorovich relaxed and generalized (MP) by allowing *transport plans* instead of strict maps. A transport plan is a measure $\gamma \in \mathscr{P}(X \times Y)$ on the product space, $X \times Y$, coupling σ and α, so that $\gamma(A \times Y) = \sigma(A)$ and $\gamma(X \times B) = \alpha(B)$

for all measurable $A \subset X$ and $B \subset Y$. Kantorovich's problem is written as follows:

$$\mathcal{T}_c = \inf_{\gamma \in \Gamma(\sigma,\alpha)} \int_{X\times Y} c \, \mathrm{d}\gamma, \tag{KP}$$

where $\Gamma(\sigma, \alpha)$ is set of transport plans, i.e.

$$\Gamma(\sigma,\alpha) = \{\gamma \in \mathscr{P}(X \times Y) : (\pi_X)_{\#}\gamma = \sigma, (\pi_Y)_{\#}\gamma = \alpha\}, \tag{1.6}$$

where π_X and π_Y are the canonical projections onto X and Y respectively. The key generalisation of Kantorovich was that he now allowed mass to be split. Intuitively, $\gamma(\mathbf{x}, \mathbf{y})$ represents how much mass is moved from location $\mathbf{x}$ to location $\mathbf{y}$. Monge's problem is recovered as the special case where γ is concentrated on the graph of a function T, i.e. no mass is split. Kantorovich's formulation turns the transport problem into a linear optimization problem over the convex set of plans, which is much easier to analyse. In particular, at least one optimal plan exists under mild conditions, by the direct method of the calculus of variations. Furthermore, under additional regularity conditions, one can often show that an optimal plan is induced by a map. For example, Brenier's Theorem [10] guarantees that for the quadratic cost, $c(\mathbf{x}, \mathbf{y}) = \frac{1}{2}\|\mathbf{x} - \mathbf{y}\|^2$, on $\mathbb{R}^n$, if the source density σ is absolutely continuous, the optimal plan is unique and is given by a transport map $T(\mathbf{x}) = \nabla\varphi(\mathbf{x})$ where φ is a convex potential. In such cases the optimal mapping satisfies a Monge–Ampère type equation, reflecting the fact that T pushes σ to α, i.e. $\det D^2\varphi$ adjusts the volume change to match the density α. The Kantorovich relaxation thus provides both the assurance of existence and a powerful framework to investigate further properties of optimal transport solutions.

Because the optimal transport problem in (KP) form is a linear programming problem with linear constraints, one can introduce a dual variational problem that plays a fundamental role in the theory. The Kantorovich *dual formulation* seeks functions $\phi \in \mathcal{C}_b(X)$ on the source and $\psi \in \mathcal{C}_b(Y)$ on the target that maximize the total "benefit"

$$\mathcal{T}_c = \max_{\varphi\oplus\psi\leq c} \int_X \phi \, \mathrm{d}\sigma + \int_Y \psi \, \mathrm{d}\alpha, \tag{DP}$$

subject to the affordability constraint $\phi(\mathbf{x}) + \psi(\mathbf{y}) \leq c(\mathbf{x}, \mathbf{y})$ for all $\mathbf{x} \in X$ and $\mathbf{y} \in Y$. Economically, ϕ and ψ can be interpreted as optimal "price" functions on mass at the source and target locations, respectively, enforcing that no transport $\mathbf{x} \to \mathbf{y}$ yields net profit, since oth-

erwise one could increase $\phi(\mathbf{x}) + \psi(\mathbf{y})$ until the inequality $\phi(\mathbf{x}) + \psi(\mathbf{y}) \leq c(\mathbf{x}, \mathbf{y})$ saturates. Duality theory guarantees that an optimal pair (ϕ, ψ) exists and that the minimum transport cost equals this maximal dual value. Moreover, one can show that optimal ϕ and ψ can be chosen to satisfy $\psi(\mathbf{y}) = \phi^c(\mathbf{y})$, where the *c-transform* $\phi^c(\mathbf{y}) := \inf_{\mathbf{x}\in X} \{c(\mathbf{x}, \mathbf{y}) - \phi(\mathbf{x})\}$ is an analogue of the Legendre transform. In particular, ψ can be taken to be *c-concave*, meaning that $\psi = \phi^c$ for some ϕ. Such ϕ and ψ are called *Kantorovich potentials*. Kantorovich potentials provide a great deal of structural insight. For instance, they encapsulate optimality conditions: $\phi(\mathbf{x}) + \phi^c(\mathbf{y}) = c(\mathbf{x}, \mathbf{y})$ on the support of any optimal plan. They also enjoy regularity properties mirroring those of the cost c: for example, if $c(\mathbf{x}, \mathbf{y}) = \|\mathbf{x} - \mathbf{y}\|^p$ and X and Y are compact, any optimal potential ϕ is Lipschitz continuous when $p \geq 1$.

The formulation (DP) is particularly valuable because, even in situations where the optimal plan is not unique, the optimal potentials, ϕ, ψ, are uniquely determined up to an additive constant. This uniqueness underpins stability results and connects optimal transport to other areas; for instance, ϕ can be seen as a generalized solution of a Hamilton–Jacobi type PDE and often carries geometric information about the transport problem. Moreover, the dual formulation provides a framework for proving existence of optimal plans via standard convex analysis arguments.

For a comprehensive and rigorous introduction to optimal transport theory, the reader is referred to the authoritative texts by Santambrogio and Friesecke [39, 59]. For a deep dive into numerical optimal transport the reader is referred to the text by Peyré and Cuturi [57].

1.5.1 Semi-Discrete Optimal Transport Theory

For us the most important branch of optimal transport theory that has emerged is the so called *semi-discrete* optimal transport where the source measure is absolutely continuous with respect to the Lebesgue measure and the target measure is discrete. We denote by $\mathcal{X} \subset \mathbb{R}^d$ the compact set representing the source space, and by $\mathcal{Y} \subset \mathbb{R}^d$ the target space. We fix $N \in \mathbb{N}$ and define the set of *seed vectors* by

$$D^N := \left\{ \mathbf{z} = \left(\mathbf{z}^1, \ldots, \mathbf{z}^N\right) \in \mathcal{Y}^N : \mathbf{z}^i \neq \mathbf{z}^j \text{ whenever } i \neq j \right\}. \tag{1.7}$$

We also define the set of admissible weights

$$\Delta^N := \left\{ \mathbf{m} = (m^1, \dots, m^N) \in (0,1]^N : \sum_{i=1}^{N} m^i = 1 \right\}, \tag{1.8}$$

and the class of discrete probability measures with N atoms as

$$\mathscr{P}^N(\mathcal{Y}) := \left\{ \sum_{i=1}^{N} m^i \delta_{\mathbf{z}^i} : \mathbf{z} \in D^N,\ \mathbf{m} \in \Delta^N \right\}. \tag{1.9}$$

Given a continuous cost function $c : \mathcal{X} \times \mathcal{Y} \to \mathbb{R}$, a source measure σ on the source domain $\mathcal{X}$, absolutely continuous with respect to the Lebesgue measure, and a discrete target measure $\alpha^N \in \mathscr{P}^N(\mathcal{Y})$, the Monge formulation of optimal transport asks for a measurable map $T : \mathcal{X} \to \mathcal{Y}$ pushing σ forward to α^N, i.e. $T_{\#}\sigma = \alpha^N$, that minimizes the total cost

$$\int_{\mathcal{X}} c(\mathbf{x}, T(\mathbf{x}))\sigma(\mathbf{x})\, \mathrm{d}\mathbf{x}. \tag{1.10}$$

Because the target measure is discrete, the transport map T must be piecewise constant, and the solution amounts to partitioning $\mathcal{X}$ into a collection of cells $\{L^i\}_{i=1}^N$ such that each cell L^i is mapped to $\mathbf{z}^i$ and has σ-measure equal to m^i. This setup captures many problems, ranging from computational geometry to optics, and it leads to a beautiful geometric description of the optimal map in terms of weighted Voronoi tessellations, called Laguerre tessellations.

Definition 1.5.2 (Voronoi Tessellation)**.** Let $P = \{\mathbf{p}_1, \mathbf{p}_2, \dots, \mathbf{p}_n\}$ be a finite set of points in R^d. The Voronoi cell C_k corresponding to a site $\mathbf{p}_k$ is the set of all points $\mathbf{x} \in \mathbb{R}^d$ whose distance to $\mathbf{p}_k$ is less than or equal to their distance to any other site $\mathbf{p}_j$. In other words

$$C_k = \{\mathbf{x} : d(\mathbf{x}, \mathbf{p}_k) \leq d(\mathbf{x}, \mathbf{p}_j) \quad \forall\, j \neq k\}, \tag{1.11}$$

where $d(\mathbf{x}, \mathbf{p})$ is the Euclidean distance. The Voronoi diagram or tessellation is the collection of all the Voronoi cells, C_k.

To describe these Laguerre cells, we introduce a vector of *weights*, $\boldsymbol{w} = (w^1, \dots, w^N) \in \mathbb{R}^N$, associated to the seeds.

Definition 1.5.3 (c-Laguerre tessellation)**.** Given $(\boldsymbol{w}, \mathbf{z}) \in \mathbb{R}^N \times D^N$, the *c-Laguerre tessella-*

tion of $\mathcal{X}$ generated by $(\boldsymbol{w}, \mathbf{z})$ is the collection of *Laguerre cells* $\{L_c^i(\boldsymbol{w}, \mathbf{z})\}_{i=1}^N$ defined by

$$L_c^i(\boldsymbol{w}, \mathbf{z}) := \big\{\mathbf{x} \in \mathcal{X} : c(\mathbf{x}, \mathbf{z}^i) - w^i \leq c(\mathbf{x}, \mathbf{z}^j) - w^j \quad \forall\, j \in \{1, \dots, N\}\big\}, \tag{1.12}$$

for $i \in \{1, \dots, N\}$.

In order to guarantee that the tessellation has desirable properties we need to introduce the following condition on the cost function.

Definition 1.5.4 (Twist Condition)**.** A cost function c is said to satisfy the *twist condition* if it is differentiable for every point $\mathbf{x} \in X$, the map $\mathbf{y} \mapsto \nabla_{\mathbf{x}} c(\mathbf{x}_0, \mathbf{y})$ is injective for every $\mathbf{x}_0 \in X$.

While we present the twist condition here due to its role in guaranteeing properties of the tessellation, it plays a substantial role in all formulations of optimal transport.

Example 1.5.5. The classical examples of twisted costs are $c(\mathbf{x}, \mathbf{y}) = \|\mathbf{x} - \mathbf{y}\|^p$ for $p > 1$ and $\mathbf{x}, \mathbf{y} \in \mathbb{R}^d$. The compressible cost in Chapter 3 is also twisted.

Under the assumption that the cost function satisfies the twist condition, the c-Laguerre cells form a tessellation of $\mathcal{X}$ in the sense that $\bigcup_{i=1}^N L_c^i(\boldsymbol{w}, \mathbf{z}) = \mathcal{X}$ and $\mathcal{L}^d\big(L_c^i(\boldsymbol{w}, \mathbf{z}) \cap L_c^j(\boldsymbol{w}, \mathbf{z})\big) = 0$ if $i \neq j$, by [53, Proposition 37]. Intuitively, changing the weight vector shifts the boundaries of the Laguerre cells, thus controlling their volumes. The twist condition is a standard assumption in optimal transport theory; it not only guarantees that the cells partition the domain, but also that the solution of the optimal transport problem is in fact a unique map.

With these Laguerre cells in hand, we define the associated semi-discrete transport map as follows:

Proposition 1.5.6 (Semi-Discrete Transport Map)**.** *Let $\sigma \in \mathscr{P}_{\mathrm{ac}}(\mathcal{X})$ be absolutely continuous. Fix a cost $c\colon \mathcal{X} \times \mathcal{Y} \to \mathbb{R}$ that satisfies the twist condition. For a weight vector $\boldsymbol{w} = (w^1, \dots, w^N) \in \mathbb{R}^N$ define*

$$T(\mathbf{x}) := \sum_{i=1}^N \mathbf{z}^i \mathbb{1}_{L_c^i(\boldsymbol{w}, \mathbf{z})}(\mathbf{x}). \tag{1.13}$$

1. ***Optimality for the Induced Target Measure.*** *For every $\boldsymbol{w} \in \mathbb{R}^N$ the map T is well defined σ-a.e. and transports σ onto*

$$\alpha := T_{\#}\sigma = \sum_{i=1}^N \sigma\big(L_c^i(\boldsymbol{w}, \mathbf{z})\big)\, \delta_{\mathbf{z}^i}.$$

Moreover T is the optimal transport map for the cost c between σ and α.

[53, Proposition 37]

2. ***Existence of Weights for a Prescribed α.*** *Conversely, given any probability measure $\alpha = \sum_{i=1}^{N} m^i \delta_{\mathbf{z}^i}$ with $m^i > 0$ and $\sum_i m^i = 1$, there exists a weight vector $\boldsymbol{w} \in \mathbb{R}^N$ (unique up to an additive constant) such that*

$$\sigma\big(L_c^i(\boldsymbol{w}, \mathbf{z})\big) = m^i, \quad i \in \{1, \dots, N\}$$

and the associated map T defined by Eq. (1.13) is therefore the optimal transport map from σ to α.

[53, Theorem 40]

It is insightful to visualize the effect of the weight adjustment in two dimensions.

Example 1.5.7. Set $d = 2$ and consider a cost function

$$c(\mathbf{x}, \mathbf{y}) = \frac{1}{2}\|\mathbf{x} - \mathbf{y}\|^2, \tag{1.14}$$

transporting

$$\sigma = \mathcal{L}^2 \quad \text{to} \quad \alpha = \frac{1}{N}\sum_{i=1}^{N} \delta_{\mathbf{z}^i}, \tag{1.15}$$

such that $m^i = \frac{1}{N}$. Initially, with $\boldsymbol{w} = \mathbf{0}$, $\{L_c^i(\boldsymbol{w}, \mathbf{z})\}_{i=1}^N$ is an unweighted Voronoi diagram where the cell areas generally do *not* match the m^i, as seen in Figure 1.1a. By progressively tuning the weights $\boldsymbol{w}$, the cell areas can be made to increase or decrease as needed. At the optimal $\boldsymbol{w}^*$, all cells $L_c^i(\boldsymbol{w}^*, \mathbf{z})$ have area $\sigma(L_c^i(\boldsymbol{w}^*, \mathbf{z})) = m^i$, meaning each seed $\mathbf{z}^i$ captures exactly its allotted mass. The resulting partition $\{L_c^i(\boldsymbol{w}^*, \mathbf{z})\}_{i=1}^N$, after optimizing the weights, is a Laguerre diagram whose cells each contain equal mass, as seen in Figure 1.1b.

Further geometric properties of these optimal Laguerre partitions, such as regularity of cell interfaces or centroids (see Definition 1.6.1), will be explored exhaustively in this thesis. In summary, the semi-discrete case provides a convenient and intuitive picture of optimal transport: the map can be thought of as carving up the continuous domain into cells of the right masses and assigning each cell to a target point at minimal cost. Each Laguerre cell acts like

a "catchment basin" for mass that travels to the corresponding site, and the optimal weights $\boldsymbol{w}^*$ adjust these basins to perfectly match the target distribution.

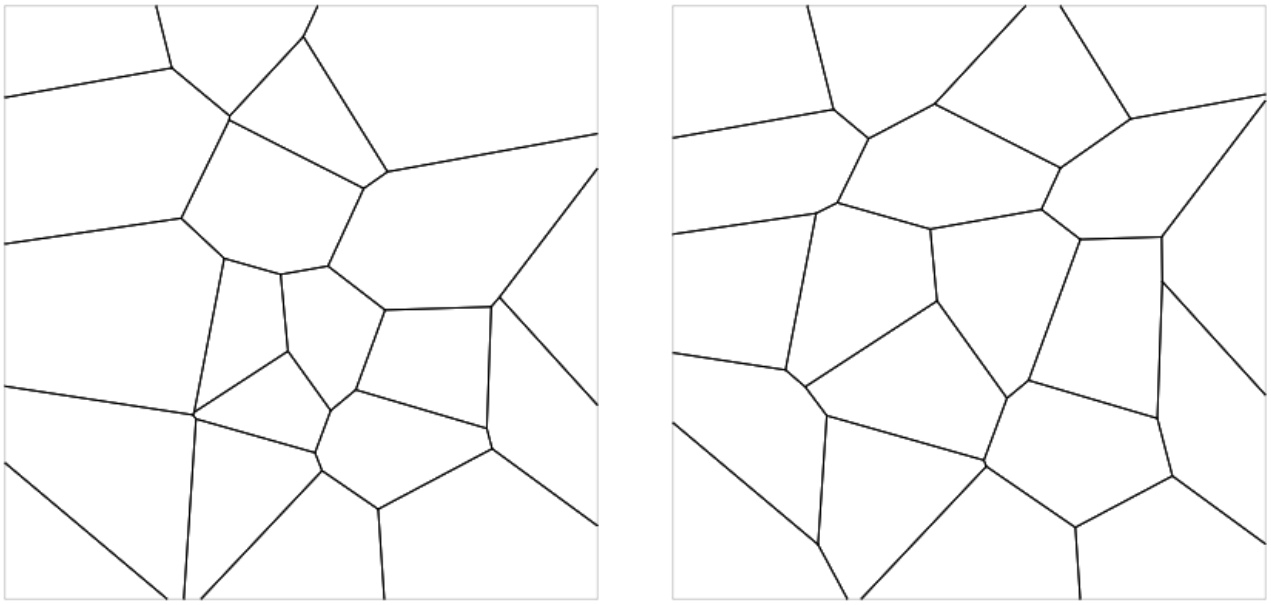

(a) Voronoi Diagram (b) Laguerre Diagram

Figure 1.1: A Voronoi diagram and the corresponding Laguerre diagram where the weights have been optimized such that all the cells have the same mass with respect to the Lebesgue measure.

For a comprehensive and rigorous introduction to semi-discrete optimal transport theory, the reader is referred to the authoritative text by Mérigot and Thibert [53].

1.6 The Semi-Geostrophic Equations

In this thesis, we are primarily concerned with the analysis and simulation of the SG equations, a system of partial differential equations used to model large-scale geophysical flows such as atmospheric fronts and ocean currents. We consider four variants of this system, distinguished by whether the fluid is compressible or incompressible, and whether the domain is two- or

three-dimensional. Despite their differences, all variants share a common structural form:

$$\begin{cases} D_t \mathbf{u}_g = \text{Momentum Forcing}, \\ D_t \theta = \text{Thermodynamic Forcing}, \\ \text{Continuity of Mass}, \\ \text{Balance Relations}, \\ \text{Boundary Conditions}, \end{cases} \tag{1.16}$$

where $D_t = \partial_t + \mathbf{u} \cdot \nabla$ denotes the material derivative with respect to the full velocity of the fluid $\mathbf{u}(\mathbf{x}, t) = (u_1(\mathbf{x}, t), u_2(\mathbf{x}, t), u_3(\mathbf{x}, t))^T$, while the geostrophic velocity is denoted by $\mathbf{u}_g(\mathbf{x}, t) = (u(\mathbf{x}, t), v(\mathbf{x}, t), 0)^T$. The full fluid velocity is related to the geostrophic velocity via

$$\mathbf{u} = \mathbf{u}_g + \mathbf{u}_a, \tag{1.17}$$

where $\mathbf{u}_a$ is the ageostrophic velocity, i.e. the component of the fluid velocity which is out of geostrophic balance. The SG equations describe the evolution of two primary state variables: the geostrophic velocity $\mathbf{u}_g(\mathbf{x}, t)$, and the potential temperature $\theta(\mathbf{x}, t)$, both advected by the full velocity field $\mathbf{u}(\mathbf{x}, t)$. The exact form of the momentum and thermodynamic forcing terms, as well as the mass continuity equation, depends on the physical assumptions of the system under consideration. In the incompressible setting, the continuity equation takes the standard divergence-free form $\nabla \cdot \mathbf{u} = 0$, and the momentum equation is coupled to the thermodynamics only through buoyancy/stratification effects related to hydrostatic balance. In the compressible settings, the continuity equation evolves the density $\rho(\mathbf{x}, t)$ of the fluid. This introduces a more complex interaction between the dynamics and thermodynamics. Dimensionality further modifies the system. In the three-dimensional setting, all components of the velocity and potential temperature gradients are retained. In two dimensions, vertical structure is suppressed, and a modified thermodynamic forcing term must be introduced to account for the absence of one component of the geostrophic velocity. This ensures consistency with the balance constraints of the SG approximation and prevents unphysical drift in the potential temperature field.

In Sections 1.6.1 and 1.6.2 we detail the reformulation in Lagrangian coordinates for two SG models, compressible and incompressible, in three dimensions, in detail. A complete derivation of the SG equations, beginning from the full primitive equations and applying the SG scaling

and coordinate transformation, is presented in Chapter 5 in the two-dimensional compressible case.

1.6.1 Incompressible PDE

We begin by considering the incompressible semi-geostrophic system in three dimensions in physical coordinates. These equations arise as an approximation of the Euler–Boussinesq equations under the geostrophic momentum approximation, and the assumption of geostrophic and hydrostatic balance. To begin let the physical (source) space $\mathcal{X} \subset \mathbb{R}^3$ be convex (in addition to our general assumptions given in Section 1.4), and let the geostrophic (target) space $\mathcal{Y} = \mathbb{R}^3$. Define the source measure as $\sigma = \mathcal{L}^3 \llcorner \mathcal{X}$ and a final time $0 < t_f < \infty$. Recall that $\theta(\mathbf{x}, t)$ is the potential temperature and the definition of all the various physical constants outlined in Section 1.4. Finally, we introduce the rotation matrix

$$J = f_{\text{cor}} \begin{pmatrix} 0 & -1 & 0 \\ 1 & 0 & 0 \\ 0 & 0 & 0 \end{pmatrix}. \tag{1.18}$$

Recall $\mathbf{u}(\mathbf{x}, t) = (u_1(\mathbf{x}, t), u_2(\mathbf{x}, t), u_3(\mathbf{x}, t))^T$ and $\mathbf{u}_g(\mathbf{x}, t) = (u(\mathbf{x}, t), v(\mathbf{x}, t), 0)^T$. Then the system of SG equations for an incompressible fluid, given by [19, Eq. 3.2], is

$$\begin{cases} D_t \mathbf{u}_g = J(\mathbf{u}_g - \mathbf{u}) & \text{in } \mathcal{X} \times [0, t_f], \\ D_t \theta = 0 & \text{in } \mathcal{X} \times [0, t_f], \\ \nabla \cdot \mathbf{u} = 0 & \text{in } \mathcal{X} \times [0, t_f], \\ \nabla p = \left(f_{\text{cor}} v,\ -f_{\text{cor}} u,\ \dfrac{g}{f_{\text{cor}}^2 \theta_0} \theta \right)^T & \text{in } \mathcal{X} \times [0, t_f], \\ \mathbf{u} \cdot \hat{\mathbf{n}} = 0 & \text{on } \partial\mathcal{X} \times [0, t_f], \end{cases} \tag{1.19}$$

where $\hat{\mathbf{n}}$ is the unit outward normal to $\partial\mathcal{X}$. Define a coordinate transform $T_t : \mathcal{X} \to \mathcal{Y}$ by

$$T_t(\mathbf{x}) = \begin{pmatrix} x_1 + f_{\text{cor}}^{-1} v(\mathbf{x}, t) \\ x_2 - f_{\text{cor}}^{-1} u(\mathbf{x}, t) \\ \frac{g}{f_{\text{cor}}^2 \theta_0} \theta(\mathbf{x}, t) \end{pmatrix}, \tag{1.20}$$

which is the coordinate transform suggested by Hoskin's in [42]. Notice that the temperature, θ, in Eq. (1.19) is constant. This arises from the adiabatic assumption which assumes that the system is perfectly thermally isolated and there is no exchange of heat. For $t \in [0, t_f]$ define $\alpha_t \in \mathscr{P}(\mathcal{Y})$ by $\alpha_t = (T_t)_{\#}\mathcal{L}^3 \llcorner \mathcal{X}$. The goal of this section is to derive a PDE for α_t, which we call the potential vorticity [19, Section 3.2.3].

In preparation for the derivation, we examine Cullen's convexity principle [19, Definition 3.2]. Cullen's convexity principle asserts that a physically stable solution at each time is one that minimizes the geostrophic energy under all admissible rearrangements of fluid particles. In practice, this principle is enforced by assuming that the modified pressure $P(\mathbf{x}, t) := p(\mathbf{x}, t) + \frac{1}{2}(x_1^2 + x_2^2)$ is convex in the spatial coordinates [19, Definition 3.2]. This convexity condition ensures both physical stability, i.e. preventing any spontaneous, unbalanced accelerations or unphysical density configurations, and mathematical stability, i.e. selecting an energy-minimizing solution [19, Theorem 3.3]. A key observation is that $T_t = \nabla P$. Indeed, since $P(\cdot, t)$ is convex, T_t is the gradient of a convex potential and hence is the unique optimal transport map for the quadratic cost for transporting σ to α_t [59, Theorem 1.48]. The cost function that emerges from the energy for the three-dimensional incompressible system is the quadratic cost, $c(\mathbf{x}, \mathbf{y}) = \frac{1}{2}\|\mathbf{x} - \mathbf{y}\|^2$ [8]. This optimal mapping property is fundamental for the subsequent weak formulation, ensuring that any weak solution respects the energy convexity principle and thus remains physically and mathematically well-behaved.

Now we derive a PDE for α_t. First take the material derivative of Eq. (1.20) :

$$D_t T_t = \begin{pmatrix} u_1 + f_{\text{cor}}^{-1} D_t v \\ u_2 - f_{\text{cor}}^{-1} D_t u \\ \frac{g}{f_{\text{cor}}^2 \theta_0} D_t \theta \end{pmatrix} \overset{(1.19)}{=} \begin{pmatrix} u_1 + u - u_1 \\ u_2 + v - u_2 \\ 0 \end{pmatrix} = \mathbf{u}_g = J(T_t - \text{Id}). \tag{1.21}$$

Via the definition of the material derivative, this implies that

$$\partial_t T_t = -(\nabla T_t)\mathbf{u} + J(T_t - \text{Id}). \tag{1.22}$$

Consider a test function $\varphi \in \mathcal{C}_c^\infty(\mathcal{Y})$. Then

$$\frac{\mathrm{d}}{\mathrm{d}t} \int_{\mathcal{Y}} \varphi(\mathbf{y}) \, \mathrm{d}\alpha_t(\mathbf{y}) = \frac{\mathrm{d}}{\mathrm{d}t} \int_{\mathcal{X}} \varphi(T_t(\mathbf{x})) \, \mathrm{d}\mathbf{x} \tag{1.23}$$

$$= \int_{\mathcal{X}} \nabla\varphi(T_t(\mathbf{x})) \cdot \partial_t T_t(\mathbf{x}) \, \mathrm{d}\mathbf{x} \tag{1.24}$$

$$= \int_{\mathcal{X}} \nabla\varphi(T_t(\mathbf{x})) \cdot (-(\nabla T_t(\mathbf{x}))\mathbf{u} + J(T_t(\mathbf{x}) - \mathbf{x})) \, \mathrm{d}\mathbf{x} \tag{1.25}$$

$$= -\int_{\mathcal{X}} \nabla[\varphi(T_t(\mathbf{x}))] \cdot \mathbf{u} \, \mathrm{d}\mathbf{x} + \int_{\mathcal{X}} \nabla\varphi(T_t(\mathbf{x})) \cdot J(T_t(\mathbf{x}) - \mathbf{x}) \, \mathrm{d}\mathbf{x} \tag{1.26}$$

$$= \int_{\mathcal{X}} \varphi(T_t(\mathbf{x})) \nabla \cdot \mathbf{u} \, \mathrm{d}\mathbf{x} - \int_{\partial\mathcal{X}} \varphi(T_t(\mathbf{x})) \mathbf{u} \cdot \hat{\mathbf{n}} \, \mathrm{d}\mathcal{H}^2 \tag{1.27}$$

$$+ \int_{\mathcal{X}} \nabla\varphi(T_t(\mathbf{x})) \cdot J(T_t(\mathbf{x}) - \mathbf{x}) \, \mathrm{d}\mathbf{x} \tag{1.28}$$

$$= \int_{\mathcal{X}} \nabla\varphi(T_t(\mathbf{x})) \cdot J\big(T_t(\mathbf{x}) - T_t^{-1}(T_t(\mathbf{x}))\big) \, \mathrm{d}\mathbf{x} \tag{1.29}$$

$$= \int_{\mathcal{Y}} \nabla\varphi(\mathbf{y}) \cdot J\big(\mathbf{y} - T_t^{-1}(\mathbf{y})\big) \, \mathrm{d}\alpha_t(\mathbf{y}). \tag{1.30}$$

Therefore

$$\frac{\mathrm{d}}{\mathrm{d}t} \int_{\mathcal{Y}} \varphi(\mathbf{y}) \, \mathrm{d}\alpha_t(\mathbf{y}) = \int_{\mathcal{Y}} \nabla\varphi(\mathbf{y}) \cdot \mathbf{w}(\mathbf{y}, t) \, \mathrm{d}\alpha_t(\mathbf{y}), \tag{1.31}$$

where

$$\mathbf{w}(\mathbf{y}, t) = J\big(\mathbf{y} - T_t^{-1}(\mathbf{y})\big), \tag{1.32}$$

which is the geostrophic velocity in geostrophic coordinates, i.e. $\mathbf{u}_g(\mathbf{x}, t) = \mathbf{w}(T_t(\mathbf{x}), t)$. Equation (1.31) holds for all φ therefore the continuity equation in geostrophic coordinates is

$$\boxed{\partial_t \alpha_t + \nabla \cdot (\alpha_t \mathbf{w}) = 0.} \tag{1.33}$$

We can discretize this PDE by plugging in the particle approximation

$$\alpha_t(\mathbf{z}) = \sum_{i=1}^{N} m^i \delta_{\mathbf{z}_t^i}. \tag{1.34}$$

In order to discretize the PDE, we define the centroids of the Laguerre cells associated with our discretization.

Definition 1.6.1 (Centroids)**.** Given $(\boldsymbol{w}, \mathbf{z}) \in \mathbb{R}^N \times D^N$, the corresponding Laguerre tessellation $\{L_c^i(\boldsymbol{w}, \mathbf{z})\}_{i=1}^N$, and a measure σ on the Laguerre cells, the centroid of the Laguerre cells is

defined by

$$\mathbf{C} := \big(\mathbf{C}^1, \dots, \mathbf{C}^N\big), \tag{1.35}$$

$$\mathbf{C}^i := \frac{1}{m^i} \int_{L_c^i(\boldsymbol{w},\mathbf{z})} \mathbf{x}\, \mathrm{d}\sigma(\mathbf{x}). \tag{1.36}$$

For the incompressible problem the measure σ on the Laguerre cells is the Lebesgue measure. Starting with the right hand side of Eq. (1.31) we can write

$$\int_{\mathcal{Y}} \nabla\varphi(\mathbf{y}) \cdot \mathbf{w}(\mathbf{y},t)\, \mathrm{d}\alpha_t(\mathbf{y}) = \int_{\mathcal{Y}} \nabla\varphi(\mathbf{y}) \cdot J\mathbf{y}\, \mathrm{d}\alpha_t(\mathbf{y}) - \int_{\mathcal{Y}} \nabla\varphi(\mathbf{y}) \cdot JT_t^{-1}(\mathbf{y})\, \mathrm{d}\alpha_t(\mathbf{y}). \tag{1.37}$$

Note by applying Proposition 1.5.6 we find

$$\int_{\mathcal{Y}} \nabla\varphi(\mathbf{y}) \cdot JT_t^{-1}(\mathbf{y})\, \mathrm{d}\alpha_t(\mathbf{y}) = \int_{\mathcal{X}} \nabla\varphi(T_t(\mathbf{x})) \cdot J\mathbf{x}\, \mathrm{d}\mathbf{x} \tag{1.38}$$

$$= \sum_{i=1}^{N} \int_{L_c^i(\boldsymbol{w},\mathbf{z})} \nabla\varphi(\mathbf{z}_t^i) \cdot J\mathbf{x}\, \mathrm{d}\mathbf{x} \tag{1.39}$$

$$= \sum_{i=1}^{N} \nabla\varphi(\mathbf{z}_t^i) \cdot m^i J \frac{1}{m^i} \int_{L_c^i(\boldsymbol{w},\mathbf{z})} \mathbf{x}\, \mathrm{d}\mathbf{x} \tag{1.40}$$

$$= \sum_{i=1}^{N} \nabla\varphi(\mathbf{z}_t^i) \cdot m^i J\mathbf{C}^i(\mathbf{z}_t), \tag{1.41}$$

where $\mathbf{C}^i$ is the centroid of the i-th Laguerre cell. Therefore

$$\int_{\mathcal{Y}} \nabla\varphi(\mathbf{y}) \cdot J\mathbf{y}\, \mathrm{d}\alpha_t(\mathbf{y}) - \int_{\mathcal{Y}} \nabla\varphi(\mathbf{y}) \cdot JT_t^{-1}(\mathbf{y})\, \mathrm{d}\alpha_t(\mathbf{y}) = \sum_{i=1}^{N} m^i \nabla\varphi(\mathbf{z}_t^i) \cdot J\big(\mathbf{z}_t^i - \mathbf{C}^i(\mathbf{z}_t)\big). \tag{1.42}$$

On the other hand, the left hand side of Eq. (1.31) yields

$$\frac{\mathrm{d}}{\mathrm{d}t} \int_{\mathcal{Y}} \varphi(\mathbf{y})\, \mathrm{d}\alpha_t(\mathbf{y}) = \frac{\mathrm{d}}{\mathrm{d}t} \sum_{i=1}^{N} m^i \varphi(\mathbf{z}_t^i) = \sum_{i=1}^{N} m^i \nabla\varphi(\mathbf{z}_t^i) \cdot \dot{\mathbf{z}}_t^i. \tag{1.43}$$

Combining equations (1.37), (1.42), and (1.43) gives

$$\sum_{i=1}^{N} m^i \nabla\varphi(\mathbf{z}_t^i) \cdot \dot{\mathbf{z}}_t^i = \sum_{i=1}^{N} m^i \nabla\varphi(\mathbf{z}_t^i) \cdot J\big(\mathbf{z}_t^i - \mathbf{C}^i(\mathbf{z}_t)\big). \tag{1.44}$$

Since φ is arbitrary, the discrete particle dynamics are governed by the following coupled system of ODEs:

$$\boxed{\dot{\mathbf{z}}_t^i = J\big(\mathbf{z}_t^i - \mathbf{C}^i(\mathbf{z}_t)\big), \quad i \in \{1, \dots, N\}.} \tag{1.45}$$

We will solve this system numerically in Chapter 2.

1.6.2 Compressible PDE

Now we consider the compressible semi-gesostrophic system in three dimensions in physical coordinates. As before these equations arise from the Euler equations under the geostrophic momentum approximation, and the assumption of geostrophic and hydrostatic balance. To begin let the physical space $\mathcal{X} \subset \mathbb{R}^3$ satisfy our standard assumptions (see Section 1.4). Let the geostrophic space $\mathcal{Y} \subset \mathbb{R}^2 \times \left(\delta, \frac{1}{\delta}\right)$ for $\delta \in (0, 1)$. Recall that $\rho(\mathbf{x}, t)$ is the fluid density and $\theta(\mathbf{x}, t)$ is the potential temperature. Furthermore, as before define a final time $0 < t_f < \infty$ and recall the definition of all the various physical constants outlined in Section 1.4. We also introduce the Exner pressure $\Pi(\mathbf{x}, t)$, which fulfils the role of a pressure-like variable in the compressible framework while accounting for density variations. For a dry ideal compressible gas, the Exner pressure and standard pressure are

$$\Pi := \left(\frac{R_d \rho \theta}{p_0}\right)^{\gamma - 1}, \tag{1.46}$$

$$p := \rho R_d \theta \Pi. \tag{1.47}$$

Taking the logarithm and then the gradient of Eq. (1.47) gives

$$\frac{\nabla p}{p} = \frac{\nabla \rho}{\rho} + \frac{\nabla \theta}{\theta} + \frac{\nabla \Pi}{\Pi}. \tag{1.48}$$

Similarly, taking the logarithm then the gradient of Eq. (1.46) yields

$$\frac{\nabla \Pi}{\Pi} = (\gamma - 1)\left(\frac{\nabla \rho}{\rho} + \frac{\nabla \theta}{\theta}\right). \tag{1.49}$$

Combining Eq. (1.48) and Eq. (1.49) leads to

$$\frac{\nabla p}{p} = \frac{\gamma}{\gamma - 1}\frac{\nabla \Pi}{\Pi}. \tag{1.50}$$

Multiplying Eq. (1.50) by p/ρ, substituting Eq. (1.47) and using the identity $c_p = \gamma R_d/(\gamma - 1)$ gives

$$\frac{1}{\rho}\nabla p = c_p \theta \nabla \Pi. \tag{1.51}$$

Finally, as before, we introduce the rotation matrix

$$J = f_{\text{cor}} \begin{pmatrix} 0 & -1 & 0 \\ 1 & 0 & 0 \\ 0 & 0 & 0 \end{pmatrix}. \tag{1.52}$$

Recall $\mathbf{u}(\mathbf{x}, t) = (u_1(\mathbf{x}, t), u_2(\mathbf{x}, t), u_3(\mathbf{x}, t))^T$ is the full velocity of the fluid and $\mathbf{u}_g(\mathbf{x}, t) = (u(\mathbf{x}, t), v(\mathbf{x}, t), 0)^T$ is the geostrophic velocity. Then the system of SG equations for a compressible fluid, given by [19, Eq. 4.1], is

$$\begin{cases} D_t \mathbf{u}_g = J(\mathbf{u}_g - \mathbf{u}) & \text{in } \mathcal{X} \times [0, t_f], \quad (1.53a) \\ D_t \theta = 0 & \text{in } \mathcal{X} \times [0, t_f], \quad (1.53b) \\ D_t \rho + \rho \nabla \cdot \mathbf{u} = 0 & \text{in } \mathcal{X} \times [0, t_f], \quad (1.53c) \\ c_p \theta \nabla \Pi = (f_{\text{cor}} v,\, -f_{\text{cor}} u,\, -g)^T & \text{in } \mathcal{X} \times [0, t_f], \quad (1.53d) \\ \mathbf{u} \cdot \hat{\mathbf{n}} = 0 & \text{on } \partial\mathcal{X} \times [0, t_f], \quad (1.53e) \end{cases}$$

where again $\hat{\mathbf{n}}$ is the unit outward normal to $\partial\mathcal{X}$. Again we take the coordinate transform as suggested by Hoskins [42] :

$$T_t(\mathbf{x}) = \begin{pmatrix} x_1 + f_{\text{cor}}^{-1} v(\mathbf{x}, t) \\ x_2 - f_{\text{cor}}^{-1} u(\mathbf{x}, t) \\ \theta(\mathbf{x}, t) \end{pmatrix}. \tag{1.54}$$

Define a new quantity $\sigma_t(\mathbf{x}) = \rho(\mathbf{x}, t)\theta(\mathbf{x}, t)$ and assume that at $t = 0$, $\int_{\mathcal{X}} \sigma_0(\mathbf{x})\, \mathrm{d}\mathbf{x} = 1$. By combining Eq. (1.53b) and Eq. (1.53c) we find

$$\begin{aligned} & \rho(D_t\theta) + \theta(D_t\rho + \rho\nabla \cdot \mathbf{u}) = 0 \\ \iff \quad & \rho\partial_t\theta + \theta\partial_t\rho = -\rho\mathbf{u} \cdot \nabla\theta - \theta\mathbf{u} \cdot \nabla\rho - \rho\theta\nabla \cdot \mathbf{u} \\ \iff \quad & \rho\partial_t\theta + \theta\partial_t\rho = -\nabla \cdot (\rho\theta\mathbf{u}) \\ \iff \quad & \partial_t\sigma_t = -\nabla \cdot (\sigma_t\mathbf{u}). \end{aligned} \tag{1.55}$$

Note that

$$\frac{\mathrm{d}}{\mathrm{d}t}\int_{\mathcal{X}} \mathrm{d}\sigma_t(\mathbf{x}) = \int_{\mathcal{X}} \partial_t \sigma_t \,\mathrm{d}\mathbf{x} \tag{1.56}$$

$$= -\int_{\mathcal{X}} \nabla \cdot (\sigma_t \mathbf{u}) \,\mathrm{d}\mathbf{x} \tag{1.57}$$

$$= \int_{\partial\mathcal{X}} \sigma_t \mathbf{u} \cdot \hat{\mathbf{n}} \,\mathrm{d}\mathcal{H}^2 = 0, \tag{1.58}$$

by Eq. (1.53e). Thus we can conclude that $\sigma_t \in \mathscr{P}_{\mathrm{ac}}(\mathcal{X})$ for all t. For $t \in [0, t_f]$, define $\alpha_t \in \mathscr{P}(\mathcal{Y})$ by $\alpha_t = (T_t)_{\#}\sigma_t$. The goal of this section is to derive a PDE for α_t.

In order to derive the PDE for the measure α_t, we first take the material derivative of Eq. (1.54) :

$$D_t T_t = \begin{pmatrix} u_1 + f_{\mathrm{cor}}^{-1} D_t v \\ u_2 - f_{\mathrm{cor}}^{-1} D_t u \\ D_t \theta \end{pmatrix} \overset{(1.53)}{=} \begin{pmatrix} u_1 + u - u_1 \\ u_2 + v - u_2 \\ 0 \end{pmatrix} = \mathbf{u}_g = J(T_t - \mathrm{Id}). \tag{1.59}$$

As before, this implies that

$$\partial T_t = -(\nabla T_t)\mathbf{u} + J(T_t - \mathrm{Id}). \tag{1.60}$$

Now we are ready to formally derive the PDE. Consider a test function $\varphi \in \mathcal{C}_c^\infty(\mathcal{Y})$. Then

$$\frac{\mathrm{d}}{\mathrm{d}t}\int_{\mathcal{Y}} \varphi(\mathbf{y}) \,\mathrm{d}\alpha_t(\mathbf{y}) = \frac{\mathrm{d}}{\mathrm{d}t}\int_{\mathcal{X}} \varphi(T_t(\mathbf{x})) \,\mathrm{d}\sigma_t(\mathbf{x}) \tag{1.61}$$

$$= \int_{\mathcal{X}} \nabla\varphi(T_t(\mathbf{x})) \cdot \partial_t T_t(\mathbf{x}) \,\mathrm{d}\sigma_t(\mathbf{x}) + \int_{\mathcal{X}} \varphi(T_t(\mathbf{x})) \partial_t \sigma_t(\mathbf{x}) \,\mathrm{d}\mathbf{x} \tag{1.62}$$

$$= \int_{\mathcal{X}} \nabla\varphi(T_t(\mathbf{x})) \cdot (-(\nabla T_t(\mathbf{x}))\mathbf{u} + J(T_t(\mathbf{x}) - \mathbf{x})) \,\mathrm{d}\sigma_t(\mathbf{x}) \tag{1.63}$$

$$- \int_{\mathcal{X}} \varphi(T_t(\mathbf{x})) \nabla \cdot (\sigma_t(\mathbf{x})\mathbf{u}) \,\mathrm{d}\mathbf{x} \tag{1.64}$$

$$= -\int_{\mathcal{X}} \nabla[\varphi(T_t(\mathbf{x}))] \cdot \mathbf{u} \,\mathrm{d}\sigma_t(\mathbf{x}) + \int_{\mathcal{X}} \nabla\varphi(T_t(\mathbf{x})) \cdot J(T_t(\mathbf{x}) - \mathbf{x}) \,\mathrm{d}\sigma_t(\mathbf{x}) \tag{1.65}$$

$$- \int_{\mathcal{X}} \varphi(T_t(\mathbf{x})) \nabla \cdot (\sigma_t(\mathbf{x})\mathbf{u}) \,\mathrm{d}\mathbf{x} \tag{1.66}$$

$$= \int_{\mathcal{X}} \varphi(T_t(\mathbf{x})) \nabla \cdot (\sigma_t(\mathbf{x})\mathbf{u}) \, \mathrm{d}\mathbf{x} - \int_{\partial\mathcal{X}} \varphi(T_t(\mathbf{x})) \mathbf{u} \cdot \hat{\mathbf{n}} \, \mathrm{d}\mathcal{H}^2 \tag{1.67}$$

$$+ \int_{\mathcal{X}} \nabla\varphi(T_t(\mathbf{x})) \cdot J(T_t(\mathbf{x}) - \mathbf{x}) \, \mathrm{d}\sigma_t(\mathbf{x}) \tag{1.68}$$

$$- \int_{\mathcal{X}} \varphi(T_t(\mathbf{x})) \nabla \cdot (\sigma_t(\mathbf{x})\mathbf{u}) \, \mathrm{d}\mathbf{x} \tag{1.69}$$

$$= \int_{\mathcal{X}} \nabla\varphi(T_t(\mathbf{x})) \cdot J\big(T_t(\mathbf{x}) - T_t^{-1}(T_t(\mathbf{x}))\big) \, \mathrm{d}\sigma_t(\mathbf{x}) \tag{1.70}$$

$$= \int_{\mathcal{Y}} \nabla\varphi(\mathbf{y}) \cdot J\big(\mathbf{y} - T_t^{-1}(\mathbf{y})\big) \, \mathrm{d}\alpha_t(\mathbf{y}). \tag{1.71}$$

Therefore

$$\frac{\mathrm{d}}{\mathrm{d}t} \int_{\mathcal{Y}} \varphi(\mathbf{y}) \, \mathrm{d}\alpha_t(\mathbf{y}) = \int_{\mathcal{Y}} \nabla\varphi(\mathbf{y}) \cdot \mathbf{w}(\mathbf{y}, t) \, \mathrm{d}\alpha_t(\mathbf{y}), \tag{1.72}$$

where

$$\mathbf{w}(\mathbf{y}, t) = J\big(\mathbf{y} - T_t^{-1}(\mathbf{y})\big), \tag{1.73}$$

which is the geostrophic velocity in geostrophic coordinates. Note that $\mathbf{u}_g(\mathbf{x}, t) = \mathbf{w}(T_t(\mathbf{x}), t)$. This holds for all φ therefore the continuity equation in geostrophic coordinates is

$$\boxed{\partial_t \alpha_t + \nabla \cdot (\alpha_t \mathbf{w}) = 0.} \tag{1.74}$$

Notice that this PDE is nearly identical to the incompressible PDE, given in Eq. (1.31). The only difference is that when we discretise it the centroids are defined with respect to a dynamic source measure σ rather than the constant Lebesgue measure. Thus the ODE system / particle approximation to this PDE is identical, modulo the change to the centroid, to the ODE system for the incompressible problem.

We further establish that the coordinate transformation T_t defined by equation (1.54) is indeed an optimal transport map. To this end, we introduce a potential function ϕ_t defined as

$$\phi_t = -c_v \gamma \Pi \overset{(1.46)}{=} -c_v \gamma \left(\frac{R_d}{p_0}\right)^{\gamma-1} \sigma^{\gamma-1} \overset{(\S 1.4)}{=} -\kappa\gamma\sigma^{\gamma-1}. \tag{1.75}$$

To understand the origin of this potential, consider the total geostrophic energy of the system given by

$$E_g(t) = \int_{\mathcal{X}} \frac{\rho}{2}\big(u^2 + v^2\big) + g\rho x_3 + c_v \rho \Pi \theta \, \mathrm{d}\mathbf{x}, \tag{1.76}$$

which is the sum of the kinetic, potential, and internal energy contributions. By Eq. (1.54), Eq. (1.76) can be rewritten as

$$\begin{aligned} &E_g(t) = F(T_t, \sigma_t, \alpha_t) \\ &:= \int_{\mathcal{X}} \frac{f_{\text{cor}}^2}{2T_t(\mathbf{x})_3}\big((x_1 - T_t(\mathbf{x})_1)^2 + (x_2 - T_t(\mathbf{x})_2)^2\big) + g\frac{x_3}{T_t(\mathbf{x})_3}\,\mathrm{d}\sigma_t(\mathbf{x}) + \int_{\mathcal{X}} f(\sigma_t(\mathbf{x}))\,\mathrm{d}\mathbf{x}, \end{aligned} \tag{1.77}$$

where the internal energy density f is defined by

$$f(s) = \begin{cases} \kappa s^\gamma & \text{if } s \geq 0, \\ +\infty & \text{otherwise.} \end{cases} \tag{1.78}$$

An optimal transport cost function, $c : \mathcal{X} \to \mathcal{Y}$, emerges naturally from this representation of energy, and it is given by

$$c(\mathbf{x}, \mathbf{y}) = \frac{f_{\text{cor}}^2}{2y_3}(x_1 - y_1)^2 + \frac{f_{\text{cor}}^2}{2y_3}(x_2 - y_2)^2 + g\frac{x_3}{y_3}. \tag{1.79}$$

The Cullen convexity principle says that $F(\cdot, \sigma_t, \alpha_t)$ is minimised over all mass-preserving rearrangements of fluid particles, i.e. that solutions of Eq. (1.53) should also satisfy

$$F(T_t, \sigma_t, \alpha_t) = \min_{(S_t)_\# \sigma_t = \alpha_t} F(S_t, \sigma_t, \alpha_t) = \mathcal{T}_c(\sigma_t, \alpha_t) + \int_{\mathcal{X}} f(\sigma_t)\,\mathrm{d}\mathbf{x} =: E(\sigma_t, \alpha_t), \tag{1.80}$$

where $\mathcal{T}_c$ is the optimal transport cost as defined in (MP).

Formal Proposition 1.6.2. *ϕ_t is c-concave for all t if and only if T_t is the optimal transport map that transports σ_t to α_t according to c.*

Remark 1.6.3. At first sight the hypothesis that the potential ϕ_t is c-concave may seem arbitrary. It is, in fact, the compressible analogue of Cullen's convexity principle for the incompressible model (see Section 1.6.1). In the incompressible setting the modified pressure

$$P(\mathbf{x}, t) = \frac{1}{2}\big(x_1^2 + x_2^2\big) + p(\mathbf{x}, t) = \frac{1}{2}\big(x_1^2 + x_2^2\big) - (-p(\mathbf{x}, t)) \tag{1.81}$$

is required to be convex. A standard result in optimal transport, [59, Proposition 1.21], is that this convexity implies that $-p$ is c-concave for the quadratic cost. Demanding c-concavity of ϕ_t with respect to the compressible cost therefore plays exactly the same structural role in the

present context: ϕ_t replaces $-p$ in Cullen's principle. Moreover, ϕ_t is not merely an auxiliary potential; it represents the negative enthalpy, a quantity with clear physical meaning.

Formal Proof of Proposition 1.6.2. This proof is only formal as it proceeds by direct calculation, assuming that the potential ϕ_t, and the relevant physical quantities are sufficiently smooth (i.e., differentiable) for the gradient operations to be well-defined. Assume that ϕ_t is c-concave for all t. First note that the gradient of the cost with respect to the spatial variable $\mathbf{x}$ is given by

$$\nabla_{\mathbf{x}} c(\mathbf{x}, \mathbf{y}) = \frac{1}{y_3} \begin{pmatrix} f_{\text{cor}}^2(x_1 - y_1) \\ f_{\text{cor}}^2(x_2 - y_2) \\ g \end{pmatrix}. \tag{1.82}$$

Evaluating this at $\mathbf{y} = T_t(\mathbf{x})$, and combining equations (1.54), (1.53d), and (1.51) we obtain

$$\nabla_{\mathbf{x}} c(\mathbf{x}, T_t(\mathbf{x})) = -\frac{1}{\rho\theta} \begin{pmatrix} \partial_{x_1} p \\ \partial_{x_2} p \\ \rho g \end{pmatrix} = -\frac{1}{\sigma_t} \nabla p. \tag{1.83}$$

Notice that

$$p \overset{(1.46)}{=} \rho\theta R_d \left(\frac{R_d \rho\theta}{p_0} \right)^{\gamma-1} = R_d \left(\frac{R_d}{p_0} \right)^{\gamma-1} \sigma_t^\gamma \overset{(\S 1.4)}{=} (\gamma c_v - c_v) \left(\frac{R_d}{p_0} \right)^{\gamma-1} \sigma_t^\gamma = \kappa(\gamma - 1)\sigma_t^\gamma. \tag{1.84}$$

Therefore

$$\nabla_{\mathbf{x}} c(\mathbf{x}, T_t(\mathbf{x})) = -\frac{1}{\sigma_t} \kappa(\gamma - 1) \nabla \sigma_t^\gamma = -\kappa(\gamma - 1)\gamma \sigma_t^{\gamma-2} \nabla \sigma_t. \tag{1.85}$$

On the other hand, computing the gradient of the potential ϕ_t gives

$$\nabla \phi_t = -\kappa\gamma \nabla \sigma_t^{\gamma-1} = -\kappa\gamma(\gamma - 1)\sigma_t^{\gamma-2} \nabla \sigma_t. \tag{1.86}$$

By comparison, we observe

$$\nabla_{\mathbf{x}} c(\mathbf{x}, T_t(\mathbf{x})) = \nabla \phi_t(\mathbf{x}). \tag{1.87}$$

The assumption that ϕ_t is c-concave then ensures, by [59, Theorem 1.47], that T_t is precisely the optimal transport map that transports σ_t onto α_t according to the cost c, and that ϕ_t is an associated Kantorovich potential.

Now assume that T_t is the optimal transport map that transports σ_t to α_t according to c.

Let $\widetilde{\phi}_t$ be an optimal c-concave Kantorovich potential for transporting σ_t to α_t with cost c. By [59, Proposition 1.15],

$$\nabla_{\mathbf{x}} c(\mathbf{x}, T_t(\mathbf{x})) = \nabla \widetilde{\phi}_t(\mathbf{x}). \tag{1.88}$$

Combining this with Eq. (1.87) we conclude that $\nabla \phi_t = \nabla \widetilde{\phi}_t$ and hence up to a constant $\widetilde{\phi}_t = \phi_t$. Therefore ϕ_t is c-concave because $\widetilde{\phi}_t$ is. □

Finally, we show that σ_t minimizes the total energy $E(\cdot, \alpha_t)$.

Corollary 1.6.4. *If ϕ_t is c-concave for all t, then σ_t minimises $E(\cdot, \alpha_t)$.*

Proof of Corollary 1.6.4. In Chapter 3 we prove that $E(\cdot, \alpha_t)$ is strictly convex and has a unique minimiser (see Lemma 3.2.4). Define σ_t^* to be the unique minimiser of $E(\cdot, \alpha_t)$. We want to prove that $\sigma_t^* = \sigma_t$. At the minimum σ_t^* of $E(\cdot, \alpha_t)$, the first variation must vanish, giving the necessary and sufficient conditions [59, §7.2] :

$$\begin{cases} \phi_t^*(\mathbf{x}) + f'(\sigma_t^*(\mathbf{x})) = \ell & \text{on } \operatorname{spt}(\sigma_t^*), \\ \phi_t^*(\mathbf{x}) + f'(\sigma_t^*(\mathbf{x})) \geq \ell & \text{everywhere}, \end{cases} \tag{1.89}$$

for some constant $\ell \in \mathbb{R}$, where ϕ_t^* is an optimal Kantorovich potential for transporting σ_t^* to α_t with cost c. This constant ℓ is a Lagrange multiplier that arises because the minimisation of the energy, $E(\cdot, \alpha_t)$, is a constrained optimisation problem. The search for the minimizer σ_t^* is restricted to the set of probability measures, which must satisfy the constraint

$$\int_{\mathcal{X}} \sigma_t^*(\mathbf{x}) \, \mathrm{d}\mathbf{x} = 1. \tag{1.90}$$

Unlike in unconstrained optimization where the gradient must be zero, here the first variation must only vanish for perturbations that preserve the total mass. The constant ℓ ensure that this condition is met, representing the marginal cost of enforcing the mass constraint. Consider the quantity $\phi_t + f'(\sigma_t)$. Note that by Proposition 1.6.2 ϕ_t is an optimal Kantorovich potential for transporting σ_t to α_t. On the support of σ_t, we have

$$\phi_t + f'(\sigma_t) = -\kappa\gamma\sigma_t^{\gamma-1} + \gamma\kappa\sigma_t^{\gamma-1} = 0, \tag{1.91}$$

and off the support of σ_t, this trivially vanishes as $\sigma_t = 0$ and $f'(0) = 0$. Thus, σ_t satisfies the first-order optimality conditions and, because $E(\cdot, \alpha_t)$ is convex, it is also a minimizer of the

total energy. Therefore, we conclude that $\sigma_t = \sigma_t^*$. □

Now that we have verified that T_t is indeed an optimal transport map, the full system in geostrophic coordinates is

$$\boxed{\begin{cases} \partial_t \alpha_t + \nabla \cdot (\alpha_t \mathbf{w}) = 0 & \text{in } \mathcal{Y} \times [0, t_f], \\ \mathbf{w} = J(\mathrm{Id} - T_t^{-1}), \\ \sigma_t = \underset{\sigma \in \mathscr{P}_{\mathrm{ac}}(\mathcal{X})}{\arg\min}\, E(\cdot, \alpha_t), \\ T_t \text{ is the optimal map from } \sigma_t \text{ to } \alpha_t. \end{cases}} \tag{1.92}$$

In Chapter 3 we prove the existence of weak solutions of this system using a particle approximation.

We have formally show that Eq. (1.53) implies Eq. (1.92). Now for completeness, we give a formal proof that Eq. (1.92) implies Eq. (1.53).

Formal Proposition 1.6.5. *Let (σ_t, α_t) satisfy equation* (1.92)*. Define $\mathbf{u}_g$, θ, $\mathbf{u}$, and ρ by Eq.* (1.97)*, Eq.* (1.101)*, Eq.* (1.102)*. Then equation* (1.53) *is satisfied.*

Formal Proof of Proposition 1.6.5. This proof is formal because, as before, we assume that ϕ_t and the relevant quantities are sufficiently differentiable for the gradient relationships to be well defined. For $E(\sigma, \alpha_t)$ defined in Eq. (1.80), note that $\sigma_t = \arg\min_{\sigma \in \mathscr{P}_{\mathrm{ac}}(\mathcal{X})} E(\sigma, \alpha_t)$, implies that the following Euler-Lagrange equations hold:

$$\begin{cases} \phi_t + f'(\sigma_t) = \ell & \text{on } \mathrm{spt}(\sigma_t), \\ \phi_t + f'(\sigma_t) \geq \ell & \text{everywhere}, \end{cases} \tag{1.93}$$

where ϕ_t is the optimal Kantorovich potential for transporting σ_t to α_t with cost c. These Euler-Lagrange equations imply that

$$\nabla \phi_t \sigma_t = -\nabla(f'(\sigma_t))\sigma_t. \tag{1.94}$$

Since ϕ_t and T_t are optimal, we know from [59, Proposition 1.15] that

$$\nabla \phi_t(\mathbf{x})\sigma_t(\mathbf{x}) = \nabla_{\mathbf{x}} c(\mathbf{x}, T_t(\mathbf{x}))\sigma_t(\mathbf{x}). \tag{1.95}$$

Thus it is immediate that

$$\nabla_{\mathbf{x}} c(\mathbf{x}, T_t(\mathbf{x}))\sigma_t = -\nabla(f'(\sigma_t))\sigma_t. \tag{1.96}$$

Define $u(\mathbf{x}, t)$ and $v(\mathbf{x}, t)$ and $\theta(\mathbf{x}, t)$ in terms of T_t by

$$\begin{aligned} u(\mathbf{x}, t) &= f_{\text{cor}}((T_t(\mathbf{x}))_1 - x_1), \\ v(\mathbf{x}, t) &= f_{\text{cor}}(x_2 - (T_t(\mathbf{x}))_2), \\ \theta(\mathbf{x}, t) &= (T_t(\mathbf{x}))_3. \end{aligned} \tag{1.97}$$

Combining Eq. (1.82) and Eq. (1.97) we find

$$\nabla_{\mathbf{x}} c(\mathbf{x}, T_t(\mathbf{x})) = \frac{1}{\theta} \begin{pmatrix} -f_{\text{cor}} v \\ f_{\text{cor}} u \\ g \end{pmatrix}. \tag{1.98}$$

Define $\Pi = \frac{\kappa}{c_v}\sigma_t^{\gamma-1}$. Then by the definition of f,

$$-\nabla(f'(\sigma_t))\sigma_t \overset{(1.78)}{=} -\kappa\gamma\nabla\big(\sigma_t^{\gamma-1}\big)\sigma_t = -c_p(\nabla\Pi)\sigma_t. \tag{1.99}$$

Therefore,

$$\begin{pmatrix} f_{\text{cor}} v \\ -f_{\text{cor}} u \\ -g \end{pmatrix} \overset{(1.98)}{=} -\theta\nabla_{\mathbf{x}} c(\mathbf{x}, T_t(\mathbf{x})) \overset{(1.96)}{=} \theta\nabla(f'(\sigma_t))\sigma_t \overset{(1.99)}{=} c_p\theta\sigma_t\nabla\Pi, \tag{1.100}$$

which is geostrophic and hydrostatic balance (see Eq. (1.53d)).

Next define

$$\rho(\mathbf{x}, t) := \frac{\sigma_t(\mathbf{x})}{\theta(\mathbf{x}, t)}. \tag{1.101}$$

By [59, Theorem 5.14], there exists a velocity $\mathbf{u}$ such that

$$\partial_t\sigma_t + \nabla \cdot (\sigma_t\mathbf{u}) = 0. \tag{1.102}$$

Consider a test function $\varphi \in \mathcal{C}_c^\infty(\mathcal{Y})$ such that $\varphi(T_t(\mathbf{x})) = 0$ for all $\mathbf{x} \in \partial\mathcal{X}$. Then by the weak

form of the PDE for α_t (see Eq. (1.62) and Eq. (1.63)),

$$\int_{\mathcal{X}} \nabla\varphi(T_t(\mathbf{x})) \cdot \partial_t T_t(\mathbf{x}) \, \mathrm{d}\sigma_t(\mathbf{x}) + \int_{\mathcal{X}} \varphi(T_t(\mathbf{x})) \partial_t \sigma_t(\mathbf{x}) \, \mathrm{d}\mathbf{x} \tag{1.103}$$

$$= \int_{\mathcal{X}} \nabla\varphi(T_t(\mathbf{x})) \cdot (-\mathbf{u} \cdot \nabla T_t(\mathbf{x}) + J(T_t(\mathbf{x}) - \mathbf{x})) \, \mathrm{d}\sigma_t(\mathbf{x}) \tag{1.104}$$

$$- \int_{\mathcal{X}} \varphi(T_t(\mathbf{x})) \nabla \cdot (\sigma_t(\mathbf{x})\mathbf{u}) \, \mathrm{d}\mathbf{x}. \tag{1.105}$$

Since this holds for any such φ, and using Eq. (1.102), we can isolate

$$\partial_t T_t(\mathbf{x}) = -\mathbf{u} \cdot \nabla T_t(\mathbf{x}) + J(T_t(\mathbf{x}) - \mathbf{x}). \tag{1.106}$$

Then Eq. (1.97) implies

$$D_t \mathbf{u}_g = J(\mathbf{u}_g - \mathbf{u}), \tag{1.107}$$

$$D_t \theta = 0, \tag{1.108}$$

which are Eq. (1.53a) and Eq. (1.53b). Then combining Eq. (1.102), Eq. (1.108) and Eq. (1.55) we get the continuity equation for ρ :

$$D_t \rho + \rho \nabla \cdot \mathbf{u} = 0. \tag{1.109}$$

Finally, start again from the weak form of Eq. (1.74) and consider any test function $\varphi \in \mathcal{C}_c^\infty(\mathcal{Y})$ (not necessarily satisfying $\varphi(T_t(\mathbf{x})) = 0$ for $\mathbf{x} \in \partial\mathcal{X}$). By the weak form of the PDE for α_t, Eq. (1.102) and Eq. (1.106),

$$\int_{\partial\mathcal{X}} \varphi(T_t(\mathbf{x})) \mathbf{u} \cdot \hat{\mathbf{n}} \, \mathrm{d}\mathcal{H}^2 = 0, \tag{1.110}$$

for all test function φ, and we conclude that $\mathbf{u} \cdot \hat{\mathbf{n}} = 0$ on $\partial\mathcal{X}$, recovering the Neumann boundary conditions, Eq. (1.53e). This completes the proof. □

Remark 1.6.6. While the full velocity is not divergence free, the geostrophic velocity, $\mathbf{w}$, is. To verify this formally, let $S_t = T_t^{-1}$ and let the pair (ϕ_t, ψ_t) be optimal potentials for transport from σ_t to α_t according to cost c. Then

$$\nabla_{\mathbf{x}} c(S_t(\mathbf{y}), \mathbf{y}) = \nabla \psi_t(\mathbf{y}). \tag{1.111}$$

Recall that

$$\nabla_{\mathbf{x}} c(\mathbf{x}, \mathbf{y}) = \frac{1}{y_3} \begin{pmatrix} f_{\text{cor}}^2(x_1 - y_1) \\ f_{\text{cor}}^2(x_2 - y_2) \\ g \end{pmatrix}. \tag{1.112}$$

Therefore

$$\frac{1}{y_3} \begin{pmatrix} f_{\text{cor}}^2(S_t(\mathbf{y})_1 - y_1) \\ f_{\text{cor}}^2(S_t(\mathbf{y})_2 - y_2) \\ g \end{pmatrix} = \begin{pmatrix} \partial_{y_1} \psi_t(\mathbf{y}) \\ \partial_{y_2} \psi_t(\mathbf{y}) \\ \partial_{y_3} \psi_t(\mathbf{y}) \end{pmatrix}. \tag{1.113}$$

Solving for $S_t(\mathbf{y})$ gives

$$S_t(\mathbf{y})_1 = y_1 + f_{\text{cor}}^{-2} y_3 \partial_{y_1} \psi_t(\mathbf{y}), \tag{1.114}$$

$$S_t(\mathbf{y})_2 = y_2 + f_{\text{cor}}^{-2} y_3 \partial_{y_2} \psi_t(\mathbf{y}). \tag{1.115}$$

Therefore

$$\mathbf{w}(\mathbf{y}, t) = J(\mathbf{y} - S_t(\mathbf{y})) \tag{1.116}$$

$$= J \begin{pmatrix} -f_{\text{cor}}^{-2} y_3 \partial_{y_1} \psi_t(\mathbf{y}) \\ -f_{\text{cor}}^{-2} y_3 \partial_{y_2} \psi_t(\mathbf{y}) \\ y_3 - S_t(\mathbf{y})_3 \end{pmatrix} \tag{1.117}$$

$$= -f_{\text{cor}}^{-2} y_3 J \nabla \psi_t(\mathbf{y}). \tag{1.118}$$

Then, recalling that the third row of J is zero,

$$\nabla \cdot \mathbf{w} = \partial_{y_1} w_1 + \partial_{y_2} w_2 + \partial_{y_3} w_3 \tag{1.119}$$

$$= -f_{\text{cor}}^{-2} y_3 (\partial_{y_1} (J \nabla \psi_t)_1 + \partial_{y_2} (J \nabla \psi_t)_2) \tag{1.120}$$

$$= -f_{\text{cor}}^{-2} y_3 (-\partial_{y_1 y_2} \psi_t + \partial_{y_2 y_1} \psi_t) \tag{1.121}$$

$$= 0. \tag{1.122}$$

This proves, formally, that the geostrophic velocity, $\mathbf{w}$, is divergence free.

With these derivations complete, we see how intimately optimal transport is coupled to the SG equations and have explained, at least formally, the relation between the physical PDE, the PDE in geostrophic coordinates, and the ODE discretisation of the PDE in geostrophic coordinates.

Chapter 2

Incompressible 3D Numerics

2.1 Introduction

In this chapter we describe what is, to our knowledge, the first mesh-free three-dimensional (3D) numerical scheme providing simulations of incompressible semi-geostrophic (SG) atmospheric flows. In particular, we use this scheme to simulate the evolution of an isolated large-scale tropical cyclone, supporting the applicability of the SG equations for modelling atmospheric and oceanic phenomenon.

The SG system is a second-order accurate reduction of the Euler equations valid for modelling large-scale atmospheric flows. Its significance in meteorology stems from the fact that the system models the formation of fronts - mathematically, that it has a natural way to admit solutions that continue past singularity formation. The recent success and interest in this system is a consequence of its reformulation, due to Brenier and Benamou, as a coupled optimal transport problem. Indeed, it is this reformulation that we exploit to devise an energy-conserving approximation that models accurately the formation of fronts and cyclones.

The scheme we present is based on semi-discrete optimal transport techniques. Two-dimensional (2D) reductions of SG dynamics, and of its incompressible Boussinesq parent model, have been approached through several complementary analytical and numerical paradigms. In the Lagrangian setting, Benamou et al. and Carlier et al. solve the SG equations with a fully discrete optimal-transport solver regularised by entropy [6, 12]. A counterpart is provided by semi-discrete optimal transport, which supplies a rigorous framework for Cullen's pioneering *geometric method* and has been investigated analytically both in 2D and 3D and simulated in the canonical 2D Eady slice [8, 25, 29]. In contrast to the mesh-free optimal-transport approaches, Yamazaki et al. examine the incompressible Eady–Boussinesq slice reproducing quasi-periodic frontogenetic life-cycles using high-resolution Eulerian compatible-finite-element solver that serve as a benchmark for the SG limit [68]. Together, the schemes of [6] and [68]

provide reference diagnostics and convergence results against which we later qualitatively evaluate our 2D benchmark and 3D simulations. Although neither their solvers nor the present one are strictly energy-conserving, all retain dissipation that is small relative to the kinetic and potential-energy budgets, so all support credible long-time diagnostics. Our semi-discrete optimal-transport framework should therefore be viewed as a complementary alternative for long-time diagnostics. Schär and Wernli [61], who originally proposed the initial conditions we investigate, used an Eulerian spectral grid with centred finite-difference time stepping to solve the SG equations. Fully discrete, entropy-regularised optimal-transport schemes are efficient, energy-stable, and convergent. They represent both the source measure and the evolving target measure on a finite discrete support and hence satisfy the semi-geostrophic equations only in a discrete sense. One recovers a weak solution of the continuous system only in the joint limit of vanishing entropic parameter [6, 12]. By contrast, in the semi-discrete approach the source measure remains continuous while the target measure is discrete, so the resulting particle trajectories are exact weak solutions of the Lagrangian form of the SG equations for every particle number N [8, 29]. Our contribution is to present what is, to the authors' knowledge the first full 3D simulation of the formation of an isolated cyclone, developing from the benchmark set of initial conditions given in [61]. We refer to this setup as a benchmark because the Schär and Wernli initial conditions represent a canonical, widely recognised problem for semi-geostrophic cyclogenesis. While previous studies have simulated this setup, they have typically been restricted to reduced two-dimensional or quasi-3D contexts, such as evolving only the top and bottom boundaries of the domain. Our work, therefore, does not serve as a benchmark for direct comparison against existing full 3D results, as none exist. Rather, by providing the first simulation of the cyclone's evolution throughout the interior, we aim to establish a new, more complete benchmark result for this canonical problem, against which other modern 3D solvers can be tested and validated in the future. Our work to implement fully 3D computations is a substantial extension of the method presented in [29].

In addition to the novel spatial particle discretisation, achieved using semi-discrete optimal transport, we briefly investigate various explicit numerical methods to solve the temporal evolution, focusing on balancing runtime with the relative error in the energy conservation. While straight forward, this exploration is novel in terms of integrating an ordinary differential equation (ODE) solver with an optimal transport solver.

We then implement our schemes, first demonstrating that the observed rate of convergence

aligns with the theoretical predictions for the space and time discretisation (see § 2.4.2). We then provide insights into large-scale SG flows and how they model the formation and development of atmospheric fronts and cyclones.

2.1.1 Background and motivation

A central theme in the study of atmospheric and oceanic dynamics is the quest for models that are both mathematically and numerically tractable and that approximate accurately the fluid motion, at least within a set of specific physical constraints. An important system of equations satisfying these requirements is the SG system. This system, which is derived under the assumptions of hydrostatic and geostrophic balance, is a second-order accurate reduction of the full Euler system and is recognised for its effectiveness in modelling shallow, rotationally-dominated flows characterised by small Rossby numbers. This contrasts with the quasi-geostrophic limit which simplifies the dynamics by neglecting ageostrophic terms beyond the first order. By retaining the second-order terms, the SG system more accurately represents ageostrophic flows and frontal dynamics [19].

The SG system was introduced by Eliassen in 1949 [30] and later revisited by Hoskins in the 1970s [43], who introduced *geostrophic* coordinates. It has played a pivotal role in our understanding of large-scale (at length scales on the order of tens of kilometers) atmospheric dynamics and of atmospheric front formation. The usefulness of the SG equations has been exemplified in operational settings, such as their use as a diagnostic tool by the UK Met Office, underscoring their value in meteorological practice [18, 19].

Mathematically, this system came to prominence following the pioneering work of Brenier and Benamou [5], who showed how the SG system in geostrophic variables is amenable to analysis using optimal transport techniques. This formulation is the one we use in this chapter as the basis of our numerical investigation.

We use the SG system to model the evolution of an isolated cyclone, starting from a standard initial profile proposed by Schär and Wernli [61]. Previous works, including those by Hoskins, Schär and Wernli, were constrained by the breakdown of the transformation between geostrophic and physical space in finite time, limiting the application of the SG system. In contrast, our approach leverages the optimal transport formulation, which overcomes this limitation and ensures that the transformation remains valid for all times - a fundamental advantage that extends beyond simply improving simulations. While existing studies focus on 2D compu-

tations of temperature and pressure evolution at the top and bottom boundaries, we go further by simulating the full 3D dynamics, capturing both the exterior surfaces and the interior of the domain.

The base state of this initial condition is a symmetric baroclinic jet combined with a uniform barotropic shear component controlled by the shear parameter, $A \in \mathbb{R}$, and given in terms of the non-dimensionalised pressure by

$$\overline{\Phi}(\mathbf{x}) = \frac{1}{2}\left(\arctan\left(\frac{x_2}{1+x_3}\right) - \arctan\left(\frac{x_2}{1-x_3}\right)\right) - 0.12x_2x_3 - \frac{1}{2}A\big(x_2^2 - x_3^2\big). \tag{2.1}$$

Importantly, this base state is harmonic and encodes the ramp-like structure observed in the presence of weather fronts. The base state is then perturbed at the top and bottom of the domain via the perturbation function given by

$$\begin{aligned} h(x_1, x_2) = &\left(1 + \left(\frac{x_1}{0.5}\right)^2 + \left(\frac{x_2}{0.5}\right)^2\right)^{-\frac{3}{2}} - \frac{1}{2}\left(1 + \left(\frac{x_1 - 1}{0.5}\right)^2 + \left(\frac{x_2}{0.5}\right)^2\right)^{-\frac{3}{2}} \\ &- \frac{1}{2}\left(1 + \left(\frac{x_1 + 1}{0.5}\right)^2 + \left(\frac{x_2}{0.5}\right)^2\right)^{-\frac{3}{2}}. \end{aligned} \tag{2.2}$$

This perturbation is applied only to the temperature, i.e. to the derivative of the pressure with respect to the vertical coordinate, x_3.

Our study seeks to advance the numerical treatment of the SG model by simulating its flow in 3D geostrophic space, continuing the research presented in [29] and iterated upon by [6, 12]. Specifically, we employ the damped Newton method recently developed by Kitagawa, Mérigot, and Thibert [46] to evaluate numerically the semi-discrete transport map, which is equivalent to computing an optimal Laguerre tessellation of the 3D space. This method represented a significant advancement for numerical semi-discrete optimal transport methods and it aligns with our goal to adopt a mathematically rigorous and consistent formulation of the geometric method first proposed by Cullen and Purser [25]. This approach is particularly desirable in view of its structural preservation qualities. It's important to clarify that these qualities are inherent to the semi-discrete optimal transport solver used for the spatial discretisation, rather than a property of the temporal integration scheme. The present study employs a standard ODE solver, not a bespoke or symplectic integrator designed for geometric conservation. Consequently, we have not explored the relationship between the number of particles N and the

necessary timestep size of the ODE solver. Establishing a rigorous 'particle CFL' condition to describe the stability of coupling OT and ODE solvers in this manner remains an open problem.

Indeed, a crucial advantage of the semi-discrete optimal transport method over traditional finite element methods such as [65, 68] is its capacity to preserve the underlying structures of the equations being discretised, so that solutions obtained through this method conserve total energy and simulate optimally mass-preserving flows within the fluid domain. Such characteristics are not only mathematically appealing but also crucial for the physical reliability of the simulations. This is particularly important when dealing with complex phenomena like frontal discontinuities, which are mathematically described as singularities occurring in finite time. Our numerical solutions, offer an accurate conservation of total energy, mirroring the physical behaviours observed in natural fluid dynamics and potentially allowing new insights into the understanding and prediction of atmospheric and oceanic phenomena.

2.1.2 Semi-geostrophic system in discrete geostrophic variables

In this section we provide the mathematical background for the model and explain, in brief, its connection to optimal transport. Consider a compact convex set $\mathcal{X} \subset \mathbb{R}^3$. $\mathcal{X}$ can be identified with the *physical or fluid* domain. Furthermore, consider an open set $\mathcal{Y} \subseteq \mathbb{R}^3$, usually called *geostrophic* space. The SG system in geostrophic space [5], is given

$$\begin{aligned} &\partial_t \alpha_t + \operatorname{div}(\alpha_t \mathbf{v}[\alpha_t]) = 0, \\ &\mathbf{v}[\alpha_t] = J(\mathrm{id} - T^{-1}), \qquad J = \begin{pmatrix} 0 & -1 & 0 \\ 1 & 0 & 0 \\ 0 & 0 & 0 \end{pmatrix}, \end{aligned} \tag{2.3}$$

where $\alpha : [0, \tau] \to \mathscr{P}(\mathcal{Y})$ is a probability measure-valued map such that $\alpha_t = \alpha(t) \in \mathscr{P}(\mathcal{Y})$ and $T : \mathcal{X} \to \mathcal{Y}$ is the optimal transport map from $\mathbb{1}_{\mathcal{X}}$ (the normalised Lebesgue measure on $\mathcal{X}$) to α_t, the potential vorticity [19], with respect to a quadratic cost. In this case the optimal transport map is defined as

$$T = \underset{\substack{T:\mathcal{X}\to\mathcal{Y} \\ T_{\#}\mathbb{1}_{\mathcal{X}}=\alpha_t}}{\arg\min} \int_{\mathcal{X}} \|\mathbf{x} - T(\mathbf{x})\|^2 \, \mathrm{d}\mathbf{x},$$

where $T_{\#}\mathbb{1}_{\mathcal{X}}$ is the pushforward of the probability measure $\mathbb{1}_{\mathcal{X}}$ under the map T [59]. This is the case that has been studied most extensively, and for which there is a fairly exhaustive theory [59].

Fix $N \in \mathbb{N}$. In our particle discretisation of this problem the target measure, α_t, becomes the discrete probability measure $\alpha_t^N = \frac{1}{N}\sum_i^N \delta_{\mathbf{z}^i(t)}$, where $\mathbf{z}^i$ are points in $\mathcal{Y} \subset \mathbb{R}^3$. This yields a system of N ODEs where the ith ODE is given formally by

$$\dot{\mathbf{z}}^i = \mathbf{v}[\alpha_t^N](\mathbf{z}^i),$$

$$\mathbf{v}\left[\alpha_t^N\right](\mathbf{z}^i) = J(\mathbf{z}^i - T^{-1}(\mathbf{z}^i)), \tag{2.4}$$

where $T : \mathcal{X} \to \mathcal{Y}$ is now the optimal transport map from $\mathbb{1}_X$ to the discrete measure α_t^N. This is a semi-discrete optimal transport problem, with respect to the quadratic cost. It is well known that its solution must be of the form $T = \frac{1}{N}\sum_{i=1}^N \mathbb{1}_{L^i}$, where L^i are cells forming a covering of the space $\mathcal{X}$. Rigorously, the i-th cell is defined, for $i \in \{1, \ldots, N\}$, by

$$L^i = \left\{\mathbf{x} \in \mathcal{X} : \|\mathbf{x} - \mathbf{z}^i\|^2 - w^i \leq \|\mathbf{x} - \mathbf{z}^j\|^2 - w^j \quad \forall\, j \in \{1, \ldots, N\}\right\},$$

where $w^j \in \mathbb{R}$ guarantee that $\mathcal{L}^d(L^i) = \frac{1}{N}$. Thus the solution of this transport problem is equivalent to solving for the *optimal tessellation* of the source space $\mathcal{X}$. For the quadratic cost, this is given by the so-called Laguerre tessellation [53]. Note that Eq. (2.4) is only formal, because T is not invertible since its inverse could map single points to regions, $T^{-1}(\mathbf{z}^i) = L^i$. Hence we replace $T^{-1}(\mathbf{z}^i)$ in Eq. (2.4) by the centroid of the cell L^i. Then α^N is an exact weak solution of Eq. (2.3) for the discrete initial data α_0^N. The resulting ODE been studied extensively [8] and is given by

$$\mathbf{z}(t) = \big(\mathbf{z}_1(t), \ldots, \mathbf{z}^N(t)\big), \qquad \dot{\mathbf{z}} = J^N(\mathbf{z} - \mathbf{C}(\mathbf{z})), \tag{2.5}$$

where $J^N \in \mathbb{R}^{3N\times 3N}$ is the block diagonal matrix $J^N := \mathrm{diag}(J, \ldots, J)$, and $\mathbf{C}(\mathbf{z}) \in \mathcal{X}^N$ is the *centroid map*, which identifies the centroid of each cell L^i of the optimal tessellation:

$$\mathbf{C}(\mathbf{z}) = \big(\mathbf{C}^1(\mathbf{z}), \ldots, \mathbf{C}^N(\mathbf{z})\big), \qquad C^i(\mathbf{z}) = \frac{1}{|L^i(\mathbf{z})|}\int_{L^i(\mathbf{z})} \mathbf{x}\,\mathrm{d}\mathbf{x}.$$

It is also energy conserving, where the total energy of the system is given by

$$E(\mathbf{z}(t)) = \sum_{i=1}^{N} \int_{L^i} \|\mathbf{x} - \mathbf{z}^i(t)\|^2 \, \mathrm{d}\mathbf{x}. \tag{2.6}$$

Numerically this problem is solved efficiently, for a very large number of point particles, via the damped Newton method of [46] already mentioned. We then select a 4th order Runge-Kutta (RK4) method as the one among existing ODE solvers for simulating the time evolution of the flow that achieves the best balance between efficiency and energy-conservation properties. This choice will be discussed further in § 2.4.

Remark 2.1.1. It would be desirable to establish that the numerical solutions converge to a solution of the underlying partial differential equation (PDE) as the number of particles N tends to infinity and the timestep size tends to zero. The result in [8] demonstrates convergence of a subsequence as $N \to \infty$, but this is not a full numerical analysis convergence result. Moreover, convergence of the full sequence may be challenging to prove, as the uniqueness of weak solutions to the underlying PDE is not known. In contrast, for the entropy-regularised fully discrete optimal transport scheme [12], convergence of the fully discrete scheme is established for $\varepsilon > 0$, providing a stronger theoretical guarantee in this setting.

2.1.3 Outline of the chapter

In Section 2.2 we reproduce the 2D results of [29] and [6] in order to validate and benchmark our code. In Section 2.3 we present and discuss the 3D initial conditions used in our simulations which are informed by the work of [61] and are designed to generate an isolated large-scale tropical cyclone. We stress that, unlike [61] and other existing results that use these initial conditions to simulate the cyclone just on the surface of the domain, we compute numerically the evolution of the full 3D problem. In the last section we collect figures, showing both the evolution of the geostrophic particles and of the cells in physical space, that illustrate the evolution of the computed cyclonic flow. Finally in the technical details at the end we show how the initial condition for the cyclonic flows is derived.

2.2 2D Benchmark

2.2.1 Incompressible Eady Slice

First we introduce the incompressible Eady slice model. This will serve as the benchmark for our code as the Eady slice model has been extensively studied and simulated. To begin let the physical (source) space $\mathcal{X} \subset \mathbb{R}^2$ be convex (in addition to our general assumptions given in Section 1.4), and let the geostrophic (target) space $\mathcal{Y} = \mathbb{R}^2$. Define the source measure as $\sigma = \mathcal{L}^2 \llcorner \mathcal{X}$ and a final time $0 < t_f < \infty$. Recall that $\theta(\mathbf{x}, t)$ is the potential temperature and the definition of all the various physical constants outlined in Section 1.4. Finally, we introduce the rotation matrix

$$J = \frac{gs}{\theta_0 f_{\text{cor}}} \begin{pmatrix} 0 & -1 \\ 1 & 0 \end{pmatrix}. \tag{2.7}$$

Note that in two dimensions we advect $v(\mathbf{x}, t)$ with the in-slice velocity $\mathbf{u}_S(\mathbf{x}, t) = (u_1(\mathbf{x}, t), u_3(\mathbf{x}, t))^T$. Note that we are "in-slice" so $\mathbf{x} = (x_1, x_3)^T$ and $\nabla = (\partial_{x_1}, \partial_{x_3})^T$. Then the system of SG equations for an incompressible fluid in two-dimensional physical coordinates given by [29] is

$$\begin{cases} D_t v + f_{\text{cor}} u_1 = -\dfrac{gs}{\theta_0} x_3 & \text{in } \mathcal{X} \times [0, t_f], \\ D_t \theta = -sv & \text{in } \mathcal{X} \times [0, t_f], \\ \nabla \cdot \mathbf{u}_S = 0 & \text{in } \mathcal{X} \times [0, t_f], \\ \nabla p = \left(f_{\text{cor}} v,\ \dfrac{g}{f_{\text{cor}}^2 \theta_0} \theta \right)^T & \text{in } \mathcal{X} \times [0, t_f], \\ \mathbf{u}_S \cdot \hat{\mathbf{n}} = 0 & \text{on } \partial\mathcal{X} \times [0, t_f], \end{cases} \tag{2.8}$$

where $\hat{\mathbf{n}}$ is the unit outward normal to $\partial\mathcal{X}$. As in the Introduction we define a coordinate transform $T_t : \mathcal{X} \to \mathcal{Y}$ by

$$T_t(\mathbf{x}) = \begin{pmatrix} x_1 + f_{\text{cor}}^{-1} v(\mathbf{x}, t) \\ \frac{g}{\theta_0 f_{\text{cor}}^2} \theta(\mathbf{x}, t) \end{pmatrix}, \tag{2.9}$$

For $t \in [0, t_f]$ define $\alpha_t \in \mathscr{P}(\mathcal{Y})$ by $\alpha_t = (T_t)_{\#} \mathcal{L}^2 \llcorner \mathcal{X}$. The goal of this section is to derive a PDE for α_t. Recall the arguments presented in § 1.6.1. These same arguments apply in the two-dimensional setting guaranteeing that T_t is in fact a unique optimal transport map for the quadratic cost transporting $\mathcal{L}^2 \llcorner \mathcal{X}$ to α_t. With this in mind we first take the material derivative

of Eq. (2.9) :

$$D_t T_t = \begin{pmatrix} u_1 + \frac{1}{f_{\text{cor}}} D_t v \\ \frac{g}{f_{\text{cor}}^2 \theta_0} D_t \theta \end{pmatrix} \overset{(2.8)}{=} \begin{pmatrix} u_1 - u_1 - \frac{gs}{\theta_0 f_{\text{cor}}} x_3 \\ -\frac{gs}{f_{\text{cor}}^2 \theta_0} v \end{pmatrix} \tag{2.10}$$

$$\overset{(2.9)}{=} \begin{pmatrix} u_1 - u_1 - \frac{gs}{\theta_0 f_{\text{cor}}} x_3 \\ -\frac{gs}{\theta_0 f_{\text{cor}}^2} f_{\text{cor}} (T_t \cdot \hat{\mathbf{e}}_1 - x_1) \end{pmatrix} = \frac{gs}{\theta_0 f_{\text{cor}}} \begin{pmatrix} -x_3 \\ x_1 - T \cdot \hat{\mathbf{e}}_1 \end{pmatrix}. \tag{2.11}$$

Via the definition of the material derivative, this implies that

$$\partial_t T_t = -(\nabla T_t)\mathbf{u}_S + J(\mathrm{Id} - (T_t \cdot \hat{\mathbf{e}}_1)\hat{\mathbf{e}}_1).$$

Consider a test function $\varphi \in \mathcal{C}_c^\infty(\mathcal{Y})$. Then

$$\begin{aligned}
\frac{\mathrm{d}}{\mathrm{d}t} \int_{\mathcal{Y}} \varphi(\mathbf{y}) \,\mathrm{d}\alpha_t(\mathbf{y}) &= \frac{\mathrm{d}}{\mathrm{d}t} \int_{\mathcal{X}} \varphi(T_t(\mathbf{x})) \,\mathrm{d}\mathbf{x} \\
&= \int_{\mathcal{X}} \nabla\varphi(T_t(\mathbf{x})) \cdot \partial_t T_t(\mathbf{x}) \,\mathrm{d}\mathbf{x} \\
&= \int_{\mathcal{X}} \nabla\varphi(T_t(\mathbf{x})) \cdot (-(\nabla T_t(\mathbf{x}))\mathbf{u}_S + J(\mathbf{x} - (T_t(\mathbf{x}) \cdot \hat{\mathbf{e}}_1)\hat{\mathbf{e}}_1)) \,\mathrm{d}\mathbf{x} \\
&= -\int_{\mathcal{X}} \nabla[\varphi(T_t(\mathbf{x}))] \cdot \mathbf{u}_S \,\mathrm{d}\mathbf{x} + \int_{\mathcal{X}} \nabla\varphi(T_t(\mathbf{x})) \cdot J(\mathbf{x} - (T_t(\mathbf{x}) \cdot \hat{\mathbf{e}}_1)\hat{\mathbf{e}}_1) \,\mathrm{d}\mathbf{x} \\
&= \int_{\mathcal{X}} \varphi(T_t(\mathbf{x})) \nabla \cdot \mathbf{u}_S \,\mathrm{d}\mathbf{x} - \int_{\partial\mathcal{X}} \varphi(T_t(\mathbf{x}))\mathbf{u}_S \cdot \hat{\mathbf{n}} \,\mathrm{d}\mathcal{H}^1 \\
&\quad + \int_{\mathcal{X}} \nabla\varphi(T_t(\mathbf{x})) \cdot J(\mathbf{x} - (T_t(\mathbf{x}) \cdot \hat{\mathbf{e}}_1)\hat{\mathbf{e}}_1) \,\mathrm{d}\mathbf{x} \\
&= \int_{\mathcal{X}} \nabla\varphi(T_t(\mathbf{x})) \cdot J\big(T_t^{-1}(T_t(\mathbf{x})) - (T_t(\mathbf{x}) \cdot \hat{\mathbf{e}}_1)\hat{\mathbf{e}}_1\big) \,\mathrm{d}\mathbf{x} \\
&= \int_{\mathcal{Y}} \nabla\varphi(\mathbf{y}) \cdot J\big(T_t^{-1}(\mathbf{y}) - (\mathbf{y} \cdot \hat{\mathbf{e}}_1)\hat{\mathbf{e}}_1\big)\alpha_t(\mathbf{y}) \,\mathrm{d}\mathbf{y}.
\end{aligned}$$

Therefore

$$\int_{\mathcal{Y}} \varphi(\mathbf{y})\partial_t\alpha_t(\mathbf{y}) \,\mathrm{d}\mathbf{y} = \int_{\mathcal{Y}} \nabla\varphi(\mathbf{y}) \cdot \mathbf{w}(\mathbf{y}, t)\alpha_t(\mathbf{y}) \,\mathrm{d}\mathbf{y}, \tag{2.12}$$

where

$$\mathbf{w}(\mathbf{y}, t) = J\big(T_t^{-1}(\mathbf{y}) - (\mathbf{y} \cdot \hat{\mathbf{e}}_1)\hat{\mathbf{e}}_1\big), \tag{2.13}$$

which is the geostrophic velocity in geostrophic coordinates. Equation (2.12) holds for all φ therefore the continuity equation in geostrophic coordinates is

$$\boxed{\partial_t \alpha_t + \nabla \cdot (\alpha_t \mathbf{w}) = 0.} \tag{2.14}$$

We can discretize this PDE by plugging in the particle approximation

$$\alpha_t(\mathbf{z}) = \sum_{i=1}^{N} m^i \delta_{\mathbf{z}_t^i}. \tag{2.15}$$

Starting with the right hand side of Eq. (2.12) we can write

$$\int_{\mathcal{Y}} \nabla\varphi(\mathbf{y}) \cdot \mathbf{w}(\mathbf{y}, t)\, \mathrm{d}\alpha_t(\mathbf{y}) = \int_{\mathcal{Y}} \nabla\varphi(\mathbf{y}) \cdot JT_t^{-1}(\mathbf{y})\, \mathrm{d}\alpha_t(\mathbf{y}) - \int_{\mathcal{Y}} \nabla\varphi(\mathbf{y}) \cdot J(\mathbf{y}\cdot\hat{\mathbf{e}}_1)\hat{\mathbf{e}}_1\, \mathrm{d}\alpha_t(\mathbf{y}). \tag{2.16}$$

Note, as was done in Section 1.6.1, by applying Proposition 1.5.6 we find

$$\begin{aligned}
\int_{\mathcal{Y}} \nabla\varphi(\mathbf{y}) \cdot JT_t^{-1}(\mathbf{y})\, \mathrm{d}\alpha_t(\mathbf{y}) &= \int_{\mathcal{X}} \nabla\varphi(T_t(\mathbf{x})) \cdot J\mathbf{x}\, \mathrm{d}\mathbf{x} && (2.17)\\
&= \sum_{i=1}^{N} \int_{L_c^i(\boldsymbol{w},\mathbf{z})} \nabla\varphi(\mathbf{z}_t^i) \cdot J\mathbf{x}\, \mathrm{d}\mathbf{x} && (2.18)\\
&= \sum_{i=1}^{N} \nabla\varphi(\mathbf{z}_t^i) \cdot m^i J \frac{1}{m^i} \int_{L_c^i(\boldsymbol{w},\mathbf{z})} \mathbf{x}\, \mathrm{d}\mathbf{x} && (2.19)\\
&= \sum_{i=1}^{N} \nabla\varphi(\mathbf{z}_t^i) \cdot m^i J\mathbf{C}^i(\mathbf{z}_t), && (2.20)
\end{aligned}$$

where $\mathbf{C}^i$ is the centroid of the i-th Laguerre cell. Therefore

$$\begin{aligned}
&\int_{\mathcal{Y}} \nabla\varphi(\mathbf{y}) \cdot JT_t^{-1}(\mathbf{y})\, \mathrm{d}\alpha_t(\mathbf{y}) - \int_{\mathcal{Y}} \nabla\varphi(\mathbf{y}) \cdot J(\mathbf{y}\cdot\hat{\mathbf{e}}_1)\hat{\mathbf{e}}_1\, \mathrm{d}\alpha_t(\mathbf{y})\\
&= \sum_{i=1}^{N} m^i \nabla\varphi(\mathbf{z}_t^i) \cdot J\big(\mathbf{C}^i(\mathbf{z}_t) - (\mathbf{z}_t^i \cdot \hat{\mathbf{e}}_1)\hat{\mathbf{e}}_1\big).
\end{aligned} \tag{2.21}$$

On the other hand, the left hand side of Eq. (2.12) equals

$$\frac{\mathrm{d}}{\mathrm{d}t} \int_{\mathcal{Y}} \varphi(\mathbf{y})\, \mathrm{d}\alpha_t(\mathbf{y}) = \frac{\mathrm{d}}{\mathrm{d}t} \sum_{i=1}^{N} m^i \varphi(\mathbf{z}_t^i) = \sum_{i=1}^{N} m^i \nabla\varphi(\mathbf{z}_t^i) \cdot \dot{\mathbf{z}}_t^i. \tag{2.22}$$

Combining equations (2.16), (2.21), and (2.22) gives

$$\sum_{i=1}^{N} m^i \nabla\varphi(\mathbf{z}_t^i)\cdot\dot{\mathbf{z}}_t^i = \sum_{i=1}^{N} m^i \nabla\varphi(\mathbf{z}_t^i)\cdot J\big(\mathbf{C}^i(\mathbf{z}_t) - (\mathbf{z}_t^i\cdot\hat{\mathbf{e}}_1)\hat{\mathbf{e}}_1\big).$$

Since φ is arbitrary, the discrete particle dynamics are governed by the following coupled system of ODES :

$$\boxed{\dot{\mathbf{z}}_t^i = J\big(\mathbf{C}^i(\mathbf{z}_t) - (\mathbf{z}_t^i\cdot\hat{\mathbf{e}}_1)\hat{\mathbf{e}}_1\big), \quad i\in\{1,\dots,N\}}. \tag{2.23}$$

Egan et al. in [29] first studied the application of a semi-discrete optimal transport scheme to solve the 2D incompressible SG equations. Given $\mathbf{z}(t) = (\mathbf{z}^1(t),\dots,\mathbf{z}^N(t)) \in \mathbb{R}^{2N}$ the ODE for the 2D system is

$$\begin{cases} \dot{\mathbf{z}}^i = J(\mathbf{C}^i(\mathbf{z}) - (\mathbf{z}^i\cdot\hat{\mathbf{e}}_1)\hat{\mathbf{e}}_1), \\ \mathbf{z}^i(0) = \overline{\mathbf{z}}^i, \end{cases}$$

for $i\in\{1,\dots,N\}$, where $\overline{\mathbf{z}}^i$ denotes the initial position of the i-th seed.

The energy for the 2D system, up to a constant depending on the physical parameters of the problem, is given by

$$E_{2\mathrm{D}}(\mathbf{z}(t)) \simeq \frac{1}{2}\sum_{i=1}^{N}\left(\int_{L^i}\|\mathbf{x}-\mathbf{z}^i(t)\|^2\,\mathrm{d}\mathbf{x} - \big(z_2^i(t)\big)^2\int_{L^i}1\,\mathrm{d}\mathbf{x}\right),$$

which is the relevant reduction of the full 3D energy given by Eq. (2.6). Benamou et al. [6] built upon this foundation by implementing a fully discrete scheme, significantly enhancing simulation resolution. To validate our code, we replicated these results, employing Egan's technique in conjunction with Benamou's improved resolution. This enhancement was facilitated by advanced numerical schemes developed by Mérigot and Leclerc [50]. We utilised the 'unstable normal mode' scenario detailed in section 5.2 of [29] as a benchmark for our code. In contrast to [29], whose highest resolution simulations were done with $N = 2678$ particles, our simulations were done with $N = 64284$ particles which is similar to the number of points used by [6] ($N = 65536$). As shown in Figure 2.1, our implementation conserves total energy with a relative error on the order of 10^{-5}, comparable to the implementations in [6, 29]. It's important to distinguish between two sources of error: the spatial discretisation error, which depends on the number of particles N, and the temporal conservation error, which reflects how well the initial discrete energy is preserved during the simulation. The relative error we

report here pertains to the latter. This conservation error is primarily a function of the ODE solver's accuracy and the chosen timestep. While the optimal transport solver is essential for the stability of the scheme, the drift in the total energy over time is introduced by the temporal integration. This study does not analyse the error in the initial energy value due to the particle discretisation. Egan et al. used a timestep of 30 seconds and Benamou et al. used a timestep of 91.44 minutes. For our benchmark we employed a timestep of 30 minutes. Notably, with these advanced numerical schemes, we achieved a relative error comparable to the one in [29] but with a timestep 60 times larger. Furthermore, as illustrated in Figure 2.2, the system's evolution over the first 10 days aligns visually with the previous results of [6, 29], where we observe the formation of a weather front and its subsequent oscillations. In order to generate the plots we extract the meridional velocity (v) and temperature (θ) from the seeds positions,

$$v(\mathbf{x}, t) = C_1 \sum_{i=1}^{N} (\mathbf{z}_1^i(t) - \mathbf{C}_1^i(\mathbf{z}, (t))) \mathbb{1}_{L^i}(\mathbf{x})$$

$$\theta(\mathbf{x}, t) = C_2 \sum_{i=1}^{N} \mathbf{z}_2^i(t) \mathbb{1}_{L^i}(\mathbf{x}),$$

where $C_1, C_2 \in \mathbb{R}$ are physical constants (see [29]).

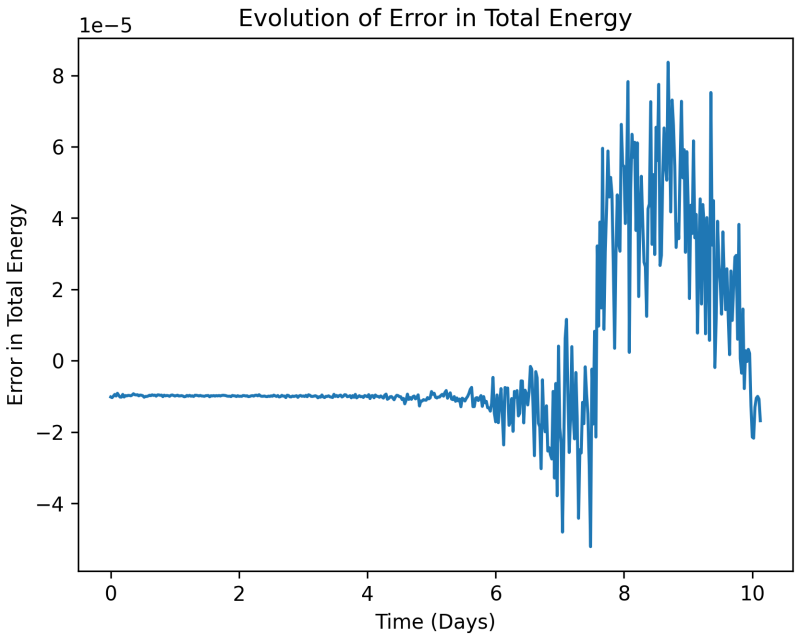

Figure 2.1: The plot shows the evolution of the relative error in the total energy as defined in Eq. (2.26). The total energy fluctuates about 2.415e10.

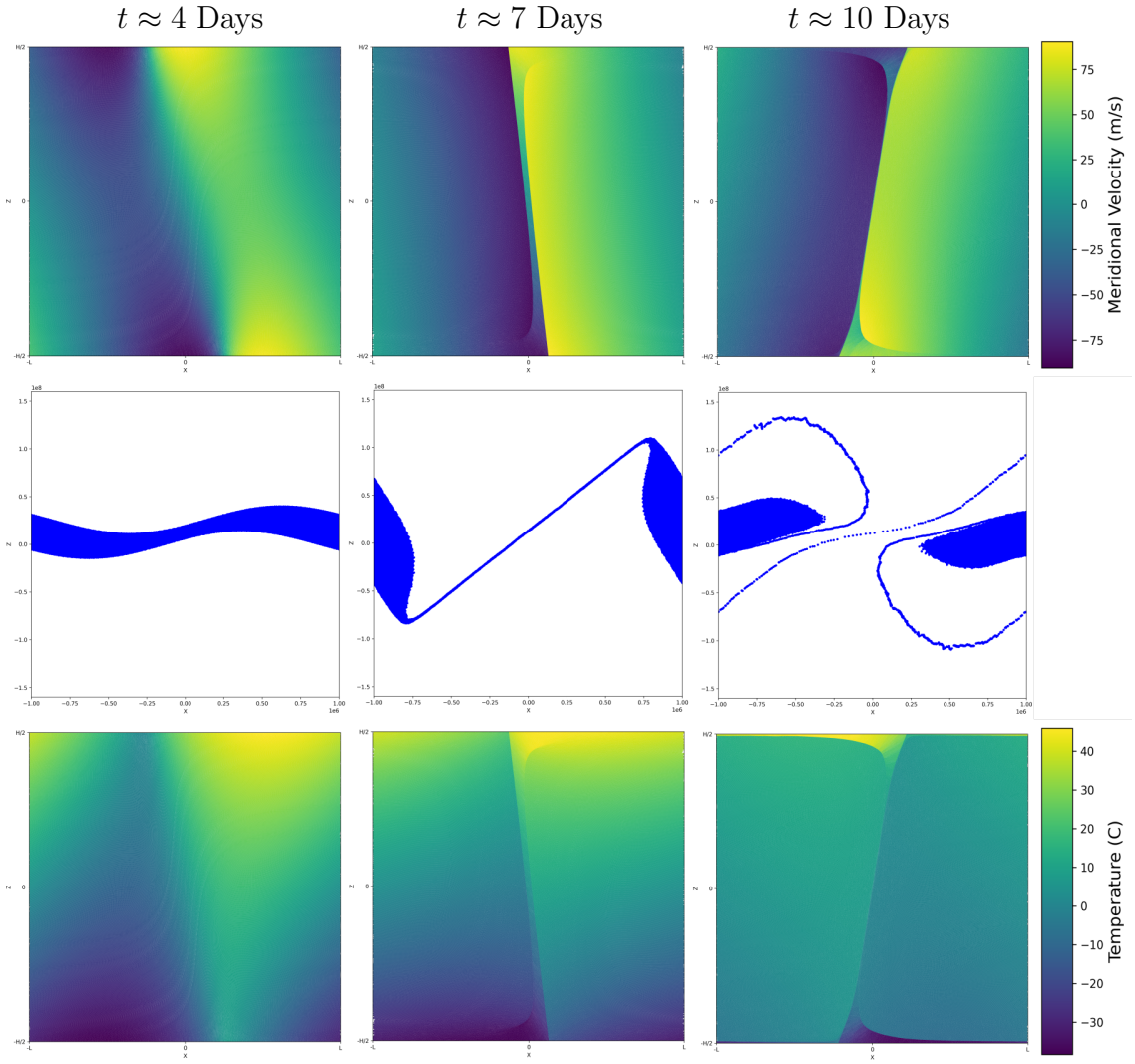

Figure 2.2: In the first row we display the evolution of the perturbation of the meridional velocity field in the physical space ($\mathcal{X}$). In the second row we display the evolution of the positions of the geostrophic particles (in $\mathcal{Y}$). Finally, in the third row we display the evolution of the perturbation of the temperature field in physical space. Over the course of 10 days we observe the formation and evolution of a weather front.

2.3 3D Benchmarks

To initialise our computations, we require a suitable initial condition. Here we explain how we generate physical initial conditions for the 3D incompressible SG equations. The initial condition presented simulates the formation of an isolated large-scale tropical cyclone with or without initial shearing winds.

2.3.1 Initial condition generating an isolated semi-geostrophic cyclone

In order to construct the initial condition for ODE (Eq. (2.5)) we need to find the initial seed positions $\overline{\mathbf{z}}$. These will be given by

$$\overline{\mathbf{z}}^i = \left(\mathrm{Id} + \widetilde{T}\right)(\mathbf{x}^i),$$

where the transport map, $T = \mathrm{Id} + \widetilde{T}$, is the gradient of a convex function, which is physically interpreted as the modified pressure. This means that the initial condition will be given by

$$\overline{\mathbf{z}}^i = \mathbf{x}^i + \nabla\Phi(\mathbf{x}^i),$$

where the $\mathbf{x}^i$ are points in a uniform grid on the domain $\mathcal{X}$, and

$$\Phi(x_1, x_2, x_3) = \overline{\Phi}(x_1, x_2, x_3) + \widetilde{\Phi}, (x_1, x_2, x_3)$$

satisfies $\Delta\Phi = 0$. Note that Laplace's equation arises from linearising of the Monge-Ampère equation (see § 2.5.1 for more details). Thus in order to construct the initial condition we need to solve for the full pressure field. Notice, however, that the steady state modified pressure $\overline{\Phi}$, Eq. (2.1), is harmonic. Therefore, to find the full pressure field we just need to find the effect that the perturbation of the temperatures on the surfaces has in the bulk of the domain. Thus we only consider $\widetilde{\Phi}$ that satisfies

$$\begin{cases} \Delta\widetilde{\Phi} = 0, \\ \widetilde{\Phi}(-a, \cdot, \cdot) = \widetilde{\Phi}(a, \cdot, \cdot), \\ \widetilde{\Phi}(\cdot, -b, \cdot) = \widetilde{\Phi}(\cdot, b, \cdot), \\ \frac{\partial\widetilde{\Phi}}{\partial x_3}\big|_{x_3=0} = 0.15h(x_1, x_2), \\ \frac{\partial\widetilde{\Phi}}{\partial x_3}\big|_{x_3=c} = -0.6h(x_1 + 1, x_2). \end{cases} \tag{2.24}$$

The solutions of the system (2.24) on a cuboid domain $\mathcal{X} = [-a, a] \times [-b, b] \times [0, c]$ approximates the effect that the surface perturbations have on the bulk. The solution satisfying the given boundary conditions, suitably adjusted for compatibility can be found explicitly (see § 2.5.2). We use the values for a, b, and c suggested in [61] : c is the height of the lid set to be 0.45 which corresponds to a physical height of 9 km, a is 3.66 and b is 1.75, which corresponds to a

channel (periodic in x) of area 14640×7000 kilometers.

2.4 Results

2.4.1 Numerical Method

The numerical method we employ consists of two main components, an optimal transport solver coupled with an ODE solver. For the optimal transport solver, we utilised the Pysdot package to generate Laguerre diagrams and solve the optimal transport problem using the damped Newton algorithm. Detailed information on this approach can be found in [29, 50, 53]. To enhance the stability and speed of convergence of the damped Newton algorithm, we applied a specific rescaling and translation of the initial configuration of geostrophic particles. Further details on this technique are provided in the work of [55]. After obtaining the centroids of the Laguerre cells from the optimal transport solver, we applied a classical RK4 scheme to solve the ODE.

A pseudocode for the numerical scheme is provided in Algorithm 1.

Algorithm 1: Semi-Discrete Optimal Transport Simulation with Weight Rescaling

Input: Initial particle positions $\mathbf{z}_0$, source domain $\mathcal{X}$, final time τ, timestep dt.

Output: Final particle positions $\mathbf{z}_\tau$.

for $k \leftarrow 0$ **to** $num\_steps - 1$ **do**

```
// Generate a stable initial guess for the OT solver's weights using
   Meyron's rescaling algorithm [55].
```

$\boldsymbol{w}_{\text{guess}} \leftarrow \text{GenerateInitialWeights}(\mathbf{z}_k, \mathcal{X})$;

```
// Solve the OT problem using the generated guess.  The solver
   returns the optimal weights and cell centroids.
```

$\boldsymbol{w}_{\text{optimal}}, \mathbf{C}_k \leftarrow \text{SolveOT}(\mathbf{z}_k, \boldsymbol{w}_{\text{guess}}, \mathcal{X})$;

```
// Compute particle velocities.
```

$\dot{\mathbf{z}}_k \leftarrow \text{CalculateVelocity}(\mathbf{z}_k, \mathbf{C}_k)$;

```
// Evolve particle positions forward in time.
```

$\mathbf{z}_{k+1} \leftarrow \text{RK4Step}(\mathbf{z}_k, \dot{\mathbf{z}}_k, dt)$;

return $\mathbf{z}$;

The full code, including links to and instructions about dependencies, is publicly available and can be found at: **github.com/thelavier/3DIncompressibleSG**

Justification of ODE Solver

We experimented with several methods besides RK4, e.g. Adams-Bashforth 2 (AB2) and Heun. Following the lead of [6] we ultimately chose RK4, even though it requires the solution of 4 optimal transport problems per timestep. We chose this method because of its energy conservation properties. Indeed, while [6] showed that there was no benefit in choosing a fourth order method over a second order method when considering the W_1 error with respect to a high resolution solution, we show that RK4 actually demonstrates a better performance over lower order methods in terms of energy conservation (see Figure 2.3). This property enabled us to run 25-day simulations in 6-8 hours because, even though more optimal transport solves were required, the step size could be much larger without affecting the conservation of the energy, carrying forward the improvements observed in the 2D benchmark to the 3D simulations.

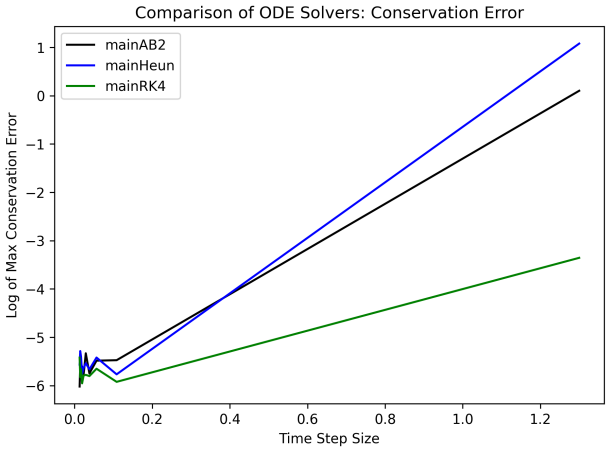

(a) Here a comparison is presented showing how the log of the maximum relative conservation error in the energy changes with solver and step size.

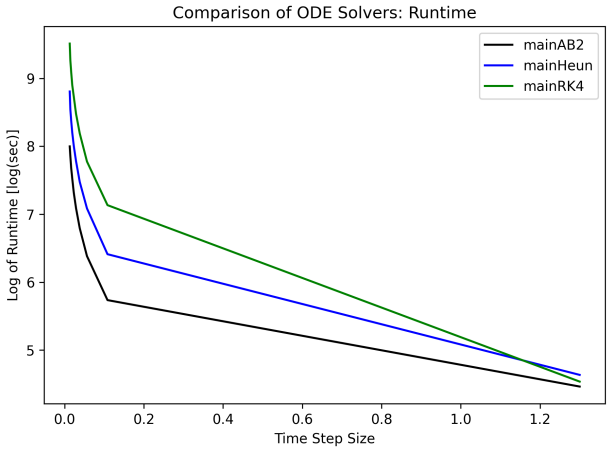

(b) Here a comparison is presented showing how the log of the simulation runtime changes changes with solver and step size.

Figure 2.3: A comparison between AB2, Heun, and RK4 when coupled to an optimal transport solver. These two plots demonstrate the trade off between run time, time step size, and maximum relative error in the conservation of the energy. These plots support the idea that a balance can be struck between runtime, step size, and maximum relative error if one wants to run simulations in a "reasonable" amount of time.

2.4.2 Experiments

All the numerical experiments that we ran and their key parameters are presented in Table 2.1.

		Wasserstein-2 Error						
		$t \approx 2$ d	$t \approx 4$ d	$t \approx 9$ d	$t \approx 13$ d	$t \approx 17$ d	$t \approx 21$ d	$t \approx 25$ d
η	1	6.8667e-10	1.1666e-5	0.0068	0.0300	0.9804	0.4346	0.3678
	0.1	7.6761e-10	1.2229e-5	0.0064	0.0291	0.0871	0.2140	0.3373
	0.01	1.9691e-10	8.6135e-7	0.0038	0.0229	0.0740	0.1996	0.3042
	0.001	-	-	-	-	-	-	-
h[sec]	10803.58	0.0091	0.0223	0.0866	0.3650	0.6162	0.5932	0.9808
	7190.46	0.0022	0.0071	0.0393	0.1865	0.5765	0.7715	0.8195
	5388.39	0.0014	0.0055	0.0428	0.1645	0.6625	0.9556	0.8565
	3595.23	0.0007	0.0032	0.0351	0.1377	0.7114	0.9401	1.0594
	2700.90	0.0004	0.0025	0.0331	0.1433	0.3229	0.5205	0.4602
	1799.11	5.2552e-5	0.0017	0.0246	0.0939	0.4740	0.9702	0.6124
	899.93	-	-	-	-	-	-	-
N	4096	0.1600	0.2594	0.6186	1.3901	1.8708	1.9466	1.4330
	5832	0.1233	0.1503	0.4656	1.0459	1.4215	1.3115	0.8541
	10648	0.0699	0.0939	0.3040	0.5674	0.9495	1.2798	0.9993
	21952	0.0246	0.0315	0.1190	0.7100	0.7642	1.4379	0.8179
	32768	-	-	-	-	-	-	-

Table 2.1: Wasserstein-2 error, as defined by Eq. (2.25), between simulations at the highest resolution (reference solution) and lower-resolution simulations as parameters vary. This table specifically presents errors resulting from the ODE solver used for temporal integration, rather than the damped Newton solver used for the optimal transport problem. The error dependence on the solver tolerance (η), timestep size (h), and particle count (N) is shown. Simulations investigating the impact of η were done with $h = 3595.23$ and $N = 32768$. Simulations investigating the impact of h were done with $\eta = 0.001$ and $N = 32768$. Simulations investigating the impact of N were done with $\eta = 0.001$ and $h = 3595.23$.

Error Computation

In order to analyse the quantitative performance of our method, we consider the following error

$$\text{Error}(t) = W_2^2\left(\frac{1}{N}\sum_{i=1}^{N}\delta_{\mathbf{z}^i_{\text{true}}(t)}, \frac{1}{N}\sum_{i=1}^{N}\delta_{\mathbf{z}^i_{\text{approx}}(t)}\right). \tag{2.25}$$

Here $\mathbf{z}_{\text{true}}(t)$ is the ensemble of seed positions generated by our finest-resolution run, which we adopt as a surrogate "ground truth", while $\mathbf{z}^i_{\text{approx}}(t)$ are the corresponding seeds produced by the lower-resolution simulation whose accuracy we wish to evaluate. The squared 2-Wasserstein distance between the two empirical measures therefore quantifies, in a physically meaningful way, how far the approximate Lagrangian configuration deviates from the reference at time t. This allows us to analyse the effect of changing the three key simulation parameters : percent tolerance of the optimal transport solver, time step size, and number of particles. We are also interested the the ability of the solver to preserve averaged quantities, in particular the energy.

In order to investigate this we also considered

$$\text{Error in Total Energy}(t) = \frac{E_{\text{mean}}(\mathbf{z}) - E(\mathbf{z}(t))}{E_{\text{mean}}(\mathbf{z})}, \tag{2.26}$$

where E_{mean} is the mean of the total energy, averaged over the entire simulation time interval $[0, \tau]$ and

$$\text{Max Conservation Error} = \max_{t \in [0,\tau]} \text{Error in Total Energy}(t).$$

In order to compute efficiently the Wasserstein-2 error for our analysis, we employed Jean Fedey's GeomLoss package to compute the Sinkhorn divergence approximation of the Wasserstein-2 distance [37]. The Sinkhorn divergence approximation of the Wasserstein-2 distance is an efficient way of measuring the distance between two probability measures. All errors were computed against a "ground-truth" simulation, defined as the highest resolution simulation. All simulations were conducted using the RK4 method.

Results of Experiments

As shown in Table 2.1, for short durations such as day 2 and 4, we observe the expected reduction in error with respect to timestep size (h^4) and particle count $\left(N^{-2/3}\right)$ [47], as illustrated in Figures 2.4 and 2.5. However, as the simulation extends to 25 days, we observe a deterioration in the accuracy, and the anticipated decay in error relative to the number of particles and timestep size no longer holds. This decline is not unexpected, as the solution develops sharp fronts that are effectively singularities in the physical space. The lack of significant change in the error when varying the tolerance on the optimal transport solver is also unsurprising, as the damped Newton method often overshoots the specified tolerance. Consequently, within reasonable bounds, the choice of tolerance for the optimal transport solver has a limited impact on the overall accuracy. Averaged properties of the system, such as total energy, remain well conserved, as shown in Figure 2.6, indicating that while the accuracy degrades, the overall physical integrity of the simulation is preserved. This highlights a crucial distinction in the system's stability: while individual particle trajectories exhibit sensitive dependence on initial conditions (a Lagrangian instability), the overall macroscopic structures and averaged properties of the flow are robust to small perturbations (an Eulerian or structural stability). Therefore, even as the precise location of a single particle becomes unpredictable, the physically

relevant collective behaviour, such as the shape of the developing fronts and the conservation of global quantities, remains reliable.

To address issues with the accuracy of the ODE solver, we plan to follow up with a study of the spectral properties of the system, particularly focusing on the centroid map, to better understand this deterioration and develop methods that maintain higher accuracy over long-term simulations. Preliminary analysis suggests that the issue may be related to a large relative spectral gap in the eigenvalues of the centroid map. The suspected presence of this spectral gap underscores why the loss of regularity presents a severe challenge for the temporal integration. Standard ODE solvers are not designed to handle such behaviour over long periods, leading to an accumulation of truncation error. The core difficulty lies not in the choice of a particular ODE scheme (e.g., RK4 vs. others), but in the inherently stiff and non-local nature of the system's evolution, which is governed by the global optimal transport problem at each step. Crafting a bespoke integrator that remains accurate in the presence of these evolving structures is a formidable open research direction and might not even be possible.

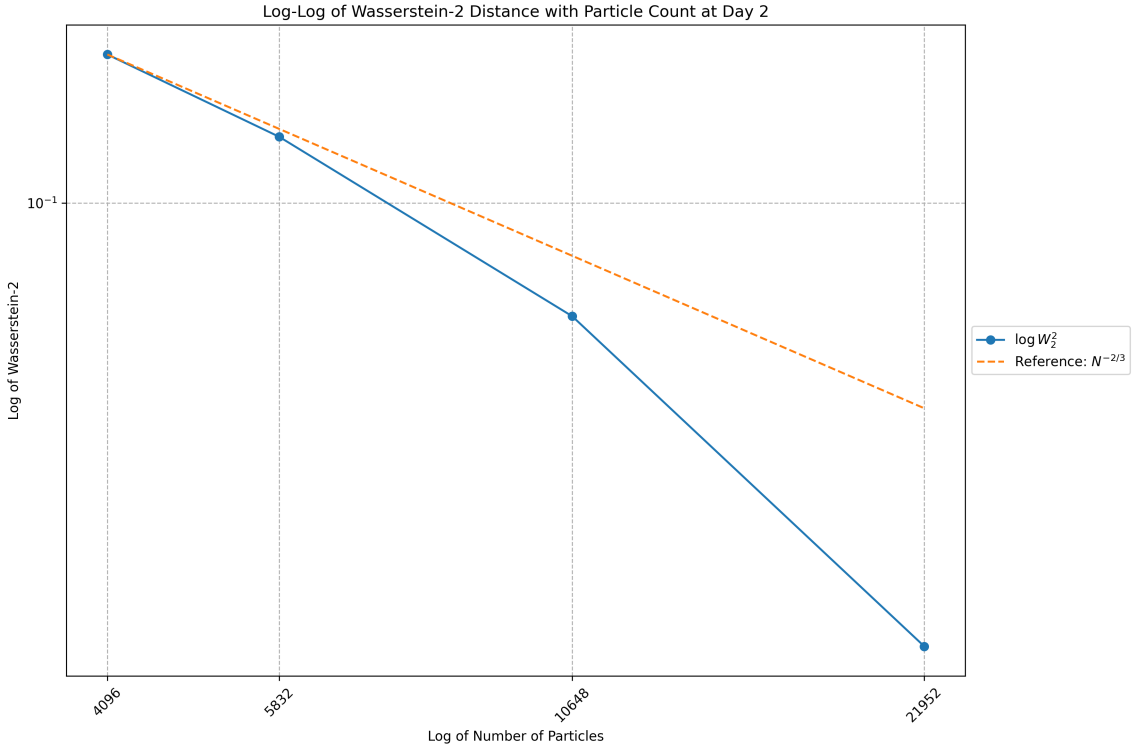

Figure 2.4: Log-log plot of the change in the Wasserstein-2 error at day 2 with respect to the change in the number of particles (in blue). In orange is a plot of the theoretical best decrease in the discretisation error with respect to the number of particles.

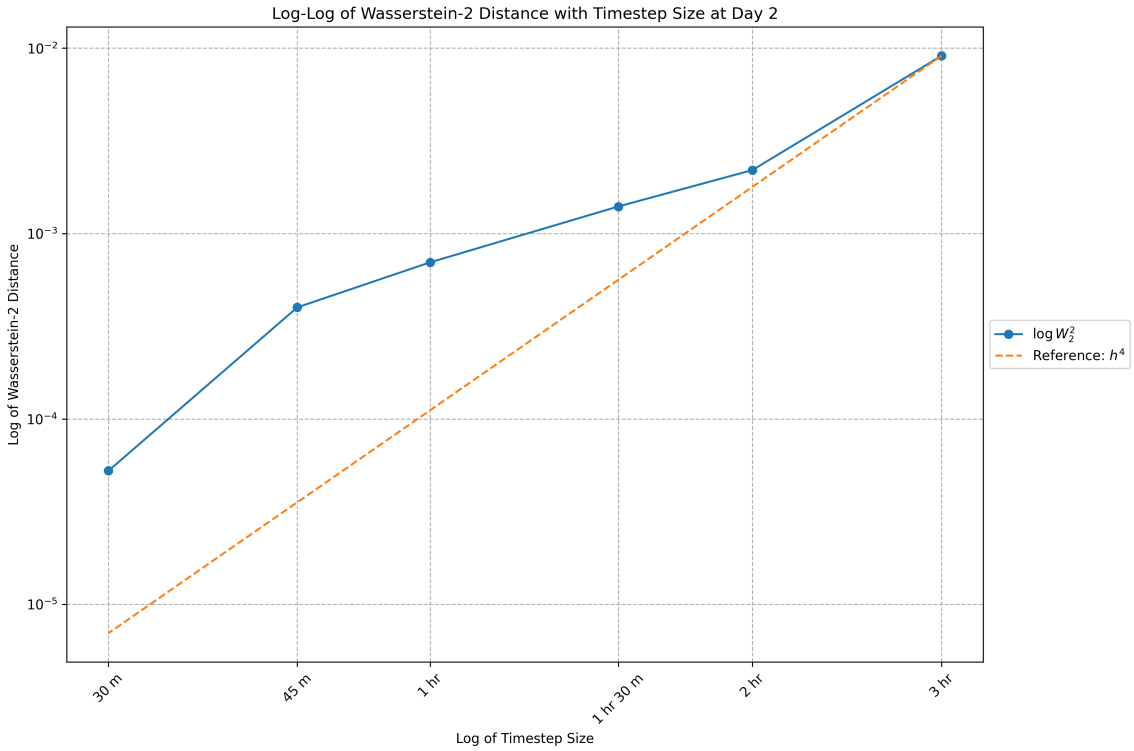

Figure 2.5: Log-log plot of the change in the Wasserstein-2 error at day 2 with respect to the change in the size of the timestep (in blue). In orange is a plot of the theoretical best decrease in the error with respect to the timestep size for Runga-Kutta 4.

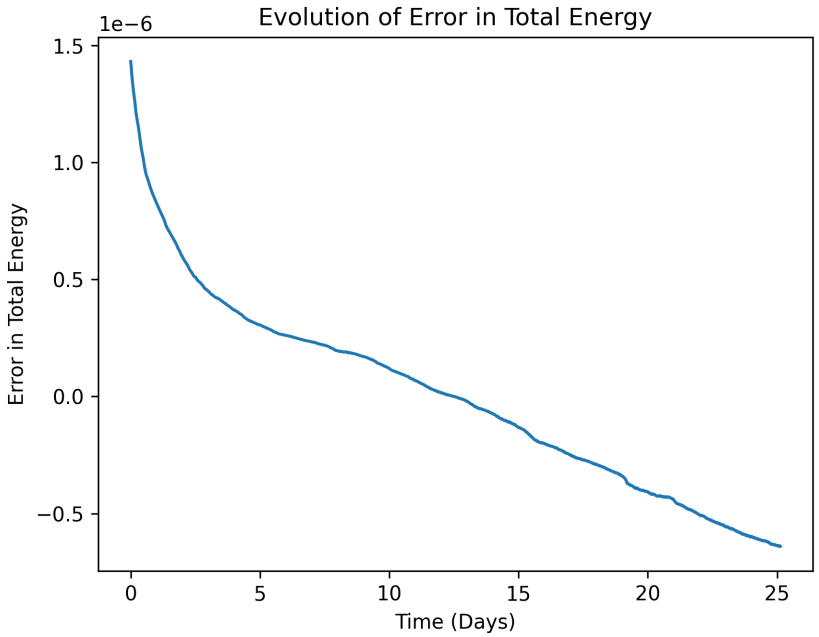

Figure 2.6: The plot shows the evolution of the relative error in the total energy as defined in Eq. (2.26). The total energy fluctuates about 3.799.

2.4.3 Observations of Cyclones

In what follows is a qualitative discussion of the evolution of an isolated large-scale tropical cyclone as controlled by the SG system. To aid in this discussion we extract the zonal velocity (ZVel), meridional velocity (MVel), geostrophic velocity, total geostrophic velocity (TVel), and temperature :

$$\mathrm{ZVel}(\mathbf{x},t) = \sum_{i=1}^{N} \left(C_2^i(\mathbf{z}(t)) - z_2^i(t)\right) \mathbb{1}_{L^i}(\mathbf{x}),$$

$$\mathrm{MVel}(\mathbf{x},t) = \sum_{i=1}^{N} \left(z_1^i(t) - C_1^i(\mathbf{z}(t))\right) \mathbb{1}_{L^i}(\mathbf{x}),$$

$$\mathbf{u}_g(\mathbf{x},t) = \left(\mathrm{ZVel}(\mathbf{x},t), \mathrm{MVel}(\mathbf{x},t)\right)^T$$

$$\mathrm{TVel}(\mathbf{x},t) = \sum_{i=1}^{N} \|\mathbf{u}_g(\mathbf{x},t)\| \mathbb{1}_{L^i}(\mathbf{x}),$$

$$\mathrm{Temperature}(\mathbf{x},t) = \sum_{i=1}^{N} z_3^i(t) \mathbb{1}_{L^i}(\mathbf{x}).$$

We also compute the root mean squared velocity (RMSv) of the three different velocities

$$\mathrm{RMSv} = \sqrt{\frac{1}{\mathcal{X}} \int_{\mathcal{X}} |v(\mathbf{x},t)|^2 \, \mathrm{d}\mathbf{x}},$$

to support our consideration of different initial shearing regimes.

In Figure 2.7, we observe the evolution of a 3D incompressible SG system where cold and hot air masses are initially separated and subsequently mix. The series of images track the development of this interaction over a period of 25 days. In rows one and three, the images display the magnitude of the total geostrophic velocity in physical space ($\mathcal{X}$). Initially, at $t \approx 4$ days, a distinct front forms between the cold and hot air masses. As time progresses to $t \approx 8$ and $t \approx 12$ days, an instability along this front propagates, evolving into a chain of rotational systems, indicative of cyclone and anticyclone formation.

Rows two and four depict the evolution of seed positions in geostrophic space ($\mathcal{Y}$), where the temperature corresponds to the vertical position in the third dimension. The geostrophic particles are color-coded to represent their vertical positions: blue for colder or "lower" and

red for hotter or "higher". At $t \approx 4$ days, the seeds are relatively evenly distributed along the front. By $t \approx 8$ and $t \approx 12$ days, the seeds begin to cluster and spiral, showing the development of vortices as the system becomes more dynamic.

By $t \approx 16$ days, the rotational structures become more pronounced, and by $t \approx 20$ and $t \approx 25$ days, the system displays fully developed cyclonic and anticyclonic patterns. This visual evidence supports the conclusion that the initial instability evolves into a series of complex, rotating systems. The continued development and interaction of these vortices demonstrate the non-linear and chaotic nature of the 3D incompressible SG dynamics, while energy is conserved throughout the process, as indicated by the stable total energy observed in long-term simulations.

Figure 2.8 complements this analysis by presenting horizontal cross-sections of the temperature and velocity magnitude at different altitudes within the domain after 12 days of evolution. These slices show the vertical structure of the flow, revealing the coupling between thermal and dynamical processes. The interaction between cold and warm air masses drives the development of baroclinic instability, leading to the characteristic rotation observed in geostrophic systems.

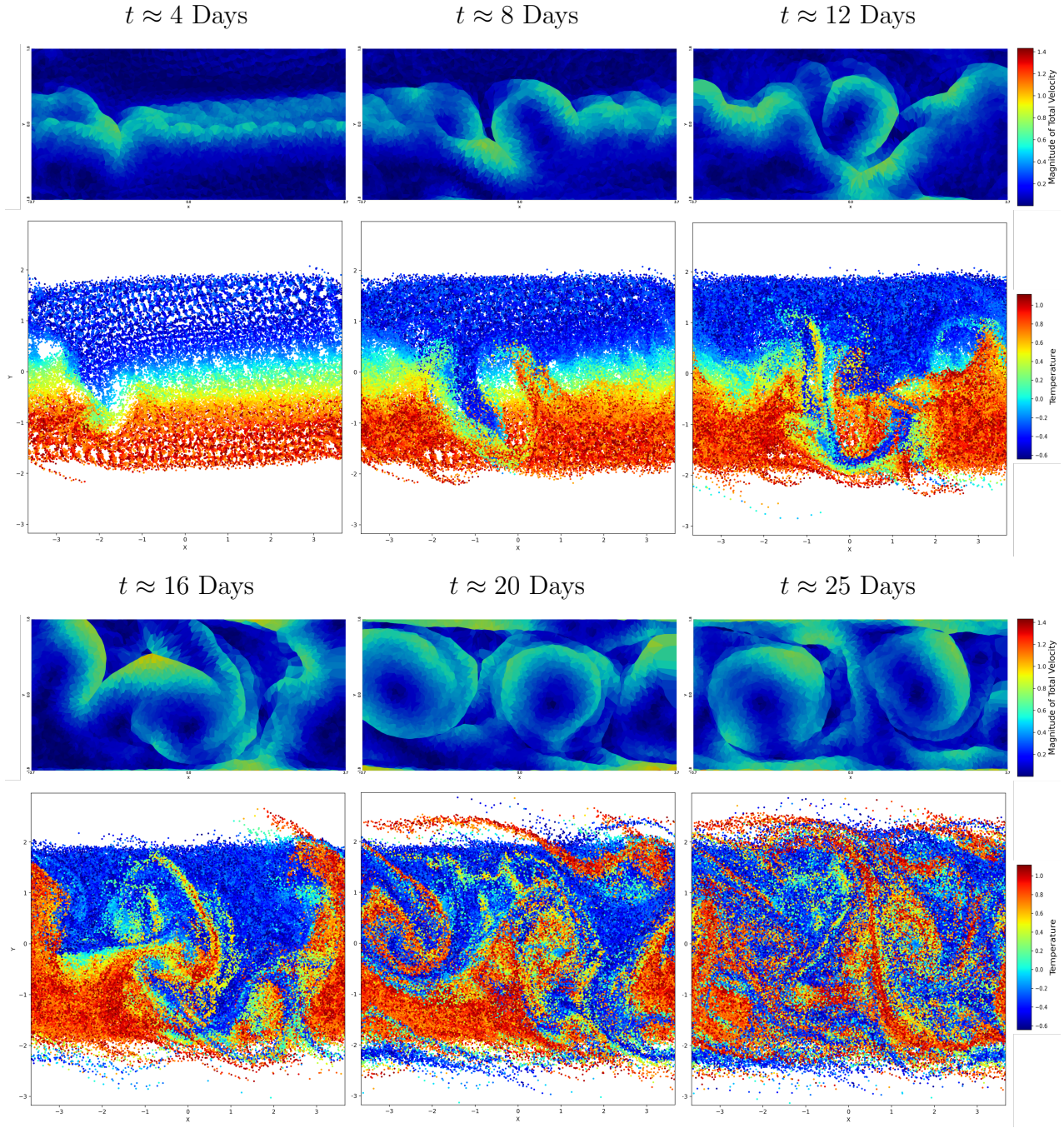

Figure 2.7: All images are done with the camera looking down on the top of the domain. In rows one and three we see the evolution of the magnitude of the total geostrophic velocity (in physical space, $\mathcal{X}$) over 25 days. In rows 2 and 4 we see the evolution of the position of the geostrophic particles over 25 days. In geostrophic space temperature corresponds to position in the third dimension. In these images this is captured in the colouring of the particles. Colder "lower" particles are blue and hotter "higher" particles are red. Simulation parameters: $N = 64000$, $\eta = 10^{-3}$, and $h = 30$ min.

Shear Parameter

Finally, as demonstrated in the seminal works by Davies et al. [26] and Wernli et al. [66], the impact of a shearing wind on cyclone development is significant, with the evolution of the system

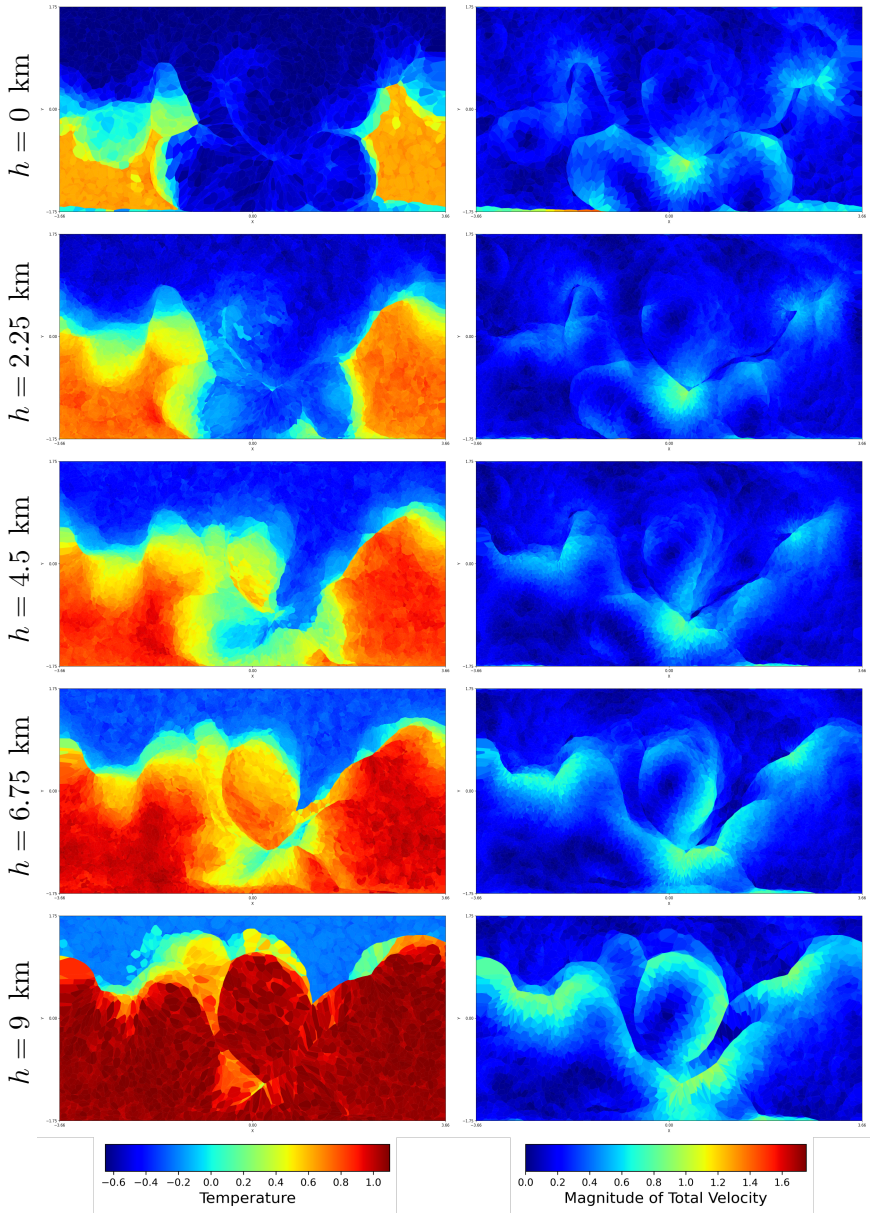

Figure 2.8: Vertical slices of temperature (left column) and total velocity magnitude (right column) at various altitudes ($h = 0$ km, 2.25 km, 4.5 km, 6.75 km, and 9 km) after 12 days of simulation. The temperature distribution highlights regions of significant thermal activity, with warmer areas denoted by red hues and cooler areas by blue, indicating the presence of convective structures and stratification. The velocity magnitude plots reveal the structure of the flow, with areas of higher velocity depicted in yellow-green, illustrating the dynamics of the developing cyclone and associated turbulence. These slices offer a detailed view of the interaction between thermal and kinematic fields throughout the bulk of the cyclone, emphasising the formation and behaviour of flow structures across multiple atmospheric layers. Simulation parameters: $N = 64000$, $\eta = 10^{-3}$, and $h = 30$ min.

being highly sensitive to the horizontal shear imposed at the initial time. These previous studies explored how variations in background shear influence the formation and characteristics of cyclonic and frontal structures. A key limitation they faced, however, was the loss of regularity

of the transformation between geostrophic and physical space occurring between 4 to 8 days, restricting their ability to investigate the long-term effects of the shear.

Our formulation overcomes this critical limitation, allowing us to maintain accuracy and continue the simulation beyond the breakdown observed in their models. This advantage enables us to explore the extended dynamics of shearing effects on cyclogenesis over a 25-day period. In Figure 2.9, we show how different initial shearing wind conditions ($A = -0.5$, $A = 0$, and $A = 0.1$) influence the intensity and organization of rotational systems. Our results reveal that with strong anticyclonic shear ($A = -0.5$), the formation of coherent rotational systems is significantly disrupted, while weaker or cyclonic shear ($A = 0.1$) promotes the intensification of cyclonic structures, mirroring the findings of [66], who observed pronounced differences in cyclone development based on the sign and magnitude of the imposed shear.

Furthermore, as shown in Figure 2.10, which separates the wind velocity into zonal and meridional components, the RMSv analysis highlights how shear conditions influence the balance between these components. For strong initial shear ($A = -0.5$), our results confirm that the zonal velocity dominates, leading to less organized and smaller-scale rotational systems, consistent with the findings by [26] where anticyclonic shear favored elongated cold fronts and weaker cyclones. Conversely, when shear is weak or absent ($A = 0$ and $A = 0.1$), the meridional velocity gains prominence, enhancing the development of more coherent cyclonic and anticyclonic structures, in line with the cyclonic shear experiments reported by [66].

The ability to extend our simulations well beyond the timescales considered in previous studies provides new insights into the stability and evolution of these systems under sustained shear conditions. This prolonged analysis underscores the critical role of initial shearing in dictating the long-term behavior of cyclonic structures, offering valuable extensions to the meteorological applications highlighted in [26] and [66]. Our results not only corroborate the sensitivity to shear observed in these foundational studies but also extend the understanding of how these dynamics evolve over longer timescales, providing a richer perspective on the impact of horizontal shear in geophysical fluid systems.

While providing detailed interpretations of the meteorological significance or specific atmospheric structures observed in the simulations goes beyond the scope of the present work, our results clearly demonstrate the utility of our optimal transport formulation. By replicating the key features of the simulations by [66], we highlight the potential of our approach as a valuable tool for investigating a broad range of SG atmospheric phenomena over extended timescales.

This capability enables the study of complex dynamics that were previously inaccessible due to the limitations of traditional numerical formulations.

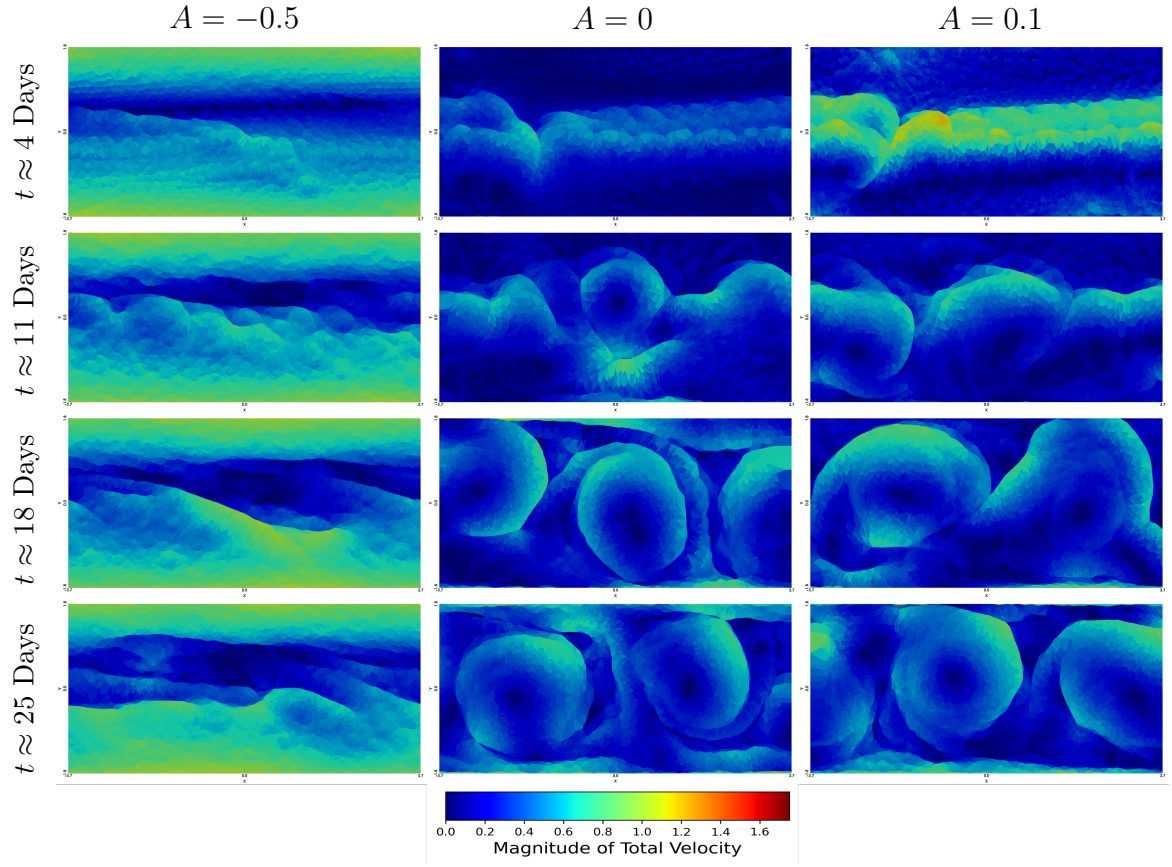

Figure 2.9: Here we demonstrate how adding a background shearing wind to the initial condition results in the disruption of or strengthening of cyclone formation over 25 days. In the first column we see the effect of a strong shear wind completely disrupting cyclone formation in the channel, in contrast with the no shear scenario in the second column, and the weak shear scenario in the third column. Each image is a view on the top of the domain and the magnitude of the total geostrophic velocity is being plotted. Simulation parameters: $N = 64000$, $\eta = 10^{-3}$, and $h = 30$ min.

2.5 Technical Details

2.5.1 The Monge-Ampère and Laplace Equations

In this section, we justify the use of Laplace's equation for establishing our initial condition. The Monge-Ampère equation, related to the optimal transport map for the quadratic cost [10], plays a central role in coupling the SG equations with a transport equation. If $\nabla u_{\#} f = g$, then the potential u satisfies the Monge-Ampère equation given by

$$f(x) = g(\nabla u(x)) \det D^2 u(x) \tag{2.27}$$

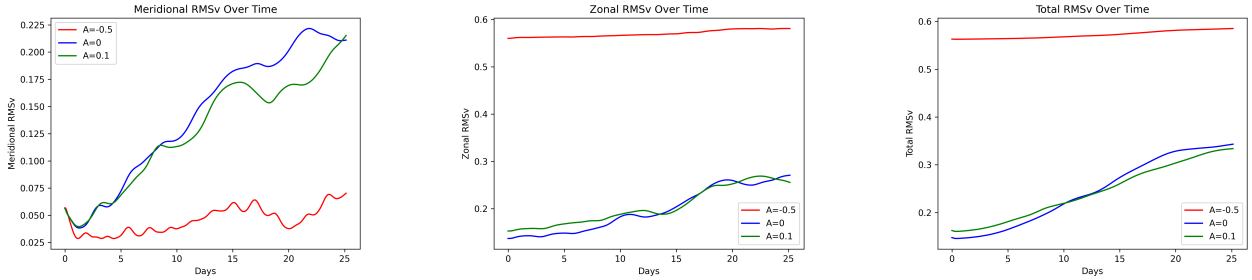

(a) Meridional RMSv (b) Zonal RMSv (c) Total RMSv

Figure 2.10: Comparison of the evolution of root mean square velocity (RMSv) components under different initial shearing conditions over 25 days. 2.10a Meridional RMSv: shows the evolution of the y-direction velocity, with higher values indicating stronger meridional flow under weaker initial shear ($A = 0$, $A = 0.1$). 2.10b Zonal RMSv: depicts the evolution of the x-direction velocity, demonstrating dominant zonal flow under strong initial shear ($A = -0.5$). 2.10c Total RMSv: presents the combined effect of both meridional and zonal components, illustrating the overall system dynamics under varying shearing conditions.

for source probability measure $f : \mathbb{R}^n \to \mathbb{R}$, target probability measure $g : \mathbb{R}^n \to \mathbb{R}$, and a convex function $u \in \mathcal{C}^2(\mathcal{X})$. Linearizing the Monge-Ampère equation around the quadratic potential leads to Poisson's equation, where the right-hand side depends on the gradient of the target measure. By neglecting this right-hand side, we obtain Laplace's equation, which is often used to approximate the initial condition in the quasi-geostrophic approximation. In the case of an incompressible fluid the source measure is the Lebesgue measure so $f(\mathbf{x}) = 1$. We linearise Eq. (2.27) about

$$u(\mathbf{x}) = \frac{1}{2}\mathbf{x}^T\mathbf{x}$$

by adding the small perturbation $\varepsilon\Phi(\mathbf{x})$ to $u(\mathbf{x})$ to get

$$1 = g(\mathbf{x} + \varepsilon\nabla\Phi(\mathbf{x}))\det\big(\mathbf{I} + \varepsilon D^2\Phi(\mathbf{x})\big),$$

and then differentiating both sides with respect to ε to get

$$\begin{aligned} 0 &= \det\big(\mathbf{I} + \varepsilon D^2\Phi(\mathbf{x})\big)\frac{\mathrm{d}}{\mathrm{d}\varepsilon}g(\mathbf{x} + \varepsilon\nabla\Phi(\mathbf{x})) + g(\mathbf{x} + \varepsilon\nabla\Phi(\mathbf{x}))\frac{\mathrm{d}}{\mathrm{d}\varepsilon}\det\big(\mathbf{I} + \varepsilon D^2\Phi(\mathbf{x})\big) \\ &= \det\big(\mathbf{I} + \varepsilon D^2\Phi(\mathbf{x})\big)\nabla g(\mathbf{x} + \varepsilon\nabla\Phi(\mathbf{x}))\cdot\nabla\Phi(\mathbf{x}) \\ &\quad + g(\mathbf{x} + \varepsilon\nabla\Phi(\mathbf{x}))\det\big(\mathbf{I} + \varepsilon D^2\Phi(\mathbf{x})\big)\,\mathrm{tr}\Big(\big(\mathbf{I} + \varepsilon D^2\Phi(\mathbf{x})\big)^{-1}\cdot D^2\Phi(\mathbf{x})\Big). \end{aligned}$$

By setting $\varepsilon = 0$ and rearranging we arrive at

$$\Delta\Phi(\mathbf{x}) = -\frac{1}{g(\mathbf{x})}\nabla g(\mathbf{x}) \cdot \nabla\Phi(\mathbf{x}).$$

Now by neglecting the right hand side we have

$$\Delta\Phi(\mathbf{x}) = 0.$$

This resulting Laplace equation is solved to derive the initial condition for the isolated large-scale tropical cyclone following the lead of [61].

2.5.2 Explicit solution for the perturbation

In this section, we solve Laplace's equation for the modified pressure, Φ, decomposed as

$$\Phi(x_1, x_2, x_3) = \overline{\Phi}(x_1, x_2, x_3) + \widetilde{\Phi}(x_1, x_2, x_3),$$

where $\overline{\Phi}$ is the background or steady state modified pressure and $\widetilde{\Phi}$ is the perturbed modified pressure. We do this to propagate the perturbation on the surfaces through the bulk of the domain. We consider a cuboid domain, subject to periodic boundary conditions in two directions and Neumann boundary conditions in the third direction. We also ensure that the compatibility condition for the Neumann problem is satisfied before proceeding with the solution. We begin with the Laplace equation

$$\Delta\Phi(\mathbf{x}) = 0$$

in the cuboid domain $[-a, a] \times [-b, b] \times [0, c]$, with periodic boundary conditions in the x_1 and x_2 directions, and Neumann boundary conditions in the x_3 direction

$$\left.\frac{\partial\widetilde{\Phi}}{\partial x_3}\right|_{x_3=0} = 0.15h(x_1, x_2) \quad \text{and} \quad \left.\frac{\partial\widetilde{\Phi}}{\partial x_3}\right|_{x_3=c} = -0.6h(x_1 + 1, x_2),$$

where $h(x_1, x_2)$ is given by Eq. (2.2). Note that $\overline{\Phi}$, introduced in Eq. (2.1), is harmonic. Thus, we only need to solve

$$\Delta\widetilde{\Phi}(\mathbf{x}) = 0.$$

Before solving Laplace's equation for $\widetilde{\Phi}$, we need to ensure the compatibility condition is satisfied. The compatibility condition requires that

$$I_0 + I_c = 0,$$

where

$$I_0 = \int_{x_1=-a}^{a} \int_{x_2=-b}^{b} 0.15h(x_1, x_2)\, \mathrm{d}x_2 \mathrm{d}x_1$$

$$I_c = -\int_{x_1=-a}^{a} \int_{x_2=-b}^{b} 0.6h(x_1+1, x_2)\, \mathrm{d}x_2 \mathrm{d}x_1.$$

This condition is necessary for the solvability of the Neumann problem. However, the Neumann boundary conditions in [61] do not satisfy this condition. Therefore, we adjust the boundary conditions to:

$$\left.\frac{\partial\widetilde{\Phi}}{\partial x_3}\right|_{x_3=0} = 0.15h(x_1, x_2) - \frac{I_0}{4ab} \quad \text{and} \quad \left.\frac{\partial\widetilde{\Phi}}{\partial x_3}\right|_{x_3=c} = -0.6h(x_1+1, x_2) - \frac{I_c}{4ab}.$$

With the compatibility condition now satisfied, we can proceed to solve Laplace's equation. We start by making the usual ansatz and expanding $\widetilde{\Phi}(x_1, x_2, x_3)$ in a Fourier series

$$\widetilde{\Phi}(x_1, x_2, x_3) = \sum_{n=-\infty}^{\infty} \sum_{m=-\infty}^{\infty} \exp\left(\frac{\pi i n x_1}{a}\right) \exp\left(\frac{\pi i m x_2}{b}\right) Z_{n,m}(x_3).$$

where $Z_{n,m}(x_3)$ are the unknown coefficient functions to be determined. By substituting this ansatz into the Laplace equation $\Delta\widetilde{\Phi}(\mathbf{x}) = 0$, we obtain the following set of ordinary differential equations for $Z_{n,m}(x_3)$:

$$\frac{\mathrm{d}^2}{\mathrm{d}x_3^2} Z_{n,m}(x_3) = k_{n,m}^2 Z_{n,m}(x_3),$$

where $k_{n,m} = \pi\sqrt{\left(\frac{n}{a}\right)^2 + \left(\frac{m}{b}\right)^2}$. The general solution for $Z_{n,m}(x_3)$ is

$$Z_{n,m}(x_3) = C_{n,m} \exp\left(k_{n,m} x_3\right) + D_{n,m} \exp\left(-k_{n,m} x_3\right),$$

where $C_{n,m}$ and $D_{n,m}$ are constants determined by the boundary conditions. Thus the solution is

$$\widetilde{\Phi}(x_1, x_2, x_3) = \sum_{n=-\infty}^{\infty} \sum_{m=-\infty}^{\infty} \exp\left(\frac{\pi i n x_1}{a}\right) \exp\left(\frac{\pi i m x_2}{b}\right) (C_{n,m} \exp(k_{n,m} x_3) + D_{n,m} \exp(-k_{n,m} x_3)).$$

Next, we apply the Neumann boundary conditions at $x_3 = 0$ and $x_3 = c$ to find $C_{n,m}$ and $D_{n,m}$. First, we compute the derivative of $\widetilde{\Phi}$ with respect to x_3

$$\frac{\partial \widetilde{\Phi}}{\partial x_3} = \sum_{n=-\infty}^{\infty} \sum_{m=-\infty}^{\infty} k_{n,m} \exp\left(\frac{\pi i n x_1}{a}\right) \exp\left(\frac{\pi i m x_2}{b}\right) (C_{n,m} \exp(k_{n,m} x_3) - D_{n,m} \exp(-k_{n,m} x_3)).$$

Now, we find the Fourier transforms of the boundary conditions. For the lower boundary $x_3 = 0$, the Fourier coefficients $A_{n,m}$ are given by

$$A_{n,m} = \frac{1}{4ab} \int_{x_1=-a}^{a} \int_{x_2=-b}^{b} \left(0.15h(x_1, x_2) - \frac{I_0}{4ab}\right) \exp\left(-\frac{\pi i n x_1}{a}\right) \exp\left(-\frac{\pi i m x_2}{b}\right) \mathrm{d}x_2 \mathrm{d}x_1.$$

For the upper boundary $x_3 = c$, the Fourier coefficients B_{nm} are given by

$$B_{n,m} = \frac{1}{4ab} \int_{x_1=-a}^{a} \int_{x_2=-b}^{b} \left(-0.6h(x_1 + 1, x_2) - \frac{I_c}{4ab}\right) \exp\left(-\frac{\pi i n x_1}{a}\right) \exp\left(-\frac{\pi i m x_2}{b}\right) \mathrm{d}x_2 \mathrm{d}x_1.$$

We then solve the following system of equations to determine C_{nm} and D_{nm} :

$$A_{nm} = k_{nm}(C_{nm} - D_{nm})$$

$$B_{nm} = k_{nm}(C_{nm} \exp(k_{nm} c) - D_{nm} \exp(-k_{nm} c)).$$

For the case $n = m = 0$, we set $C_{00} = D_{00} = 0$, which corresponds to the average perturbation on the surfaces of the domain. With the coefficients C_{nm} and D_{nm} determined, the initial condition is fully established, and we are now ready to proceed with the numerical solution of the system.

Chapter 3

Compressible Analysis

3.1 Introduction

In this chapter we study the compressible system formulated in terms of the so-called *geostrophic variables*. In these variables, the governing evolution equation is a continuity equation for a time-dependent probability measure α_t, usually called the *potential vorticity*.[1] The equation for α_t is given by

$$\partial_t \alpha_t + \nabla \cdot (\alpha_t \mathcal{W}[\alpha_t]) = 0. \tag{3.1}$$

The non-local velocity field $\mathcal{W}[\alpha_t]$ (defined in (3.4) below) is known as the *geostrophic wind*. It is defined at each time t by minimising the *geostrophic energy* given the potential vorticity α_t. The PDE (3.1) is derived in [24] by starting from Euler's equations for a compressible fluid, assuming a shallow atmosphere in hydrostatic balance, a rotation-dominated flow, and making the geostrophic approximation, which is valid for large-scale flows, then transforming the resulting equations to geostrophic coordinates.

The main goal of this chapter is to construct global-in-time weak solutions of (3.1) as the limit of spatially discrete approximations. This generalises and extends the semi-discrete optimal transport strategy presented in [8] for the incompressible setting, a generalisation that requires substantial changes and poses new technical challenges.

There are several benefits of using semi-discrete optimal transport: this approach highlights an intuitive connection between flows in geostrophic coordinates and corresponding flows in the fluid domain, it provides the means to construct explicit solutions, and it serves as the theoretical foundation for adapting Cullen and Purser's groundbreaking geometric method [25, 29] to solve the compressible SG equations numerically.

[1] In physical terms, α_t is the inverse of the physical potential vorticity; see [19].

3.1.1 Summary of results

We denote by $\mathcal{X} \subset \mathbb{R}^3$ the compact set representing the physical fluid domain, and by $\mathcal{Y} \subset \mathbb{R}^3$ the *geostrophic domain* where the equations are defined after the change to geostrophic variables. For further details about the assumptions on the fluid and geostrophic domains see Section 3.2.1.

To define the geostrophic energy of the system, consider an absolutely continuous probability measure $\sigma \in \mathscr{P}_{\mathrm{ac}}(\mathcal{X})$. The measure σ is a physical variable, representing the product of the fluid density and potential temperature. For a given probability measure $\alpha_t \in \mathscr{P}(\mathcal{Y})$ representing the potential vorticity, let $\mathcal{T}_c(\sigma, \alpha_t)$ be the *optimal transport cost* between σ and α_t, given below by (3.10), for the cost function $c : \mathcal{X} \times \mathcal{Y} \to \mathbb{R}$ given by equation (3.9). The corresponding *geostrophic energy* $E(\sigma, \alpha_t)$ is given by

$$E(\sigma, \alpha_t) = \mathcal{T}_c(\sigma, \alpha_t) + \kappa \int_{\mathcal{X}} \sigma^\gamma \, \mathrm{d}\mathbf{x}, \tag{3.2}$$

where $\gamma \in (1, 2)$ and $\kappa > 0$ are physical constants[2]. The geostrophic energy is the sum of the kinetic energy of the fluid, its gravitational potential energy, and its internal energy.

The geostrophic wind $\mathcal{W}$ that appears in (3.1) is defined by minimising the geostrophic energy over all σ. We show that this minimisation problem has a unique solution

$$\sigma_*[\alpha_t] = \operatorname*{arg\,min}_{\sigma \in \mathscr{P}_{\mathrm{ac}}(\mathcal{X})} E(\sigma, \alpha_t), \tag{3.3}$$

which we call the *optimal source measure*. Let T_{α_t} denote the *optimal transport map* from $\sigma_*[\alpha_t]$ to α_t for the cost c. Then the velocity field $\mathcal{W}[\alpha_t] : \mathcal{Y} \to \mathbb{R}^3$ in (3.1) can be formally defined by

$$\mathcal{W}[\alpha_t] = J\left(\mathrm{Id} - T_{\alpha_t}^{-1}\right), \qquad J = f_{\mathrm{cor}} \begin{pmatrix} 0 & -1 & 0 \\ 1 & 0 & 0 \\ 0 & 0 & 0 \end{pmatrix}, \tag{3.4}$$

where Id denotes the identity on $\mathcal{Y}$, and $f_{\mathrm{cor}} > 0$ is the Coriolis parameter, which we take to be constant. The optimal transport map T_{α_t} exists and is unique because the cost function c given by (3.9) satisfies the classical *twist* condition. We can recover the physical variables from the

[2]Interpreted physically, γ is the ratio $\frac{c_{\mathrm{p}}}{c_{\mathrm{v}}}$, where c_{p} is the specific heat at constant pressure and c_{v} is the specific heat at constant volume, and $\kappa = c_v\left(\frac{R_d}{p_0}\right)^{\gamma-1}$, where R_d is the specific gas constant for dry air, and p_0 is the reference pressure.

components of T_{α_t}. It can be shown that $T_{\alpha_t}(\mathbf{x}) = (x_1 + f_{\text{cor}}^{-2} v_2^g(\mathbf{x}, t), x_2 - f_{\text{cor}}^{-2} v_1^g(\mathbf{x}, t), \theta(\mathbf{x}, t))$, where $\mathbf{v}^g = (v_1^g, v_2^g, 0)$ is the geostrophic velocity of the fluid and θ is its potential temperature [24, equation (5)]. In general, the transport map T_{α_t} is not invertible, so equation (3.4) is only formal; we give a rigorous meaning to the PDE (3.1) in Definition 3.2.6.

To state the first of our results, we formulate the discrete analogue of the PDE (3.1) by making the discrete ansatz

$$\alpha_t^N = \sum_{i=1}^{N} m^i \delta_{\mathbf{z}^i(t)}, \tag{3.5}$$

where $\mathbf{z}^i(t) \in \mathcal{Y}$. Let $\mathbf{z}(t) = \big(\mathbf{z}^1(t), \dots, \mathbf{z}^N(t)\big) \in \mathcal{Y}^N$. Then this ansatz gives rise to the ODE

$$\dot{\mathbf{z}} = J^N(\mathbf{z} - \mathbf{C}(\mathbf{z})), \tag{3.6}$$

where $J^N \in \mathbb{R}^{3N \times 3N}$ is the block diagonal matrix $J^N := \operatorname{diag}(J, \dots, J)$, and $\mathbf{C}$ is the *centroid map*, which is defined in Definition 3.4.2 (see Figure 3.1). This centroid map is the discrete analogue of the map $T_{\alpha_t}^{-1}$ appearing in (3.4).

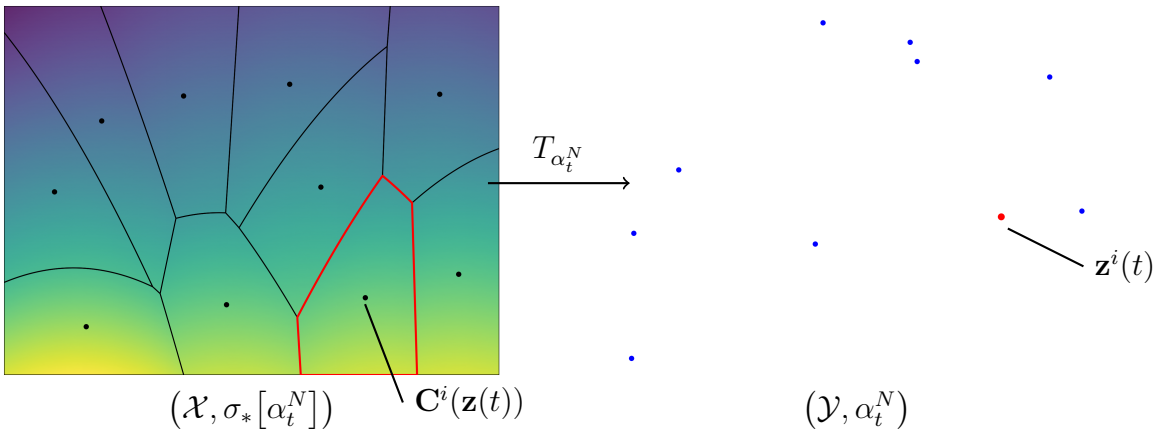

Figure 3.1: On the left is the source space $\mathcal{X}$ coloured by the density of the optimal source measure $\sigma_*[\alpha_t^N]$. The boundaries and centroids $\mathbf{C}^j(\mathbf{z}(t))$ of the corresponding c-Laguerre cells are plotted in black, with the boundary of the i-th cell, L_c^i, highlighted in red. On the right is the target space $\mathcal{Y}$ with the seeds $\mathbf{z}^j(t)$ in blue. The i-th seed, $\mathbf{z}^i(t)$, corresponding to the i-th cell is highlighted in red. The union of the seeds is the support of the target measure α_t^N.

We now state our two main results. The notation we use is listed in Section 2. In particular, by $\mathcal{C}^{0,1}([0, \tau]; \mathscr{P}(\mathcal{Y}))$ we mean Lipschitz continuity with respect to the W^1 Wasserstein metric on $\mathscr{P}(\mathcal{Y})$ and the standard metric on $[0, \tau]$.

Our first theorem asserts the existence and uniqueness of solutions of the ODE (3.6) and correspondingly of the PDE (3.1) with discrete initial data.

Theorem 3.1.1 (Existence of discrete geostrophic solutions)**.** *Fix $N \in \mathbb{N}$, an arbitrary final time $\tau > 0$, and an initial discrete probability measure $\overline{\alpha}^N = \sum_{i=1}^N m^i \delta_{\overline{\mathbf{z}}^i} \in \mathscr{P}^N(\mathcal{Y})$ that is well-prepared in the sense of* (3.15)*. Then there exists a unique solution $\mathbf{z} \in \mathcal{C}^2([0,\tau]; D^N)$ of the ODE* (3.6) *with initial condition $\mathbf{z}(0) = (\overline{\mathbf{z}}^1, \dots, \overline{\mathbf{z}}^N)$. Define $\alpha^N \in \mathcal{C}^{0,1}([0,\tau]; \mathscr{P}^N(\mathcal{Y}))$ by*

$$\alpha_t^N = \sum_{i=1}^N m^i \delta_{\mathbf{z}^i(t)}.$$

Then α^N is the unique weak solution of the compressible SG equations (in the sense of Definition 3.2.6) with discrete initial data $\alpha_0^N = \overline{\alpha}^N$. Moreover, α^N is energy-conserving in the sense that

$$E(\sigma_*[\alpha_t^N], \alpha_t^N) = E(\sigma_*[\alpha_0^N], \alpha_0^N) \quad \forall\, t \in [0,\tau].$$

Our second theorem states the existence of global-in-time weak solutions of the compressible SG equations (3.1) for arbitrary, compactly supported initial data.

Theorem 3.1.2 (Existence of weak geostrophic solutions)**.** *Let $\tau > 0$ be an arbitrary final time, and let $\overline{\alpha} \in \mathscr{P}_{\mathrm{c}}(\mathcal{Y})$ be an initial compactly-supported probability measure. Then there exists a weak solution $\alpha \in \mathcal{C}^{0,1}([0,\tau]; \mathscr{P}_{\mathrm{c}}(\mathcal{Y}))$ of the compressible SG equations with initial measure $\overline{\alpha}$ (in the sense of Definition 3.2.6). Moreover, there exist discrete weak solutions $\alpha^N \in \mathcal{C}^{0,1}([0,\tau]; \mathscr{P}^N(\mathcal{Y}))$ of the compressible SG equations that approximate α uniformly in the sense that*

$$\lim_{N\to\infty} \sup_{t\in[0,\tau]} W_1(\alpha_t^N, \alpha_t) = 0.$$

We stress that while the incompressible SG system considered in [8] involves the standard quadratic cost and a fixed source measure, the compressible SG system involves a non-standard cost c and a time-dependent source measure, defined by the minimisation problem (3.3). This presents new, significant challenges regarding the regularity of the centroid map $\mathbf{C}$.

Our method of proof gives rise naturally to a numerical method. Indeed, to show that the ODE (3.6) has a unique solution, we first derive a concave dual formulation of the energy minimisation problem (3.3) in the case where α_t is a discrete measure; see Section 3.3. We show that this dual problem is solvable and that its solution can be used to define the optimal source measure $\sigma_*[\alpha_t]$. While we do not compute numerical solutions here, the dual problem is an unconstrained, finite-dimensional, concave maximisation problem, which is numerically tractable. (The analogous problem with the quadratic cost is solved numerically for example

in [60].) Hence the velocity field in the ODE (3.6) can, in principle, be computed numerically. Importantly, solutions of the ODE (3.6) give rise to discrete, energy-conserving solutions of the PDE (3.1). It has been observed in the incompressible setting that numerical solutions inherit this conservation property [29, 48]. Implementing a numerical scheme based on these observations would be a natural extension to the compressible setting of Cullen and Purser's geometric method [25, 29].

3.1.2 Background

The Navier-Stokes equations are the fundamental mathematical model used by meteorologists to simulate the dynamics of the atmosphere and oceans. Since the viscosity of air is low, the atmosphere is often modelled as inviscid, so that the diffusion coefficient in the Navier-Stokes equations can be set to zero to obtain the Euler equations. At length scales on the order of tens of kilometres, such flows develop singularities known as atmospheric fronts. These can be modelled using the SG approximation, which is a good approximation for shallow, rotationally-dominated flows (small Rossby numbers). This approximation was first formulated in 1949 by Eliassen [30] and rediscovered in the 1970s by Hoskins [42]. Since then it has been studied extensively (see for example the book [19] and the bibliography therein) and the SG equations have been used as a diagnostic tool at the UK Met Office [18].

The SG approximation is based on two balances that dictate the dynamics of the system. The first is *hydrostatic balance*, namely the assumption that the vertical component of the pressure gradient is balanced by the gravitational force. The second is *geostrophic balance*, which assumes that the first two components of the pressure gradient are balanced by the Coriolis force [30]. The corresponding *geostrophic wind* (in physical variables) is a large-scale, two-dimensional approximation of the fluid velocity and is directed along isobars.

From a physical point of view, the model described by the SG equations conserves the *geostrophic energy*: the sum of kinetic, potential and internal energy. However, mathematically, the equations do not appear to be in a conservative form, as is the case for the well-known *quasi-geostrophic* reduction. This inconsistency was considered by Hoskins [42], who clarified the mathematical structure of the incompressible SG equations by an ingenious change of variables to the so-called *geostrophic* coordinates, sometimes called *dual coordinates*.

3.1.3 Previous results

The change of coordinates to geostrophic variables was made mathematically rigorous in the groundbreaking work of Benamou and Brenier [5], where the incompressible SG equations are formulated in geostrophic variables as a transport equation coupled to a Monge-Ampère equation. Brenier's solution of the optimal transport problem for the quadratic cost in [10] was used to prove the existence of global-in-time weak solutions of the incompressible SG equations in geostrophic variables. This seminal work provided the foundation for much of the subsequent analysis of the SG equations. Indeed, similar reformulations are established in [21] for the SG shallow water equations and in [24] for the compressible SG equations, which we study in this chapter, where the template of the proof given in [5] is used to prove global existence of weak solutions.

In [24] the existence of global-in-time solutions of the compressible SG equations is established for compactly-supported initial potential vorticity $\overline{\alpha} \in L^r(\mathcal{Y})$ for $r \in (1, \infty)$. The case $r = 1$ was added by Faria in [32]. We extend this result to $\overline{\alpha} \in \mathscr{P}_c(\mathcal{Y})$. However, in [24] the term in the cost function c representing the gravitational potential energy is taken to be any C^2 function whose derivative with respect to the vertical variable is non-zero, which is more general than the case we treat. The same result is proved in [23] using the general theory for Hamiltonian ODEs in Wasserstein space developed by Ambrosio and Gangbo in [4]. Additionally, [23] presents a proof of the existence of weak Lagrangian solutions in physical space, analogous to the results of Cullen, Feldman & Tudorascu for the incompressible SG equations [20, 33, 35, 36].

In [8] a *semi-discrete* optimal transport approach is used to prove the global existence of weak solutions for the *incompressible* SG equations for measure-valued initial data. Exact solutions of the incompressible SG equations are constructed starting from spatially discrete initial data. These discrete solutions are then used to approximate solutions for arbitrary initial data. Similar existence results were already established in increasing levels of generality in [5, 34, 38, 52]. The approach of [8] is distinct from those of earlier papers in its use of a spatial discretisation based on semi-discrete optimal transport, rather than a combination of time discretisation and spatial mollification as used in [5]. It is also distinct from the fully discrete approach used to study a variant of the incompressible SG equations in [22], where both physical and geostrophic variables are spatially discretised. While we cannot give here an exhaustive reference list to what is now a very substantial body of work, other important

contributions to the analysis of the SG equations include the works of Ambrosio et al. [1, 2] and recent work on the incompressible SG equations with non-constant Coriolis term [62]. In this chapter we assume that the Coriolis term is constant.

Numerical methods for the SG equations date back to the development of the geometric method of Cullen & Purser [25]. More recently, major developments in the field of numerical optimal transport have given rise to efficient numerical methods for solving the SG equations. Semi-discrete optimal transport has been used to obtain solutions of the 2D SG Eady slice equations [29] and the 3D incompressible SG equations [48], while entropy-regularised discrete optimal transport [6, 12] has also been used to solve the Eady slice equations. Other applications of semi-discrete optimal transport in fluid dynamics are studied for example in [40, 41]. The finite element method has recently been used to solve a 2D version of the compressible SG equations [67].

3.1.4 Outline of the chapter

Section 3.2 includes notation, background material, and the definition of a weak solution of (3.1). In Section 3.3 we derive a dual formulation of the energy minimisation problem (3.3) and in Section 3.4 we prove Theorem 3.1.1. Our main theorem, Theorem 3.1.2, is proved in Section 3.5. In Section 3.6 we give two explicit solutions of the compressible SG equations, namely an absolutely continuous steady state solution and a discrete solution with a single particle. In § 3.7.1 we discuss a technical assumption on the fluid domain. In § 3.7.2 we prove a technical lemma, Lemma 3.3.6, which is important for establishing the regularity of the centroid map $\mathbf{C}$.

3.2 Preliminaries

3.2.1 Assumptions

Throughout this chapter we make the following assumptions:

- $\mathcal{X} \subset \mathbb{R}^3$ denotes the fluid domain. We assume that $\mathcal{X}$ is nonempty, connected, compact, and that it coincides with the closure of its interior. Moreover, we assume that the set $\Phi^{-1}(\mathcal{X})$ is convex, where $\Phi : \mathbb{R}^3 \to \mathbb{R}^3$ is defined by

$$\Phi(\mathbf{x}) = \left(f_{\text{cor}}^{-2}\, x_1,\ f_{\text{cor}}^{-2}\, x_2,\ g^{-1}\left(x_3 - \tfrac{1}{2} f_{\text{cor}}^{-2}\left(x_1^2 + x_2^2\right)\right)\right). \tag{3.7}$$

  In Section 3.7.1 we give examples of domains satisfying this assumption and show that it

is equivalent to assuming that $\mathcal{X}$ is *c-convex* [46, Definition 1.2], which is an important notion in regularity theory for semi-discrete optimal transport. We require this technical assumption to prove Lemma 3.3.6.

- $\mathcal{Y} = \mathbb{R}^2 \times (\delta, \frac{1}{\delta})$ denotes the geostrophic domain, where $\delta \in (0, 1)$. This is equivalent to assuming that the initial potential temperature of the fluid is bounded away from zero and infinity.

- We always equip $\mathscr{P}_{\mathrm{c}}(\mathcal{Y})$ with the W_1 Wasserstein metric, which is defined by $W_1 : \mathscr{P}_{\mathrm{c}}(\mathcal{Y}) \times \mathscr{P}_{\mathrm{c}}(\mathcal{Y}) \to [0, \infty)$,

$$W_1(\alpha, \beta) = \inf \left\{ \int_{\mathcal{Y}\times\mathcal{Y}} \|\mathbf{y} - \tilde{\mathbf{y}}\| \, \mathrm{d}\gamma(\mathbf{y}, \tilde{\mathbf{y}}) : \gamma \in \mathscr{P}(\mathcal{Y} \times \mathcal{Y}) \right\}, \tag{3.8}$$

  where $\pi_{1\#}\gamma = \alpha$ and $\pi_{2\#}\gamma = \beta$ such that $\pi_1 : \mathcal{Y} \times \mathcal{Y} \to \mathcal{Y}$ is defined by $\pi_1(\mathbf{y}, \tilde{\mathbf{y}}) = \mathbf{y}$ and $\pi_2 : \mathcal{Y} \times \mathcal{Y} \to \mathcal{Y}$ is defined by $\pi_1(\mathbf{y}, \tilde{\mathbf{y}}) = \tilde{\mathbf{y}}$.

3.2.2 The compressible SG equations

In this section we define weak solutions of (3.1).

Definition 3.2.1 (The cost function)**.** The cost function $c : \mathcal{X} \times \mathcal{Y} \to \mathbb{R}$ associated with the compressible SG equations is given by

$$c(\mathbf{x}, \mathbf{y}) = \frac{1}{y_3} \left(\frac{f_{\mathrm{cor}}^2}{2}(x_1 - y_1)^2 + \frac{f_{\mathrm{cor}}^2}{2}(x_2 - y_2)^2 + g x_3 \right). \tag{3.9}$$

It is easy to check that c is *twisted*, namely that c is differentiable in $\mathbf{x}$ and that the map $\mathbf{y} \mapsto \nabla_{\mathbf{x}} c(\mathbf{x}, \mathbf{y})$ is injective for all $\mathbf{x} \in \mathcal{X}$ [59, Definition 1.16].

Note that, while the term gx_3 in (3.9) is physically motivated, it could be replaced by $\phi(\mathbf{x})$ for any function $\phi \in \mathcal{C}^2(\mathcal{X})$ such that $\partial_{x_3}\phi \neq 0$ (so that c is twisted). In [24] the existence of weak solutions of the compressible SG equations is proved in this more general setting, while the assumptions on the initial data in [24], as well as the subsequent [23] and [32], are more restrictive than ours.

Definition 3.2.2 (Optimal transport cost)**.** The optimal transport cost from $\sigma \in \mathscr{P}(\mathcal{X})$ to

$\alpha \in \mathscr{P}(\mathcal{Y})$ for the cost function c is defined by

$$\mathcal{T}_c(\sigma, \alpha) := \inf_{\substack{T:\mathcal{X}\to\mathcal{Y} \\ T_\#\sigma=\alpha}} \int_{\mathcal{X}} c(\mathbf{x}, T(\mathbf{x}))\, \mathrm{d}\sigma(\mathbf{x}). \tag{3.10}$$

If $\sigma \in \mathscr{P}_{\mathrm{ac}}(\mathcal{X})$ and $\alpha \in \mathscr{P}_{\mathrm{c}}(\mathcal{Y})$, then there exists a unique map $T : \mathcal{X} \to \mathcal{Y}$ achieving the minimum in (3.10); see, for example, [59]. We call T the *optimal transport map* from σ to α for the cost c.

Definition 3.2.3 (Geostrophic energy)**.** We define the compressible geostrophic energy functional $E : \mathscr{P}(\mathcal{X}) \times \mathscr{P}_{\mathrm{c}}(\mathcal{Y}) \to \mathbb{R} \cup \{+\infty\}$ by

$$E(\sigma, \alpha) = \mathcal{T}_c(\sigma, \alpha) + F(\sigma), \tag{3.11}$$

where $F : \mathscr{P}(\mathcal{X}) \to \mathbb{R} \cup \{+\infty\}$ is defined by

$$F(\sigma) = \begin{cases} \kappa \displaystyle\int_{\mathcal{X}} \sigma(\mathbf{x})^\gamma \, \mathrm{d}\mathbf{x} & \text{if } \sigma \in \mathscr{P}_{\mathrm{ac}}(\mathcal{X}), \\ +\infty & \text{otherwise,} \end{cases}$$

where $\gamma \in (1, 2)$ and $\kappa > 0$ are constants.

Lemma 3.2.4 (Existence and uniqueness of minimisers of E)**.** *Given $\alpha \in \mathscr{P}_{\mathrm{c}}(\mathcal{Y})$, the functional on $\mathscr{P}(\mathcal{X})$ defined by $\sigma \mapsto E(\sigma, \alpha)$ is strictly convex and has a unique minimiser $\sigma_* \in \mathscr{P}_{\mathrm{ac}}(\mathcal{X})$.*

Proof. This is proved in [24, Theorem 4.1] for the special case $\alpha \in \mathscr{P}_{\mathrm{ac}}(\mathcal{X})$. The functional $\mathscr{P}(\mathcal{X}) \ni \sigma \mapsto \mathcal{T}_c(\sigma, \alpha)$ is continuous and convex [59, Propositions 7.4 & 7.17], and F is lower semi-continuous and strictly convex [59, Proposition 7.7 & Section 7.2]. Therefore E is lower semi-continuous and strictly convex. Since $\mathcal{X}$ is compact, $\mathscr{P}(\mathcal{X})$ is compact with respect to weak convergence of measures. Therefore $E(\cdot, \alpha)$ has a minimiser σ_*, which belongs to $\mathscr{P}_{\mathrm{ac}}(\mathcal{X})$ because $E(\cdot, \alpha)$ takes the value $+\infty$ on $\mathscr{P}(\mathcal{X}) \setminus \mathscr{P}_{\mathrm{ac}}(\mathcal{X})$. Since E is strictly convex, its minimiser is unique. □

Definition 3.2.5 (Optimal source measure and transport map)**.** Given $\alpha \in \mathscr{P}_{\mathrm{c}}(\mathcal{Y})$, we define the map $\sigma_* : \mathscr{P}_{\mathrm{c}}(\mathcal{Y}) \to \mathscr{P}_{\mathrm{ac}}(\mathcal{X})$ by

$$\sigma_*[\alpha] = \operatorname*{arg\,min}_{\sigma \in \mathscr{P}_{\mathrm{ac}}(\mathcal{X})} E(\sigma, \alpha). \tag{3.12}$$

We denote by $T_\alpha : \mathcal{X} \to \mathcal{Y}$ the optimal transport map from $\sigma_*[\alpha]$ to α for the cost c.

The formulation of the compressible SG equations given in (3.1) and (3.4) is formal because the inverse of T_{α_t} may not be well defined. For example, if α_t is discrete, then T_{α_t} sends a set of positive Lebesgue measure to each point in the support of α_t, violating injectivity. We therefore introduce a suitable weak formulation of (3.1).

To derive the weak formulation, we assume provisionally that $T_{\alpha_t}^{-1}$ exists and that all functions appearing in (3.1) are sufficiently regular. Multiplying (3.1) by $\varphi \in \mathcal{C}_c^\infty(\mathcal{Y} \times \mathbb{R})$ and integrating by parts over the domain $\mathcal{Y} \times [0, \tau]$ yields

$$\int_0^\tau \int_{\mathcal{Y}} \big(\partial_t \varphi_t(\mathbf{y}) + J\big(\mathbf{y} - T_{\alpha_t}^{-1}(\mathbf{y})\big) \cdot \nabla \varphi_t(\mathbf{y})\big) \, \mathrm{d}\alpha_t(\mathbf{y}) \mathrm{d}t = \int_{\mathcal{Y}} \varphi_\tau(\mathbf{y}) \, \mathrm{d}\alpha_\tau(\mathbf{y}) - \int_{\mathcal{Y}} \varphi_0(\mathbf{y}) \, \mathrm{d}\alpha_0(\mathbf{y}),$$

where we have used the notation $\varphi_t(\mathbf{y}) := \varphi(\mathbf{y}, t)$. By using the push-forward constraint $(T_{\alpha_t})_\# \sigma_*[\alpha_t] = \alpha_t$ to rewrite the term involving $T_{\alpha_t}^{-1}$, we arrive at the following weak formulation of the compressible SG equations.

Definition 3.2.6 (Weak solution)**.** We say that $\alpha \in \mathcal{C}([0, \tau]; \mathscr{P}_{\mathrm{c}}(\mathcal{Y}))$ is a *weak solution* of the compressible SG equation (3.1) with initial condition $\alpha_0 = \overline{\alpha} \in \mathscr{P}_{\mathrm{c}}(\mathcal{Y})$ if for all $\varphi \in \mathcal{C}_c^\infty(\mathcal{Y} \times \mathbb{R})$,

$$\int_0^\tau \int_{\mathcal{Y}} \left[\partial_t \varphi_t(\mathbf{y}) + (J\mathbf{y}) \cdot \nabla \varphi_t(\mathbf{y})\right] \, \mathrm{d}\alpha_t(\mathbf{y}) \, \mathrm{d}t - \int_0^\tau \int_{\mathcal{X}} (J\mathbf{x}) \cdot \nabla \varphi_t(T_{\alpha_t}(\mathbf{x})) \, \mathrm{d}\sigma_*[\alpha_t](\mathbf{x}) \, \mathrm{d}t$$
$$= \int_{\mathcal{Y}} \varphi_\tau(\mathbf{y}) \, \mathrm{d}\alpha_\tau(\mathbf{y}) - \int_{\mathcal{Y}} \varphi_0(\mathbf{y}) \, \mathrm{d}\overline{\alpha}(\mathbf{y}). \quad (3.13)$$

Remark 3.2.7 (Equivalent weak formulation)*.* Following [6, 12], the nonlinear term in (3.13) can be rewritten as a term that is *linear* in the optimal transport plan:

$$\int_0^\tau \int_{\mathcal{X}} (J\mathbf{x}) \cdot \nabla \varphi_t(T_{\alpha_t}(\mathbf{x})) \, \mathrm{d}\sigma_*[\alpha_t](\mathbf{x}) \, \mathrm{d}t = \int_0^\tau \int_{\mathcal{X} \times \mathcal{Y}} (J\mathbf{x}) \cdot \nabla \varphi_t(\mathbf{y}) \, \mathrm{d}\gamma[\alpha_t](\mathbf{x}, \mathbf{y}) \, \mathrm{d}t, \quad (3.14)$$

where $\gamma[\alpha_t] = (\mathrm{Id}_{\mathcal{X}} \times T_{\alpha_t})_\# \sigma_*[\alpha_t]$ is the optimal plan for transporting $\sigma_*[\alpha_t]$ to α_t.

3.2.3 Semi-discrete optimal transport

In this section we summarise a key definition used throughout this chapter. Here $N \in \mathbb{N}$ is any natural number.

We say that a discrete probability measure $\sum_{i=1}^{N} m^i \delta_{\mathbf{z}^i} \in \mathscr{P}^N(\mathcal{Y})$ is *well-prepared* if

$$\mathbf{z} \in D_0^N \text{ where } D_0^N \coloneqq \left\{ \mathbf{z} \in D^N \,:\, z_3^i \neq z_3^j \;\forall\, i,j \in \{1,\dots,N\},\, i \neq j \right\}. \tag{3.15}$$

In other words, a discrete measure is well-prepared if the seeds $\mathbf{z}^i$ lie in distinct horizontal planes.

Definition 3.2.8 (c-Laguerre tessellation)**.** Given $(\boldsymbol{w}, \mathbf{z}) \in \mathbb{R}^N \times D^N$, the *$c$-Laguerre tessellation of $\mathcal{X}$ generated by* $(\boldsymbol{w}, \mathbf{z})$ is the collection of *Laguerre cells* $\{L_c^i(\boldsymbol{w}, \mathbf{z})\}_{i=1}^N$ defined by

$$L_c^i(\boldsymbol{w}, \mathbf{z}) \coloneqq \left\{ \mathbf{x} \in \mathcal{X} : c(\mathbf{x}, \mathbf{z}^i) - w^i \leq c(\mathbf{x}, \mathbf{z}^j) - w^j \;\forall\, j \in \{1,\dots,N\} \right\}, \quad i \in \{1,\dots,N\}.$$

The c-Laguerre cells form a tessellation of $\mathcal{X}$ in the sense that $\bigcup_{i=1}^N L_c^i(\boldsymbol{w}, \mathbf{z}) = \mathcal{X}$ and $\mathcal{L}^3\big(L_c^i(\boldsymbol{w}, \mathbf{z}) \cap L_c^j(\boldsymbol{w}, \mathbf{z})\big) = 0$ if $i \neq j$ (by [53, Proposition 37]). Intuitively, changing the *weight vector* $\boldsymbol{w} = (w^1, \dots, w^N)$ shifts the boundaries of the Laguerre cells, thus controlling their volumes. It is easy to check that if $\mathbf{z} \in D_0^N$, then each Laguerre cell $L_c^i(\boldsymbol{w}, \mathbf{z})$ is the intersection of $\mathcal{X}$ with $N-1$ paraboloids of the form

$$\left\{ \mathbf{x} \in \mathbb{R}^3 : x_3 \leq -\frac{f_{\mathrm{cor}}^2}{2g} \left((x_1 - a_1)^2 + (x_2 - a_2)^2 \right) + b \right\},$$

where $a_1, a_2 \in \mathbb{R}$ depend on $\mathbf{z}$ and $b \in \mathbb{R}$ depends on $(\boldsymbol{w}, \mathbf{z})$. In Figure 3.2 we plot c-Laguerre tessellations in two dimensions for the following 2D version of the cost (3.9):

$$c_{\mathrm{2d}}((x_1, x_3), (y_1, y_3)) = \frac{1}{y_3} \left(\frac{f_{\mathrm{cor}}^2}{2} (x_1 - y_1)^2 + g x_3 \right). \tag{3.16}$$

Characterisation of the optimal transport map

It is well known (e.g., [53, Section 4]) that the optimal transport map $T : \mathcal{X} \to \mathcal{Y}$ from an absolutely continuous source measure $\sigma \in \mathcal{P}_{\mathrm{ac}}(\mathcal{X})$ to a discrete measure $\alpha^N \in \mathscr{P}^N(\mathcal{Y})$ for the cost c is given by

$$T = \sum_{i=1}^{N} \mathbf{z}^i \mathbb{1}_{L_c^i(\boldsymbol{w}, \mathbf{z})}, \tag{3.17}$$

where $\boldsymbol{w} \in \mathbb{R}^N$ satisfies

$$\sigma(L_c^i(\boldsymbol{w}, \mathbf{z})) = m^i \quad \forall\, i \in \{1, \dots, N\}. \tag{3.18}$$

In other words, T is the piecewise constant function given by $T(\mathbf{x}) = \mathbf{z}^i$ if $\mathbf{x} \in L_c^i(\boldsymbol{w}, \mathbf{z})$. As a consequence of the fact that c is twisted and of [53, Proposition 37], the intersection of any two c-Laguerre cells has zero Lebesgue measure, and hence T is well-defined $\mathcal{L}^3$-almost everywhere. In addition, by [53, Theorem 40], $\boldsymbol{w}$ satisfies (3.18) if and only if it maximises the *dual transport functional*, namely, if and only if it satisfies

$$\begin{aligned}
&\sum_{i=1}^N \left(m^i w^i + \int_{L_c^i(\boldsymbol{w},\mathbf{z})} \big(c(\mathbf{x}, \mathbf{z}^i) - w^i\big)\, \mathrm{d}\sigma(\mathbf{x}) \right) \\
&= \max_{\widetilde{\boldsymbol{w}} \in \mathbb{R}^N} \sum_{i=1}^N \left(m^i \widetilde{w}^i + \int_{L_c^i(\widetilde{\boldsymbol{w}},\mathbf{z})} \big(c(\mathbf{x}, \mathbf{z}^i) - \widetilde{w}^i\big)\, \mathrm{d}\sigma(\mathbf{x}) \right) = \mathcal{T}_c(\sigma, \alpha^N),
\end{aligned} \tag{3.19}$$

where the second equality follows from the well-known Kantorovich Duality Theorem.

3.3 The dual problem

In this section we derive a dual formulation of the minimisation problem (3.12) for the case where α is a discrete measure. Additionally, we prove necessary and sufficient optimality conditions that characterise the optimal source measure $\sigma_*[\alpha]$ in terms of the solution of the dual problem. The main results are contained in Theorem 3.3.4.

Given $(\boldsymbol{w}, \mathbf{z}) \in \mathbb{R}^N \times D^N$, recall that the c-transform of $\boldsymbol{w}$ is the function $\boldsymbol{w}^c(\,\cdot\,; \mathbf{z}) : \mathcal{X} \to \mathbb{R}$ defined by

$$\boldsymbol{w}^c(\mathbf{x}; \mathbf{z}) = \min_{i \in \{1,\dots,N\}} \big\{ c(\mathbf{x}, \mathbf{z}^i) - w^i \big\}.$$

In particular, $\boldsymbol{w}^c(\mathbf{x}; \mathbf{z}) = c(\mathbf{x}, \mathbf{z}^i) - w^i$ if and only if $\mathbf{x} \in L_c^i(\boldsymbol{w}, \mathbf{z})$.

Definition 3.3.1 (Dual functional)**.** Given $\mathbf{m} \in \Delta^N$, define the dual functional $\mathcal{G} : \mathbb{R}^N \times D^N \to \mathbb{R}$ by

$$\mathcal{G}(\boldsymbol{w}, \mathbf{z}) = \sum_{i=1}^N m^i w^i - \int_{\mathcal{X}} f^*(-\boldsymbol{w}^c(\mathbf{x}; \mathbf{z}))\, \mathrm{d}\mathbf{x} = \sum_{i=1}^N \left(m^i w^i - \int_{L_c^i(\boldsymbol{w},\mathbf{z})} f^*(w^i - c(\mathbf{x}, \mathbf{z}^i))\, \mathrm{d}\mathbf{x} \right),$$

where $f^* : \mathbb{R} \to \mathbb{R}$ is the Legendre-Fenchel transform of the function $f : \mathbb{R} \to \mathbb{R}$ given by

$$f(s) = \begin{cases} \kappa s^\gamma & \text{if } s \geq 0, \\ +\infty & \text{if } s < 0, \end{cases}$$

where $\gamma \in (1, 2)$ and $\kappa > 0$.

Remark 3.3.2 (Properties of f). The function f is strictly convex on $[0, \infty)$, lower semi-continuous, and its Legendre-Fenchel transform is given by

$$f^*(t) \coloneqq \sup_{s \in \mathbb{R}} (st - f(s)) = \begin{cases} \frac{1}{\gamma'}(\kappa\gamma)^{1-\gamma'} t^{\gamma'} & \text{if } t > 0, \\ 0 & \text{if } t \leq 0, \end{cases}$$

where $\gamma' \in (2, \infty)$ satisfies $\frac{1}{\gamma} + \frac{1}{\gamma'} = 1$. Note that $f^* \in \mathcal{C}^2(\mathbb{R})$.

Remark 3.3.3 (Derivation of the dual functional). We give a short derivation of the dual functional before stating a rigorous duality theorem below (see Theorem 3.3.4). Here we identify vectors $\boldsymbol{w} \in \mathbb{R}^N$ with real-valued functions on the discrete set $\{\mathbf{z}^i\}_{i=1}^N$ via $\boldsymbol{w}(\mathbf{z}^i) = w^i$. Applying the standard Kantorovich Duality Theorem from optimal transport theory gives

$$\begin{aligned}
\inf_{\sigma \in \mathscr{P}_{\mathrm{ac}}(\mathcal{X})} E(\sigma, \alpha^N) &= \inf_{\sigma \in \mathscr{P}_{\mathrm{ac}}(\mathcal{X})} \Big(\mathcal{T}_c(\sigma, \alpha^N) + F(\sigma) \Big) \\
&= \inf_{\sigma \in \mathscr{P}_{\mathrm{ac}}(\mathcal{X})} \left(\sup_{\boldsymbol{w} \in \mathbb{R}^N} \left(\int_{\mathcal{X}} \boldsymbol{w}^c \, \mathrm{d}\sigma + \int_{\mathcal{Y}} \boldsymbol{w} \, \mathrm{d}\alpha^N \right) + F(\sigma) \right) \\
&\geq \sup_{\boldsymbol{w} \in \mathbb{R}^N} \inf_{\sigma \in \mathscr{P}_{\mathrm{ac}}(\mathcal{X})} \left(\int_{\mathcal{X}} \boldsymbol{w}^c \, \mathrm{d}\sigma + \int_{\mathcal{Y}} \boldsymbol{w} \, \mathrm{d}\alpha^N + F(\sigma) \right) \\
&= \sup_{\boldsymbol{w} \in \mathbb{R}^N} \left(\int_{\mathcal{Y}} \boldsymbol{w} \, \mathrm{d}\alpha^N - \underbrace{\sup_{\sigma \in \mathscr{P}_{\mathrm{ac}}(\mathcal{X})} \left(\int_{\mathcal{X}} (-\boldsymbol{w}^c) \, \mathrm{d}\sigma - F(\sigma) \right)}_{= F^*(-\boldsymbol{w}^c)} \right) \\
&= \sup_{\boldsymbol{w} \in \mathbb{R}^N} \left(\sum_{i=1}^N m^i w^i - \int_{\mathcal{X}} f^*(-\boldsymbol{w}^c) \, \mathrm{d}\mathbf{x} \right) \\
&= \sup_{\boldsymbol{w} \in \mathbb{R}^N} \mathcal{G}(\boldsymbol{w}, \mathbf{z}).
\end{aligned}$$

In Theorem 3.3.4 we prove that the inf on the left-hand side is in fact a min, the sup on the right-hand side is in fact a max, and the inequality is an equality.

Theorem 3.3.4 (Duality Theorem). *Let $\mathbf{z} \in D^N$, $\mathbf{m} \in \Delta^N$ and define*

$$\alpha^N := \sum_{i=1}^{N} m^i \delta_{\mathbf{z}^i}.$$

Assume that $z_3^i \neq z_3^j$ for all $i, j \in \{1, \dots, N\}$ with $i \neq j$. Then the map $\sigma \mapsto E(\sigma, \alpha^N)$ is strictly convex and has a unique minimiser, and the map $\boldsymbol{w} \mapsto \mathcal{G}(\boldsymbol{w}, \mathbf{z})$ is concave and has a unique maximiser. Moreover,

$$\min_{\sigma \in \mathscr{P}_{\mathrm{ac}}(\mathcal{X})} E(\sigma, \alpha^N) = \max_{\boldsymbol{w} \in \mathbb{R}^N} \mathcal{G}(\boldsymbol{w}, \mathbf{z}). \tag{3.20}$$

Furthermore, $\sigma \in \mathscr{P}_{\mathrm{ac}}(\mathcal{X})$ minimises $E(\cdot, \alpha^N)$ and $\boldsymbol{w} \in \mathbb{R}^N$ maximises $\mathcal{G}(\cdot, \mathbf{z})$ if and only if

$$m^i = \int_{L_c^i(\boldsymbol{w}, \mathbf{z})} (f^*)'(w^i - c(\mathbf{x}, \mathbf{z}^i)) \, \mathrm{d}\mathbf{x} \quad \forall\, i \in \{1, \dots, N\}, \tag{3.21}$$

$$\sigma(\mathbf{x}) = (f^*)'(-\boldsymbol{w}^c(\mathbf{x}; \mathbf{z})) \quad \textit{for } \mathcal{L}^3\textit{-almost every } \mathbf{x} \in \mathcal{X}. \tag{3.22}$$

Theorem 3.3.4 is analogous to the duality result given in [60, Proposition 12] but with the cost c rather than the quadratic cost. Other closely related results include [51, Proposition 5.3] and [9, Theorems 3.1 and 3.2]. In addition, the Euler-Lagrange equation (3.22) can be derived from [59, Proposition 7.20].

Remark 3.3.5 (Optimal transport map). If $\sigma \in \mathscr{P}_{\mathrm{ac}}(\mathcal{X})$ minimises $E(\cdot, \alpha^N)$ and $\boldsymbol{w} \in \mathbb{R}^N$ maximises $\mathcal{G}(\cdot, \mathbf{z})$, then the optimality conditions (3.21) and (3.22) imply that the mass constraint (3.18) holds. In particular, this means that the map T given by (3.17) is the optimal transport map from σ to α^N for the cost c.

We begin by establishing the regularity of $\mathcal{G}$; see Proposition 3.3.8. To do this we use the following two lemmas, which will also be used in Section 3.4 to prove that the centroid map is continuously differentiable.

Lemma 3.3.6 (Regularity of integrals over Laguerre cells). *Let $U \subset \mathbb{R}^N \times D_0^N$ be the open set*

$$U = \left\{ (\boldsymbol{w}, \mathbf{z}) \in \mathbb{R}^N \times D_0^N \,:\, \mathcal{L}^3(L_c^i(\boldsymbol{w}, \mathbf{z})) > 0 \;\forall\, i \in \{1, \dots, N\} \right\}.$$

Define $\boldsymbol{\Psi} = (\Psi^1, \dots, \Psi^N) : U \to \mathbb{R}^N$ by

$$\Psi^i(\boldsymbol{w}, \mathbf{z}) := \int_{L_c^i(\boldsymbol{w}, \mathbf{z})} \zeta(\mathbf{x}, \boldsymbol{w}, \mathbf{z}) \, \mathrm{d}\mathbf{x},$$

where $\zeta : \mathcal{X} \times \mathbb{R}^N \times D^N \to \mathbb{R}$ *satisfies the following:*

- $\zeta(\cdot, \boldsymbol{w}, \mathbf{z}) \in \mathcal{C}(\mathcal{X})$ *for all* $(\boldsymbol{w}, \mathbf{z}) \in \mathbb{R}^N \times D^N$*;*
- *for each compact set* $K \subset \mathbb{R}^N \times D^N$, $\zeta(\mathbf{x}, \cdot, \cdot) \in \mathcal{C}^{0,1}(K)$ *for all* $\mathbf{x} \in \mathcal{X}$ *and there exists a constant* $L(K) > 0$ *such that* $\sup_{\mathbf{x} \in \mathcal{X}} \operatorname{Lip}(\zeta(\mathbf{x}, \cdot, \cdot)|_K) \leq L(K)$*;*
- *for each* $(\boldsymbol{w}_0, \mathbf{z}_0) \in \mathbb{R}^N \times D^N$*, there exists an open set* $S(\boldsymbol{w}_0, \mathbf{z}_0) \subseteq \mathcal{X}$ *with* $\mathcal{L}^3(\mathcal{X} \setminus S(\boldsymbol{w}_0, \mathbf{z}_0)) = 0$ *such that the partial derivatives* $\partial\zeta/\partial\boldsymbol{w}(\mathbf{x}, \cdot, \cdot)$, $\partial\zeta/\partial\mathbf{z}(\mathbf{x}, \cdot, \cdot)$ *exist and are continuous at* $(\boldsymbol{w}_0, \mathbf{z}_0)$ *for all* $\mathbf{x} \in S(\boldsymbol{w}_0, \mathbf{z}_0)$*.*

Then $\boldsymbol{\Psi}$ *is continuously differentiable. Moreover, for all* $i, j \in \{1, \dots, N\}$, $i \neq j$,

$$\frac{\partial \Psi^i}{\partial w^j}(\boldsymbol{w}, \mathbf{z}) = \int_{L_c^i(\boldsymbol{w}, \mathbf{z})} \frac{\partial \zeta}{\partial w^j}(\mathbf{x}, \boldsymbol{w}, \mathbf{z}) \, \mathrm{d}\mathbf{x} - \int_{L_c^i(\boldsymbol{w}, \mathbf{z}) \cap L_c^j(\boldsymbol{w}, \mathbf{z})} \frac{\zeta(\mathbf{x}, \boldsymbol{w}, \mathbf{z})}{\|\nabla_{\mathbf{x}} c(\mathbf{x}, \mathbf{z}^i) - \nabla_{\mathbf{x}} c(\mathbf{x}, \mathbf{z}^j)\|} \, \mathrm{d}\mathcal{H}^2(\mathbf{x}),$$

$$\frac{\partial \Psi^i}{\partial \mathbf{z}^j}(\boldsymbol{w}, \mathbf{z}) = \int_{L_c^i(\boldsymbol{w}, \mathbf{z})} \frac{\partial \zeta}{\partial \mathbf{z}^j}(\mathbf{x}, \boldsymbol{w}, \mathbf{z}) \, \mathrm{d}\mathbf{x} + \int_{L_c^i(\boldsymbol{w}, \mathbf{z}) \cap L_c^j(\boldsymbol{w}, \mathbf{z})} \frac{\nabla_{\mathbf{y}} c(\mathbf{x}, \mathbf{z}^j) \, \zeta(\mathbf{x}, \boldsymbol{w}, \mathbf{z})}{\|\nabla_{\mathbf{x}} c(\mathbf{x}, \mathbf{z}^i) - \nabla_{\mathbf{x}} c(\mathbf{x}, \mathbf{z}^j)\|} \, \mathrm{d}\mathcal{H}^2(\mathbf{x}),$$

and

$$\frac{\partial \Psi^i}{\partial w^i}(\boldsymbol{w}, \mathbf{z}) = \int_{L_c^i(\boldsymbol{w}, \mathbf{z})} \frac{\partial \zeta}{\partial w^i}(\mathbf{x}, \boldsymbol{w}, \mathbf{z}) \, \mathrm{d}\mathbf{x} + \sum_{j \neq i} \int_{L_c^i(\boldsymbol{w}, \mathbf{z}) \cap L_c^j(\boldsymbol{w}, \mathbf{z})} \frac{\zeta(\mathbf{x}, \boldsymbol{w}, \mathbf{z})}{\|\nabla_{\mathbf{x}} c(\mathbf{x}, \mathbf{z}^i) - \nabla_{\mathbf{x}} c(\mathbf{x}, \mathbf{z}^j)\|} \, \mathrm{d}\mathcal{H}^2(\mathbf{x}),$$

$$\frac{\partial \Psi^i}{\partial \mathbf{z}^i}(\boldsymbol{w}, \mathbf{z}) = \int_{L_c^i(\boldsymbol{w}, \mathbf{z})} \frac{\partial \zeta}{\partial \mathbf{z}^i}(\mathbf{x}, \boldsymbol{w}, \mathbf{z}) \, \mathrm{d}\mathbf{x} - \sum_{j \neq i} \int_{L_c^i(\boldsymbol{w}, \mathbf{z}) \cap L_c^j(\boldsymbol{w}, \mathbf{z})} \frac{\nabla_{\mathbf{y}} c(\mathbf{x}, \mathbf{z}^j) \, \zeta(\mathbf{x}, \boldsymbol{w}, \mathbf{z})}{\|\nabla_{\mathbf{x}} c(\mathbf{x}, \mathbf{z}^i) - \nabla_{\mathbf{x}} c(\mathbf{x}, \mathbf{z}^j)\|} \, \mathrm{d}\mathcal{H}^2(\mathbf{x}).$$

Proof. The proof is rather technical and is given in § 3.7.2. □

Note that the set U in the statement of Lemma 3.3.6 is open because the map $(\boldsymbol{w}, \mathbf{z}) \mapsto \mathcal{L}^3(L_c^i(\boldsymbol{w}, \mathbf{z}))$ is continuous; cf. [53, Proposition 38(vii)]. The constraint that the seeds in U satisfy $|z_3^i - z_3^j| > 0$ is not necessary, but it is sufficient for our purposes and it slightly simplifies the proof.

Lemma 3.3.7. *Define* $\zeta : \mathcal{X} \times \mathbb{R}^N \times D^N \to \mathbb{R}$ *by*

$$\zeta(\mathbf{x}, \boldsymbol{w}, \mathbf{z}) := (f^*)'(-\boldsymbol{w}^c(\mathbf{x}; \mathbf{z})).$$

Then ζ *satisfies the assumptions of Lemma 3.3.6.*

Proof. Since $(f^*)'$ is non-decreasing, we have that

$$\zeta(\mathbf{x}, \boldsymbol{w}, \mathbf{z}) = (f^*)'\Big(- \min_{i\in\{1,\dots,N\}} (c(\mathbf{x}, \mathbf{z}^i) - w^i)\Big) = \max_{i\in\{1,\dots,N\}} (f^*)'(w^i - c(\mathbf{x}, \mathbf{z}^i)).$$

For each $i \in \{1, \dots, N\}$, define $\zeta^i : \mathcal{X} \times \mathbb{R}^N \times D^N \to \mathbb{R}$ by

$$\zeta^i(\mathbf{x}, \boldsymbol{w}, \mathbf{z}) = (f^*)'(w^i - c(\mathbf{x}, \mathbf{z}^i)). \tag{3.23}$$

Then ζ^i is continuously differentiable because $(f^*)'$ and c are continuously differentiable.

Fix $(\boldsymbol{w}, \mathbf{z}) \in \mathbb{R}^N \times D^N$ and consider the function $\zeta(\cdot, \boldsymbol{w}, \mathbf{z}) = \max_i \zeta^i(\cdot, \boldsymbol{w}, \mathbf{z})$. For each $i \in \{1, \dots, N\}$ the function $\zeta^i(\cdot, \boldsymbol{w}, \mathbf{z})$ is globally Lipschitz on $\mathcal{X}$ because ζ^i is continuously differentiable and $\mathcal{X}$ is compact. Therefore $\zeta(\cdot, \boldsymbol{w}, \mathbf{z})$ is the pointwise maximum of a finite family of Lipschitz functions, hence Lipschitz. In particular, it is continuous.

Now we consider the functions $\zeta(\mathbf{x}, \cdot, \cdot) = \max_i \zeta^i(\mathbf{x}, \cdot, \cdot)$ indexed by $\mathbf{x} \in \mathcal{X}$. Let $K \subset \mathbb{R}^N \times D^N$ be compact. As above, $\zeta(\mathbf{x}, \cdot, \cdot)|_K$ is the pointwise maximum of a finite family of of Lipschitz functions, hence Lipschitz. Moreover, the Lipschitz constant of $\zeta^i(\mathbf{x}, \cdot, \cdot)|_K$ can be bounded from above by a constant $L^i(K)$ independent of $\mathbf{x}$ since $\partial\zeta^i/\partial\boldsymbol{w}$, $\partial\zeta^i/\partial\mathbf{z}$ are continuous, and $\mathcal{X}$ and K are compact. Therefore $\sup_{\mathbf{x}\in\mathcal{X}} \operatorname{Lip}(\zeta(\mathbf{x}, \cdot, \cdot)|_K) \le \max_i L^i(K) =: L(K)$, as required.

Let $(\boldsymbol{w}_0, \mathbf{z}_0) \in \mathbb{R}^N \times D^N$ and define $S(\boldsymbol{w}_0, \mathbf{z}_0) = \bigcup_{j=1}^N \operatorname{int}(L_c^j(\boldsymbol{w}_0, \mathbf{z}_0))$. Since the cost c is twisted, $\mathcal{L}^3(\mathcal{X} \setminus S(\boldsymbol{w}_0, \mathbf{z}_0)) = 0$ by [53, Proposition 37]. For all $\mathbf{x} \in S(\boldsymbol{w}_0, \mathbf{z}_0)$, we have

$$\frac{\partial\zeta}{\partial w^i}(\mathbf{x}, \boldsymbol{w}_0, \mathbf{z}_0) = \begin{cases} (f^*)''(w_0^i - c(\mathbf{x}, \mathbf{z}_0^i)) & \text{if } \mathbf{x} \in \operatorname{int}(L_c^i(\boldsymbol{w}_0, \mathbf{z}_0)), \\ 0 & \text{if } \mathbf{x} \in \operatorname{int}(L_c^j(\boldsymbol{w}_0, \mathbf{z}_0)) \text{ for } j \neq i, \end{cases}$$

$$\frac{\partial\zeta}{\partial \mathbf{z}^i}(\mathbf{x}, \boldsymbol{w}_0, \mathbf{z}_0) = \begin{cases} -\nabla_{\mathbf{y}} c(\mathbf{x}, \mathbf{z}_0^i)(f^*)''(w_0^i - c(\mathbf{x}, \mathbf{z}_0^i)) & \text{if } \mathbf{x} \in \operatorname{int}(L_c^i(\boldsymbol{w}_0, \mathbf{z}_0)), \\ 0 & \text{if } \mathbf{x} \in \operatorname{int}(L_c^j(\boldsymbol{w}_0, \mathbf{z}_0)) \text{ for } j \neq i. \end{cases}$$

(Note that the partial derivatives do not exist if $\mathbf{x} \in L_c^i(\boldsymbol{w}_0, \mathbf{z}_0) \cap L_c^j(\boldsymbol{w}_0, \mathbf{z}_0)$ for $j \neq i$.) In particular, for all $\mathbf{x} \in S(\boldsymbol{w}_0, \mathbf{z}_0)$, the partial derivatives $\partial\zeta/\partial\boldsymbol{w}(\mathbf{x}, \cdot, \cdot)$, $\partial\zeta/\partial\mathbf{z}(\mathbf{x}, \cdot, \cdot)$ exist at $(\boldsymbol{w}_0, \mathbf{z}_0)$. Now we prove that the partial derivatives are continuous. Let $\mathbf{x} \in S(\boldsymbol{w}_0, \mathbf{z}_0)$. Then

there exists $i \in \{1, \dots, N\}$ such that $\mathbf{x} \in \operatorname{int}(L_c^i(\boldsymbol{w}_0, \mathbf{z}_0))$, so

$$c(\mathbf{x}, \mathbf{z}_0^i) - w_0^i < c(\mathbf{x}, \mathbf{z}_0^j) - w_0^j \quad \forall\, j \in \{1, \dots, N\} \setminus \{i\}.$$

Since the inequality is strict and c is continuous, $\mathbf{x} \in \operatorname{int}(L_c^i(\boldsymbol{w}, \mathbf{z}))$ for all $(\boldsymbol{w}, \mathbf{z})$ sufficiently close to $(\boldsymbol{w}_0, \mathbf{z}_0)$, and

$$\frac{\partial \zeta}{\partial w^i}(\mathbf{x}, \boldsymbol{w}, \mathbf{z}) - \frac{\partial \zeta}{\partial w^i}(\mathbf{x}, \boldsymbol{w}_0, \mathbf{z}_0) =$$

$$\begin{cases} (f^*)''(w^i - c(\mathbf{x}, \mathbf{z}^i)) - (f^*)''(w_0^i - c(\mathbf{x}, \mathbf{z}_0^i)) & \text{if } \mathbf{x} \in \operatorname{int}(L_c^i(\boldsymbol{w}_0, \mathbf{z}_0)), \\ 0 & \text{if } \mathbf{x} \in \operatorname{int}(L_c^j(\boldsymbol{w}_0, \mathbf{z}_0)) \text{ for } j \neq i. \end{cases}$$

Since $(f^*)''$ and c are continuous, it follows that $\partial\zeta/\partial\boldsymbol{w}(\mathbf{x}, \cdot, \cdot)$ is continuous at $(\boldsymbol{w}_0, \mathbf{z}_0)$. Similarly, it can be shown that $\partial\zeta/\partial\mathbf{z}(\mathbf{x}, \cdot, \cdot)$ is continuous at $(\boldsymbol{w}_0, \mathbf{z}_0)$. This completes the proof. □

Proposition 3.3.8 (Regularity of $\mathcal{G}$)**.** *Let $\mathbf{z} \in D^N$ and $\boldsymbol{w} \in \mathbb{R}^N$. Then $\mathcal{G}(\cdot, \mathbf{z}) \in \mathcal{C}^1(\mathbb{R}^N)$, $\mathcal{G}(\boldsymbol{w}, \cdot) \in \mathcal{C}^1(D^N)$, and*

$$\frac{\partial \mathcal{G}}{\partial w^i}(\boldsymbol{w}, \mathbf{z}) = m^i - \int_{L_c^i(\boldsymbol{w}, \mathbf{z})} (f^*)'(w^i - c(\mathbf{x}, \mathbf{z}^i))\, \mathrm{d}\mathbf{x}, \tag{3.24}$$

$$\frac{\partial \mathcal{G}}{\partial \mathbf{z}^i}(\boldsymbol{w}, \mathbf{z}) = \int_{L_c^i(\boldsymbol{w}, \mathbf{z})} \nabla_{\mathbf{y}} c(\mathbf{x}, \mathbf{z}^i)\, (f^*)'(w^i - c(\mathbf{x}, \mathbf{z}^i))\, \mathrm{d}\mathbf{x}, \tag{3.25}$$

for all $i \in \{1, \dots, N\}$. Moreover, if $\mathbf{z} \in D^N$ satisfies $z_3^i \neq z_3^j$ for all $i, j \in \{1, \dots, N\}$, $i \neq j$, and $\boldsymbol{w} \in \mathbb{R}^N$ satisfies $\mathcal{L}^3(L_c^i(\boldsymbol{w}, \mathbf{z})) > 0$ for all $i \in \{1, \dots, N\}$, then $\mathcal{G}$ is twice continuously differentiable at $(\boldsymbol{w}, \mathbf{z})$, and the second-order partial derivatives of $\mathcal{G}$ with respect to $\boldsymbol{w}$ are

$$\begin{cases} \dfrac{\partial^2 \mathcal{G}}{\partial w^i \partial w^j}(\boldsymbol{w}, \mathbf{z}) & = \displaystyle\int_{L_c^i(\boldsymbol{w}, \mathbf{z}) \cap L_c^j(\boldsymbol{w}, \mathbf{z})} \frac{(f^*)'(w^i - c(\mathbf{x}, \mathbf{z}^i))}{\|\nabla_{\mathbf{x}} c(\mathbf{x}, \mathbf{z}^i) - \nabla_{\mathbf{x}} c(\mathbf{x}, \mathbf{z}^j)\|}\, \mathrm{d}\mathcal{H}^2(\mathbf{x}) \quad \text{for } j \neq i, \\ \dfrac{\partial^2 \mathcal{G}}{\partial w^i \partial w^i}(\boldsymbol{w}, \mathbf{z}) & = -\displaystyle\int_{L_c^i(\boldsymbol{w}, \mathbf{z})} (f^*)''(w^i - c(\mathbf{x}, \mathbf{z}^i))\, \mathrm{d}\mathbf{x} - \sum_{j \neq i} \frac{\partial^2 \mathcal{G}}{\partial w^i \partial w^j}(\boldsymbol{w}, \mathbf{z}). \end{cases} \tag{3.26}$$

If in addition

$$\int_{L_c^i(\boldsymbol{w}, \mathbf{z})} (f^*)'(w^i - c(\mathbf{x}, \mathbf{z}^i))\, \mathrm{d}\mathbf{x} > 0 \tag{3.27}$$

for all $i \in \{1, \dots, N\}$, then the Hessian matrix $D^2_{\boldsymbol{ww}} \mathcal{G}(\boldsymbol{w}, \mathbf{z})$ is negative definite.

Proof. Fix $\mathbf{z}_0 \in D^N$. We begin by showing that $\mathcal{G}(\cdot, \mathbf{z}_0) \in \mathcal{C}^1(\mathbb{R}^N)$. Let $\boldsymbol{w}_0 \in \mathbb{R}^N$ and, as in the proof of Lemma 3.3.7, define the set

$$S(\boldsymbol{w}_0, \mathbf{z}_0) \coloneqq \bigcup_{j=1}^{N} \operatorname{int}(L_c^j(\boldsymbol{w}_0, \mathbf{z}_0)).$$

For any $\mathbf{x} \in S(\boldsymbol{w}_0, \mathbf{z}_0)$ there exists $i \in \{1, \dots, N\}$ and $\varepsilon > 0$ such that, for all $\boldsymbol{w} \in B_\varepsilon(\boldsymbol{w}_0)$,

$$c(\mathbf{x}, \mathbf{z}_0^i) - w^i < c(\mathbf{x}, \mathbf{z}_0^j) - w^j \quad \forall\, j \in \{1, \dots, N\}.$$

In particular, $\mathbf{x} \in L_c^i(\boldsymbol{w}, \mathbf{z}_0)$ for all $\boldsymbol{w} \in B_\varepsilon(\boldsymbol{w}_0)$, i.e.,

$$-\boldsymbol{w}^c(\mathbf{x}; \mathbf{z}) = w^i - c(\mathbf{x}, \mathbf{z}_0^i) \quad \forall\, \boldsymbol{w} \in B_\varepsilon(\boldsymbol{w}_0).$$

It follows that

$$\forall\, \mathbf{x} \in \operatorname{int}(L_c^i(\boldsymbol{w}_0, \mathbf{z}_0)), \quad \frac{\partial}{\partial w^j} f^*(-\boldsymbol{w}^c(\mathbf{x}; \mathbf{z}))\Big|_{\boldsymbol{w}=\boldsymbol{w}_0} = \begin{cases} (f^*)'(w_0^i - c(\mathbf{x}, \mathbf{z}_0^i)) & \text{if } j = i, \\ 0 & \text{otherwise.} \end{cases} \tag{3.28}$$

By continuity of $(f^*)'$,

$$\lim_{\boldsymbol{w} \to \boldsymbol{w}_0} (f^*)'(w^j - c(\mathbf{x}, \mathbf{z}_0^j)) \mathbb{1}_{L_c^j(\boldsymbol{w}, \mathbf{z}_0)}(\mathbf{x}) = (f^*)'(w_0^j - c(\mathbf{x}, \mathbf{z}_0^j)) \mathbb{1}_{L_c^j(\boldsymbol{w}_0, \mathbf{z}_0)}(\mathbf{x}) \tag{3.29}$$

for all $j \in \{1, \dots, N\}$.

As in the proof of Lemma 3.3.7, the map $\boldsymbol{w} \mapsto f^*(-\boldsymbol{w}^c(\mathbf{x}; \mathbf{z}))$ is locally Lipschitz continuous for all $\mathbf{x} \in \mathcal{X}$, and its Lipschitz constant can be bounded uniformly, independently of $\mathbf{x} \in \mathcal{X}$. Moreover, for all $\mathbf{x} \in S(\boldsymbol{w}_0, \mathbf{z}_0)$ this map is differentiable at $\boldsymbol{w}_0$ with derivative given by (3.28). Then, since $\mathcal{X}$ is compact and $\mathcal{X} \setminus S(\boldsymbol{w}_0, \mathbf{z}_0)$ is Lebesgue negligible, by the Dominated Convergence Theorem

$$\begin{aligned} \frac{\partial \mathcal{G}}{\partial w^j}(\boldsymbol{w}_0, \mathbf{z}_0) &= \frac{\partial}{\partial w^j} \left(\sum_{i=1}^{N} m^i w^i - \int_{\mathcal{X}} f^*(-\boldsymbol{w}^c(\mathbf{x}; \mathbf{z}))\, \mathrm{d}\mathbf{x} \right) \Bigg|_{\boldsymbol{w}=\boldsymbol{w}_0} \\ &= m^j - \int_{\mathcal{X}} \frac{\partial}{\partial w^j} f^*(-\boldsymbol{w}^c(\mathbf{x}; \mathbf{z}))\Big|_{\boldsymbol{w}=\boldsymbol{w}_0} \mathrm{d}\mathbf{x} \end{aligned}$$

$$= m^j - \int_{L_c^j(\boldsymbol{w}_0, \mathbf{z}_0)} (f^*)'(w_0^j - c(\mathbf{x}, \mathbf{z}_0^j))\,\mathrm{d}\mathbf{x}.$$

This establishes (3.24). Similarly, using (3.29) and applying the Dominated Convergence Theorem proves continuity of the partial derivatives of $\mathcal{G}(\cdot, \mathbf{z}_0)$ at $\boldsymbol{w}_0$. Since $\boldsymbol{w}_0$ was arbitrary, it follows that $\mathcal{G}(\cdot, \mathbf{z}_0) \in \mathcal{C}^1(\mathbb{R}^N)$. Analogously, it can be proved that (3.25) holds and that $\mathcal{G}(\boldsymbol{w}_0, \cdot) \in \mathcal{C}^1(D^N)$ for all $\boldsymbol{w}_0 \in \mathbb{R}^N$; we omit the proof for brevity.

Now suppose that $\mathbf{z} \in D^N$ satisfies $z_3^i \neq z_3^j$ for all $i, j \in \{1, \ldots, N\}$, $i \neq j$, and $\boldsymbol{w} \in \mathbb{R}^N$ satisfies $\mathcal{L}^3(L_c^i(\boldsymbol{w}, \mathbf{z})) > 0$ for all $i \in \{1, \ldots, N\}$. By Lemmas 3.3.6 and 3.3.7, and equations (3.24) and (3.25), $\mathcal{G}$ is twice continuously differentiable in a neighbourhood of $(\boldsymbol{w}, \mathbf{z})$ and its second-order partial derivatives with respect to $\boldsymbol{w}$ are given by (3.26).

In addition, suppose that the positivity constraint (3.27) holds. Then

$$\int_{L_c^i(\boldsymbol{w}, \mathbf{z})} (f^*)''(w^i - c(\mathbf{x}, \mathbf{z}^i))\,\mathrm{d}\mathbf{x} > 0$$

for all $i \in \{1, \ldots, N\}$. Using this inequality and the non-negativity of $(f^*)'$ and $(f^*)''$ gives

$$\left|\frac{\partial^2 \mathcal{G}}{\partial w^i \partial w^i}(\boldsymbol{w}, \mathbf{z})\right| - \sum_{j \neq i} \left|\frac{\partial^2 \mathcal{G}}{\partial w^i \partial w^j}(\boldsymbol{w}, \mathbf{z})\right| = \int_{L_c^i(\boldsymbol{w}, \mathbf{z})} (f^*)''(w^i - c(\mathbf{x}, \mathbf{z}^i))\,\mathrm{d}\mathbf{x} > 0.$$

Altogether, the Hessian $D^2_{\boldsymbol{w}\boldsymbol{w}}\mathcal{G}(\boldsymbol{w}, \mathbf{z})$ is strictly diagonally dominant, symmetric, and has negative diagonal entries, which implies that it is negative definite, as claimed. □

Now we prove the duality theorem, Theorem 3.3.4.

Proof of Theorem 3.3.4. By Lemma 3.2.4, $E(\cdot, \alpha^N)$ is strictly convex and has a unique minimiser over $\mathscr{P}_{\mathrm{ac}}(\mathcal{X})$.

Now we show that the maximum of $\mathcal{G}(\cdot, \mathbf{z})$ over $\mathbb{R}^N$ is attained. Since $\mathcal{G}(\cdot, \mathbf{z})$ is continuous, it suffices to show that $\lim_{\|\boldsymbol{w}\| \to \infty} \mathcal{G}(\boldsymbol{w}, \mathbf{z}) = -\infty$. Since $\mathcal{X}$ is compact and c is continuous, there exists a constant $M(\mathbf{z}) > 0$ such that

$$\max_{j \in \{1, \ldots, N\}} \max_{\mathbf{x} \in \mathcal{X}} |c(\mathbf{x}, \mathbf{z}^j)| \leq M(\mathbf{z}).$$

Since f^* is non-decreasing,

$$f^*(-\boldsymbol{w}^c(\mathbf{x}; \mathbf{z})) = f^*\left(\max_{j \in \{1, \ldots, N\}} \left(w^j - c(\mathbf{x}, \mathbf{z}^j)\right)\right) \geq f^*\left(\max_j \boldsymbol{w} - M(\mathbf{z})\right).$$

For each $\boldsymbol{w} \in \mathbb{R}^N$, write $\boldsymbol{w} = \boldsymbol{w}_+ - \boldsymbol{w}_-$, where $\boldsymbol{w}_+, \boldsymbol{w}_-$ are the positive and negative parts of $\boldsymbol{w}$, namely, $w_+^i = \max\{w^i, 0\}$, $w_-^i = -\min\{w^i, 0\}$ for all $i \in \{1, \dots, N\}$. Since $\sum_{i=1}^N m^i = 1$,

$$\begin{aligned}
\mathcal{G}(\boldsymbol{w}) &\leq \sum_{i=1}^N m^i (w_+^i - w_-^i) - \mathcal{L}^3(\mathcal{X}) f^* \left(\max_j \boldsymbol{w} - M(\mathbf{z}) \right) \\
&\leq \|\boldsymbol{w}_+\|_\infty - \min_i m^i \, \|\boldsymbol{w}_-\|_\infty - \mathcal{L}^3(\mathcal{X}) f^* \left(\max_j \boldsymbol{w} - M(\mathbf{z}) \right) \\
&= -\min_i m^i \, \|\boldsymbol{w}_-\|_\infty + \begin{cases} 0 & \text{if } \boldsymbol{w}_+ = 0, \\ \|\boldsymbol{w}_+\|_\infty - \mathcal{L}^3(\mathcal{X}) f^* \left(\|\boldsymbol{w}_+\|_\infty - M(\mathbf{z}) \right) & \text{if } \boldsymbol{w}_+ \neq 0. \end{cases}
\end{aligned}$$

The first term tends to $-\infty$ as $\|\boldsymbol{w}_-\|_\infty \to \infty$, and the second term tends to $-\infty$ as $\|\boldsymbol{w}_+\|_\infty \to \infty$ because f^* grows superlinearly at $+\infty$. Therefore $\lim_{\|\boldsymbol{w}\| \to \infty} \mathcal{G}(\boldsymbol{w}, \mathbf{z}) = -\infty$, as claimed.

Next we show that $\mathcal{G}(\cdot, \mathbf{z})$ is concave. Since f^* is non-decreasing,

$$\mathcal{G}(\boldsymbol{w}, \mathbf{z}) = \sum_{i=1}^N m^i w^i - \int_{\mathcal{X}} f^*(-\boldsymbol{w}^c(\mathbf{x}; \mathbf{z}))\, \mathrm{d}\mathbf{x} = \sum_{i=1}^N m^i w^i - \int_{\mathcal{X}} \max_{j \in \{1, \dots, N\}} f^*(w^j - c(\mathbf{x}, \mathbf{z}^j))\, \mathrm{d}\mathbf{x}.$$

Note that the map $\boldsymbol{w} \mapsto \max_{j \in \{1, \dots, N\}} f^*(w^j - c(\mathbf{x}, \mathbf{z}^j))$ is convex because f^* is convex and the pointwise maximum over a family of convex functions is convex. Therefore it follows by linearity of integration that $\mathcal{G}(\cdot, \mathbf{z})$ is concave.

Now we prove that the maximiser of $\mathcal{G}(\cdot, \mathbf{z})$ is unique. Let $\boldsymbol{w}$ be a maximiser of $\mathcal{G}(\cdot, \mathbf{z})$. By Lemma 3.3.8 the Hessian of $\mathcal{G}(\cdot, \mathbf{z})$ at $\boldsymbol{w}$ is negative definite, so $\boldsymbol{w}$ is an isolated maximiser. Since $\mathcal{G}(\cdot, \mathbf{z})$ is concave, its set of maximisers must be convex, hence connected. Therefore, $\boldsymbol{w}$ is the unique maximiser of $\mathcal{G}(\cdot, \mathbf{z})$.

Next we prove weak duality. Recall the Fenchel-Young inequality:

$$ab \leq f(a) + f^*(b) \quad \forall\, a, b \in \mathbb{R}, \tag{3.30}$$

$$ab = f(a) + f^*(b) \quad \iff \quad a \in \partial f^*(b) = \{(f^*)'(b)\} \quad \iff \quad b \in \partial f(a). \tag{3.31}$$

By the Kantorovich Duality Theorem (see (3.19)) and the Fenchel-Young inequality (3.30), for all $\sigma \in \mathscr{P}_{\mathrm{ac}}(\mathcal{X})$, $\boldsymbol{w} \in \mathbb{R}^N$,

$$E(\sigma, \alpha^N) = \mathcal{T}_c(\sigma, \alpha^N) + \int_{\mathcal{X}} f(\sigma(\mathbf{x}))\, \mathrm{d}\mathbf{x}$$

$$= \max_{\widetilde{\boldsymbol{w}} \in \mathbb{R}^N} \left(\sum_{i=1}^N m^i \widetilde{w}^i + \int_{\mathcal{X}} \widetilde{\boldsymbol{w}}^c(\mathbf{x}; \mathbf{z}) \sigma(\mathbf{x}) \, \mathrm{d}\mathbf{x} \right) + \int_{\mathcal{X}} f(\sigma(\mathbf{x})) \, \mathrm{d}\mathbf{x}$$

$$\geq \sum_{i=1}^N m^i w^i + \int_{\mathcal{X}} \left(\boldsymbol{w}^c(\mathbf{x}; \mathbf{z}) \sigma(\mathbf{x}) + f(\sigma(\mathbf{x})) \right) \mathrm{d}\mathbf{x}$$

$$\geq \sum_{i=1}^N m^i w^i - \int_{\mathcal{X}} f^*(-\boldsymbol{w}^c(\mathbf{x}; \mathbf{z})) \, \mathrm{d}\mathbf{x} = \mathcal{G}(\boldsymbol{w}, \mathbf{z}). \tag{3.32}$$

In particular, we have the weak duality

$$\min_{\sigma \in \mathscr{P}_{\mathrm{ac}}(\mathcal{X})} E(\sigma, \alpha^N) \geq \max_{\boldsymbol{w} \in \mathbb{R}^N} \mathcal{G}(\boldsymbol{w}, \mathbf{z}). \tag{3.33}$$

It follows that if $E(\sigma, \alpha^N) = \mathcal{G}(\boldsymbol{w}, \mathbf{z})$, then $\boldsymbol{w}$ is a maximiser of $\mathcal{G}(\cdot, \mathbf{z})$ and σ is a minimiser of $E(\cdot, \alpha^N)$.

Now we prove that there exists a pair $(\sigma, \boldsymbol{w}) \in \mathscr{P}_{\mathrm{ac}}(\mathcal{X}) \times \mathbb{R}^N$ satisfying (3.21) and (3.22). Let $\boldsymbol{w} \in \mathbb{R}^N$ be the unique maximiser of $\mathcal{G}(\cdot, \mathbf{z})$. Then $\nabla_{\boldsymbol{w}} \mathcal{G}(\boldsymbol{w}, \mathbf{z}) = 0$ and hence, by (3.24), $\boldsymbol{w}$ satisfies (3.21). Define $\sigma : \mathcal{X} \to \mathbb{R}$ by

$$\sigma(\mathbf{x}) = (f^*)'(-\boldsymbol{w}^c(\mathbf{x}; \mathbf{z})).$$

Since $\sum_{i=1}^N m^i = 1$ and (3.21) holds, it follows that σ is a probability measure. Therefore the pair $(\sigma, \boldsymbol{w}) \in \mathscr{P}_{\mathrm{ac}}(\mathcal{X}) \times \mathbb{R}^N$ satisfies (3.21) and (3.22), as claimed.

Finally, we prove strong duality and that (3.21) and (3.22) are necessary and sufficient for optimality. Let $(\sigma, \boldsymbol{w}) \in \mathscr{P}_{\mathrm{ac}}(\mathcal{X}) \times \mathbb{R}^N$ satisfy (3.21) and (3.22). Then

$$\int_{L_c^i(\boldsymbol{w}, \mathbf{z})} \sigma(\mathbf{x}) \, \mathrm{d}\mathbf{x} = m^i \quad \forall \, i \in \{1, \ldots, N\}.$$

Therefore $\boldsymbol{w}$ is an optimal Kantorovich potential for transporting σ to α^N, and

$$\mathcal{T}_c(\sigma, \alpha^N) = \int_{\mathcal{X}} w^c(\mathbf{x}; \mathbf{z}) \, \mathrm{d}\sigma(\mathbf{x}) + \sum_{i=1}^N m^i w^i. \tag{3.34}$$

By (3.22),

$$\sigma(\mathbf{x}) = (f^*)'(-\boldsymbol{w}^c(\mathbf{x}; \mathbf{z})) \in \partial f^*(-\boldsymbol{w}^c(\mathbf{x}; \mathbf{z})) \quad \forall \, \mathbf{x} \in \mathcal{X}.$$

Then by the Fenchel-Young inequality (3.31),

$$-\boldsymbol{w}^c(\mathbf{x};\mathbf{z})\,\sigma(\mathbf{x}) = f(\sigma(\mathbf{x})) + f^*(-\boldsymbol{w}^c(\mathbf{x};\mathbf{z})) \quad \forall\, \mathbf{x} \in \mathcal{X}. \tag{3.35}$$

Combining (3.34) and (3.35) gives

$$E(\sigma, \alpha^N) = \sum_{i=1}^{N} m^i w^i - \int_{\mathcal{X}} f^*(-\boldsymbol{w}^c(\mathbf{x};\mathbf{z}))\,\mathrm{d}\mathbf{x} = \mathcal{G}(\boldsymbol{w}, \mathbf{z}).$$

Therefore, by (3.33), $\boldsymbol{w}$ is a maximiser of $\mathcal{G}(\cdot, \mathbf{z})$, σ is a minimiser of $E(\cdot, \alpha^N)$, and strong duality holds, (3.20).

Conversely, let $\sigma \in \mathscr{P}_{\mathrm{ac}}(\mathcal{X})$ minimise $E(\cdot, \alpha^N)$ and $\boldsymbol{w} \in \mathbb{R}^N$ maximise $\mathcal{G}(\cdot, \mathbf{z})$. We will show that (3.21) and (3.22) hold. Since $\mathcal{G}(\cdot, \mathbf{z})$ is continuously differentiable and w is its maximiser, $\nabla_{\boldsymbol{w}}\, G(\boldsymbol{w}, \mathbf{z}) = 0$. Therefore $\boldsymbol{w}$ satisfies (3.21) by (3.24). By strong duality, (3.20), the inequality in (3.32) is in fact an equality with this choice of σ and $\boldsymbol{w}$. In particular,

$$\boldsymbol{w}^c(\mathbf{x};\mathbf{z})\,\sigma(\mathbf{x}) + f(\sigma(\mathbf{x})) = -f^*(-\boldsymbol{w}^c(\mathbf{x};\mathbf{z})) \quad \text{for } \mathcal{L}^3\text{-almost every } \mathbf{x} \in \mathcal{X}.$$

Hence, by the Fenchel-Young inequality (3.31), for $\mathcal{L}^3$-almost every $\mathbf{x} \in \mathcal{X}$,

$$\sigma(\mathbf{x}) \in \partial f^*(-\boldsymbol{w}^c(\mathbf{x};\mathbf{z})) = \{\, (f^*)'(-\boldsymbol{w}^c(\mathbf{x};\mathbf{z}))\,\}.$$

This proves (3.22) and completes the proof. □

An immediate consequence of Theorem 3.3.4 and Lemma 3.3.7 is the following.

Corollary 3.3.9 (Regularity of the optimal source measure for discrete target measures)**.** *Let $\alpha^N \in \mathscr{P}^N(\mathcal{Y})$ be a discrete measure and $\sigma_*[\alpha^N] \in \mathscr{P}_{\mathrm{ac}}(\mathcal{X})$ be the optimal source measure given in Definition 3.2.5. Then $\sigma_*[\alpha^N]$ is Lipschitz continuous.*

3.4 Discrete solutions of the compressible SG equations

The goal of this section is to prove Theorem 3.1.1, namely, that for well-prepared initial data, discrete solutions of the compressible semi-geostrophic equations exist, are unique, and are energy conserving.

We first define the centroid map $\mathbf{C}$ that appears in the ODE (3.6) and show that it is

continuously differentiable.

Definition 3.4.1 (Optimal weight map)**.** Given $\mathbf{m} \in \Delta^N$, define the map $\boldsymbol{w}_* : D_0^N \to \mathbb{R}^N$ by

$$\boldsymbol{w}_*(\mathbf{z}) := \operatorname*{arg\,max}_{\boldsymbol{w} \in \mathbb{R}^N} \mathcal{G}(\boldsymbol{w}, \mathbf{z}). \tag{3.36}$$

Note that $\boldsymbol{w}_*$ is well defined by Theorem 3.3.4.

Definition 3.4.2 (Centroid map)**.** Given $\mathbf{m} \in \Delta^N$, define the centroid map $\mathbf{C} : D_0^N \to (\mathbb{R}^3)^N$ by $\mathbf{C}(\mathbf{z}) \coloneqq (\mathbf{C}^1(\mathbf{z}), \dots, \mathbf{C}^N(\mathbf{z}))$, where

$$\mathbf{C}^i(\mathbf{z}) \coloneqq \frac{1}{m^i} \int_{L_c^i(\boldsymbol{w}_*(\mathbf{z}), \mathbf{z})} \mathbf{x} \, \mathrm{d}\sigma_*[\alpha^N](\mathbf{x}), \tag{3.37}$$

where

$$\alpha^N = \sum_{i=1}^N m^i \delta_{\mathbf{z}^i}.$$

That is, $\mathbf{C}^i(\mathbf{z})$ is the centroid (or barycentre) of the set of points $T_{\alpha^N}^{-1}(\{\mathbf{z}^i\})$ transported to $\mathbf{z}^i$ in the optimal transport from $\sigma_*[\alpha^N]$ to α^N for the cost c.

To prove the existence of solutions of the ODE (3.6), we show that the transport velocity $W : D_0^N \to \mathbb{R}^{3N}$ is continuously differentiable, where W is defined by

$$W(\mathbf{z}) = J^N(\mathbf{z} - \mathbf{C}(\mathbf{z})),$$

where J^N is the block diagonal matrix $J^N := \operatorname{diag}(J, \dots, J) \in \mathbb{R}^{3N \times 3N}$.

Lemma 3.4.3 (Regularity of $\boldsymbol{w}_*$)**.** *The optimal weight map $\boldsymbol{w}_*$ is continuously differentiable.*

Proof. By definition of $\boldsymbol{w}_*$, $\nabla_{\boldsymbol{w}} \mathcal{G}(\boldsymbol{w}_*(\mathbf{z}), \mathbf{z}) = 0$ for all $\mathbf{z} \in D^N$. In order to show that $\boldsymbol{w}_*$ is continuously differentiable, we will apply the Implicit Function Theorem to the function $\nabla_{\boldsymbol{w}} \mathcal{G}$. Fix any point $\mathbf{z}_0 \in D_0^N$ and define $\boldsymbol{w}_0 = \boldsymbol{w}_*(\mathbf{z}_0)$. By Proposition 3.3.8 and equation (3.21), $\mathcal{G}$ is twice continuously differentiable in a neighbourhood of $(\boldsymbol{w}_0, \mathbf{z}_0)$ and $D^2_{\boldsymbol{w}\boldsymbol{w}} \mathcal{G}(\boldsymbol{w}_0, \mathbf{z}_0)$ is negative definite, hence invertible. By the Implicit Function Theorem, there exists an open set $U \subset D_0^N$ containing $\mathbf{z}_0$ and a unique, continuously differentiable function $\widetilde{\boldsymbol{w}} : U \to \mathbb{R}^N$ such that $\widetilde{\boldsymbol{w}}(\mathbf{z}_0) = \boldsymbol{w}_0$ and $\nabla_{\boldsymbol{w}} \mathcal{G}(\widetilde{\boldsymbol{w}}(\mathbf{z}), \mathbf{z}) = 0$ for all $\mathbf{z} \in U$. By uniqueness, $\widetilde{\boldsymbol{w}}$ coincides with $\boldsymbol{w}_*$ on U. Therefore $\boldsymbol{w}_*$ is continuously differentiable in a neighbourhood of $\mathbf{z}_0$, as required. □

Lemma 3.4.4 (Regularity of $\mathbf{C}$)**.** *The centroid map $\mathbf{C}$ is continuously differentiable.*

Proof. Recalling the expression for $\sigma_*[\alpha^N]$ derived in Theorem 3.3.4, we have

$$\mathbf{C}^i(\mathbf{z}) = \frac{1}{m^i} \int_{L_c^i(\boldsymbol{w}_*(\mathbf{z}),\mathbf{z})} \mathbf{x}\, (f^*)'(-(\boldsymbol{w}_*(\mathbf{z}))^c(\mathbf{x};\mathbf{z}))\, \mathrm{d}\mathbf{x}.$$

Define $\boldsymbol{\Psi} = (\Psi^1, \dots, \Psi^N) : \mathbb{R}^N \times D_0^N \to (\mathbb{R}^3)^N$ by

$$\Psi^i(\boldsymbol{w}, \mathbf{z}) = \frac{1}{m^i} \int_{L_c^i(\boldsymbol{w},\mathbf{z})} \mathbf{x}\, (f^*)'(-\boldsymbol{w}^c(\mathbf{x};\mathbf{z}))\, \mathrm{d}\mathbf{x}.$$

Then $\mathbf{C} = \Psi \circ (\boldsymbol{w}_*, \mathrm{Id})$. For $j \in \{1,2,3\}$, define the functions $\zeta_j : \mathcal{X} \times \mathbb{R}^N \times D^N \to \mathbb{R}$ by $\zeta_j(\mathbf{x}, \boldsymbol{w}, \mathbf{z}) = x_j\, (f^*)'(-\boldsymbol{w}^c(\mathbf{x};\mathbf{z}))$. It follows from Lemma 3.3.7 that ζ_j satisfy the assumptions of Lemma 3.3.6, so Ψ is continuously differentiable by Lemma 3.3.6. Therefore $\mathbf{C}$ is continuously differentiable by Lemma 3.4.3 and the Chain Rule. □

We now show that solutions of the ODE (3.6) correspond to weak solutions of the PDE (3.1) with discrete initial data.

Proposition 3.4.5 (cf. [8, Lemma 4.2])**.** *Let $\overline{z} \in D^N$ and let $\overline{\alpha}^N \in \mathscr{P}^N(\mathcal{Y})$ be the corresponding discrete initial measure given by*

$$\overline{\alpha}^N = \sum_{i=1}^N m^i \delta_{\overline{\mathbf{z}}^i}. \tag{3.38}$$

Fix a final time $\tau > 0$ and let $\mathbf{z} \in \mathcal{C}^1([0,\tau]; \mathcal{Y}^N)$. Define $\alpha^N : [0,\tau] \to \mathscr{P}^N(\mathcal{Y})$ by

$$\alpha_t^N = \sum_{i=1}^N m^i \delta_{\mathbf{z}^i(t)} \quad \forall\, t \in [0,\tau]. \tag{3.39}$$

Then α^N is a weak solution of the compressible semi-geostrophic equations (in the sense of Definition 3.2.6) with initial data $\alpha_0^N = \overline{\alpha}^N$ if and only if $\mathbf{z}$ is a solution of the ODE (3.6) with initial data $\mathbf{z}(0) = \overline{\mathbf{z}}$.

Proof. Suppose that $\mathbf{z} \in C^1([0,\tau]; \mathcal{Y}^N)$ is a solution of the ODE (3.6) and let α^N be given by (3.39). We show that α^N satisfies (3.13). For all $\varphi \in \mathcal{C}_c^\infty(\mathcal{Y} \times \mathbb{R})$,

$$\int_0^\tau \int_{\mathcal{Y}} \left[\partial_t \varphi_t(\mathbf{y}) + (J\mathbf{y}) \cdot \nabla \varphi_t(\mathbf{y})\right] \mathrm{d}\alpha_t^N(\mathbf{y})\, \mathrm{d}t - \int_0^\tau \int_{\mathcal{X}} (J\mathbf{x}) \cdot \nabla \varphi_t(T_{\alpha_t^N}(\mathbf{x}))\, \mathrm{d}\sigma_*[\alpha_t^N](\mathbf{x})\, \mathrm{d}t$$

$$= \sum_{i=1}^N m^i \int_0^\tau \left[\partial_t \varphi_t(\mathbf{z}^i(t)) + (J\mathbf{z}^i(t)) \cdot \nabla \varphi_t(\mathbf{z}^i(t))\right] \mathrm{d}t$$

$$
\begin{aligned}
&- \int_0^\tau \sum_{i=1}^N \int_{L_c^i(\boldsymbol{w}_*(\mathbf{z}(t)),\mathbf{z}(t))} (J\mathbf{x}) \cdot \nabla \varphi_t(\mathbf{z}^i(t)) \, \mathrm{d}\sigma_*[\alpha_t^N](\mathbf{x}) \, \mathrm{d}t \\
&= \sum_{i=1}^N m^i \int_0^\tau \left[\partial_t \varphi_t(\mathbf{z}^i(t)) + J\left(\mathbf{z}^i(t) - \mathbf{C}^i(\mathbf{z}(t))\right) \cdot \nabla \varphi_t(\mathbf{z}^i(t)) \right] \mathrm{d}t \\
&= \sum_{i=1}^N m^i \int_0^\tau \left[\partial_t \varphi_t(\mathbf{z}^i(t)) + \dot{\mathbf{z}}^i(t) \cdot \nabla \varphi_t(\mathbf{z}^i(t)) \right] \mathrm{d}t \\
&= \sum_{i=1}^N m^i \int_0^\tau \frac{d}{dt} \varphi_t(\mathbf{z}^i(t)) \, \mathrm{d}t \\
&= \sum_{i=1}^N m^i \left(\varphi_\tau(\mathbf{z}^i(\tau)) - \varphi_0(\mathbf{z}^i(0)) \right) \\
&= \int_{\mathcal{Y}} \varphi_\tau(\mathbf{y}) \, \mathrm{d}\alpha_\tau^N(\mathbf{y}) - \int_{\mathcal{Y}} \varphi_0(\mathbf{y}) \, \mathrm{d}\overline{\alpha}^N(\mathbf{y}),
\end{aligned}
$$

as required. From here, the proof follows exactly the proof of Lemma 4.2 given in [8]. □

Next we prove global existence and uniqueness of solutions of the ODE (3.6) using the following *a priori* estimates.

Lemma 3.4.6 (*A priori* estimates)**.** *Let* $\mathbf{z} : [0,\tau] \to D^N$ *be continuously differentiable and satisfy the ODE* (3.6) *on the interval* $[0,\tau]$*. Let* $R = R(\mathcal{X}) > 0$ *satisfy* $\mathcal{X} \subset B_R(0)$*. Then, for each* $i \in \{1,\dots,N\}$ *and* $t \in [0,\tau]$*,*

$$\|\mathbf{z}^i(t)\| \le \|\mathbf{z}^i(0)\| + f_{\mathrm{cor}} R\tau, \tag{3.40}$$

$$\|\dot{\mathbf{z}}^i(t)\| \le f_{\mathrm{cor}} \left(\|\mathbf{z}^i(0)\| + R(f_{\mathrm{cor}}\tau + 1) \right). \tag{3.41}$$

Proof. By (3.6), and since J is skew-symmetric with $\|J\|_2 = f_{\mathrm{cor}}$,

$$\frac{d}{dt}\|\mathbf{z}^i(t)\| = \frac{\mathbf{z}^i}{\|\mathbf{z}^i(t)\|} \cdot \dot{\mathbf{z}}^i(t) = -\frac{\mathbf{z}^i(t) \cdot J\,\mathbf{C}^i(\mathbf{z}(t))}{\|\mathbf{z}^i(t)\|} \le f_{\mathrm{cor}} \|\mathbf{C}^i(\mathbf{z}(t))\| \le f_{\mathrm{cor}} R.$$

Integrating gives (3.40). By (3.6) and (3.40),

$$\|\dot{\mathbf{z}}^i(t)\| = \|J(\mathbf{z}^i(t) - \mathbf{C}^i(\mathbf{z}(t)))\| \le f_{\mathrm{cor}} \left(\|\mathbf{z}^i(t)\| + \|\mathbf{C}^i(\mathbf{z}(t))\| \right) \le f_{\mathrm{cor}} \left(\|\mathbf{z}^i(0)\| + f_{\mathrm{cor}} R\tau + R \right),$$

as required. □

Proposition 3.4.7 (Existence and uniqueness of solutions of the ODE (3.6))**.** *Let the final time $\tau \in (0, \infty)$ be arbitrary and let the initial data $\overline{\mathbf{z}} \in D_0^N$. Then there exists a unique function $\mathbf{z} \in \mathcal{C}^2([0,\tau]; D_0^N)$ such that $\mathbf{z}$ satisfies the ODE (3.6) on the interval $[0,\tau]$ and $\mathbf{z}(0) = \overline{\mathbf{z}}$.*

Proof. The proof of Proposition 3.4.7 follows exactly the proof of Proposition 4.4 of [8]. Indeed, local existence and uniqueness follows from the Picard–Lindelöf Theorem, Lemma 3.4.4, and the assumption on the initial data $\overline{\mathbf{z}}$. Global existence then follows from the *a priori* estimates (Lemma 3.4.6) and the fact that the third row of the matrix J is zero, which implies that any solution $\mathbf{z}$ of the ODE satisfies $z_3^i(t) = z_3^i(0)$ for all t and i. In particular, for all t, $\mathbf{z}(t)$ belongs to the subset D_0^N of D^N where the centroid map $\mathbf{C}$ is continuously differentiable. □

Furthermore, we prove that the discrete solutions conserve energy.

Proposition 3.4.8 (Solutions are energy-conserving)**.** *Any solution $\mathbf{z} \in \mathcal{C}^1([0,\tau]; D_0^N)$ of the ODE (3.6) is energy-conserving in the sense that*

$$\frac{d}{dt} E(\sigma_*[\alpha_t^N], \alpha_t^N) = 0 \quad \forall\, t \in [0,\tau],$$

where

$$\alpha_t^N = \sum_{i=1}^N m^i \delta_{\mathbf{z}^i(t)}.$$

Proof. By the duality theorem (Theorem 3.3.4),

$$\begin{aligned}
\frac{d}{dt} E(\sigma_*[\alpha_t^N], \alpha_t^N) &= \frac{d}{dt} \mathcal{G}(\boldsymbol{w}_*(\mathbf{z}(t)), \mathbf{z}(t)) \\
&= \sum_{i=1}^N \left(\frac{\partial \mathcal{G}}{\partial w^i}(\boldsymbol{w}_*(\mathbf{z}(t)), \mathbf{z}(t)) \frac{d}{dt} w_*^i(\mathbf{z}(t)) + \frac{\partial \mathcal{G}}{\partial \mathbf{z}^i}(\boldsymbol{w}_*(\mathbf{z}(t)), \mathbf{z}(t)) \cdot \dot{\mathbf{z}}^i(t) \right) \\
&= \sum_{i=1}^N \frac{\partial \mathcal{G}}{\partial \mathbf{z}^i}(\boldsymbol{w}_*(\mathbf{z}(t)), \mathbf{z}(t)) \cdot \dot{\mathbf{z}}^i(t) \qquad (3.42)
\end{aligned}$$

because $\boldsymbol{w}_*(\mathbf{z}(t))$ is the maximiser (and hence a critical point) of $\mathcal{G}(\cdot, \mathbf{z}(t))$. For brevity, define

$$L_c^i(t) := L_c^i(\boldsymbol{w}_*(\mathbf{z}(t)), \mathbf{z}(t)),$$

and let $\mathbf{C}^i(t) = \mathbf{C}^i(\mathbf{z}(t))$. By (3.22) and (3.25),

$$\begin{aligned}\frac{\partial \mathcal{G}}{\partial \mathbf{z}^i}(\boldsymbol{w}_*(\mathbf{z}(t)), \mathbf{z}(t)) \cdot \dot{\mathbf{z}}^i(t) &= \left(\int_{L_c^i(t)} \nabla_{\mathbf{y}} c(\mathbf{x}, \mathbf{z}^i(t))\, \sigma_*[\alpha_t^N](\mathbf{x})\, \mathrm{d}\mathbf{x} \right) \cdot \dot{\mathbf{z}}^i(t) \\ &= \frac{1}{z_3^i(t)} \left(\int_{L_c^i(t)} \begin{pmatrix} f_{\mathrm{cor}}^2(z_1^i(t) - x_1) \\ f_{\mathrm{cor}}^2(z_2^i(t) - x_2) \\ -c(\mathbf{x}, \mathbf{z}^i(t)) \end{pmatrix} \sigma_*[\alpha_t^N](\mathbf{x})\, \mathrm{d}\mathbf{x} \right) \cdot \dot{\mathbf{z}}^i(t) \\ &= \frac{m^i f_{\mathrm{cor}}^2}{z_3^i(t)} (\mathbf{z}^i - \mathbf{C}^i(t)) \cdot J(\mathbf{z}^i - \mathbf{C}^i(t)) = 0 \end{aligned} \tag{3.43}$$

where the final two equalities hold by (3.6), skew-symmetry of J, and the fact that the third row of J is zero. Combining (3.42) and (3.43) completes the proof. □

Finally, we prove Theorem 3.1.1.

Proof of Theorem 3.1.1. Let $\overline{\alpha}^N = \sum_{i=1}^N m^i \delta_{\overline{\mathbf{z}}^i} \in \mathscr{P}^N(\mathcal{Y})$ be well-prepared in the sense of (3.15). By Proposition 3.4.7 the ODE (3.6) has a unique solution $\mathbf{z} \in \mathcal{C}^2([0,\tau]; D_0^N)$ satisfying $\mathbf{z}(0) = \overline{\mathbf{z}}$. Define $\alpha^N : [0,\tau] \to \mathscr{P}^N(\mathcal{Y})$ by $\alpha_t^N = \sum_{i=1}^N m^i \delta_{\mathbf{z}^i(t)}$. By Proposition 3.4.5 α^N is weak solution of the compressible SG equations (in the sense of Definition 3.2.6) with $\alpha_0^N = \overline{\alpha}^N$. Furthermore, α^N is energy-conserving by Proposition 3.4.8. □

3.5 Existence of weak solutions

In this section we prove Theorem 3.1.2. The strategy is to approximate the initial measure $\overline{\alpha} \in \mathscr{P}_c(\mathcal{Y})$ by a sequence of discrete measures $\overline{\alpha}^N \in \mathscr{P}^N(\mathcal{Y})$, apply Theorem 3.1.1 to obtain a weak solution of (3.1) for each initial data $\overline{\alpha}^N$, and then pass to the limit $N \to \infty$ to obtain a weak solution of (3.1) with initial data $\overline{\alpha}$. This is the same proof strategy as for the *incompressible* system given in [8]. Indeed, some of the preliminary lemmas, namely Lemmas 3.5.1 and 3.5.2, are identical and are stated here without proof. The first lemma asserts that any probability measure $\mu \in \mathscr{P}_c(\mathcal{Y})$ can be approximated in the W_1 metric by a discrete measure $\mu^N \in \mathscr{P}^N(\mathcal{Y})$ with seeds in distinct horizontal planes.

Lemma 3.5.1 (Quantization, [8, Lemma 5.1])**.** *Let $\mu \in \mathscr{P}_c(\mathcal{Y})$. There exists a compact set $K \subset \mathcal{Y}$ and a sequence of well-prepared discrete probability measures $\mu^N \in \mathscr{P}^N(\mathcal{Y})$ (in the*

sense of (3.15)*) such that*

$$\operatorname{spt}(\mu^N) \subset K \quad \forall\, N \in \mathbb{N}, \qquad \lim_{N\to\infty} W_1(\mu^N, \mu) = 0.$$

Lemma 3.5.2 (Compactness, [8, Lemma 5.2])**.** *Let $\overline{\alpha} \in \mathscr{P}_{\mathrm{c}}(\mathcal{Y})$ and let $\overline{\alpha}^N \in \mathscr{P}^N(\mathcal{Y})$ given by Lemma 3.5.1 be a sequence of well-prepared discrete discrete probability measures converging to $\overline{\alpha}$ in W_1. Fix $\tau \in (0,\infty)$. Let $\alpha^N \in \mathcal{C}^{0,1}([0,\tau];\mathscr{P}^N(\mathcal{Y}))$ given by Theorem 3.1.1 be a discrete weak solution of* (3.1) *with initial data $\overline{\alpha}^N$. Then the sequence $(\alpha^N)_{N\in\mathbb{N}}$ has a uniformly convergent subsequence in $\mathcal{C}([0,\tau];\mathscr{P}_{\mathrm{c}}(\mathcal{Y}))$. To be precise, there exists a subsequence (which we do not relabel) and a Lipschitz map $\alpha \in \mathcal{C}^{0,1}([0,\tau];\mathscr{P}_{\mathrm{c}}(\mathcal{Y}))$ such that*

$$\lim_{N\to\infty} \sup_{t\in[0,\tau]} W_1\big(\alpha_t^N, \alpha_t\big) = 0. \tag{3.44}$$

Moreover, there exists a compact set $K \subset \mathcal{Y}$ such that $\operatorname{spt}(\alpha_t^N) \subset K$ and $\operatorname{spt}(\alpha_t) \subset K$ for all $t \in [0,\tau]$ and $N \in \mathbb{N}$.

The final task is to show that α in Lemma 3.5.2 satisfies the PDE (3.1). One of the ingredients of the proof is the following.

Lemma 3.5.3 (Uniform convergence of source measures)**.** *Given a compact set $K \subset \mathcal{Y}$ and a sequence $\beta^N \in \mathscr{P}^N(\mathcal{Y}) \cap \mathscr{P}(K)$ converging weakly to $\beta \in \mathscr{P}(K)$, the sequence of optimal source measures $\sigma_*[\beta^N]$ converges uniformly to $\sigma_*[\beta]$.*

Proof. Recall from Corollary 3.3.9 that $\sigma_*[\beta^N]$ is Lipschitz continuous for all $N \in \mathbb{N}$. Moreover, it follows from the proof of Lemma 3.3.7 that its $W^{1,\infty}$-norm can be bounded independently of N (by noting that $\max_{\mathbf{z}\in D^N\cap K^N} \|\zeta^i(\cdot, \boldsymbol{w}_*(\mathbf{z}), \mathbf{z})\|_{\mathcal{C}^1(\mathcal{X})}$ is independent of N, where ζ^i was defined in equation (3.23)). Therefore the sequence $\sigma_*[\beta^N]$ is uniformly bounded and equicontinuous. By the Ascoli-Arzelá Theorem, there exists $\widetilde{\sigma} \in \mathcal{C}(\mathcal{X}) \cap \mathscr{P}_{\mathrm{ac}}(\mathcal{X})$ such that $\sigma_*[\beta^N]$ converges uniformly in $\mathcal{X}$ to $\widetilde{\sigma}$ (up to a subsequence that we do not relabel).

Next we show that $\widetilde{\sigma} = \sigma_*[\beta]$. The continuity of $\mathcal{T}_c$ (see [59, Theorem 1.51]) and the uniform convergence of $\sigma_*[\beta^N]$ imply that

$$E\big(\sigma_*[\beta^N], \beta^N\big) \to E(\widetilde{\sigma}, \beta) \quad \text{and} \quad E(\sigma_*[\beta], \beta^N) \to E(\sigma_*[\beta], \beta) \quad \text{as} \quad N \to \infty.$$

Assume for a contradiction that $E(\widetilde{\sigma}, \beta) > E(\sigma_*[\beta], \beta)$. Then $E(\sigma_*[\beta^N], \beta^N) > E(\sigma_*[\beta], \beta^N)$ for N sufficiently large, which contradicts the fact that $\sigma_*[\beta^N]$ is the global minimiser of $E(\cdot, \beta^N)$.

Hence $E(\widetilde{\sigma}, \beta) = E(\sigma_*[\beta], \beta)$ and so $\widetilde{\sigma} = \sigma_*[\beta]$ by the uniqueness of the minimiser of $E(\cdot, \beta)$. Finally, note that all convergent subsequences of $\sigma_*[\beta^N]$ converge to $\sigma_*[\beta]$, hence the whole sequence must converge. □

For the proof of Theorem 3.1.2, weak convergence of $\sigma_*[\alpha_t^N]$ is in fact sufficient. However, uniform convergence of $\sigma_*[\alpha_t^N]$, along with the fact that $\sigma_*[\alpha_t^N]$ is Lipschitz continuous uniformly in α_t^N (see Lemma 3.3.7), implies the following.

Corollary 3.5.4 (Regularity of the optimal source measure for general target measures)**.** *Let $\beta \in \mathscr{P}_{\mathrm{c}}(\mathcal{Y})$ and $\sigma_*[\beta] \in \mathscr{P}_{\mathrm{ac}}(\mathcal{X})$ be the optimal source measure. Then $\sigma_*[\beta]$ is Lipschitz continuous.*

Proof. This is an immediate consequence of Corollary 3.3.9 and Lemmas 3.3.7, 3.5.1 and 3.5.3. □

Finally we prove our main theorem.

Proof of Theorem 3.1.2. Let $\alpha \in \mathcal{C}^{0,1}([0,\tau]; \mathscr{P}_{\mathrm{c}}(\mathcal{Y}))$ be the limit of the sequence $(\alpha^N)_{N\in\mathbb{N}}$ obtained in Lemma 3.5.2, and let $K \subset \mathcal{Y}$ be a compact set such that $\mathrm{spt}(\alpha_t^N) \subset K$ and $\mathrm{spt}(\alpha_t) \subset K$ for all $t \in [0,\tau]$ and $N \in \mathbb{N}$. By (3.13) and (3.14), for all $\varphi \in \mathcal{C}_c^\infty(\mathcal{Y} \times \mathbb{R})$,

$$\int_0^\tau \int_{\mathcal{Y}} [\partial_t \varphi_t(\mathbf{y}) + (J\mathbf{y}) \cdot \nabla \varphi_t(\mathbf{y})] \, \mathrm{d}\alpha_t^N(\mathbf{y}) \, \mathrm{d}t - \int_0^\tau \int_{\mathcal{X}\times\mathcal{Y}} (J\mathbf{x}) \cdot \nabla \varphi_t(\mathbf{y}) \, \mathrm{d}\gamma[\alpha_t^N](\mathbf{x},\mathbf{y}) \, \mathrm{d}t$$
$$= \int_{\mathcal{Y}} \varphi_\tau(\mathbf{y}) \, \mathrm{d}\alpha_\tau^N(\mathbf{y}) - \int_{\mathcal{Y}} \varphi_0(\mathbf{y}) \, \mathrm{d}\overline{\alpha}^N(\mathbf{y}). \quad (3.45)$$

A standard estimate in optimal transport theory (see [59, Exercise 38] or [63, Theorem 1.14]) gives

$$\left| \int_0^\tau \int_{\mathcal{Y}} [\partial_t \varphi_t(\mathbf{y}) + (J\mathbf{y}) \cdot \nabla \varphi_t(\mathbf{y})] \, \mathrm{d}\big(\alpha_t^N - \alpha_t\big)(\mathbf{y}) \, \mathrm{d}t \right|$$
$$\leq \int_0^\tau \max_{\mathbf{y}\in K} \big\{ \|\nabla_{\mathbf{y}} [\partial_t \varphi_t(\mathbf{y}) + (J\mathbf{y}) \cdot \nabla \varphi_t(\mathbf{y})]\| \big\} \, W_1(\alpha_t^N, \alpha_t) \, \mathrm{d}t$$
$$\leq \tau \max_{\substack{t\in[0,\tau] \\ \mathbf{y}\in K}} \big\{ \|\nabla_{\mathbf{y}} [\partial_t \varphi_t(\mathbf{y}) + (J\mathbf{y}) \cdot \nabla \varphi_t(\mathbf{y})]\| \, W_1(\alpha_t^N, \alpha_t) \big\} \to 0 \quad \text{as} \quad N \to \infty \quad (3.46)$$

by uniform convergence of α^N (seee (3.44)). Pointwise-in-time convergence of α^N implies that

$$\lim_{N\to\infty}\int_{\mathcal{Y}}\varphi_\tau(\mathbf{y})\,\mathrm{d}\big(\alpha_\tau^N-\alpha_\tau\big)(\mathbf{y})=0\quad\text{and}\quad\lim_{N\to\infty}\int_{\mathcal{Y}}\varphi_0(\mathbf{y})\,\mathrm{d}\big(\overline{\alpha}^N-\overline{\alpha}\big)(\mathbf{y})=0.$$

By Lemma 3.5.3, for all $t\in[0,\tau]$, $\sigma_*[\alpha_t^N]\rightharpoonup\sigma_*[\alpha_t]$ in $\mathscr{P}(\mathcal{X})$. Also, $\alpha_t^N\rightharpoonup\alpha_t$ in $\mathscr{P}(K)$. Therefore $\gamma[\alpha_t^N]\rightharpoonup\gamma[\alpha_t]$ in $\mathscr{P}(\mathcal{X}\times K)$, where $\gamma[\alpha_t]$ is the unique optimal transport plan for transporting $\sigma_*[\alpha_t]$ to α_t; see [64, Theorem 5.20] . Define $F,F_N\in L^1([0,\tau])$ by

$$F(t)=\int_{\mathcal{X}\times\mathcal{Y}}(J\mathbf{x})\cdot\nabla\varphi_t(\mathbf{y})\,\mathrm{d}\gamma[\alpha_t](\mathbf{x},\mathbf{y}),\quad F_N(t)=\int_{\mathcal{X}\times\mathcal{Y}}(J\mathbf{x})\cdot\nabla\varphi_t(\mathbf{y})\,\mathrm{d}\gamma[\alpha_t^N](\mathbf{x},\mathbf{y}).$$

Then $\lim_{N\to\infty}F_N(t)=F(t)$ for all $t\in[0,\tau]$ and

$$\|F_N\|_{L^\infty([0,\tau])}\le f_{\mathrm{cor}}\max_{\mathbf{x}\in\mathcal{X}}\|\mathbf{x}\|\max_{t\in[0,\tau]}\|\nabla\varphi_t\|_{L^\infty(K)}.$$

By the Lebesgue Dominated Convergence Theorem,

$$\lim_{N\to\infty}\int_0^\tau\int_{\mathcal{X}\times\mathcal{Y}}(J\mathbf{x})\cdot\nabla\varphi_t(\mathbf{y})\,\mathrm{d}\gamma[\alpha_t^N](\mathbf{x},\mathbf{y})\,\mathrm{d}t=\int_0^\tau\int_{\mathcal{X}\times\mathcal{Y}}(J\mathbf{x})\cdot\nabla\varphi_t(\mathbf{y})\,\mathrm{d}\gamma[\alpha_t](\mathbf{x},\mathbf{y})\,\mathrm{d}t.\quad(3.47)$$

Combining equations (3.45)–(3.47) shows that α is a weak solution of (3.1), as required. □

Remark 3.5.5 (Convergence of the transport maps). It can be shown that $T_{\alpha_t^N}\to T_{\alpha_t}$ as $N\to\infty$ in L^p for $p\in(1,\infty)$. This can be combined with the uniform convergence of the source measures to pass to the limit in the nonlinear term

$$\int_0^\tau\int_{\mathcal{X}}(J\mathbf{x})\cdot\nabla\varphi_t(T_{\alpha_t^N}(\mathbf{x}))\,\mathrm{d}\sigma_*[\alpha_t^N](\mathbf{x})\,\mathrm{d}t$$

to give an alternative, though more involved, proof of Theorem 3.1.2.

3.6 Explicit examples

In this section we present two explicit solutions of (3.1): a steady state solution and a discrete solution with a single seed.

3.6.1 Steady state example

In this section we make the additional assumption that the fluid domain satisfies $\mathcal{X}\subset\mathcal{Y}$.

Here, the geostrophic space $\mathcal{Y} = \mathbb{R}^2 \times (\delta, 1/\delta)$ represents the set of all mathematically valid coordinates for the model, where the vertical coordinate x_3 is bounded away from zero and infinity for some small $\delta \in (0, 1)$. The domain $\mathcal{X}$ is the support of the fluid's mass distribution within this coordinate system. The assumption $\mathcal{X} \subset \mathcal{Y}$ is therefore a statement of physical consistency: the region actually occupied by the fluid must be a subset of the space of valid coordinates.

Furthermore, in a steady state, the system is by definition stationary, implying the optimal transport map is the identity ($T_t = \mathrm{Id}$). From the definition of the geostrophic velocity in terms of T_t, this immediately forces the velocity to be zero, a state which is trivially bounded. The uniqueness of this steady-state solution is not a general property of the time-dependent PDE, but rather a direct consequence of these highly restrictive steady-state conditions. As shown in Remark 3.6.2, the requirement that $T_t = \mathrm{Id}$ forces any solution into a specific functional form. Within this highly constrained family, the general mass conservation requirement becomes powerful enough to uniquely determine the single parameter ℓ_*. Thus, the uniqueness arises from the combination of the restrictive steady-state conditions reducing the problem to a single degree of freedom, which is then fixed by the mass constraint.

Proposition 3.6.1 (Time-independent solution)**.** *Given $\ell \in \mathbb{R}$, define $\sigma_\ell : \mathcal{X} \to \mathbb{R}$ by*

$$\sigma_\ell(\mathbf{x}) := (f^*)'(\ell - g \ln x_3).$$

Then there exists $\ell_* \in \mathbb{R}$ such that

$$\int_{\mathcal{X}} \sigma_{\ell_*}(\mathbf{x}) \, \mathrm{d}\mathbf{x} = 1.$$

Define $\alpha : [0, \tau] \to \mathscr{P}_{\mathrm{c}}(\mathcal{Y})$ by

$$\alpha_t = \sigma_{\ell_*} \mathcal{L}^3 \llcorner \mathcal{X} \quad \forall\, t \in [0, \tau].$$

Then α is a weak steady state solution of the compressible SG equation (3.1)*.*

Remark 3.6.2 (Formal derivation). We give a formal derivation of the steady state α before giving a rigorous proof of Proposition 3.6.1. By Definition 3.2.6, we take a weak solution $\alpha \in \mathcal{C}([0, \tau]; \mathscr{P}_{\mathrm{c}}(\mathcal{Y}))$ of (3.1) and define it as a steady state if it is independent of time, is its own energy-minimising source measure (i.e. $\alpha_t = \sigma_*[\alpha_t]$, in particular, $\mathrm{spt}(\alpha_t) \subseteq \mathcal{X}$), and has

the identity as its optimal transport map $T_{\alpha_t} = \mathrm{Id}$. Then

$$\alpha_t = \operatorname*{arg\,min}_{\sigma \in \mathscr{P}_{\mathrm{ac}}(\mathcal{X})} E(\sigma, \alpha_t)$$

for all $t \in [0, \tau]$. It follows from [59, Proposition 7.20] that α_t satisfies the Euler-Lagrange equations

$$\begin{cases} \dfrac{\delta E}{\delta \sigma}(\alpha_t, \alpha_t) = \ell & \text{on the support of } \alpha_t, \\ \dfrac{\delta E}{\delta \sigma}(\alpha_t, \alpha_t) \geq \ell & \text{otherwise,} \end{cases}$$

for some $\ell \in \mathbb{R}$, where $\delta E / \delta \sigma$ denotes the first variation of E with respect to σ. Formally we expect

$$\frac{\delta E}{\delta \sigma}(\alpha_t, \alpha_t) = \varphi + f'(\alpha_t),$$

where $\varphi : \mathcal{X} \to \mathbb{R}$ is an optimal c-concave Kantorovich potential for transporting α_t to itself with cost c; see [59, Section 7.2]. Then

$$\begin{cases} \varphi + f'(\alpha_t) = \ell & \text{on the support of } \alpha_t, \\ \varphi + f'(\alpha_t) \geq \ell & \text{otherwise.} \end{cases}$$

If $T_{\alpha_t} = \mathrm{Id}$ is the optimal transport map from α_t to itself , then $\nabla \varphi(\mathbf{x}) = \nabla_{\mathbf{x}} c(\mathbf{x}, \mathbf{x})$ for almost all $\mathbf{x}$ in the support of α_t [59, Proposition 1.15]. Integrating this expression gives $\varphi(\mathbf{x}) = g \ln x_3$, up to a constant. Then solving the Euler-Lagrange equations yields

$$\alpha_t(\mathbf{x}) = (f')^{-1}(\ell - \varphi(\mathbf{x})) = (f^*)'(\ell - g \ln x_3)$$

for all $\mathbf{x}$ in the support of α_t. This is the steady state given in Proposition 3.6.1. The constant ℓ is determined by the constraint that α_t is a probability measure.

Proof of Proposition 3.6.1. First we show that there exists $\ell_* \in \mathbb{R}$ such that $\int_{\mathcal{X}} \sigma_{\ell_*}(\mathbf{x}) \, \mathrm{d}\mathbf{x} = 1$. Since $X \subset \mathcal{Y} = \mathbb{R}^2 \times (\delta, 1/\delta)$ and $(f^*)'$ is non-decreasing, then for $\ell \in \mathbb{R}$

$$(f^*)'(\ell - g \ln x_3) \geq (f^*)'(\ell - g \ln(1/\delta))$$

for all $\mathbf{x} \in \mathcal{X}$. Therefore

$$\int_{\mathcal{X}} \sigma_\ell(\mathbf{x})\,\mathrm{d}\mathbf{x} \geq (f^*)'(\ell - g\ln(1/\delta))|\mathcal{X}| \to \infty \quad \text{as} \quad \ell \to \infty.$$

Let $\ell_\delta = g\ln\delta$. Since $x_3 \geq \delta$ for all $\mathbf{x} \in \mathcal{X}$,

$$\int_{\mathcal{X}} \sigma_{\ell_\delta}(\mathbf{x})\,\mathrm{d}\mathbf{x} = \int_{\mathcal{X}} (f^*)'(\ell_\delta - g\ln x_3)\,\mathrm{d}\mathbf{x} \leq \int_{\mathcal{X}} (f^*)'(\ell_\delta - g\ln\delta)\,\mathrm{d}\mathbf{x} = (f^*)'(0)|\mathcal{X}| = 0.$$

The map $\ell \mapsto \int_{\mathcal{X}} \sigma_\ell(\mathbf{x})\,\mathrm{d}\mathbf{x}$ is continuous. Therefore, by the Intermediate Value Theorem, there exists $\ell_* \in \mathbb{R}$ such that

$$\int_{\mathcal{X}} \sigma_{\ell_*}(\mathbf{x})\,\mathrm{d}\mathbf{x} = 1,$$

as claimed. For the remainer of this proof, we take $\ell = \ell_*$

Next we show that the identity map is the optimal transport map for transporting any measure $\sigma \in \mathscr{P}(\mathcal{X})$ to itself, and that an optimal Kantorovich potential pair is (φ, φ^c), where $\varphi : \mathcal{X} \to \mathbb{R}$ is given by $\varphi(\mathbf{x}) = g\ln x_3$, and $\varphi^c : \mathcal{Y} \to \mathbb{R}$ is given by

$$\varphi^c(\mathbf{y}) = \min_{\mathbf{x}\in\mathcal{X}} (c(\mathbf{x},\mathbf{y}) - \varphi(\mathbf{x})) = \min_{\mathbf{x}\in\mathcal{X}} (c(\mathbf{x},\mathbf{y}) - g\ln x_3).$$

First we compute an explicit expression for $\varphi^c(\mathbf{y})$ for the special case $\mathbf{y} \in \mathcal{X} \cap \mathcal{Y} = \mathcal{X}$. Given $\mathbf{y} \in \mathcal{X}$, define $\theta_{\mathbf{y}} : \mathcal{X} \to \mathbb{R}$ by $\theta_{\mathbf{y}}(\mathbf{x}) = c(\mathbf{x},\mathbf{y}) - g\ln x_3$. Then

$$\nabla\theta_{\mathbf{y}}(\mathbf{x}) = \begin{pmatrix} \frac{f_{\mathrm{cor}}^2}{y_3}(x_1 - y_1) \\ \frac{f_{\mathrm{cor}}^2}{y_3}(x_2 - y_2) \\ \frac{g}{y_3} - \frac{g}{x_3} \end{pmatrix}, \qquad D^2\theta_{\mathbf{y}}(\mathbf{x}) = \begin{pmatrix} \frac{f_{\mathrm{cor}}^2}{y_3} & 0 & 0 \\ 0 & \frac{f_{\mathrm{cor}}^2}{y_3} & 0 \\ 0 & 0 & \frac{g}{x_3^2} \end{pmatrix}.$$

Therefore $D^2\theta_{\mathbf{y}}(\mathbf{x})$ is positive definite for all $\mathbf{x} \in \mathcal{X}$. Hence $\theta_{\mathbf{y}}$ is strictly convex, its minimiser is $\mathbf{y}$, and its minimum value is

$$\varphi^c(\mathbf{y}) = \min_{\mathbf{x}\in\mathcal{X}} \theta_{\mathbf{y}}(\mathbf{x}) = \theta_{\mathbf{y}}(\mathbf{y}) = c(\mathbf{y},\mathbf{y}) - g\ln y_3 = g - g\ln y_3.$$

Note that $\varphi(\mathbf{x}) + \varphi^c(\mathbf{x}) = g$ for all $\mathbf{x} \in \mathcal{X}$ and that σ is supported on $\mathcal{X} \subset \mathcal{Y}$. Then

$$\mathcal{T}_c(\sigma,\sigma) \leq \int_{\mathcal{X}} c(\mathbf{x},\mathbf{x})\,\mathrm{d}\sigma(\mathbf{x}) = g = \int_{\mathcal{X}} \varphi\,\mathrm{d}\sigma + \int_{\mathcal{Y}} \varphi^c\,\mathrm{d}\sigma \leq \mathcal{T}_c(\sigma,\sigma),$$

which proves that the identity map is optimal for transporting $\sigma \in \mathscr{P}(\mathcal{X})$ to itself, and that (φ, φ^c) is an optimal Kantorovich potential pair, as claimed.

Lastly, we show that $\sigma_\ell = \arg\min_{\sigma \in \mathscr{P}_{\mathrm{ac}}(\mathcal{X})} E(\sigma, \sigma_\ell)$. If $\mathbf{x} \in \mathcal{X}$ satisfies $\sigma_\ell(\mathbf{x}) = 0$, then $(f^*)'(\ell - g \ln x_3) = 0$ because $\sigma_\ell(\mathbf{x}) = (f^*)'(\ell - g \ln x_3)$. By the definition of f^* (see Remark 3.3.2), then

$$0 \geq \ell - g \ln x_3 = \ell - \varphi(\mathbf{x}).$$

Therefore, since $\sigma_\ell(\mathbf{x}) = 0$ in this case, we have $f'(\sigma_\ell(\mathbf{x})) = f'(0)$ which is zero by the definition of f. It follows that

$$\varphi(\mathbf{x}) + f'(\sigma_\ell(\mathbf{x})) = \varphi(\mathbf{x}) \geq \ell.$$

On the other hand, if $\mathbf{x} \in \mathcal{X}$ satisfies $\sigma_\ell(\mathbf{x}) > 0$, then

$$\varphi(\mathbf{x}) + f'(\sigma_\ell(\mathbf{x})) = g \ln x_3 + f'((f^*)'(\ell - g \ln x_3)) = g \ln x_3 + \ell - g \ln x_3 = \ell$$

because $f'((f^*)'(t)) = t$, which holds since $(f^*)'$ is the inverse of f', a standard property of the Legendre transform for convex functions, for all $t > 0$ in the range of f'. In summary,

$$\varphi(\mathbf{x}) + f'(\sigma_\ell(\mathbf{x})) \geq \ell \quad \forall\, \mathbf{x} \in \mathcal{X}, \tag{3.48}$$

and

$$\big(\varphi(\mathbf{x}) + f'(\sigma_\ell(\mathbf{x}))\big)\sigma_\ell(\mathbf{x}) = \ell \sigma_\ell(\mathbf{x}) \quad \forall\, \mathbf{x} \in \mathcal{X}. \tag{3.49}$$

By the Kantorovich Duality Theorem and the convexity of f, for all $\sigma \in \mathscr{P}_{\mathrm{ac}}(\mathcal{X})$,

$$\begin{aligned} E(\sigma, \sigma_\ell) &= \mathcal{T}_c(\sigma, \sigma_\ell) + \int_{\mathcal{X}} f(\sigma)\, \mathrm{d}\mathcal{L}^3 \\ &\geq \int_{\mathcal{X}} \varphi\, \mathrm{d}\sigma + \int_{\mathcal{Y}} \varphi^c\, \mathrm{d}\sigma_\ell + \int_{\mathcal{X}} \big(f(\sigma_\ell) + f'(\sigma_\ell)(\sigma - \sigma_\ell)\big)\, \mathrm{d}\mathcal{L}^3 \\ &= E(\sigma_\ell, \sigma_\ell) + \int_{\mathcal{X}} \big(\varphi + f'(\sigma_\ell)\big)(\sigma - \sigma_\ell)\, \mathrm{d}\mathcal{L}^3 \end{aligned} \tag{3.50}$$

since φ is an optimal Kantorovich potential for the transport from σ_ℓ to itself. Therefore, by (3.48), (3.49) and (3.50),

$$E(\sigma, \sigma_\ell) \geq E(\sigma_\ell, \sigma_\ell) + \ell \int_{\mathcal{X}} (\sigma - \sigma_\ell)\, \mathrm{d}\mathcal{L}^3 = E(\sigma_\ell, \sigma_\ell),$$

and so $\sigma_\ell = \arg\min_{\sigma \in \mathscr{P}_{\mathrm{ac}}(\mathcal{X})} E(\sigma, \sigma_\ell)$, as claimed.

In conclusion, we have shown that $\sigma_*[\sigma_\ell] = \sigma_\ell$ and $T_{\sigma_\ell} = \mathrm{Id}$. Therefore the time-independent map $[0, \tau] \ni t \mapsto \alpha_t = \sigma_\ell$ is a weak solution of (3.1), as required. □

3.6.2 Single particle example

In the case of a single seed particle (N=1), the semi-discrete optimal transport problem becomes trivial, allowing for the construction of an explicit solution. With only one particle, its associated Laguerre cell encompasses the entire domain $\mathcal{X}$, effectively collapsing the problem of domain partitioning. This is guaranteed under the conditions on the particle's location that we make explicit in the following proposition. This simplification means the optimal weight and the cell's centroid can be calculated directly by integrating over the known domain. Consequently, the ordinary differential equation governing the particle's motion can be written in a closed form.

To ensure these integrals yield a clean, analytical solution, we select the specific value of $\gamma = 2$. It's important to note that the more physically meaningful range is $\gamma \in (1, 2)$; however, deriving a similarly explicit solution for these non-integer values is not straightforward.

Proposition 3.6.3 (Elliptic orbit of a single seed)**.** *Fix $\gamma = 2$, $\kappa = \frac{1}{2}$ and $\tau > 0$. Let $\mathcal{X} = [-a, a] \times [-b, b] \times [0, h]$, where $a, b, h > 0$. Let $\overline{\mathbf{z}} \in \mathcal{Y}$ be the initial position of the particle. Define $\mathbf{z} : (-\infty, \infty) \to \mathcal{Y}$ to be the solution of the linear ODE*

$$\dot{\mathbf{z}}(t) = f_{\mathrm{cor}} \begin{pmatrix} 0 & -A & 0 \\ B & 0 & 0 \\ 0 & 0 & 0 \end{pmatrix} \mathbf{z}(t),$$

$$\mathbf{z}(0) = \overline{\mathbf{z}},$$

where

$$A = 1 - \frac{|\mathcal{X}| f_{\mathrm{cor}}^2}{3\overline{z}_3} b^2, \qquad B = 1 - \frac{|\mathcal{X}| f_{\mathrm{cor}}^2}{3\overline{z}_3} a^2, \qquad |\mathcal{X}| = 4abh.$$

Assume that $\overline{z}_3 > \frac{|\mathcal{X}| f_{\mathrm{cor}}^2}{3} \max\{a^2, b^2\}$ so that $A > 0$ and $B > 0$. Define the ellipse $\mathcal{E} \subset \mathcal{Y}$ by

$$\mathcal{E} \coloneqq \{\mathbf{z}(t) : t \in (-\infty, \infty)\} = \left\{ (y_1, y_2, \overline{z}_3) \in \mathbb{R}^2 \times \{\overline{z}_3\} \ : \ \frac{y_1^2}{A} + \frac{y_2^2}{B} = \frac{\overline{z}_1^2}{A} + \frac{\overline{z}_2^2}{B} \right\}.$$

Assume additionally that $\overline{z}_3$ is sufficiently large so that

$$c(\mathbf{x},\mathbf{y}) - \frac{1}{|\mathcal{X}|}\int_{\mathcal{X}} c(\cdot,\mathbf{y})\,\mathrm{d}\mathcal{L}^3 < \frac{1}{|\mathcal{X}|} \quad \forall\,(\mathbf{x},\mathbf{y}) \in \mathcal{X}\times\mathcal{E}. \tag{3.51}$$

Define $\alpha : [0,\tau] \to \mathscr{P}_{\mathrm{c}}(\mathcal{Y})$ by $\alpha_t = \delta_{\mathbf{z}(t)}$. Then the following hold:

1. *The optimal weight map $w_* : D \to \mathbb{R}$ (defined in* (3.4.1)*) satisfies the following:*

$$w_*(\mathbf{z}(t)) = \frac{1}{|\mathcal{X}|}\left(1 + \int_{\mathcal{X}} c(\mathbf{x},\mathbf{z}(t))\,\mathrm{d}\mathbf{x}\right) \quad \forall\, t \in (-\infty,\infty).$$

2. *The optimal source measure $\sigma_*[\alpha_t] \in \mathscr{P}_{\mathrm{ac}}(\mathcal{X})$ is given by*

$$\sigma_*[\alpha_t](\mathbf{x}) = w_*(\mathbf{z}(t)) - c(\mathbf{x},\mathbf{z}(t)).$$

3. *α is a weak solution of the compressible SG equation* (3.1)*. In particular, the trajectory of the seed is the ellipse $\mathcal{E}$. Moreover, if $a = b$, then the seed moves on a circle. If $\overline{z}_1 = \overline{z}_2 = 0$, then the seed is stationary.*

Proof. Since $\gamma = 2$ and $\kappa = \frac{1}{2}$,

$$f^*(t) = \begin{cases} \frac{1}{2}t^2 & \text{if } t > 0, \\ 0 & \text{if } t \le 0. \end{cases}$$

Define $w : (-\infty,\infty) \to \mathbb{R}$ by

$$w(t) = \frac{1}{|\mathcal{X}|}\left(1 + \int_{\mathcal{X}} c(\mathbf{x},\mathbf{z}(t))\,\mathrm{d}\mathbf{x}\right).$$

Then, for all $\mathbf{x} \in \mathcal{X}$, $t \in (-\infty,\infty)$,

$$w(t) - c(\mathbf{x},\mathbf{z}(t)) = \frac{1}{|\mathcal{X}|}\left(1 + \int_{\mathcal{X}} c(\tilde{\mathbf{x}},\mathbf{z}(t))\,\mathrm{d}\tilde{\mathbf{x}}\right) - c(\mathbf{x},\mathbf{z}(t)) > 0$$

by (3.51). Therefore

$$\frac{\partial \mathcal{G}}{\partial w}(w(t),\mathbf{z}(t)) = 1 - \int_{\mathcal{X}} (f^*)'(w(t) - c(\mathbf{x},\mathbf{z}(t)))\,\mathrm{d}\mathbf{x} = 1 - \int_{\mathcal{X}} (w(t) - c(\mathbf{x},\mathbf{z}(t)))\,\mathrm{d}\mathbf{x} = 0,$$

hence $w(t)$ maximises the concave function $\mathcal{G}(\cdot,\mathbf{z}(t))$. Since the maximiser of $\mathcal{G}(\cdot,\mathbf{z}(t))$ is unique by Theorem 3.3.4, it follows that $w_*(\mathbf{z}(t)) = w(t)$, as claimed. The expression for $\sigma_*[\alpha_t]$ then

follows immediately from (3.22).

It remains to prove that α is a weak solution the compressible SG equation (3.1). By Proposition 3.4.5, it suffices to show that $\mathbf{z}$ satisfies the following ODE:

$$\dot{z}_1(t) = f_{\text{cor}}(-z_2(t) + C_2(\mathbf{z}(t))),$$

$$\dot{z}_2(t) = f_{\text{cor}}(z_1(t) - C_1(\mathbf{z}(t))),$$

$$\dot{z}_3(t) = 0.$$

In other words, we need to show that

$$C_1(\mathbf{z}(t)) = (1 - B)z_1(t), \qquad C_2(\mathbf{z}(t)) = (1 - A)z_2(t).$$

We will just verify the expression for C_1; the expression for C_2 is similar. By Definition 3.4.2 and the symmetry of the domain $\mathcal{X}$,

$$\begin{aligned}
C_1(\mathbf{z}(t)) &= \int_{\mathcal{X}} x_1 \, \sigma_*[\alpha_t](\mathbf{x}) \, \mathrm{d}\mathbf{x} \\
&= \int_{\mathcal{X}} x_1 \left(w_*(\mathbf{z}(t)) - c(\mathbf{x}, \mathbf{z}(t))\right) \, \mathrm{d}\mathbf{x} \\
&= -\frac{1}{\overline{z}_3} \int_{-a}^{a} \int_{-b}^{b} \int_{0}^{h} x_1 \left(\frac{f_{\text{cor}}^2}{2}(x_1 - z_1(t))^2 + \frac{f_{\text{cor}}^2}{2}(x_2 - z_2(t))^2 + g x_3 \right) \mathrm{d}x_3 \, \mathrm{d}x_2 \, \mathrm{d}x_1 \\
&= \frac{f_{\text{cor}}^2}{\overline{z}_3} \int_{-a}^{a} \int_{-b}^{b} \int_{0}^{h} x_1^2 z_1(t) \, \mathrm{d}x_3 \, \mathrm{d}x_2 \, \mathrm{d}x_1 \\
&= \frac{4a^3 b h f_{\text{cor}}^2}{3\overline{z}_3} z_1(t) \\
&= (1 - B)z_1(t),
\end{aligned}$$

as required. □

3.7 Technical Details

3.7.1 Assumptions on the fluid domain $\mathcal{X}$

Recall that $\Phi : \mathbb{R}^3 \to \mathbb{R}^3$ is the diffeomorphism defined by

$$\Phi(\mathbf{x}) = \left(f_{\text{cor}}^{-2}\, x_1,\ f_{\text{cor}}^{-2}\, x_2,\ g^{-1}\left(x_3 - \tfrac{1}{2} f_{\text{cor}}^{-2}\left(x_1^2 + x_2^2\right)\right)\right).$$

In this section we discuss the assumption that the fluid domain $\mathcal{X}$ satisfies

$$\Phi^{-1}(\mathcal{X}) \text{ is convex.} \tag{3.52}$$

In particular, we give examples of domains $\mathcal{X}$ satisfying (3.52), we prove that (3.52) is equivalent to $\mathcal{X}$ being c-convex [46, Definition 1.2], and we prove that, given any c-Laguerre tessellation $\{L_c^i(\boldsymbol{w}, \mathbf{z})\}_{i=1}^N$, then $\{\Phi^{-1}(L_c^i(\boldsymbol{w}, \mathbf{z}))\}_{i=1}^N$ is a classical Laguerre tessellation (with respect to the quadratic cost). In particular, $\Phi^{-1}(L_c^i(\boldsymbol{w}, \mathbf{z}))$ is a convex polyhedron for all i. Moreover, we will see that the cost c satisfies Loeper's condition [46, Definition 1.1].

Remark 3.7.1 (Interpreting Φ in terms of c-exponential maps). Let $\mathbf{y}_0 = (0, 0, 1)$. It is easy to check that Φ is the c-exponential map $\exp_{\mathbf{y}_0}^c$ [46, Remark 4.4]:

$$\Phi = \exp_{\mathbf{y}_0}^c := (-D_{\mathbf{y}} c(\cdot, \mathbf{y}_0))^{-1}.$$

In other words,

$$-D_{\mathbf{y}} c(\Phi(\mathbf{x}), \mathbf{y}_0) = \mathbf{x}.$$

Note that c-exponential maps play an important role in regularity theory for semi-discrete optimal transport [46].

Example 3.7.2 (Domains satisfying assumption (3.52)). Let $(a_1, a_2, a_3) \in \mathbb{R}^3$. It can be shown that any paraboloid of the form

$$\mathcal{X}_1 = \left\{\mathbf{x} \in \mathbb{R}^3 : x_3 \leq -\frac{f_{\text{cor}}^2}{2g}\left((x_1 - a_1)^2 + (x_2 - a_2)^2\right) + a_3\right\} \tag{3.53}$$

satisfies (3.52). Its inverse image $\Phi^{-1}(\mathcal{X}_1)$ is a half-space of the form

$$\Phi^{-1}(\mathcal{X}_1) = \{\mathbf{p} \in \mathbb{R}^3 : p_3 \leq b_1 p_1 + b_2 p_2 + c\},$$

where $b_1, b_2, c \in \mathbb{R}$. In particular, it is convex. Replacing the inequality $\leq$ in (3.53) by $\geq$ gives another example of a set satisfying (3.52). Another example is the half-space

$$\mathcal{X}_2 = \{\mathbf{x} \in \mathbb{R}^3 : \mathbf{x} \cdot \mathbf{n} \geq d\}$$

where $d \in \mathbb{R}$ and $\mathbf{n} \in \mathbb{R}^3$ with $n_3 \geq 0$. Its inverse image $\Phi^{-1}(\mathcal{X}_2)$ has the following form for some $\mathbf{b} \in \mathbb{R}^3$, $c \in \mathbb{R}$:

$$\Phi^{-1}(\mathcal{X}_2) = \left\{\mathbf{p} \in \mathbb{R}^3 : \frac{n_3}{g f_{\text{cor}}^2}(p_1^2 + p_2^2) + \mathbf{b} \cdot \mathbf{p} + c \leq 0\right\}. \tag{3.54}$$

This is convex because it has the form $\{\mathbf{p} \in \mathbb{R}^3 : F(\mathbf{p}) \leq 0\}$ with F convex. We can build other examples by using the fact that any intersection of sets satisfying (3.52) also satisfies (3.52). For example, "blister pack" sets of the form

$$\mathcal{X}_3 = \left\{\mathbf{x} \in \mathbb{R}^3 : 0 \leq x_3 \leq -\frac{f_{\text{cor}}^2}{2g}\left((x_1 - a_1)^2 + (x_2 - a_2)^2\right) + a_3\right\}$$

satisfy (3.52) for all $\mathbf{a} \in \mathbb{R}^3$. It can be seen from (3.54) that the half-space $\{\mathbf{x} \in \mathbb{R}^3 : \mathbf{x} \cdot \mathbf{n} \geq d\}$ does *not* satisfy (3.52) if $n_3 < 0$.

Remark 3.7.3 (Rectangular domains do not satisfy (3.52)). Rectangular domains of the form $\mathcal{X} = [a_1, b_1] \times [a_2, b_2] \times [a_3, b_3]$ do not satisfy assumption (3.52). These domains are perhaps the most natural from a physical point of view. However, in this case an alternative, bespoke argument can be used to prove Corollary 3.7.7, and hence Theorems 3.1.1, 3.1.2; see [49].

Recall the following from [46, Definitions 1.1 and 1.2]: The cost c satisfies *Loeper's condition* if, for each $\mathbf{y} \in \mathcal{Y}$, there exists a diffeomorphism $\Phi_{\mathbf{y}} : \mathbb{R}^3 \to \mathbb{R}^3$ such that the map

$$\mathbb{R}^3 \ni \mathbf{x} \mapsto c(\Phi_{\mathbf{y}}(\mathbf{x}), \mathbf{y}) - c(\Phi_{\mathbf{y}}(\mathbf{x}), \mathbf{z})$$

is quasi-convex for all $\mathbf{z} \in \mathcal{Y}$ (meaning that its sublevel sets are convex). If in addition the set $\Phi_{\mathbf{y}}^{-1}(\mathcal{X})$ is convex for each $\mathbf{y} \in \mathcal{Y}$, then we say that $\mathcal{X}$ is *c-convex*.

Lemma 3.7.4 (Loeper's condition and c-convexity)**.** *Let* $\mathbf{x} \in \mathcal{X}$*,* $\mathbf{y}, \mathbf{z} \in \mathcal{Y}$*. Then*

$$c(\Phi(\mathbf{x}), \mathbf{y}) = -\frac{1}{y_3}\begin{pmatrix} x_1 \\ x_2 \\ x_3 \end{pmatrix} \cdot \begin{pmatrix} y_1 \\ y_2 \\ -1 \end{pmatrix} + \frac{f_{\text{cor}}^2}{2y_3}\left(y_1^2 + y_2^2\right). \tag{3.55}$$

In particular, $u : \mathbb{R}^3 \to \mathbb{R}$ *defined by*

$$u(\mathbf{x}) = c(\Phi(\mathbf{x}), \mathbf{y}) - c(\Phi(\mathbf{x}), \mathbf{z})$$

is affine and the cost c *satisfies Loeper's condition. Moreover,* $\mathcal{X}$ *satisfies assumption* (3.52) *if and only if* $\mathcal{X}$ *is* c*-convex.*

Proof. Equation (3.55) is a direct computation. Since u is affine, then it is quasi-convex. Therefore, by definition, c satisfies Loeper's condition (with $\Phi_{\mathbf{y}} = \Phi$ independent of $\mathbf{y}$), and assumption (3.52) is equivalent to c-convexity of $\mathcal{X}$. □

To prove that c satisfies Loeper's condition, we could have also chosen the c-exponential maps $\Phi_{\mathbf{y}} = \exp^c_{\mathbf{y}} := (-D_{\mathbf{y}} c(\cdot, \mathbf{y}))^{-1}$ depending on $\mathbf{y}$. However, the fact that Φ is independent of $\mathbf{y}$ (and that u is affine) has important consequences, as we will now see. Let

$$D_2^N := \left\{ \mathbf{y} = \left(\mathbf{y}^1, \dots, \mathbf{y}^N\right) \in (\mathbb{R}^3)^N : \mathbf{y}^i \neq \mathbf{y}^j \text{ whenever } i \neq j \right\}.$$

Recall the following definition:

Definition 3.7.5 (Classical Laguerre tessellations)**.** Given $(\boldsymbol{\psi}, \mathbf{y}) \in \mathbb{R}^N \times D_2^N$, the (classical) *Laguerre tessellation* of $\Phi^{-1}(\mathcal{X})$ generated by $(\boldsymbol{\psi}, \mathbf{y})$ is the partition $\{L_2^i(\boldsymbol{\psi}, \mathbf{y})\}_{i=1}^N$ defined by

$$L_2^i(\boldsymbol{\psi}, \mathbf{y}) = \left\{ \mathbf{x} \in \Phi^{-1}(\mathcal{X}) : \|\mathbf{x} - \mathbf{y}^i\|^2 - \psi^i \leq \|\mathbf{x} - \mathbf{y}^j\|^2 - \psi^j \ \forall\, j \in \{1, \dots, N\} \right\}.$$

The Laguerre cells $L_2^i(\boldsymbol{\psi}, \mathbf{y})$ are the intersection of $\Phi^{-1}(\mathcal{X})$ with convex polyhedra. Consequently, unlike c-Laguerre cells, they can be computed very efficiently. Classical Laguerre tessellations arise in semi-discrete optimal transport problems with *quadratic* cost. The following lemma asserts that c-Laguerre tessellations are just classical Laguerre tessellations in disguise. It also gives a practical way of computing them.

Lemma 3.7.6 (Rewriting c-Laguerre tessellations as classical Laguerre tessellations)**.** *Define* $\widehat{\mathbf{y}} : \mathcal{Y}^N \to (\mathbb{R}^3)^N$ *by* $\widehat{\mathbf{y}}(\mathbf{z}) = (\widehat{\mathbf{y}}^1(\mathbf{z}), \dots, \widehat{\mathbf{y}}^N(\mathbf{z}))$*, where*

$$\widehat{\mathbf{y}}^i(\mathbf{z}) = \frac{1}{2z_3^i} \begin{pmatrix} z_1^i \\ z_2^i \\ -1 \end{pmatrix}.$$

Define $\widehat{\boldsymbol{\psi}} : \mathbb{R}^N \times \mathcal{Y}^N \to \mathbb{R}^N$ *by*

$$\widehat{\psi}^i(\boldsymbol{w}, \mathbf{z}) = w^i + \left(\frac{z_1^i}{2z_3^i}\right)^2 + \left(\frac{z_2^i}{2z_3^i}\right)^2 + \left(\frac{1}{2z_3^i}\right)^2 - \frac{f_{\text{cor}}^2}{2z_3^i}\left(\left(z_1^i\right)^2 + \left(z_2^i\right)^2\right).$$

Then, for all $i \in \{1, \dots, N\}$ *and* $(\boldsymbol{w}, \mathbf{z}) \in \mathbb{R}^N \times D^N$,

$$\Phi^{-1}(L_c^i(\boldsymbol{w}, \mathbf{z})) = L_2^i(\widehat{\boldsymbol{\psi}}(\boldsymbol{w}, \mathbf{z}), \widehat{\mathbf{y}}(\mathbf{z})).$$

Proof. By (3.55), for all $\mathbf{x} \in \mathbb{R}^3$, $\mathbf{z} \in \mathcal{Y}$, $\boldsymbol{w} \in \mathbb{R}^N$,

$$\begin{aligned} c(\Phi(\mathbf{x}), \mathbf{z}^i) - w^i &= -\frac{1}{z_3^i}\begin{pmatrix} x_1 \\ x_2 \\ x_3 \end{pmatrix} \cdot \begin{pmatrix} z_1^i \\ z_2^i \\ -1 \end{pmatrix} + \frac{f_{\text{cor}}^2}{2z_3^i}\left(\left(z_1^i\right)^2 + \left(z_2^i\right)^2\right) - w^i \\ &= \|\mathbf{x} - \widehat{\mathbf{y}}^i(\mathbf{z})\|^2 - \widehat{\psi}^i(\boldsymbol{w}, \mathbf{z}) - \|\mathbf{x}\|^2. \end{aligned} \tag{3.56}$$

Let $\mathbf{x} \in \Phi^{-1}(\mathcal{X})$. Then

$$\begin{aligned} \mathbf{x} \in \Phi^{-1}(L_c^i(\boldsymbol{w}, \mathbf{z})) \quad &\iff \quad c(\Phi(\mathbf{x}), \mathbf{z}^i) - w^i \le c(\Phi(\mathbf{x}), \mathbf{z}^j) - w^j \quad \forall\, j \\ &\iff \quad \|\mathbf{x} - \widehat{\mathbf{y}}^i(\mathbf{z})\|^2 - \widehat{\psi}^i(\boldsymbol{w}, \mathbf{z}) \le \|\mathbf{x} - \widehat{\mathbf{y}}^j(\mathbf{z})\|^2 - \widehat{\psi}^j(\boldsymbol{w}, \mathbf{z}) \quad \forall\, j \\ &\iff \quad \mathbf{x} \in L_2^i(\widehat{\boldsymbol{\psi}}(\boldsymbol{w}, \mathbf{z}), \widehat{\mathbf{y}}(\mathbf{z})), \end{aligned}$$

as required. □

3.7.2 Proof of Lemma 3.3.6

In this section we prove Lemma 3.3.6. The main ingredient of the proof is the following lemma.

Lemma 3.7.7 (Regularity theory for semi-discrete optimal transport)**.** *Let* $\zeta : \mathcal{X} \to \mathbb{R}$ *be continuous. Let* $U \subset \mathbb{R}^N \times D_0^N$ *be the open set*

$$U = \left\{(\boldsymbol{w}, \mathbf{z}) \in \mathbb{R}^N \times D_0^N \,:\, \mathcal{L}^3(L_c^i(\boldsymbol{w}, \mathbf{z})) > 0 \;\forall\, i \in \{1, \dots, N\}\right\}.$$

Define $\boldsymbol{\Psi} = (\Psi^1, \dots, \Psi^N) : U \to \mathbb{R}^N$ *by*

$$\Psi^i(\boldsymbol{w}, \mathbf{z}) := \int_{L_c^i(\boldsymbol{w},\mathbf{z})} \zeta(\mathbf{x}) \, \mathrm{d}\mathbf{x}.$$

Then $\boldsymbol{\Psi}$ *is continuously differentiable. Moreover, for all* $j \in \{1, \dots, N\} \setminus \{i\}$,

$$\frac{\partial \Psi^i}{\partial w^j}(\boldsymbol{w}, \mathbf{z}) = -\int_{L_c^i(\boldsymbol{w},\mathbf{z}) \cap L_c^j(\boldsymbol{w},\mathbf{z})} \frac{\zeta(\mathbf{x})}{\|\nabla_{\mathbf{x}} c(\mathbf{x}, \mathbf{z}^i) - \nabla_{\mathbf{x}} c(\mathbf{x}, \mathbf{z}^j)\|} \, \mathrm{d}\mathcal{H}^2(\mathbf{x}), \tag{3.57}$$

$$\frac{\partial \Psi^i}{\partial \mathbf{z}^j}(\boldsymbol{w}, \mathbf{z}) = \int_{L_c^i(\boldsymbol{w},\mathbf{z}) \cap L_c^j(\boldsymbol{w},\mathbf{z})} \frac{\nabla_{\mathbf{y}} c(\mathbf{x}, \mathbf{z}^j) \, \zeta(\mathbf{x})}{\|\nabla_{\mathbf{x}} c(\mathbf{x}, \mathbf{z}^i) - \nabla_{\mathbf{x}} c(\mathbf{x}, \mathbf{z}^j)\|} \, \mathrm{d}\mathcal{H}^2(\mathbf{x}), \tag{3.58}$$

and

$$\frac{\partial \Psi^i}{\partial w^i}(\boldsymbol{w}, \mathbf{z}) = -\sum_{j \neq i} \frac{\partial \Psi^j}{\partial w^i}(\boldsymbol{w}, \mathbf{z}), \qquad \frac{\partial \Psi^i}{\partial \mathbf{z}^i}(\boldsymbol{w}, \mathbf{z}) = -\sum_{j \neq i} \frac{\partial \Psi^j}{\partial \mathbf{z}^i}(\boldsymbol{w}, \mathbf{z}). \tag{3.59}$$

This lemma could be proved using [27, Theorem 1], by proving that our transport cost c satisfies assumptions (Diff-2) and (Cont-2) of [27]. However, this is very involved. We give a shorter proof using Lemma 3.7.6 to reduce to the case of the classical quadratic transport cost.

Proof. Note that $\det(D\Phi) = f_{\mathrm{cor}}^{-4} g^{-1} > 0$ is constant. By the change of variables formula and Lemma 3.7.6,

$$\Psi^i(\boldsymbol{w}, \mathbf{z}) = \int_{L_c^i(\boldsymbol{w},\mathbf{z})} \zeta \, \mathrm{d}\mathcal{L}^3 = \int_{\Phi^{-1}(L_c^i(\boldsymbol{w},\mathbf{z}))} \zeta \circ \Phi \det(D\Phi) \, \mathrm{d}\mathcal{L}^3 = \det(D\Phi) \int_{L_2^i(\widehat{\boldsymbol{\psi}}(\boldsymbol{w},\mathbf{z}), \widehat{\mathbf{y}}(\mathbf{z}))} \zeta \circ \Phi \, \mathrm{d}\mathcal{L}^3.$$

Let $U_2 \subset \mathbb{R}^N \times D_2^N$ be the open set

$$U_2 = \left\{ (\boldsymbol{\psi}, \mathbf{y}) \in \mathbb{R}^N \times D_2^N \, : \, \mathcal{L}^3(L_2^i(\boldsymbol{\psi}, \mathbf{y})) > 0 \; \forall \, i \in \{1, \dots, N\} \right\}.$$

Define $\boldsymbol{\Psi}_2 = (\Psi_2^1, \dots, \Psi_2^N) : U_2 \to \mathbb{R}^N$ by

$$\Psi_2^i(\boldsymbol{\psi}, \mathbf{y}) := \int_{L_2^i(\boldsymbol{\psi},\mathbf{y})} \zeta(\Phi(\mathbf{x})) \, \mathrm{d}\mathbf{x}.$$

Then

$$\boldsymbol{\Psi}(\boldsymbol{w}, \mathbf{z}) = \det(D\Phi) \boldsymbol{\Psi}_2(\widehat{\boldsymbol{\psi}}(\boldsymbol{w}, \mathbf{z}), \widehat{\mathbf{y}}(\mathbf{z})). \tag{3.60}$$

By assumption (3.52) and [27, Proposition 2], $\boldsymbol{\Psi}_2$ is continuously differentiable and, for all

$j \in \{1, \dots, N\} \setminus \{i\}$,

$$\frac{\partial \Psi_2^i}{\partial \psi^j}(\boldsymbol{\psi}, \mathbf{y}) = -\frac{1}{2\|\mathbf{y}^i - \mathbf{y}^j\|} \int_{L_2^i(\boldsymbol{\psi},\mathbf{y}) \cap L_2^j(\boldsymbol{\psi},\mathbf{y})} \zeta(\Phi(\mathbf{x}))\, \mathrm{d}\mathcal{H}^2(\mathbf{x}), \tag{3.61}$$

$$\frac{\partial \Psi_2^i}{\partial \mathbf{y}^j}(\boldsymbol{\psi}, \mathbf{y}) = \frac{1}{\|\mathbf{y}^i - \mathbf{y}^j\|} \int_{L_2^i(\boldsymbol{\psi},\mathbf{y}) \cap L_2^j(\boldsymbol{\psi},\mathbf{y})} (\mathbf{y}^j - \mathbf{x}) \zeta(\Phi(\mathbf{x}))\, \mathrm{d}\mathcal{H}^2(\mathbf{x}), \tag{3.62}$$

and

$$\frac{\partial \Psi_2^i}{\partial \psi^i}(\boldsymbol{\psi}, \mathbf{y}) = -\sum_{j \neq i} \frac{\partial \Psi_2^j}{\partial \psi^i}(\boldsymbol{\psi}, \mathbf{y}), \qquad \frac{\partial \Psi_2^i}{\partial \mathbf{y}^i}(\boldsymbol{\psi}, \mathbf{y}) = -\sum_{j \neq i} \frac{\partial \Psi_2^j}{\partial \mathbf{y}^i}(\boldsymbol{\psi}, \mathbf{y}). \tag{3.63}$$

Note that $(\widehat{\boldsymbol{\psi}}(\boldsymbol{w}, \mathbf{z}), \widehat{\mathbf{y}}(\mathbf{z})) \in U_2$ for all $(\boldsymbol{w}, \mathbf{z}) \in U$. Therefore, by the Chain Rule and the smoothness of $\widehat{\boldsymbol{\psi}}$ and $\widehat{\mathbf{y}}$, it follows that $\boldsymbol{\Psi}$ is also continuously differentiable.

Next we compute $\partial \Psi^i / \partial w^j$ for $i \neq j$. For brevity let

$$L_2^{ij} = L_2^i(\widehat{\boldsymbol{\psi}}(\boldsymbol{w}, \mathbf{z}), \widehat{\mathbf{y}}(\mathbf{z})) \cap L_2^j(\widehat{\boldsymbol{\psi}}(\boldsymbol{w}, \mathbf{z}), \widehat{\mathbf{y}}(\mathbf{z})).$$

Then

$$\begin{aligned}
\frac{\partial \Psi^i}{\partial w^j}(\boldsymbol{w}, \mathbf{z}) &= \det(D\Phi) \sum_{k=1}^{N} \frac{\partial \Psi_2^i}{\partial \psi^k}(\widehat{\boldsymbol{\psi}}(\boldsymbol{w}, \mathbf{z}), \widehat{\mathbf{y}}(\mathbf{z})) \frac{\partial \widehat{\psi}^k}{\partial w^j}(\boldsymbol{w}, \mathbf{z}) \\
&= \det(D\Phi) \frac{\partial \Psi_2^i}{\partial \psi^j}(\widehat{\boldsymbol{\psi}}(\boldsymbol{w}, \mathbf{z}), \widehat{\mathbf{y}}(\mathbf{z})) \\
&= -\frac{\det(D\Phi)}{2\|\widehat{\mathbf{y}}^i(\mathbf{z}) - \widehat{\mathbf{y}}^j(\mathbf{z})\|} \int_{L_2^{ij}} \zeta \circ \Phi \, \mathrm{d}\mathcal{H}^2.
\end{aligned} \tag{3.64}$$

By the generalised area formula (see, e.g., [3, Theorem 2.91] or [11, Equation (2.7)]),

$$\int_{L_2^{ij}} \zeta \circ \Phi \, \mathrm{d}\mathcal{H}^2 = \int_{\Phi(L_2^{ij})} \frac{\zeta}{J_\Phi \circ \Phi^{-1}} \, \mathrm{d}\mathcal{H}^2 = \int_{L_c^i(\boldsymbol{w},\mathbf{z}) \cap L_c^j(\boldsymbol{w},\mathbf{z})} \frac{\zeta}{J_\Phi \circ \Phi^{-1}} \, \mathrm{d}\mathcal{H}^2, \tag{3.65}$$

where $J_\Phi : \mathbb{R}^3 \to \mathbb{R}$ is the Jacobian

$$J_\Phi = \|(D\Phi)^{-T}\mathbf{n}\| \det(D\Phi), \qquad \mathbf{n} = \frac{\widehat{\mathbf{y}}^j(\mathbf{z}) - \widehat{\mathbf{y}}^i(\mathbf{z})}{\|\widehat{\mathbf{y}}^j(\mathbf{z}) - \widehat{\mathbf{y}}^i(\mathbf{z})\|}.$$

Note that $\mathbf{n}$ is the outer unit normal to $L_2^i(\widehat{\boldsymbol{\psi}}(\boldsymbol{w}, \mathbf{z}), \widehat{\mathbf{y}}(\mathbf{z}))$ on the face L_2^{ij}. We will prove below that $J_\Phi \circ \Phi^{-1}$ is uniformly bounded from below by a positive constant, hence the integrals in (3.65) are well defined and the generalised area formula is valid.

By equation (3.56),

$$c(\mathbf{x}, \mathbf{z}^i) - \boldsymbol{w}^i = -2\Phi^{-1}(\mathbf{x}) \cdot \widehat{\mathbf{y}}^i(\mathbf{z}) + \|\widehat{\mathbf{y}}^i(\mathbf{z})\|^2 - \widehat{\psi}^i(\boldsymbol{w}, \mathbf{z}). \tag{3.66}$$

Differentiating this with respect to $\mathbf{x}$ gives

$$\nabla_{\mathbf{x}} c(\mathbf{x}, \mathbf{z}^i) = -2(D\Phi^{-1}(\mathbf{x}))^T \widehat{\mathbf{y}}^i(\mathbf{z}) = -2(D\Phi(\Phi^{-1}(\mathbf{x}))^{-T} \widehat{\mathbf{y}}^i(\mathbf{z}).$$

Therefore

$$\|\nabla_{\mathbf{x}} c(\mathbf{x}, \mathbf{z}^i) - \nabla_{\mathbf{x}} c(\mathbf{x}, \mathbf{z}^j)\| = \frac{2J_\Phi(\Phi^{-1}(\mathbf{x}))\|\widehat{\mathbf{y}}^j(\mathbf{z}) - \widehat{\mathbf{y}}^i(\mathbf{z})\|}{\det(D\Phi)}. \tag{3.67}$$

Combining equations (3.64), (3.65) and (3.67) proves (3.57), as required.

Next we prove a lower bound on $J_\Phi \circ \Phi^{-1}$. Let $\mathbf{z} \in D_0^N$ and $\eta = \min_{i \neq j} |z_3^i - z_3^j| > 0$. Then

$$\|\nabla_{\mathbf{x}} c(\mathbf{x}, \mathbf{z}^i) - \nabla_{\mathbf{x}} c(\mathbf{x}, \mathbf{z}^j)\| \geq |\partial_{x_3} c(\mathbf{x}, \mathbf{z}^i) - \partial_{x_3} c(\mathbf{x}, \mathbf{z}^j)| = g\frac{|z_3^i - z_3^j|}{z_3^i z_3^j} \geq g\eta\delta^2 \tag{3.68}$$

since $\mathbf{z}^i, \mathbf{z}^j \in \mathcal{Y} = \mathbb{R}^2 \times (\delta, 1/\delta)$. By (3.67), for all $\mathbf{x} \in \mathcal{X}$,

$$J_\Phi(\Phi^{-1}(\mathbf{x})) = \frac{\det(D\Phi)\|\nabla_{\mathbf{x}} c(\mathbf{x}, \mathbf{z}^i) - \nabla_{\mathbf{x}} c(\mathbf{x}, \mathbf{z}^j)\|}{2\|\widehat{\mathbf{y}}^j(\mathbf{z}) - \widehat{\mathbf{y}}^i(\mathbf{z})\|} \geq \frac{f_{\text{cor}}^{-4}\,\eta\,\delta^2}{2\|\widehat{\mathbf{y}}^j(\mathbf{z}) - \widehat{\mathbf{y}}^i(\mathbf{z})\|},$$

which is the required uniform lower bound.

Next we prove (3.58). Differentiating (3.66) with respect to $\mathbf{z}^i$ gives

$$\nabla_{\mathbf{y}} c(\mathbf{x}, \mathbf{z}^i) = 2\left(\frac{\partial \widehat{\mathbf{y}}^i}{\partial \mathbf{z}^i}(\mathbf{z})\right)^T (-\Phi^{-1}(\mathbf{x}) + \widehat{\mathbf{y}}^i(\mathbf{z})) - \frac{\partial \widehat{\psi}^i}{\partial \mathbf{z}^i}(\boldsymbol{w}, \mathbf{z}). \tag{3.69}$$

By (3.60), for all $i \neq j$,

$$\begin{aligned}
&\frac{\partial \Psi^i}{\partial \mathbf{z}^j}(\boldsymbol{w}, \mathbf{z}) = \\
&= \det(D\Phi)\left(\frac{\partial \Psi_2^i}{\partial \psi^j}(\widehat{\boldsymbol{\psi}}(\boldsymbol{w}, \mathbf{z}), \widehat{\mathbf{y}}(\mathbf{z}))\frac{\partial \widehat{\psi}^j}{\partial \mathbf{z}^j}(\boldsymbol{w}, \mathbf{z}) + \left(\frac{\partial \widehat{\mathbf{y}}^j}{\partial \mathbf{z}^j}(\mathbf{z})\right)^T \frac{\partial \Psi_2^i}{\partial \mathbf{y}^j}(\widehat{\boldsymbol{\psi}}(\boldsymbol{w}, \mathbf{z}), \widehat{\mathbf{y}}(\mathbf{z}))\right) \\
&= -\frac{\det(D\Phi)}{2\|\widehat{\mathbf{y}}^i(\mathbf{z}) - \widehat{\mathbf{y}}^j(\mathbf{z})\|}\int_{L_2^{ij}} \zeta(\Phi(\mathbf{x}))\,\mathrm{d}\mathcal{H}^2(\mathbf{x})\,\frac{\partial \widehat{\psi}^j}{\partial \mathbf{z}^j}(\boldsymbol{w}, \mathbf{z}) \\
&\quad + \left(\frac{\partial \widehat{\mathbf{y}}^j}{\partial \mathbf{z}^j}(\mathbf{z})\right)^T \frac{\det(D\Phi)}{\|\widehat{\mathbf{y}}^i(\mathbf{z}) - \widehat{\mathbf{y}}^j(\mathbf{z})\|}\int_{L_2^{ij}} (\widehat{\mathbf{y}}^j(\mathbf{z}) - \mathbf{x})\zeta(\Phi(\mathbf{x}))\,\mathrm{d}\mathcal{H}^2(\mathbf{x})
\end{aligned}$$

$$= -\frac{\det(D\Phi)}{2\|\widehat{\mathbf{y}}^i(\mathbf{z}) - \widehat{\mathbf{y}}^j(\mathbf{z})\|} \int_{\Phi(L_2^{ij})} \frac{\zeta(\mathbf{x})}{J_\Phi(\Phi^{-1}(\mathbf{x}))}\, \mathrm{d}\mathcal{H}^2(\mathbf{x})\, \frac{\partial \widehat{\psi}^j}{\partial \mathbf{z}^j}(\boldsymbol{w}, \mathbf{z})$$

$$+ \left(\frac{\partial \widehat{\mathbf{y}}^j}{\partial \mathbf{z}^j}(\mathbf{z})\right)^T \frac{\det(D\Phi)}{\|\widehat{\mathbf{y}}^i(\mathbf{z}) - \widehat{\mathbf{y}}^j(\mathbf{z})\|} \int_{\Phi(L_2^{ij})} \frac{(\widehat{\mathbf{y}}^j(\mathbf{z}) - \Phi^{-1}(\mathbf{x}))\zeta(\mathbf{x})}{J_\Phi(\Phi^{-1}(\mathbf{x}))}\, \mathrm{d}\mathcal{H}^2(\mathbf{x})$$

$$= \frac{\det(D\Phi)}{2\|\widehat{\mathbf{y}}^i(\mathbf{z}) - \widehat{\mathbf{y}}^j(\mathbf{z})\|} \int_{\Phi(L_2^{ij})} \frac{\zeta}{J_\Phi \circ \Phi^{-1}} \left(2\left(\frac{\partial \widehat{\mathbf{y}}^j}{\partial \mathbf{z}^j}(\mathbf{z})\right)^T (\widehat{\mathbf{y}}^j(\mathbf{z}) - \Phi^{-1}) - \frac{\partial \widehat{\psi}^j}{\partial \mathbf{z}^j}(\boldsymbol{w}, \mathbf{z})\right) \mathrm{d}\mathcal{H}^2.$$

Combining this with (3.67) and (3.69) proves (3.58), as desired.

Finally, (3.59) follows by differentiating

$$\sum_{j=1}^{N} \Psi^j(\boldsymbol{w}, \mathbf{z}) = \int_{\mathcal{X}} \zeta(\mathbf{x})\, \mathrm{d}\mathbf{x}$$

with respect to w^i and $\mathbf{z}^i$. □

Finally we are in a position to prove Lemma 3.3.6.

Proof of Lemma 3.3.6. For each $i \in \{1, \dots, N\}$, define the auxiliary function $h^i : U \times U \to \mathbb{R}$ by

$$h^i(\boldsymbol{w}_1, \mathbf{z}_1, \boldsymbol{w}_2, \mathbf{z}_2) = \int_{L_c^i(\boldsymbol{w}_1, \mathbf{z}_1)} \zeta(\mathbf{x}, \boldsymbol{w}_2, \mathbf{z}_2)\, \mathrm{d}\mathbf{x}.$$

Then $\Psi^i(\boldsymbol{w}, \mathbf{z}) = h^i(\boldsymbol{w}, \mathbf{z}, \boldsymbol{w}, \mathbf{z})$. Fix an arbitrary point $(\boldsymbol{w}_0, \mathbf{z}_0) \in U$ and let $K \subset U$ be a compact neighbourhood of $(\boldsymbol{w}_0, \mathbf{z}_0)$ such that $|z_3^i - z_3^j| \geq \eta$ for all $i, j \in \{1, \dots, N\}$, $i \neq j$, for some $\eta > 0$. We will prove that h^i is continuously differentiable at $(\boldsymbol{w}_0, \mathbf{z}_0, \boldsymbol{w}_0, \mathbf{z}_0)$, and hence Ψ^i is continuously differentiable at $(\boldsymbol{w}_0, \mathbf{z}_0)$. To be precise, firstly we will prove that

$$\forall\, (\boldsymbol{w}_2, \mathbf{z}_2) \in U,\ \frac{\partial h^i}{\partial \boldsymbol{w}_1}(\cdot, \cdot, \boldsymbol{w}_2, \mathbf{z}_2) \text{ and } \frac{\partial h^i}{\partial \mathbf{z}_1}(\cdot, \cdot, \boldsymbol{w}_2, \mathbf{z}_2) \text{ are continuous in } U, \tag{3.70}$$

$$\left\{\frac{\partial h^i}{\partial \boldsymbol{w}_1}(\boldsymbol{w}_1, \mathbf{z}_1, \cdot, \cdot)\right\}_{(\boldsymbol{w}_1, \mathbf{z}_1) \in K} \text{ is uniformly Lipschitz continuous in } K, \tag{3.71}$$

$$\left\{\frac{\partial h^i}{\partial \mathbf{z}_1}(\boldsymbol{w}_1, \mathbf{z}_1, \cdot, \cdot)\right\}_{(\boldsymbol{w}_1, \mathbf{z}_1) \in K} \text{ is uniformly Lipschitz continuous in } K. \tag{3.72}$$

Here *uniformly Lipschitz* means that the Lipschitz constants are independent of $(\boldsymbol{w}_1, \mathbf{z}_1) \in K$. It follows from (3.70)–(3.72) that the partial derivatives $\partial h^i / \partial \boldsymbol{w}_1$ and $\partial h^i / \partial \mathbf{z}_1$ are continuous

at $(\boldsymbol{w}_0, \mathbf{z}_0, \boldsymbol{w}_0, \mathbf{z}_0)$. Secondly we will prove that

$$\forall\, (\boldsymbol{w}_1, \mathbf{z}_1) \in U,\ \frac{\partial h^i}{\partial \boldsymbol{w}_2}(\boldsymbol{w}_1, \mathbf{z}_1, \cdot, \cdot) \text{ and } \frac{\partial h^i}{\partial \mathbf{z}_2}(\boldsymbol{w}_1, \mathbf{z}_1, \cdot, \cdot) \text{ are continuous in } U, \tag{3.73}$$

$$\left\{\frac{\partial h^i}{\partial \boldsymbol{w}_2}(\cdot, \cdot, \boldsymbol{w}_2, \mathbf{z}_2)\right\}_{(\boldsymbol{w}_2, \mathbf{z}_2) \in K} \text{ and } \left\{\frac{\partial h^i}{\partial \mathbf{z}_2}(\cdot, \cdot, \boldsymbol{w}_2, \mathbf{z}_2)\right\}_{(\boldsymbol{w}_2, \mathbf{z}_2) \in K} \text{ are equicontinuous in } K. \tag{3.74}$$

Therefore the partial derivatives $\partial h^i/\partial \boldsymbol{w}_2$ and $\partial h^i/\partial \mathbf{z}_2$ are also continuous at $(\boldsymbol{w}_0, \mathbf{z}_0, \boldsymbol{w}_0, \mathbf{z}_0)$.

Step 1: proof of (3.70)–(3.72). By Lemma 3.7.7, the function $h^i(\cdot, \cdot, \boldsymbol{w}_2, \mathbf{z}_2)$ is continuously differentiable in U for all $(\boldsymbol{w}_2, \mathbf{z}_2) \in U$. (Here we have used the assumption in Lemma 3.3.6 that $\zeta(\cdot, \boldsymbol{w}_2, \mathbf{z}_2)$ is continuous.) This proves (3.70). Moreover, we read off from Lemma 3.7.7 that, for all $j \in \{1, \dots, N\} \setminus \{i\}$,

$$\frac{\partial h^i}{\partial w_1^j}(\boldsymbol{w}_1, \mathbf{z}_1, \boldsymbol{w}_2, \mathbf{z}_2) = -\int_{L_c^i(\boldsymbol{w}_1, \mathbf{z}_1) \cap L_c^j(\boldsymbol{w}_1, \mathbf{z}_1)} \frac{\zeta(\mathbf{x}, \boldsymbol{w}_2, \mathbf{z}_2)}{\|\nabla_{\mathbf{x}} c(\mathbf{x}, \mathbf{z}_1^i) - \nabla_{\mathbf{x}} c(\mathbf{x}, \mathbf{z}_1^j)\|}\, \mathrm{d}\mathcal{H}^2(\mathbf{x}), \tag{3.75}$$

$$\frac{\partial h^i}{\partial \mathbf{z}_1^j}(\boldsymbol{w}_1, \mathbf{z}_1, \boldsymbol{w}_2, \mathbf{z}_2) = \int_{L_c^i(\boldsymbol{w}_1, \mathbf{z}_1) \cap L_c^j(\boldsymbol{w}_1, \mathbf{z}_1)} \frac{\nabla_{\mathbf{y}} c(\mathbf{x}, \mathbf{z}_1^j)\, \zeta(\mathbf{x}, \boldsymbol{w}_2, \mathbf{z}_2)}{\|\nabla_{\mathbf{x}} c(\mathbf{x}, \mathbf{z}_1^i) - \nabla_{\mathbf{x}} c(\mathbf{x}, \mathbf{z}_1^j)\|}\, \mathrm{d}\mathcal{H}^2(\mathbf{x}), \tag{3.76}$$

and

$$\frac{\partial h^i}{\partial w_1^i}(\boldsymbol{w}_1, \mathbf{z}_1, \boldsymbol{w}_2, \mathbf{z}_2) = -\sum_{j \neq i} \frac{\partial h^j}{\partial w_1^i}(\boldsymbol{w}_1, \mathbf{z}_1, \boldsymbol{w}_2, \mathbf{z}_2), \tag{3.77}$$

$$\frac{\partial h^i}{\partial \mathbf{z}_1^i}(\boldsymbol{w}_1, \mathbf{z}_1, \boldsymbol{w}_2, \mathbf{z}_2) = -\sum_{j \neq i} \frac{\partial h^j}{\partial \mathbf{z}_1^i}(\boldsymbol{w}_1, \mathbf{z}_1, \boldsymbol{w}_2, \mathbf{z}_2). \tag{3.78}$$

Next we prove (3.71). For all $\mathbf{x} \in \mathcal{X}$, $(\boldsymbol{w}_1, \mathbf{z}_1) \in K$,

$$\|\nabla_{\mathbf{x}} c(\mathbf{x}, \mathbf{z}_1^i) - \nabla_{\mathbf{x}} c(\mathbf{x}, \mathbf{z}_1^k)\| \geq g\eta\delta^2$$

by (3.68). For all $(\boldsymbol{w}_1, \mathbf{z}_1)$, $(\boldsymbol{w}_2, \mathbf{z}_2)$, $(\widetilde{\boldsymbol{w}}_2, \widetilde{\mathbf{z}}_2) \in K$ and all $i, j \in \{1, \dots, N\}$, $i \neq j$,

$$\begin{aligned}
&\left|\frac{\partial h^i}{\partial w_1^j}(\boldsymbol{w}_1, \mathbf{z}_1, \boldsymbol{w}_2, \mathbf{z}_2) - \frac{\partial h^i}{\partial w_1^j}(\boldsymbol{w}_1, \mathbf{z}_1, \widetilde{\boldsymbol{w}}_2, \widetilde{\mathbf{z}}_2)\right| \\
&\quad \leq \int_{L_c^i(\boldsymbol{w}_1, \mathbf{z}_1) \cap L_c^j(\boldsymbol{w}_1, \mathbf{z}_1)} \frac{|\zeta(\mathbf{x}, \boldsymbol{w}_2, \mathbf{z}_2) - \zeta(\mathbf{x}, \widetilde{\boldsymbol{w}}_2, \widetilde{\mathbf{z}}_2)|}{\|\nabla_{\mathbf{x}} c(\mathbf{x}, \mathbf{z}_1^i) - \nabla_{\mathbf{x}} c(\mathbf{x}, \mathbf{z}_1^j)\|}\, \mathrm{d}\mathcal{H}^2(\mathbf{x})
\end{aligned}$$

$$\leq \mathcal{H}^2(L_c^i(\boldsymbol{w}_1, \mathbf{z}_1) \cap L_c^j(\boldsymbol{w}_1, \mathbf{z}_1)) \frac{L(K)}{g\eta\delta^2} \|(\boldsymbol{w}_2, \mathbf{z}_2) - (\widetilde{\boldsymbol{w}}_2, \widetilde{\mathbf{z}}_2)\|, \tag{3.79}$$

where $L(K)$ was defined in the statement of Lemma 3.3.6. Define

$$f^{ij} = \left\{\mathbf{x} \in \mathbb{R}^3 : c(\mathbf{x}, \mathbf{z}_1^i) - w_1^i = c(\mathbf{x}, \mathbf{z}_1^j) - w_1^j\right\}.$$

Note that $L_c^i(\boldsymbol{w}_1, \mathbf{z}_1) \cap L_c^j(\boldsymbol{w}_1, \mathbf{z}_1) \subseteq f^{ij}$. By [31, Theorem 2.8],

$$\begin{aligned}
\mathcal{H}^2(L_c^i(\boldsymbol{w}_1, \mathbf{z}_1) \cap L_c^j(\boldsymbol{w}_1, \mathbf{z}_1)) &\leq \mathcal{H}^2(\mathcal{X} \cap f^{ij}) \\
&\leq \mathrm{Lip}(\Phi|_{\mathcal{X}})^2 \mathcal{H}^2\left(\Phi^{-1}(\mathcal{X} \cap f^{ij})\right) \\
&= \mathrm{Lip}(\Phi|_{\mathcal{X}})^2 \mathcal{H}^2\left(\Phi^{-1}(\mathcal{X}) \cap \Phi^{-1}(f^{ij})\right) \\
&\leq \mathrm{Lip}(\Phi|_{\mathcal{X}})^2 \, \pi \left(\frac{\mathrm{diam}(\Phi^{-1}(\mathcal{X}))}{2}\right)^2,
\end{aligned} \tag{3.80}$$

where in the last line we used the fact that $\Phi^{-1}(f^{ij})$ is a plane (by Lemma 3.7.4) and the isodiametric inequality. Combining (3.79) and (3.80) proves that $\partial h^i / \partial w_1^j(\boldsymbol{w}_1, \mathbf{z}_1, \cdot, \cdot)$ is Lipschitz continuous in K with Lipschitz constant independent of $(\boldsymbol{w}_1, \mathbf{z}_1) \in K$. By (3.77), the same holds for $\partial h^i / \partial w_1^i(\boldsymbol{w}_1, \mathbf{z}_1, \cdot, \cdot)$. This proves (3.71). The proof of (3.72) is very similar.

Step 2: proof of (3.73), (3.74). First we show that the partial derivative $\partial h^i / \partial \boldsymbol{w}_2$ exists. Fix $(\boldsymbol{w}_1, \mathbf{z}_1, \boldsymbol{w}_2, \mathbf{z}_2) \in U \times U$ and let $k \in \{1, \ldots, N\}$ and $\varepsilon \in (0, 1)$. To show that h^i is differentiable with respect to $\boldsymbol{w}_2$, consider the difference quotient

$$\frac{h^i(\boldsymbol{w}_1, \mathbf{z}_1, \boldsymbol{w}_2 + \varepsilon \mathbf{e}_k, \mathbf{z}_2) - h^i(\boldsymbol{w}_1, \mathbf{z}_1, \boldsymbol{w}_2, \mathbf{z}_2)}{\varepsilon} = \int_{L_c^i(\boldsymbol{w}_1, \mathbf{z}_1)} \frac{\zeta(\mathbf{x}, \boldsymbol{w}_2 + \varepsilon \mathbf{e}_k, \mathbf{z}_2) - \zeta(\mathbf{x}, \boldsymbol{w}_2, \mathbf{z}_2)}{\varepsilon} \, \mathrm{d}\mathbf{x},$$

where $\{\mathbf{e}_j\}_{j=1}^N$ is the standard basis of $\mathbb{R}^N$. Note that

$$\lim_{\varepsilon \to 0} \frac{\zeta(\mathbf{x}, \boldsymbol{w}_2 + \varepsilon \mathbf{e}_k, \mathbf{z}_2) - \zeta(\mathbf{x}, \boldsymbol{w}_2, \mathbf{z}_2)}{\varepsilon} = \frac{\partial \zeta}{\partial \boldsymbol{w}}(\mathbf{x}, \boldsymbol{w}_2, \mathbf{z}_2)$$

for all $\mathbf{x} \in S(\boldsymbol{w}_2, \mathbf{z}_2)$, in particular, for $\mathcal{L}^3$-almost every $\mathbf{x} \in L_c^i(\boldsymbol{w}_1, \mathbf{z}_1)$. Moreover,

$$\left| \frac{\zeta(\mathbf{x}, \boldsymbol{w}_2 + \varepsilon \mathbf{e}_k, \mathbf{z}_2) - \zeta(\mathbf{x}, \boldsymbol{w}_2, \mathbf{z}_2)}{\varepsilon} \right| \leq L(\widetilde{K}),$$

where $\widetilde{K} = \{(\boldsymbol{w}_2 + \rho \mathbf{e}_k, \mathbf{z}_2) : \rho \in [0, 1]\}$ and L was defined in the statement of Lemma 3.3.6.

Therefore, by the Lebesgue Dominated Convergence Theorem,

$$\frac{\partial h^i}{\partial \boldsymbol{w}_2}(\boldsymbol{w}_1, \mathbf{z}_1, \boldsymbol{w}_2, \mathbf{z}_2) = \int_{L_c^i(\boldsymbol{w}_1, \mathbf{z}_1)} \frac{\partial \zeta}{\partial \boldsymbol{w}}(\mathbf{x}, \boldsymbol{w}_2, \mathbf{z}_2)\, \mathrm{d}\mathbf{x}. \tag{3.81}$$

Similarly,

$$\frac{\partial h^i}{\partial \mathbf{z}_2}(\boldsymbol{w}_1, \mathbf{z}_1, \boldsymbol{w}_2, \mathbf{z}_2) = \int_{L_c^i(\boldsymbol{w}_1, \mathbf{z}_1)} \frac{\partial \zeta}{\partial \mathbf{z}}(\mathbf{x}, \boldsymbol{w}_2, \mathbf{z}_2)\, \mathrm{d}\mathbf{x}. \tag{3.82}$$

Then (3.73) follows from the assumption that the partial derivatives $\partial\zeta/\partial\boldsymbol{w}(\mathbf{x}, \cdot, \cdot)$, $\partial\zeta/\partial\mathbf{z}(\mathbf{x}, \cdot, \cdot)$ are continuous at $(\boldsymbol{w}_2, \mathbf{z}_2)$ for all $\mathbf{x} \in S(\boldsymbol{w}_2, \mathbf{z}_2)$, along with another application of the Lebesgue Dominated Convergence Theorem.

Finally we prove (3.74). For all $(\boldsymbol{w}_1, \mathbf{z}_1)$, $(\widetilde{\boldsymbol{w}}_1, \widetilde{\mathbf{z}}_1)$, $(\boldsymbol{w}_2, \mathbf{z}_2) \in K$,

$$\begin{aligned}
&\left\| \frac{\partial h^i}{\partial \boldsymbol{w}_2}(\widetilde{\boldsymbol{w}}_1, \widetilde{\mathbf{z}}_1, \boldsymbol{w}_2, \mathbf{z}_2) - \frac{\partial h^i}{\partial \boldsymbol{w}_2}(\boldsymbol{w}_1, \mathbf{z}_1, \boldsymbol{w}_2, \mathbf{z}_2) \right\| \\
&\quad = \left\| \int_{L_c^i(\widetilde{\boldsymbol{w}}_1, \widetilde{\mathbf{z}}_1)} \frac{\partial \zeta}{\partial \boldsymbol{w}}(\mathbf{x}, \boldsymbol{w}_2, \mathbf{z}_2)\, \mathrm{d}\mathbf{x} - \int_{L_c^i(\boldsymbol{w}_1, \mathbf{z}_1)} \frac{\partial \zeta}{\partial \boldsymbol{w}}(\mathbf{x}, \boldsymbol{w}_2, \mathbf{z}_2)\, \mathrm{d}\mathbf{x} \right\| \\
&\quad \le \max_{\mathbf{x} \in \mathcal{X}} \left\| \frac{\partial \zeta}{\partial \boldsymbol{w}}(\mathbf{x}, \boldsymbol{w}_2, \mathbf{z}_2) \right\| \left\| \chi_{L_c^i(\widetilde{\boldsymbol{w}}_1, \widetilde{\mathbf{z}}_1)} - \chi_{L_c^i(\boldsymbol{w}_1, \mathbf{z}_1)} \right\|_{L^1(\mathcal{X})} \\
&\quad \le L(K) \left\| \chi_{L_c^i(\widetilde{\boldsymbol{w}}_1, \widetilde{\mathbf{z}}_1)} - \chi_{L_c^i(\boldsymbol{w}_1, \mathbf{z}_1)} \right\|_{L^1(\mathcal{X})}.
\end{aligned} \tag{3.83}$$

It can be read off from the proof of [53, Proposition 38(vii)] that

$$\|\chi_{L_c^i(\widetilde{\boldsymbol{w}}_1, \widetilde{\mathbf{z}}_1)} - \chi_{L_c^i(\boldsymbol{w}_1, \mathbf{z}_1)}\|_{L^1(\mathcal{X})} \to 0 \quad \text{as} \quad (\widetilde{\boldsymbol{w}}_1, \widetilde{\mathbf{z}}_1) \to (\boldsymbol{w}_1, \mathbf{z}_1).$$

Then, by (3.83), $\partial h^i/\partial \boldsymbol{w}_2(\cdot, \cdot, \boldsymbol{w}_2, \mathbf{z}_2)$ is continuous on the compact set K, hence uniformly continuous, and moreover its modulus of continuity is independent of $(\boldsymbol{w}_2, \mathbf{z}_2)$. The same holds for $\partial h^i/\partial \mathbf{z}_2(\cdot, \cdot, \boldsymbol{w}_2, \mathbf{z}_2)$. This proves (3.74).

Step 3. The expressions for the partial derivatives of Ψ^i in the statement of Lemma 3.3.6 can be read off immediately from (3.75)–(3.78), (3.81) and (3.82). □

(a) 5 Laguerre cells

(b) 10 Laguerre cells

(c) 25 Laguerre cells

(d) 50 Laguerre cells

Figure 3.2: c-Laguerre tessellations (see Definition 3.2.8) in the (x_1, x_3)-plane for the cost function $c = c_{2d}$ (see (3.16)). The colours distinguish the cells. For each plot, $\mathcal{X} = [0,1]^2$, $f_{cor} = 1$, $g = 1$, the seeds $\mathbf{z}^i$ were sampled uniformly from $\mathcal{X}$, and the weights w^i were chosen so that the cells have equal area (by maximising the dual function as in (3.19)).

Chapter 4

Geometric Conditions on the Physical Domain

4.1 Introduction

In Chapter 3 we proved the existence of weak solutons under the assumption that $\mathcal{X}$ is c-concave. This excludes rectangular domains. In this chapter we give a bespoke proof for rectangular domains.

4.1.1 The dGKL Conditions

The solution to the semi-discrete optimal transport problem partitions the source domain into regions called Laguerre cells. The boundaries between these cells are key to the dGKL conditions, which involve measuring the volume or area of a small neighbourhood around these boundaries.

Given $\varepsilon > 0$ and a set $A \subset \mathbb{R}^d$, we define the ε-neighbourhood of A by

$$\mathcal{N}_\varepsilon(A) = \left\{ \mathbf{x} \in \mathbb{R}^3 : \inf_{\mathbf{y} \in A} \|\mathbf{x} - \mathbf{y}\| \leq \varepsilon \right\}.$$

Thus the neighbourhood $\mathcal{N}_{L_\varepsilon \varepsilon}$ is the set $\{\mathbf{x} : |d_{ik}(\mathbf{x})| \leq L_\varepsilon \varepsilon\}$. Let $(\boldsymbol{w}, \mathbf{z}) \in \mathbb{R}^N \times D^N$. The face between two cells, L_c^i and L_c^j, is contained in the set

$$f^{ij}(\boldsymbol{w}, \mathbf{z}) = \left\{ \mathbf{x} \in \mathbb{R}^d : c(\mathbf{x}, \mathbf{z}^i) - w^i = c(\mathbf{x}, \mathbf{z}^j) - w^j \right\}, \tag{4.1}$$

for $i, j \in \{1, \ldots, N\}$, $i \neq j$. In addition, following the notation of [27], for all $i \in \{1, \ldots, N\}$, define $f^{i0}(\boldsymbol{w}, \mathbf{z}) := \partial\mathcal{X}$. We will opt for more classical notation in the proof.

Since the cost c is twisted, the sets f^{ij} are $\mathcal{C}^{1,1}$, 2-manifolds by [54, proof of Proposition 37]. We characterise them below in Lemma 4.2.1. If the Laguerre cells $L_c^i(\boldsymbol{w}, \mathbf{z})$ and $L_c^j(\boldsymbol{w}, \mathbf{z})$ share a face, then this face is contained in f^{ij}. To be precise, $L_c^i(\boldsymbol{w}, \mathbf{z}) \cap L_c^j(\boldsymbol{w}, \mathbf{z}) \subseteq f^{ij}(\boldsymbol{w}, \mathbf{z})$.

The following technical conditions were introduced in [27]. These are a set of geometric requirements designed to ensure the Laguerre tessellation is sufficiently well-behaved, which is a crucial prerequisite for establishing the regularity of the right-hand side of our governing ODE (Eq. (3.6)). The baseline assumption is the $\mathcal{C}^2$ smoothness of the cost function, which allows the cell boundaries to be defined as smooth surfaces. The remaining conditions prevent these surfaces from forming pathological configurations. The non-degeneracy condition ensures that the boundaries between any two cells are sharply defined, while the uniform bound on their surface area controls their geometric complexity. The final conditions govern how these boundaries intersect to form edges, ruling out pathological features like cusps or tangential intersections. Taken together, these conditions guarantee that the geometric quantities defining the ODE's right-hand side are stable and regular functions of the particle positions.

Definition 4.1.1 (The dGKL Conditions [27])**.** Let $(\boldsymbol{w}, \mathbf{z}) \in \mathbb{R}^N \times D^N$. The *dGKL Conditions* consist of the following requirements from [27, Definitions 1 & 2]:

1. $c \in \mathcal{C}^2(\mathcal{X} \times \mathcal{Y})$.

2. There exists $\eta > 0$ such that for all $i, k \in \{1, \dots, N\}$, $i \neq k$, and all $\mathbf{x} \in f^{ik}(\boldsymbol{w}, \mathbf{z})$,

$$\left\|\nabla_{\mathbf{x}} c(\mathbf{x}, \mathbf{z}^i) - \nabla_{\mathbf{x}} c(\mathbf{x}, \mathbf{z}^k)\right\| \geq \eta.$$

3. For all $i \in \{1, \dots, N\}$, there exists $\varepsilon_0 > 0$ and $C > 0$ such that for all $j, k \in \{0, \dots, N\}$, $j \neq k$, and all $\varepsilon_1, \varepsilon_2 \in (0, \varepsilon_0)$,

$$\mathcal{L}^3\big(\mathcal{X} \cap \mathcal{N}_{\varepsilon_1}\big(f^{ik}(\boldsymbol{w}, \mathbf{z})\big) \cap \mathcal{N}_{\varepsilon_2}\big(f^{ij}(\boldsymbol{w}, \mathbf{z})\big)\big) \leq C\varepsilon_1\varepsilon_2. \tag{3a}$$

   Moreover,

$$\lim_{\varepsilon_1 \to 0} \mathcal{H}^2\big(\mathcal{X} \cap f^{ik}(\boldsymbol{w}, \mathbf{z}) \cap \mathcal{N}_{\varepsilon_1}\big(f^{ij}(\boldsymbol{w}, \mathbf{z})\big)\big) = 0. \tag{3b}$$

4. There exists $C > 0$ such that for all $i, j \in \{0, \dots, N\}$, $i \neq j$,

$$\mathcal{H}^2(f^{ij}(\boldsymbol{w}, \mathbf{z}) \cap \mathcal{X}) \leq C.$$

Remark 4.1.2. Conditions (*3a*) and (*3b*) in Theorem 4.1.1 correspond to conditions (Diff-2-b) and (Diff-2-c) in [27, Definition 1]. Note that there is a minor typo in [27, Definition 1]; in

(Diff-2-b) and (Diff-2-c) the ε-neighbourhoods should be intersected with the domain, just as we intersect the ε-neighbourhoods with $\mathcal{X}$ in (*3a*) and (*3b*). Moreover, in [27, Theorem 1] it is assumed that $\mathcal{X}$ is convex, which is not necessary unless the cost is quadratic. In general, it is sufficient that the measure σ is Hölder continuous on a c-convex set containing its support (see Definition 3.7.1 for the definition of c-convexity).

4.1.2 Main Results

Having established the necessary definitions, we can now formally state the main theorem of this chapter.

Theorem 4.1.3. *Consider the compressible SG cost $c \in \mathcal{C}^2(\mathcal{X} \times \mathcal{Y})$ given by Eq.* (3.9)*, which is twisted. Let $\mathcal{X}$ be a rectangular domain aligned with the canonical axes, which we define as $\mathcal{X} := [x_l, x_r] \times [y_l, y_r] \times [B, T]$, where the constants x_l, x_r, y_l, y_r determine the lateral boundaries, while B and T define the bottom and top boundaries, respectively. If the seeds $\mathbf{z}^i$ lie in distinct horizontal planes and $\mathcal{L}^3(L_c^i(\boldsymbol{w}, \mathbf{z})) > 0$ then this choice of cost and domain satisfy the dGKL conditions (Definition 4.1.1).*

Corollary 4.1.4. *An immediate consequence of Theorem 4.1.3 is that the conditions of Lemma 3.3.6 are satisfied. Theorem 4.1.3 establishes that our choice of cost and domain satisfy the dGKL conditions, which in turn ensures that the regularity results for Laguerre cells from [27] hold. These regularity properties are precisely the hypotheses required by Lemma 3.3.6. The key implication is that the theoretical framework developed in Chapter 3 is therefore applicable to our specific case of a rectangular domain.*

4.2 Proof Theorem 4.1.3

In this section, we prove the four conditions listed in the statement of Definition 4.1.1 for a rectangular domain, which is not c-convex with respect to the compressible SG cost

$$c(\mathbf{x}, \mathbf{y}) = \frac{1}{y_3}\left(\frac{f_{\text{cor}}^2}{2}(x_1 - y_1)^2 + \frac{f_{\text{cor}}^2}{2}(x_2 - y_2)^2 + g x_3\right). \tag{4.3}$$

Recall that the compressible cost maps from $\mathcal{X}$ to $\mathcal{Y} = \mathbb{R}^2 \times (\delta, 1/\delta$ for $\delta \in (0, 1)$.

Our verification of the dGKL conditions relies on a key technical result, presented in the lemma below. This lemma provides a crucial bound by relating the geometric ε-neighbourhoods of the boundary and cell edges to more analytically tractable level sets.

Recall that we assumed $\mathcal{X}$ is a rectangle. Consequently, its boundary $\partial\mathcal{X}$ is the union of six hyper-planes, each with a constant normal vector parallel to a coordinate axis.

Lemma 4.2.1 (Laguerre cells in physical space)**.** *For the compressible SG cost function given in Eq.* (4.3)*, the set* $f^{ik} = \{\mathbf{x} \in \mathbb{R}^3 : c(\mathbf{x}, \mathbf{z}^i) - w^i = c(\mathbf{x}, \mathbf{z}^k) - w^k\}$*, which contains the face between the Laguerre cells of two distinct seeds* $\mathbf{z}^i$ *and* $\mathbf{z}^k$*, has the following geometric form :*

1. *If the seeds are at the same height* ($z_3^i = z_3^k$)*, the face* f^{ik} *is a vertical plane.*
2. *If the seeds are at different heights* ($z_3^i \neq z_3^k$)*, the face* f^{ik} *is a paraboloid*

$$x_3 = -\frac{f_{\text{cor}}^2}{2g}\Big(\big(x_1 - A(\mathbf{z}^i, \mathbf{z}^k)\big)^2 + \big(x_2 - B(\mathbf{z}^i, \mathbf{z}^k)\big)^2\Big) + C(\mathbf{z}^i, \mathbf{z}^k, w^i, w^k). \tag{4.4}$$

Consequently, any two faces f^{ik} *and* f^{ij} *that are generated by three vertically aligned seeds are parallel paraboloids.*

Proof. The edge f^{ik} is defined by the equation $c(\mathbf{x}, \mathbf{z}^i) - w^i = c(\mathbf{x}, \mathbf{z}^k) - w^k$. We analyse this equation in two cases.

When $\mathbf{z}^i$ and $\mathbf{z}^k$ satisfy $z_3^i = z_3^k = z_3$, the defining equation becomes

$$(z_1^k - z_1^i)x_1 + (z_2^k - z_2^i)x_2 = \frac{1}{2}\Big(\big(z_1^k\big)^2 + \big(z_2^k\big)^2 - \big(z_1^i\big)^2 - \big(z_2^i\big)^2\Big) + \frac{z_3 g}{f_{\text{cor}}^2}\big(w^i - w^k\big). \tag{4.5}$$

This is the equation of a vertical plane.

If $z_3^i \neq z_3^k$, we rearrange the defining equation to solve for x_3. Grouping the terms gives

$$x_3 = -\frac{f_{\text{cor}}^2}{2g}\big(x_1^2 + x_2^2\big) + \frac{f_{\text{cor}}^2}{g}\frac{z_1^i z_3^k - z_1^k z_3^i}{z_3^k - z_3^i}x_1 + \frac{f_{\text{cor}}^2}{g}\frac{z_2^i z_3^k - z_2^k z_3^i}{z_3^k - z_3^i}x_2 - D(\mathbf{z}^i, \mathbf{z}^k, w^i, w^k), \tag{4.6}$$

where

$$D(\mathbf{z}^i, \mathbf{z}^k, w^i, w^k) = \frac{f_{\text{cor}}^2}{2g}\frac{z_3^k((z_1^i)^2 + (z_2^i)^2) - z_3^i\big((z_1^k)^2 + (z_2^k)^2\big)}{z_3^k - z_3^i} + \frac{z_3^i z_3^k(w^k - w^i)}{g(z_3^k - z_3^i)}. \tag{4.7}$$

This is the equation of a paraboloid of revolution with a vertical axis. Crucially, the leading quadratic coefficient, $-\frac{f_{\text{cor}}^2}{2g}$, is a universal constant, independent of the specific seeds $\mathbf{z}^i$ and $\mathbf{z}^k$.

Finally, consider two faces f^{ik} and f^{ij} generated by three vertically aligned seeds, which share the same (z_1, z_2) coordinates. From the derivation above, both faces are described by

paraboloids of the form

$$x_3 = -\frac{f_{\text{cor}}^2}{2g}\left(x_1^2 + x_2^2\right) + \frac{f_{\text{cor}}^2}{g}(z_1 x_1 + z_2 x_2) + C, \tag{4.8}$$

where $C = -D(\mathbf{z}^i, \mathbf{z}^k, w^i, w^k)$ for f^{ik} and $C = -D(\mathbf{z}^i, \mathbf{z}^j, w^i, w^j)$ for f^{ij}. □

Lemma 4.2.2. *Let $\mathcal{X} \subset \mathbb{R}^3$ be a compact set. Let $G : \mathbb{R}^3 \to \mathbb{R}$ be a $\mathcal{C}^2$ function. Assume that its gradient does not vanish on its zero-level set, i.e., $\nabla G \neq 0$ for all $\mathbf{x}$ where $G(\mathbf{x}) = 0$. For $\varepsilon \in (0, 1]$ and $\varepsilon_0 \geq 1$, the tubular neighbourhood of the hyper-surface $G^{-1}(\{0\})$ can be bounded by thickened level sets. This principle is illustrated in Figure 4.1. Formally*

$$\mathcal{X} \cap \mathcal{N}_\varepsilon(G^{-1}(\{0\})) \subseteq \mathcal{X} \cap G^{-1}([-a\varepsilon, a\varepsilon]),$$

where the constant a is defined by

$$a := \sup_{\mathbf{y} \in \mathcal{N}_{\varepsilon_0}(\mathcal{X})} \|\nabla G(\mathbf{y})\| + \frac{1}{2} \sup_{\mathbf{y} \in \mathcal{N}_{\varepsilon_0}(\mathcal{X})} \left\|\nabla^2 G(\mathbf{y})\right\|_2. \tag{4.9}$$

Proof. Let $\mathbf{p}$ be an arbitrary point in the neighbourhood $\mathcal{N}_\varepsilon(G^{-1}(\{0\}))$. By definition of the tubular neighbourhood, $\mathbf{p}$ can be expressed as $\mathbf{p} = \mathbf{x} + t\hat{\mathbf{n}}(\mathbf{x})$ for some point $\mathbf{x} \in \mathcal{X} \cap G^{-1}(\{0\})$, some $t \in (-\varepsilon, \varepsilon)$, and where $\hat{\mathbf{n}}(\mathbf{x})$ is the unit normal vector to the surface $G^{-1}(\{0\})$ at $\mathbf{x}$. We define this normal vector using the gradient of G :

$$\hat{\mathbf{n}}(\mathbf{x}) = \frac{\nabla G(\mathbf{x})}{\|\nabla G(\mathbf{x})\|}. \tag{4.10}$$

Our goal is to bound the value of $\|G(\mathbf{p})\|$. Since $G \in \mathcal{C}^2$, we can apply Taylor's theorem with the Lagrange form of the remainder to expand $G(\mathbf{p}) = G(\mathbf{x} + t\hat{\mathbf{n}}(\mathbf{x}))$ around the point $\mathbf{x}$:

$$G(\mathbf{p}) = G(\mathbf{x}) + t\nabla G(\mathbf{x}) \cdot \hat{\mathbf{n}}(\mathbf{x}) + \frac{t^2}{2}\hat{\mathbf{n}}(\mathbf{x})^T \nabla^2 G(\xi)\hat{\mathbf{n}}(\mathbf{x}), \tag{4.11}$$

for some point ξ on the line segment between $\mathbf{x}$ and $\mathbf{p}$. Since $\mathbf{x} \in G^{-1}(\{0\})$, $G(\mathbf{x}) = 0$. Substituting the definition of $\hat{\mathbf{n}}(\mathbf{x})$, the second term becomes

$$t\nabla G(\mathbf{x}) \cdot \frac{\nabla G(\mathbf{x})}{\|\nabla G(\mathbf{x})\|} = t\|\nabla G(\mathbf{x})\|. \tag{4.12}$$

The remainder term can be bounded using the Cauchy-Schwarz inequality :

$$\left\|\hat{\mathbf{n}}(\mathbf{x})^T \nabla^2 G(\xi) \hat{\mathbf{n}}(\mathbf{x})\right\| \leq \|\hat{\mathbf{n}}(\mathbf{x})\|^2 \left\|\nabla^2 G(\xi)\right\|_2 = \left\|\nabla^2 G(\xi)\right\|_2. \tag{4.13}$$

To establish the desired inclusion, we take the norm of the Taylor expansion

$$\|G(\mathbf{p})\| = \left\| G(\mathbf{x}) + t\nabla G(\mathbf{x}) \cdot \hat{\mathbf{n}}(\mathbf{x}) + \frac{t^2}{2} \hat{\mathbf{n}}(\mathbf{x})^T \nabla^2 G(\xi) \hat{\mathbf{n}}(\mathbf{x}) \right\|, \tag{4.14}$$

and, using the triangle inequality and the bounds we derived, find

$$\|G(\mathbf{p})\| \leq |t| \cdot \|\nabla G(\mathbf{x})\| + \frac{t^2}{2} \left\|\nabla^2 G(\xi)\right\|_2. \tag{4.15}$$

Since $|t| \leq \varepsilon$, we can establish an upper bound

$$\|G(\mathbf{p})\| \leq \varepsilon \cdot \|\nabla G(\mathbf{x})\| + \frac{\varepsilon^2}{2} \left\|\nabla^2 G(\xi)\right\|_2. \tag{4.16}$$

Since $\varepsilon \in (0, 1]$, we have $\varepsilon^2 \leq \varepsilon$. Furthermore, since $\mathbf{x} \in \mathcal{X}$ and $\mathbf{p} \in \mathcal{N}_{\varepsilon_0}(\mathcal{X})$, the point ξ must also lie in $\mathcal{N}_{\varepsilon_0}(\mathcal{X})$. We can therefore bound the gradient and the Hessian norms by their suprema over this set

$$\|G(\mathbf{p})\| < \varepsilon \left(\sup_{\mathbf{y} \in \mathcal{N}_{\varepsilon_0}(\mathcal{X})} \|\nabla G(\mathbf{y})\| + \frac{1}{2} \sup_{\mathbf{y} \in \mathcal{N}_{\varepsilon_0}(\mathcal{X})} \left\|\nabla^2 G_1(\xi)\right\| \right) = a\varepsilon. \tag{4.17}$$

This shows that if $\mathbf{p} \in \mathcal{N}_\varepsilon(G^{-1}(\{0\}))$, then $\mathbf{p} \in G^{-1}([-a\varepsilon, a\varepsilon])$, which implies the set inclusion

$$\mathcal{X} \cap \mathcal{N}_\varepsilon(G^{-1}(\{0\})) \subseteq \mathcal{X} \cap G^{-1}([-a\varepsilon, a\varepsilon]). \tag{4.18}$$

This completes the proof. □

4.2.1 Properties (1) and (4)

The proof of property (1) is immediate by the assumptions on the cost and property (4) follows equally quickly from the fact that the edges are paraboloids and the domain $\mathcal{X}$ is compact.

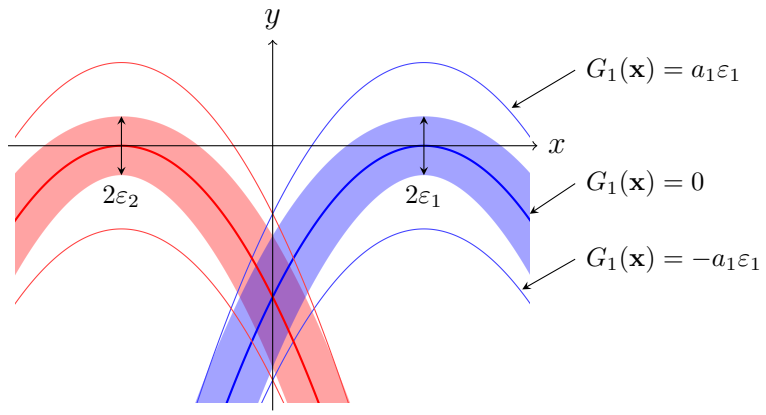

Figure 4.1: A schematic illustration of the principle in Lemma 4.2.2. The intersection of the tubular neighbourhoods (the dark overlapping region of the red and blue shaded bands) of two hyper-surfaces, $G_1^{-1}(\{0\})$ and $G_2^{-1}(\{0\})$, is shown to be contained within the intersection of their corresponding thickened level sets, which are bounded by the outer curves. The lemma formalizes this by relating the neighbourhood widths $\varepsilon_1, \varepsilon_2$ to the level set values $a_1\varepsilon_1, a_2\varepsilon_2$.

4.2.2 Property (2)

Let $i, k \in \{1, \dots, N\}$, $i \neq k$, and $\mathbf{x} \in f^{ik}(\boldsymbol{w}, \mathbf{z})$. Then

$$\nabla_{\mathbf{x}} c(\mathbf{x}, \mathbf{z}^i) - \nabla_{\mathbf{x}} c(\mathbf{x}, \mathbf{z}^k) = \frac{1}{z_3^i} \begin{pmatrix} f_{\text{cor}}^2(x_1 - z_1^i) \\ f_{\text{cor}}^2(x_2 - z_2^i) \\ g \end{pmatrix} - \frac{1}{z_3^k} \begin{pmatrix} f_{\text{cor}}^2(x_1 - z_1^k) \\ f_{\text{cor}}^2(x_2 - z_2^k) \\ g \end{pmatrix}$$

$$= \frac{f_{\text{cor}}^2}{z_3^i z_3^k} \begin{pmatrix} z_3^k(x_1 - z_1^i) - z_3^i(x_1 - z_1^k) \\ z_3^k(x_2 - z_2^i) - z_3^i(x_2 - z_2^k) \\ g(z_3^k - z_3^i)/f_{\text{cor}}^2 \end{pmatrix}.$$

Define

$$\eta_1 = \min\{|z_3^l - z_3^m| : l, m \in \{1, \dots, N\},\ z_3^l \neq z_3^m\}.$$

Then

$$\|\nabla_{\mathbf{x}} c(\mathbf{x}, \mathbf{z}^i) - \nabla_{\mathbf{x}} c(\mathbf{x}, \mathbf{z}^k)\| \geq |\partial_{x_3} c(\mathbf{x}, \mathbf{z}^i) - \partial_{x_3} c(\mathbf{x}, \mathbf{z}^k)| = g\frac{|z_3^k - z_3^i|}{z_3^i z_3^k} \geq g\eta_1\delta^2 =: \eta \qquad (4.19)$$

since $\mathbf{z}^i, \mathbf{z}^k \in \mathcal{Y} = \mathbb{R}^2 \times (\delta, 1/\delta)$. This proves Definition 4.1.1, property (2).

4.2.3 Property (3a) and (3b) for Edge-Edge Intersections ($j, k \neq 0$)

Properties (3a) and (3b) for $k \neq 0$ follow immediately from Chapter 3. Specifically from the fact that we can rewrite the diagram as a standard quadratic power diagram, along with the proof of [27, Proposition 1].

4.2.4 Property (3a) for Edge-Boundary Intersections

We now prove property (3a) for the case of an edge-boundary intersection, $j = 0$, where one of the surfaces is the boundary of the domain, $\partial\mathcal{X}$. We are bounding the volume

$$\mathcal{L}^3\big(\mathcal{X} \cap \mathcal{N}_{\varepsilon_1}(f^{ik}) \cap \mathcal{N}_{\varepsilon_2}(\partial\mathcal{X})\big). \tag{4.20}$$

The geometry of the domain is now critical. The faces f^{ik} are paraboloids (see Lemma 4.2.1). We express each face as the zero level set of the function $F_{ik}(\mathbf{x}) := c(\mathbf{x}, \mathbf{z}^i) - w^i - c(\mathbf{x}, \mathbf{z}^k) + w^k$, so that $f^{ik} = F_{ik}^{-1}(\{0\})$. Similarly, each face of the boundary is the zero level set of an affine function G (e.g. $G(\mathbf{x}) = x_3 - T$ for the top face). We thus express the boundary of the domain as $\partial\mathcal{X} = \bigcup_\ell G_\ell$ for $G_\ell : \mathcal{X} \to \mathbb{R}$ and $\ell \in \{1, \ldots, 6\}$.

Thus the volume we seek to bound can be controled by:

$$\mathcal{L}^3\big(\mathcal{X} \cap \mathcal{N}_{\varepsilon_1}(f^{ik}) \cap \mathcal{N}_{\varepsilon_2}(\partial\mathcal{X})\big) \leq \sum_\ell \mathcal{L}^3\big(\mathcal{N}_{\varepsilon_1}(f^{ik}) \cap \mathcal{N}_{\varepsilon_2}(G_\ell^{-1}(\{0\}))\big). \tag{4.21}$$

We prove an upper bound on the terms of this sum. The nature of the intersection between these surfaces determines our approach. The normal vector to a face, ∇F_{ik}, is parallel to a boundary normal (e.g. $(0, 0, 1)^T$) only in the specific case where the vertex of the paraboloid is tangent to the top or bottom face of the domain. This observation leads to two distinct cases for the proof. Before tackling these cases we introduce a key tool that we will use throughout the rest of the proof.

Theorem 4.2.3 (Coarea Formula, Theorem 3.13 of [31]). *Assume $f : \mathbb{R}^n \to \mathbb{R}$ is Lipschitz continuous. Then*

$$\int_{\mathbb{R}^n} |Df| \, \mathrm{d}\mathbf{x} = \int_{-\infty}^{\infty} \mathcal{H}^{n-1}(\{f = t\}) \, \mathrm{d}t. \tag{4.22}$$

Assume also

$$\operatorname{ess\,inf} |Df| > 0, \tag{4.23}$$

and suppose $g : \mathbb{R}^n \to \mathbb{R}$ *is* $\mathcal{L}^n$*-summable. Then*

$$\int_{\{f>t\}} g \, \mathrm{d}\mathbf{x} = \int_t^\infty \int_{\{f=s\}} \frac{g}{|Df|} \, \mathrm{d}\mathcal{H}^{n-1} \mathrm{d}s. \tag{4.24}$$

Transversal Intersection (Normals are Not Parallel)

This is the general case, occurring when a face f^{ik} intersects a side face of the rectangle (e.g., at $x_1 = x_l$) or when it intersects the top ($x_3 = T$) or bottom ($x_3 = B$) face away from its vertex. Here, the normal vectors $\nabla F_{ik}(\mathbf{x})$ and $\nabla G_\ell(\mathbf{x})$ are not parallel.

Since the normals are not parallel, the Jacobian of the map $\mathbf{x} \mapsto (F_{ik}(\mathbf{x}), G_\ell(\mathbf{x}))$ is uniformly bounded away from zero. Let

$$F_G(\mathbf{x}) = \begin{pmatrix} F_{ik}(\mathbf{x}) \\ G_\ell(\mathbf{x}) \end{pmatrix}. \tag{4.25}$$

Then, applying Lemma 4.2.2, we can bound the intersection of neighbourhoods by the intersection of the thickened level sets

$$\mathcal{L}^3\big(\mathcal{X} \cap \mathcal{N}_{\varepsilon_1}(f^{ik}) \cap \mathcal{N}_{\varepsilon_2}(\partial\mathcal{X})\big) \leq \mathcal{L}^3\big(\mathcal{X} \cap F_G^{-1}\{[-a\varepsilon_1, a\varepsilon_1] \times [-b\varepsilon_2, b\varepsilon_2]\}\big), \tag{4.26}$$

where the constants a and b are determined by separate applications of Lemma 4.2.2 to the functions $G_1 = F_{ik}$ and $G_2 = G_\ell$, and the bound is formed by intersecting the resulting sets. Specifically, $a = a_{F_{ik}}$ and $b = a_{G_\ell}$, where for a function ϕ

$$a_\phi := \sup_{\mathbf{y} \in \mathcal{N}_{\varepsilon_0}(\mathcal{X})} \|\nabla\phi(\mathbf{y})\| + \frac{1}{2} \sup_{\mathbf{y} \in \mathcal{N}_{\varepsilon_0}(\mathcal{X})} \big\|\nabla^2\phi(\mathbf{y})\big\|_2, \tag{4.27}$$

for fixed $\varepsilon_0 \geq 1$. We then apply the coarea formula

$$\mathcal{L}^3\big(\mathcal{X} \cap \mathcal{N}_{\varepsilon_1}(f^{ik}) \cap \mathcal{N}_{\varepsilon_2}(\partial\mathcal{X})\big) \leq \int_{s=-a\varepsilon_1}^{a\varepsilon_1} \int_{t=-b\varepsilon_2}^{b\varepsilon_2} \int_{\mathcal{X} \cap F_G^{-1}(\{(s,t)\})} \frac{1}{J_{F_G}(\mathbf{x})} \, \mathrm{d}\mathcal{H}^1(\mathbf{x}) \, \mathrm{d}t \mathrm{d}s, \tag{4.28}$$

where the Jacobian is $J_{F_G}(\mathbf{x}) = \|\nabla F_{ik}(\mathbf{x}) \times \nabla G_\ell(\mathbf{x})\|$. The crucial step is to establish a uniform lower bound for the Jacobian. In the the transversal case, the normal vectors are not parallel by assumption. The set where the edge f^{ik} intersects the boundary face within $\mathcal{X}$ is a compact set. Since F_{ik} and G_ℓ are $\mathcal{C}^2$ functions, the Jacobian J_{F_G} is continuous. A continuous function that is strictly positive on a compact set must attain a strictly positive minimum. We can

therefore define a uniform lower bound $\delta_{ik}^{\ell} > 0$

$$\delta_{ik}^{\ell} := \min_{\mathbf{x} \in f^{ik} \cap \partial\mathcal{X}} \|\nabla F_{ik}(\mathbf{x}) \times \nabla G_{\ell}(\mathbf{x})\| > 0. \tag{4.29}$$

This provides the necessary uniform bound for all relevant $\mathbf{x}$:

$$\frac{1}{J_{F_G}(\mathbf{x})} \leq \frac{1}{\delta_{ik}^{\ell}}. \tag{4.30}$$

This bound can be made explicit. For an intersection with a side-wall, e.g., $G(\mathbf{x}) = x_1 - x_l = 0$ (so $\nabla G = (1,0,0)^T$), the Jacobian is bounded below by

$$J_{F_G}(\mathbf{x}) = \left\|\nabla F_{ik}(\mathbf{x}) \times (1,0,0)^T\right\| \geq |\partial_{x_3} F_{ik}(\mathbf{x})| = \left|\frac{g}{z_3^i} - \frac{g}{z_3^k}\right|. \tag{4.31}$$

Since the seeds $\mathbf{z}^i$ and $\mathbf{z}^k$ lie in distinct horizontal planes ($z_3^i \neq z_3^k$), this value is a strictly positive constant, providing a concrete realization of the lower bound δ_{ik}^{ℓ}.

Using the uniform lower bound on the Jacobian, and by noting that the curve lengths $\mathcal{H}^1(\mathcal{X} \cap F_G^{-1}(\{(s,t)\}))$ are uniformly bounded by a constant $D_{\max}$, due to the compactness of $\mathcal{X}$ and the paraboloid nature of f^{ik}, the coarea integral is bounded by

$$\mathcal{L}^3(\mathcal{X} \cap \mathcal{N}_{\varepsilon_1}(f^{ik}) \cap \mathcal{N}_{\varepsilon_2}(\partial\mathcal{X})) \leq \int_{-a\varepsilon_1}^{a\varepsilon_1} \int_{-b\varepsilon_2}^{b\varepsilon_2} \int_{\mathcal{X} \cap F_G^{-1}(\{(s,t)\})} \frac{1}{\delta_{ik}^{\ell}} \, \mathrm{d}\mathcal{H}^1(\mathbf{x}) \mathrm{d}t \mathrm{d}s \tag{4.32}$$

$$\leq \frac{D_{\max}}{\delta_{ik}^{\ell}} \int_{-a\varepsilon_1}^{a\varepsilon_1} \int_{-b\varepsilon_2}^{b\varepsilon_2} \mathrm{d}t \mathrm{d}s \tag{4.33}$$

$$= \frac{4abD_{\max}}{\delta_{ik}^{\ell}} \varepsilon_1 \varepsilon_2. \tag{4.34}$$

Finally, to obtain a single constant C_{trans} valid for all transversal intersections as required by Definition 4.1.1, we must establish uniform bounds. There are a finite number of edges and a finite number of boundary faces. We can therefore define universal constants by taking the maximum over all possibilities. Let $a_{\max} := \max_{i \neq k} \{a_{F_{ik}}\}$. Let $b_{\max} := \max_{\ell} \{b_{G_\ell}\}$. Let $\delta_{\min} := \min_{i \neq k, \ell} \left\{\delta_{ik}^{\ell}\right\}$, where the minimum is taken over all pairs that intersect transversally. Since the number of functions is finite, $a_{\max}$ and $b_{\max}$ are finite, and $\delta_{\min}$ is strictly positive.

We can now define a single constant C_{trans} that works for any transversal intersection:

$$C_{\text{trans}} := \frac{4a_{\max}b_{\max}D_{\max}}{\delta_{\min}}. \tag{4.35}$$

This gives the required bound $C_{\text{trans}}\varepsilon_1\varepsilon_2$ and proves condition (3a), $j = 0$, for the transversal case.

Tangential Intersection (Normals are Parallel)

This special case occurs when the vertex of the paraboloid f^{ik} is tangent to the top ($x_3 = T$) boundary of the domain. If the vertex of the paraboloid is tangent to the bottom of the domain the cell is empty which cannot happen.

At this point of tangency, the face normal $\nabla F_{ik}(\mathbf{x})$ is parallel to the boundary normal (e.g., $(0, 0, 1)^T$). Consequently, the Jacobian $J_{F_G}(\mathbf{x})$ is zero, and the coarea-based argument form the transversal case fails. We therefore turn to a direct geometric argument, illustrated in Figure 4.2 and Figure 4.3.

We need to bound the volume of the intersection between the ε_1-neighbourhood of the face, $\mathcal{N}_{\varepsilon_1}(f^{ik})$, and the ε_2-neighbourhood of the boundary, $\mathcal{N}_{\varepsilon_2}(\partial\mathcal{X})$. Near the point of tangency, this corresponds to the intersection of a paraboloid shell of thickness $2\varepsilon_1$ and a planar slab of thickness ε_2 within the domain $\mathcal{X}$. The volume of this region can be calculated as the difference between the the volumes of two paraboloid caps. The volume of a paraboloid cap of height h with radius r at height h from the vertex is given by

$$V(h) = \frac{\pi r^2 h}{2}. \tag{4.36}$$

For the specific paraboloids f^{ik}, the radius r at a given height h from the vertex is given by

$$r^2 = \frac{2gh}{f_{\text{cor}}^2}. \tag{4.37}$$

This follows from Lemma 4.2.1.

Consider Figure 4.2 and Figure 4.3, these illustrate the two possible scenarios that can occur in the case of a tangential intersection, $\varepsilon_1 \leq \varepsilon_2$ or $\varepsilon_1 \geq \varepsilon_2$. As the figures illustrate, regardless of the scenario, the height of the larger cap is $h_{\text{outer}} = \varepsilon_1 + \varepsilon_2$ and the height of the inner cap is

$h_{\text{inner}} = |\varepsilon_1 - \varepsilon_2|$. This leads to a single computation that is valid for both $\varepsilon_1 \leq \varepsilon_2$ and $\varepsilon_1 \geq \varepsilon_2$

$$\mathcal{L}^3\big(\mathcal{X} \cap \mathcal{N}_{\varepsilon_1}(f^{ik}) \cap \mathcal{N}_{\varepsilon_2}(\partial\mathcal{X})\big) \leq \mathcal{L}^3(\mathcal{N}_{\varepsilon_1}(f^{ik}) \cap \mathcal{N}_{\varepsilon_2}(\partial\mathcal{X})) \tag{4.38}$$

$$\leq V(h_{\text{outer}}) - V(h_{\text{inner}}) \tag{4.39}$$

$$= \frac{\pi r_{\text{outer}}^2 h_{\text{outer}}}{2} - \frac{\pi r_{\text{inner}}^2 h_{\text{inner}}}{2} \tag{4.40}$$

$$= \frac{\pi g}{f_{\text{cor}}^2} h_{\text{outer}}^2 - \frac{\pi g}{f_{\text{cor}}^2} h_{\text{inner}}^2 \tag{4.41}$$

$$= \frac{\pi g}{f_{\text{cor}}^2} \big((\varepsilon_1 + \varepsilon_2)^2 - (\varepsilon_1 - \varepsilon_2)^2\big) \tag{4.42}$$

$$= \frac{4\pi g}{f_{\text{cor}}^2} \varepsilon_1 \varepsilon_2. \tag{4.43}$$

This gives the required bound with a constant $C_{\text{tang}} = \frac{4\pi g}{f_{\text{cor}}^2}$.

We have shown that in both the transversal and tangential intersection cases, the volume of intersection is bounded by $C\varepsilon_1\varepsilon_2$. By defining a single constant $C = \max\{C_{\text{trans}}, C_{\text{tang}}\}$, we have a uniform bound that holds for all edge-boundary intersections. This completes the proof of property (3a) for the rectangular domain.

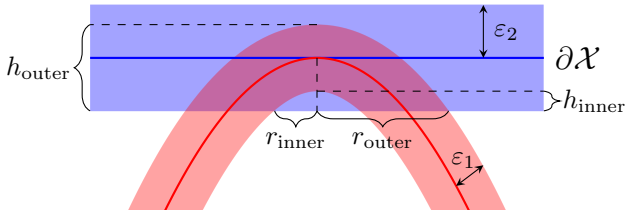

Figure 4.2: The tangential intersection of a face f^{ij} and the domain boundary $\partial\mathcal{X}$ when the edge neighbourhood (ε_1) is smaller than the boundary neighbourhood (ε_2). The intersection volume is bounded by the volume of the paraboloid cap formed by the outer shell of the edge neighbourhood.

4.2.5 Property (3b) for Edge-Boundary Intersections

This property requires us to show that the area of an edge lying in a neighbourhood of the boundary vanishes as the neighbourhood shrinks, and vice-versa. Formally, we prove

1. $\lim_{\varepsilon_1 \to 0} \mathcal{H}^2\big(\mathcal{X} \cap \partial\mathcal{X} \cap \mathcal{N}_{\varepsilon_1}(f^{ik})\big) = 0$,

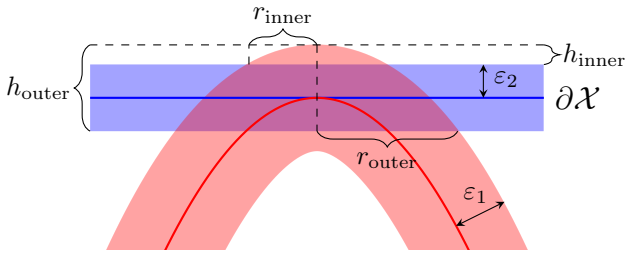

Figure 4.3: The tangential intersection of a face f^{ij} and the domain boudary $\partial\mathcal{X}$ when the edge neighbourhood (ε_1) is larger than the boundary neighbourhood (ε_2). The intersection volume is computed as the difference between two paraboloid caps, with heights $h_{\text{outer}} = \varepsilon_1 + \varepsilon_2$ and $h_{\text{inner}} = \varepsilon_1 - \varepsilon_2$.

2. $\lim_{\varepsilon_2 \to 0} \mathcal{H}^2\big(\mathcal{X} \cap f^{ik} \cap \mathcal{N}_{\varepsilon_2}(\partial\mathcal{X})\big) = 0.$

The proof splits into the two cases as in Section 4.2.4.

Transversal Intersection

We will prove the first limit in detail. The proof for the second limit follows by a symmetric argument. We seek to bound the area $\mathcal{H}^2\big(\mathcal{X} \cap \partial\mathcal{X} \cap \mathcal{N}_{\varepsilon_1}(f^{ik})\big)$. Applying Lemma 4.2.2, this is bounded by $\mathcal{H}^2\big(\mathcal{X} \cap \partial\mathcal{X} \cap F_{ik}^{-1}([-a\varepsilon_1, a\varepsilon_1])\big)$, where $a = a_{F_{ik}}$ is the constant form the lemma. We now apply the coarea formula by integrating the function $F_{ik}(\mathbf{x})$ over the surface $S = \mathcal{X} \cap \partial\mathcal{X}$

$$\mathcal{H}^2\big(\mathcal{X} \cap \partial\mathcal{X} \cap F_{ik}^{-1}([-a, \varepsilon_1, a\varepsilon_1])\big) = \int_{t=-a\varepsilon_1}^{a\varepsilon_1} \int_{S \cap F_{ik}^{-1}(\{t\})} \frac{1}{\|\nabla_S F_{ik}(\mathbf{x})\|} \, \mathrm{d}\mathcal{H}^1(\mathbf{x}) \mathrm{d}t. \tag{4.44}$$

The Jacobian is the tangential gradient $\|\nabla_S F_{ik}(\mathbf{x})\|$. This is the norm of the gradient of the edge function projected onto the boundary surface, given by $\|\nabla F_{ik}(\mathbf{x}) \times \hat{\mathbf{n}}(\mathbf{x})\|$, where $\hat{\mathbf{n}}(\mathbf{x})$ is the normal to the boundary $\partial\mathcal{X}$. This is exactly the Jacobian J_{F_G} from the proof of property (3a), which we established is uniformly bounded below in the transversal case by a constant $\delta_{\min} > 0$. Again, the length of the intersection curves $\mathcal{H}^1(S \cap F_{ik}^{-1}(\{t\}))$ is uniformly bounded by a constant $D_{\max}$ due to compactness and the paraboloid nature of f^{ik}. The integral is therefore bounded

$$\mathcal{H}^2\big(\mathcal{X} \cap \partial\mathcal{X} \cap \mathcal{N}_{\varepsilon_1}(f^{ik})\big) \leq \int_{t=-a\varepsilon_1}^{a\varepsilon_1} \int_{S \cap F_{ik}^{-1}(\{t\})} \frac{1}{\|\nabla_S F_{ik}(\mathbf{x})\|} \, \mathrm{d}\mathcal{H}^1(\mathbf{x}) \mathrm{d}t \tag{4.45}$$

$$\leq \int_{t=-a\varepsilon_1}^{a\varepsilon_1} \frac{D_{\max}}{\delta_{\min}} \mathrm{d}t \tag{4.46}$$

$$= \frac{2aD_{\max}}{\delta_{\min}}\varepsilon_1 \tag{4.47}$$

$$= C'\varepsilon_1. \tag{4.48}$$

Since this bound is linear in ε_1, it vanishes as $\varepsilon_1 \to 0$, proving the first limit. A symmetric argument, which involves integrating over the edge surface f^{ik} instead of the boundary, proves the second limit.

Tangential Intersection

When the edge f^{ik} and the boundary $\partial\mathcal{X}$ intersect at a single point, two distinct scenarios arise regarding how the intersection vanishes.

The first scenario, illustrated in Figure 4.4, focuses on the measure $\mathcal{H}^2\big(\mathcal{X} \cap \partial\mathcal{X} \cap \mathcal{N}_{\varepsilon_1}(f^{ik})\big)$. As ε_1 approaches 0, we demonstrate that this measure also approaches 0.

As depicted in Figure 4.4, the region of intersection can be described by a circle. Following the proof for tangential intersection in property (3a), the radius of this circle is given by :

$$r^2(h) = \frac{2gh}{f_{\text{cor}}^2}. \tag{4.49}$$

Therefore, the limit of the measure as ε_1 approaches 0 is :

$$\lim_{\varepsilon_1 \to 0} \mathcal{H}^2\big(\mathcal{X} \cap \partial\mathcal{X} \cap \mathcal{N}_{\varepsilon_1}(f^{ik})\big) = \lim_{\varepsilon_1 \to 0} \frac{2g\pi}{f_{\text{cor}}^2}\varepsilon_1 = 0. \tag{4.50}$$

The second scenario, shown in Figure 4.5, concerns the measure $\mathcal{H}^2\big(\mathcal{X} \cap f^{ik} \cap \mathcal{N}_{\varepsilon_2}(\partial\mathcal{X})\big)$. We aim to show that this measure tends to 0 as ε_2 goes to 0. As shown in Figure 4.5, the area of intersection is described by the surface area of paraboloid, given by :

$$S(h) = \frac{\pi r(h)}{6h^2}\left(\sqrt{\left(r(h)^2 + 4h^2\right)^3} - r(h)^3\right). \tag{4.51}$$

Consequently, the limit of the measures as ε_2 approaches 0 is :

$$\lim_{\varepsilon_2 \to 0} \mathcal{H}^2\big(\mathcal{X} \cap f^{ik} \cap \mathcal{N}_{\varepsilon_2}(\partial\mathcal{X})\big) = \lim_{\varepsilon_2 \to 0} \frac{8g\pi}{3f_{\text{cor}}^8\varepsilon_2}\left(-g^3\varepsilon_2^3 + f_{\text{cor}}^6\sqrt{\frac{\left(f_{\text{cor}}^4 + g^2\right)^3\varepsilon_2^6}{f_{\text{cor}}^{12}}}\right) = 0. \tag{4.52}$$

This concludes the proof of property (3b) for all edge-boundary intersections.

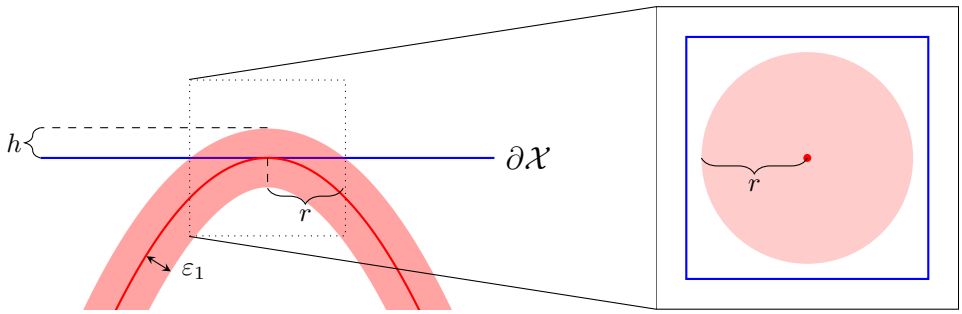

Figure 4.4: Scenario 1 : The intersection of $\partial\mathcal{X}$ with a neighbourhood of f^{ik}. The main figure (left) shows the edge f^{ik} (red curve) tangentially intersecting the boundary $\partial\mathcal{X}$ (blue line) at the origin. The shaded red region represents the ε_1-neighbourhood around f^{ik}. The dashed box indicates the region zoomed in on the right. The zoom-in figure (right) is a view from the top down on the point of intersection and illustrates the circular region of intersection, with its radius r marked.

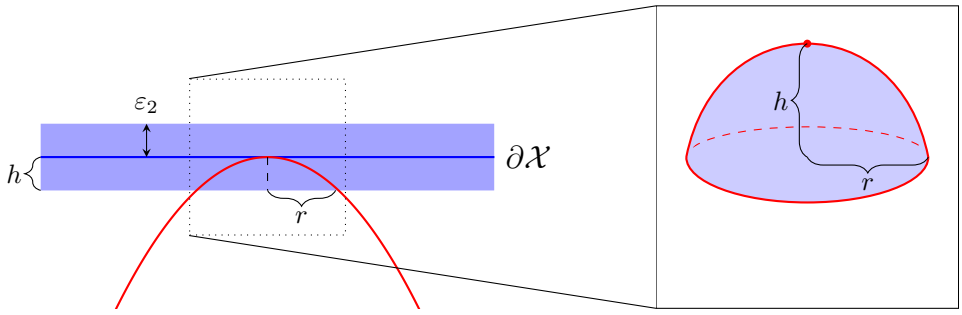

Figure 4.5: Scenario 2 : The intersection of f^{ik} with a neighbourhood of $\partial\mathcal{X}$. The main figure (left) shows the edge f^{ik} (red curve) intersecting the boundary $\partial\mathcal{X}$ (blue line) at the origin. The shaded blue region represents the ε_2-neighbourhood around $\partial\mathcal{X}$. The dashed box indicates the region zoomed in on the right. The zoom-in figure (right) illustrates the paraboloid region of the intersection, with its height h and radius r marked.

Chapter 5

2D Compressible Model

5.1 Introduction

In this chapter we derive a 2D version of the compressible SG equations and its weak formulation. This will serve in future work as the first model for numerical simulations, on the way to a numerical solution of the full 3D SG equations.

5.1.1 Outline of the Chapter

This chapter is organized as follows. In Section 2, we introduce the 2D compressible SG equations. To derive a reduced model for a compressible, stratified, and rotating atmosphere we start from the full compressible Euler equations and apply the hydrostatic, vertical slice, and semi-geostrophic approximations. A coordinate transformation to geostrophic variables then leads to a novel variational formulation and an optimal transport problem. We present the weak form and non-dimensionalization of the system to highlight the key governing parameters.

5.2 Derivation of the Slice Compressible Model

In this section we derive the slice compressible model, a system designed to emulate key atmospheric dynamics within a two-dimensional vertical slice. While this model is not a direct reduction of its three-dimensional counterpart, it is constructed from the compressible Euler equations by incorporating a series of physically-motivated approximations. We begin by presenting the governing equations and the necessary thermodynamic closure before applying the vertical slice, hydrostatic, and semi-geostrophic approximations to arrive at a simplified system capturing the essential dynamical balances. Subsequently, we introduce a coordinate transformation to geostrophic variables and derive the corresponding weak form of the governing equations. This systematic derivation provides the foundation for the discrete particle system

we intend to simulate in the future.

5.2.1 Governing Equations and Physical Assumptions

The crucial step is the introduction of a vertical slice geometry, which is necessary because, unlike in the incompressible case, a quasi-2D solution cannot be found by simple reduction of the 3D compressible model. The system is then further simplified using the semi-geostrophic approximation to isolate the large-scale balanced flow relevant to frontogenesis. These steps, combined with the necessary thermodynamic closure relations, define the final model equations for our analysis.

Fully Compressible Model

We begin with the three-dimensional *compressible Euler equations*, formulated for a stratified, rotating atmosphere. The state of the system at a point $\mathbf{x} = (x_1, x_2, x_3)$, corresponding to longitude, latitude, and altitude, respectively, is described by the velocity field $\mathbf{u} = (u, v, w)$, the density ρ, and the potential temperature θ. The thermodynamic state is closed by the equation of state for a dry ideal gas, which relates the pressure p to the density and temperature via the Exner pressure Π :

$$\begin{aligned} p &= \rho R_d \theta \Pi, \\ \Pi(\rho, \theta) &= \left(\frac{\rho R_d \theta}{p_0} \right)^{\gamma - 1}, \end{aligned} \tag{5.1}$$

where p_0 is a reference pressure, $\gamma = c_p/c_v$ is the adiabatic index, and $R_d = c_p - c_v$ is the specific gas constant for dry air.

Once again we adopt the hydrostatic approximation, which assumes a balance between the vertical pressure gradient and gravity. Under this assumption, the governing equations in a reference frame rotating with frequency f_{cor} about the vertical axis $\hat{\mathbf{e}}_3$ are the following:

$$\begin{cases} D_t \mathbf{u} + f_{\text{cor}} \hat{\mathbf{e}}_3 \times \mathbf{u} + c_p \theta \nabla \Pi + g \hat{\mathbf{e}}_3 = 0, \\ \partial_t \rho + \nabla \cdot (\rho \mathbf{u}) = 0, \\ D_t \Theta = 0, \end{cases} \tag{5.2}$$

where Θ is the full potential temperature and the material derivative D_t is given by :

$$D_t = \frac{\partial}{\partial t} + \mathbf{u} \cdot \nabla = \frac{\partial}{\partial t} + u\frac{\partial}{\partial x_1} + v\frac{\partial}{\partial x_2} + w\frac{\partial}{\partial x_3}. \tag{5.3}$$

Vertical Slice and Semi-Geostrophic Approximation

To construct the model, we first apply the *vertical slice approximation*. Following the framework in [17], we consider a two-dimensional domain

$$\mathcal{X} := [-L, L) \times [0, H], \tag{5.4}$$

which represents a vertical slice of the atmosphere in the x_1-x_3 plane. The model is periodic in the x_1-direction and we assume rigid boundaries at the top and bottom. The velocity field $\mathbf{u} = (u, v, w)$ is decomposed into its in-slice component $\mathbf{u}_S = (u, w)$, and the transverse component, v.

The central assumption is that all fields are independent of the transverse coordinate x_2, except for a background temperature gradient that is necessary to support baroclinic instability. Accordingly, the in-slice velocity $\mathbf{u}_S$, density ρ, and the in-slice potential temperature perturbation θ are assumed to depend only on (x_1, x_3, t). The total potential temperature Θ is decomposed as

$$\Theta(x_1, x_2, x_3, t) = \theta_0 + \overline{\theta}(x_2) + \theta(x_1, x_3, t), \tag{5.5}$$

where θ_0 is a constant reference temperature and $\overline{\theta}(x_2) = sx_2$ is a background stratification profile, with s representing the background vertical shear. The model is then formulated in terms of the in-slice perturbation θ.

The momentum equations from the parent model are replaced by diagnostic balance relations, which represent an assumed geostrophic and hydrostatic equilibrium :

$$v = \frac{1}{f_{\text{cor}}} c_p \theta \partial_{x_1} \Pi, \tag{5.6}$$

$$\theta = -\frac{g}{c_p \partial_{x_3} \Pi}. \tag{5.7}$$

The model is completed by the remaining prognostic equations from the Euler equations. These are modified with the ad-hoc terms identified in [67] to emulate the effect of the transverse

temperature gradient, forming the *semi-geostrophic slice compressible model* first introduced in [17, Remark 5.3]. It was derived from the Euler equations (Eq. (5.2)) by making the slice ansatz, using the SG approximation (Eq. (5.6) and Eq. (5.7)), and adding an adhoc term to the right hand side of Eq. (5.2) to emulate the Eady Slice model, which we presented as a benchmark case in Chapter 2.

$$\begin{cases} D_t v + f_{\text{cor}} u = s c_p (\Pi - \Pi_0) & \text{in } \mathcal{X} \times [0, t_f], \quad (5.8a) \\ D_t \theta + s v = 0 & \text{in } \mathcal{X} \times [0, t_f], \quad (5.8b) \\ D_t \rho + \rho \nabla \cdot \mathbf{u}_S = 0 & \text{in } \mathcal{X} \times [0, t_f], \quad (5.8c) \\ c_p \theta \nabla \Pi = (f_{\text{cor}} v, -g)^T & \text{in } \mathcal{X} \times [0, t_f], \quad (5.8d) \\ \mathbf{u}_S \cdot \hat{\mathbf{n}} = 0 & \text{on } \mathcal{X} \times [0, t_f] \cap \{x_3 = 0, H\}, \quad (5.8e) \\ \mathbf{u}_S(-L, x_3) = \mathbf{u}_S(L, x_3) & \text{on } \mathcal{X} \times [0, t_f]. \quad (5.8f) \end{cases}$$

Here the in-slice material derivative is $D_t = \frac{\partial}{\partial t} + \mathbf{u}_S \cdot \nabla_2 = \partial_t + u\partial_{x_1} + w\partial_{x_3}$, and Π_0 is the initial spatial average of the Exner pressure,

$$\Pi_0 = \fint_{\mathcal{X}} \Pi \, \mathrm{d}\mathbf{x}, \tag{5.9}$$

which is included to reduce the mean horizontal flow. In this formulation, the transverse velocity v is influenced by both the Coriolis force and the background shear s.

This system of equations has not been analysed rigorously, hence we assume the existence of a solution and we proceed formally.

5.2.2 Derivation of the Semi-Geostrophic Equations in Geostrophic Coordinates

Define a new quantity $\sigma_t(\mathbf{x}) = \rho(\mathbf{x}, t)\theta(\mathbf{x}, t)$ and assume that at $t = 0$, $\int_{\mathcal{X}} \sigma_0(\mathbf{x}) \, \mathrm{d}\mathbf{x} = 1$. By combining Eq. (5.8c) and Eq. (5.8b) we find

$$\rho(D_t\theta + sv) + \theta(D_t\rho + \rho\nabla \cdot \mathbf{u}_S) = 0 \tag{5.10}$$

$$\iff \quad \rho\partial_t\theta + \theta\partial_t\rho = -\rho\mathbf{u}_S \cdot \nabla\theta - \theta\mathbf{u}_S \cdot \nabla\rho - \rho\theta\nabla \cdot \mathbf{u}_S - \rho sv \tag{5.11}$$

$$\iff \quad \rho\partial_t\theta + \theta\partial_t\rho = -\nabla \cdot (\rho\theta\mathbf{u}_S) - \rho sv \tag{5.12}$$

$$\iff \quad \partial_t\sigma_t = -\nabla \cdot (\sigma_t\mathbf{u}_S) - \frac{\sigma_t}{\theta} sv. \tag{5.13}$$

Lemma 5.2.1 (σ_t is a Probability Measure)**.** *Assume at time $t = 0$ that $\int_{\mathcal{X}} \mathrm{d}\sigma_0(\mathbf{x}) = 1$, then $\sigma_t \in \mathscr{P}_{\mathrm{ac}}(\mathcal{X})$ for all t.*

Proof. Our goal is to show that the time derivative of $\int_{\mathcal{X}} \mathrm{d}\sigma_t(\mathbf{x})$ is zero. Note the following relationship

$$\sigma_t \partial_{x_1}\left(\sigma_t^{\gamma-1}\right) = (\gamma-1)\sigma_t\sigma_t^{\gamma-2}\partial_{x_1}\sigma_t = \left(\frac{\gamma-1}{\gamma}\right)\partial_{x_1}\sigma_t^{\gamma}. \tag{5.14}$$

Using the geostrophic balance relation Eq. (5.7) and the equation of state (Eq. (5.1)), the source term in Eq. (5.13), can be rewritten as

$$\frac{\sigma_t}{\theta} sv \overset{(5.6)}{=} \frac{sc_p}{f_{\mathrm{cor}}}\sigma_t\partial_{x_1}\Pi \overset{(5.1)}{=} \frac{sc_p}{f_{\mathrm{cor}}}\left(\frac{R_d}{p_0}\right)^{\gamma-1}\sigma_t\partial_{x_1}\sigma_t^{\gamma-1} \overset{(5.14)}{=} C\partial_{x_1}\sigma_t^{\gamma}, \tag{5.15}$$

where the constant C is defined as

$$C = \frac{sc_p}{f_{\mathrm{cor}}}\left(\frac{R_d}{p_0}\right)^{\gamma-1}\left(\frac{\gamma-1}{\gamma}\right). \tag{5.16}$$

Thus, the evolution equation for σ_t, Eq. (5.13) can be written as

$$\partial_t\sigma_t + \nabla\cdot(\sigma_t\mathbf{u}_S) = -C\partial_{x_1}\sigma_t^{\gamma}. \tag{5.17}$$

Now we compute directly

$$\frac{\mathrm{d}}{\mathrm{d}t}\int_{\mathcal{X}} \mathrm{d}\sigma_t(\mathbf{x}) = \int_{\mathcal{X}} \partial_t\sigma_t(\mathbf{x})\,\mathrm{d}\mathbf{x} = -\int_{\mathcal{X}} \nabla\cdot(\sigma_t\mathbf{u}_S)\,\mathrm{d}\mathbf{x} - C\int_{\mathcal{X}} \partial_{x_1}\sigma_t^{\gamma}\,\mathrm{d}\mathbf{x} \tag{5.18}$$

$$= \int_{\partial\mathcal{X}} \sigma_t\mathbf{u}_S\cdot\hat{\mathbf{n}}\,\mathrm{d}\mathcal{H}^1 - C\int_{\mathcal{X}} \partial_{x_1}\sigma_t^{\gamma}\,\mathrm{d}\mathbf{x} \tag{5.19}$$

$$= \int_{\partial\mathcal{X}} \sigma_t\mathbf{u}_S\cdot\hat{\mathbf{n}}\,\mathrm{d}\mathcal{H}^1 - C\int_0^H\int_{-L}^L \partial_{x_1}\sigma_t^{\gamma}\,\mathrm{d}x_1\mathrm{d}x_3 \tag{5.20}$$

$$= \int_{\partial\mathcal{X}} \sigma_t\mathbf{u}_S\cdot\hat{\mathbf{n}}\,\mathrm{d}\mathcal{H}^1 - C\int_0^H \sigma_t^{\gamma}(-L,x_2) - \sigma_t^{\gamma}(L,x_2)\,\mathrm{d}x_3 \tag{5.21}$$

$$= \int_{\partial\mathcal{X}} \sigma_t\mathbf{u}_S\cdot\hat{\mathbf{n}}\,\mathrm{d}\mathcal{H}^1 - C\int_0^H 0\,\mathrm{d}x_3 \tag{5.22}$$

$$= \int_{-L}^L \sigma_t(x_1,H)w((x_1,H),t)\,\mathrm{d}x_1 - \int_{-L}^L \sigma_t(x_1,H)w((x_1,H),t)\,\mathrm{d}x_1 \tag{5.23}$$

$$+ \int_0^H \sigma_t(L, x_3) u((L, x_3), t)\, \mathrm{d}x_3 - \int_0^H \sigma_t(-L, x_3) u((-L, x_3), t)\, \mathrm{d}x_3 \tag{5.24}$$

$$= 0, \tag{5.25}$$

by the boundary conditions (5.8e) and (5.8f). Therefore $\sigma_t \in \mathscr{P}_{\mathrm{ac}}(\mathcal{X})$. □

Again, as in Section 1.6.2, we take the coordinate transform as suggested by Hoskins [42] :

$$T_t(\mathbf{x}) = \begin{pmatrix} x_1 + f_{\mathrm{cor}}^{-1} v(\mathbf{x}, t) \\ \frac{g}{\theta_0 f_{\mathrm{cor}}^2} \theta(\mathbf{x}, t) \end{pmatrix}, \tag{5.26}$$

where $\mathbf{x} = (x_1, x_3)$.

For $t \in [0, t_f]$, define $\alpha_t \in \mathscr{P}(\mathcal{Y})$ by $\alpha_t = (T_t)_{\#}\sigma_t$. The goal of this section is to derive a PDE for α_t. We introduce

$$J = \frac{sg}{f_{\mathrm{cor}}\theta_0} \begin{pmatrix} 0 & -1 \\ 1 & 0 \end{pmatrix}. \tag{5.27}$$

In order to derive the PDE for the measure α_t, we first take the material derivative of Eq. (5.26):

$$D_t T_t = \begin{pmatrix} D_t x_1 + f_{\mathrm{cor}}^{-1} D_t v \\ \frac{g}{f_{\mathrm{cor}}^2 \theta_0} D_t \theta \end{pmatrix} = \begin{pmatrix} u_1 + s c_p f_{\mathrm{cor}}^{-1} (\Pi - \Pi_0) - u_1 \\ -\frac{sg}{f_{\mathrm{cor}}^2 \theta_0} v \end{pmatrix} = \frac{sg}{f_{\mathrm{cor}}\theta_0} \begin{pmatrix} \frac{c_p \theta_0}{g} (\Pi - \Pi_0) \\ (\mathbf{x} - T_t) \cdot \hat{\mathbf{e}}_1 \end{pmatrix}. \tag{5.28}$$

Define on $\mathcal{X}$ the velocity $\mathbf{W}(\cdot, t)$ as

$$\mathbf{W} := J \begin{pmatrix} (\mathrm{Id} - T_t) \cdot \hat{\mathbf{e}}_1 \\ \frac{c_p \theta_0}{g} (\Pi_0 - \Pi) \end{pmatrix}, \tag{5.29}$$

so that

$$\partial_t T_t = -(\nabla T_t)\mathbf{u}_S + \mathbf{W}.$$

Using the coordinate transformation we can rewrite the term

$$\frac{sv}{\theta} = \frac{sg}{f_{\mathrm{cor}}\theta_0} \frac{(T_t - \mathrm{Id}) \cdot \hat{\mathbf{e}}_1}{T_t \cdot \hat{\mathbf{e}}_3} =: \mathcal{S}. \tag{5.30}$$

Note that the value of $\mathcal{S}$ can be extracted from θ and v.

Now we are ready to formally derive the PDE. Consider a test function $\varphi \in \mathcal{C}_c^\infty(\mathcal{Y})$. Then

$$\frac{\mathrm{d}}{\mathrm{d}t}\int_{\mathcal{Y}} \varphi(\mathbf{y})\,\mathrm{d}\alpha_t(\mathbf{y}) = \frac{\mathrm{d}}{\mathrm{d}t}\int_{\mathcal{X}} \varphi(T_t(\mathbf{x}))\,\mathrm{d}\sigma_t(\mathbf{x}) \tag{5.31}$$

$$= \int_{\mathcal{X}} \nabla\varphi(T_t(\mathbf{x}))\cdot\partial_t T_t(\mathbf{x})\,\mathrm{d}\sigma_t(\mathbf{x}) + \int_{\mathcal{X}} \varphi(T_t(\mathbf{x}))\partial_t\sigma_t(\mathbf{x})\,\mathrm{d}\mathbf{x} \tag{5.32}$$

$$= \int_{\mathcal{X}} \nabla\varphi(T_t(\mathbf{x}))\cdot(-(\nabla T_t(\mathbf{x}))\mathbf{u}_S + \mathbf{W}(\mathbf{x},t))\,\mathrm{d}\sigma_t(\mathbf{x}) \tag{5.33}$$

$$- \int_{\mathcal{X}} \varphi(T_t(\mathbf{x}))\nabla\cdot(\sigma_t(\mathbf{x})\mathbf{u}_S)\,\mathrm{d}\mathbf{x} - \int_{\mathcal{X}} \varphi(T_t(\mathbf{x}))\mathcal{S}(\mathbf{x},t)\,\mathrm{d}\sigma_t(\mathbf{x}) \tag{5.34}$$

$$= -\int_{\mathcal{X}} \nabla[\varphi(T_t(\mathbf{x}))]\cdot\mathbf{u}_S\,\mathrm{d}\sigma_t(\mathbf{x}) - \int_{\mathcal{X}} \varphi(T_t(\mathbf{x}))\nabla\cdot(\sigma_t(\mathbf{x})\mathbf{u}_S)\,\mathrm{d}\mathbf{x} \tag{5.35}$$

$$+ \int_{\mathcal{X}} \nabla\varphi(T_t(\mathbf{x}))\cdot\mathbf{W}(\mathbf{x},t)\,\mathrm{d}\sigma_t(\mathbf{x}) - \int_{\mathcal{X}} \varphi(T_t(\mathbf{x}))\mathcal{S}(\mathbf{x},t)\,\mathrm{d}\sigma_t(\mathbf{x}). \tag{5.36}$$

Then by integration by parts and our boundary conditions the two terms in expression (5.35) cancel and we are left with the equation

$$\frac{\mathrm{d}}{\mathrm{d}t}\int_{\mathcal{X}} \varphi(\mathbf{y})\,\mathrm{d}\alpha_t(\mathbf{y}) = \int_{\mathcal{X}} \nabla\varphi(T_t(\mathbf{x}))\cdot\mathbf{W}(\mathbf{x},t)\,\mathrm{d}\sigma_t(\mathbf{x}) - \int_{\mathcal{X}} \varphi(T_t(\mathbf{x}))\mathcal{S}(\mathbf{x},t)\,\mathrm{d}\sigma_t(\mathbf{x}). \tag{5.37}$$

Therefore

$$\frac{\mathrm{d}}{\mathrm{d}t}\int_{\mathcal{Y}} \varphi(\mathbf{y})\,\mathrm{d}\alpha_t(\mathbf{y}) = \int_{\mathcal{Y}} \nabla\varphi(\mathbf{y})\cdot\mathbf{w}(\mathbf{y},t)\,\mathrm{d}\alpha_t(\mathbf{y}) - \int_{\mathcal{Y}} \varphi(\mathbf{y})S(\mathbf{y},t)\,\mathrm{d}\alpha_t(\mathbf{y}), \tag{5.38}$$

where

$$\mathbf{w}(\mathbf{y},t) = \mathbf{W}(T_t^{-1}(\mathbf{y}),t) = J\begin{pmatrix} \big(T_t^{-1}(\mathbf{y}) - \mathbf{y}\big)\cdot\hat{\mathbf{e}}_1 \\ \frac{c_p\theta_0}{g}\big(\Pi_0 - \Pi(T_t^{-1}(\mathbf{y}),t)\big)\end{pmatrix} \tag{5.39}$$

$$S(\mathbf{y},t) = \mathcal{S}(T_t^{-1}(\mathbf{y}),t) = \frac{sg}{f_{\mathrm{cor}}\theta_0}\frac{\big(\mathbf{y} - T_t^{-1}(\mathbf{y})\big)\cdot\hat{\mathbf{e}}_1}{\mathbf{y}\cdot\hat{\mathbf{e}}_3}, \tag{5.40}$$

which are the geostrophic velocity and the source/sink in geostrophic coordinates. Eq. (5.38) holds for all φ therefore the continuity equation in geostrophic coordinates is

$$\boxed{\partial_t\alpha_t + \nabla\cdot(\alpha_t\mathbf{w}) = -\alpha_t S.} \tag{5.41}$$

Consider the total geostrophic energy associated to the semi-geostrophic approximation (5.8) given by

$$E_g(t) = \int_\Omega \frac{\rho}{2} v^2 + g\rho x_3 - c_p \rho \Pi_0 \theta + c_v \rho \Pi \theta \, \mathrm{d}\mathbf{x}, \tag{5.42}$$

which is the sum of the kinetic, potential, and internal energy contributions. By Eq. (5.26), Eq. (5.42) can be rewritten as

$$\begin{aligned} E_g(t) &= F(T_t, \sigma_t, \alpha_t) \\ &:= \int_\Omega \left(\frac{f_{\mathrm{cor}}^2}{2T_t(\mathbf{x})_3} (x_1 - T_t(\mathbf{x})_1)^2 + g \frac{x_3}{T_t(\mathbf{x})_3} - c_p \Pi_0 \right) \sigma \, \mathrm{d}\mathbf{x} + \int_\Omega f(\sigma_t(\mathbf{x})) \, \mathrm{d}\mathbf{x}, \end{aligned} \tag{5.43}$$

where the internal energy density f is defined by

$$f(s) = \begin{cases} \kappa s^\gamma & \text{if } s \geq 0, \\ +\infty & \text{otherwise.} \end{cases} \tag{5.44}$$

An optimal transport cost function, $c : \mathcal{X} \to \mathcal{Y}$, emerges naturally from this representation of the energy, and it is given by

$$c(\mathbf{x}, \mathbf{y}) = \frac{f_{\mathrm{cor}}^2}{2y_3} (x_1 - y_1)^2 + g \frac{x_3}{y_3} - c_p \Pi_0. \tag{5.45}$$

As before, the Cullen convexity principle says that $F(\cdot, \sigma_t, \alpha_t)$ is minimised over all mass-preserving rearrangements of fluid particles, i.e. that solutions of Eq. (5.8) should also satisfy

$$F(T_t, \sigma_t, \alpha_t) = \min_{(S_t)_\# \sigma_t = \alpha_t} F(S_t, \sigma_t, \alpha_t) = \mathcal{T}_c(\sigma_t, \alpha_t) + \int_{\mathcal{X}} f(\sigma_t) \, \mathrm{d}\mathbf{x} =: E(\sigma_t, \alpha_t), \tag{5.46}$$

where again $\mathcal{T}_c$ is the optimal transport cost as defined in (MP).

Remark 5.2.2. The energy functional for the slice model and the corresponding optimal transport cost function in Eq. (5.45) are structurally almost identical to their three-dimensional counterparts discussed in Section 1.6.2. The only difference in the cost function is the addition of the constant term $-c_p \Pi_0$.

This addition does not alter the core arguments used to establish the link between the system dynamics and optimal transport and we can choose $\phi_t = -\kappa\gamma\sigma_t^{\gamma-1}$. Specifically, the proof of Proposition 1.6.2, which states that the potential ϕ_t is c-concave if and only if T_t is

the optimal transport map, relies on the spatial gradient of the cost function, $\nabla_{\mathbf{x}} c(\mathbf{x}, \mathbf{y})$. Since the new term is a constant, its gradient is zero, leaving this crucial calculation unchanged.

Furthermore, adding a constant to the cost function only shifts the total energy $E(\sigma_t, \alpha_t)$ by that same constant; it does not change the minimizer σ_t with respect to which the energy is minimized. Therefore, the arguments presented in the introduction directly apply. These observations justify the conclusion that, for this slice compressible model, the coordinate transform T_t is the unique optimal transport map that transports σ_t to α_t, and that σ_t is the unique minimizer of the energy functional $E(\sigma_t, \alpha_t)$.

Discretisation

In light of this we can discretise this PDE by plugging in the particle approximation

$$\alpha_t(\mathbf{z}) = \sum_{i=1}^{N} m_t^i \delta_{\mathbf{z}_t^i}. \tag{5.47}$$

As was done in Chapter 1 we use the centroids, $\mathbf{C}^i$. Starting with the velocity term on the right-hand side of Eq. (5.38) we can write

$$\int_{\mathcal{Y}} \nabla\varphi(\mathbf{y}) \cdot \mathbf{w}(\mathbf{y}, t)\, \mathrm{d}\alpha_t(\mathbf{y}) = \sum_{i=1}^{N} m_t^i \nabla\varphi(\mathbf{z}_t^i) \cdot J \begin{pmatrix} (\mathbf{C}^i(\mathbf{z}_t) - \mathbf{z}_t^i) \cdot \hat{\mathbf{e}}_1 \\ \frac{c_p \theta_0}{g} E_I(\mathbf{z}_t) \end{pmatrix}, \tag{5.48}$$

where

$$E_I(\mathbf{z}_t) := \frac{1}{m_t^i} \int_{L_c^i(\boldsymbol{w}, \mathbf{z}_t)} \Pi_0 - \Pi(\mathbf{x})\, \mathrm{d}\sigma_t(\mathbf{x}). \tag{5.49}$$

The source/sink term gives

$$\int_{\mathcal{Y}} \varphi(\mathbf{y}) S(\mathbf{y}, t)\, \mathrm{d}\alpha_t(\mathbf{y}) = \sum_{i=1}^{N} m_t^i \varphi(\mathbf{z}_t^i) \frac{(\mathbf{z}_t^i - \mathbf{C}^i(\mathbf{z}_t)) \cdot \hat{\mathbf{e}}_1}{\mathbf{z}_t^i \cdot \hat{\mathbf{e}}_3}. \tag{5.50}$$

The left-hand side of Eq. (5.38) yields

$$\frac{\mathrm{d}}{\mathrm{d}t} \int_{\mathcal{Y}} \varphi(\mathbf{y})\, \mathrm{d}\alpha_t(\mathbf{y}) = \sum_{i=1}^{N} \left[\dot{m}_t^i \varphi(\mathbf{z}_t^i) + m_t^i \nabla\varphi(\mathbf{z}_t^i) \cdot \dot{\mathbf{z}}_t^i \right]. \tag{5.51}$$

Combining equations (5.48), (5.50), and (5.51) gives

$$\begin{aligned}&\sum_{i=1}^{N}\left[\dot{m}_t^i\varphi(\mathbf{z}_t^i)+m_t^i\nabla\varphi(\mathbf{z}_t^i)\cdot\dot{\mathbf{z}}_t^i\right]\\&=\sum_{i=1}^{N}m_t^i\nabla\varphi(\mathbf{z}_t^i)\cdot J\begin{pmatrix}(\mathbf{C}^i(\mathbf{z}_t)-\mathbf{z}_t^i)\cdot\hat{\mathbf{e}}_1\\ \frac{c_p\theta_0}{g}E_I(\mathbf{z}_t)\end{pmatrix}-\sum_{i=1}^{N}m_t^i\varphi(\mathbf{z}_t^i)\frac{(\mathbf{z}_t^i-\mathbf{C}^i(\mathbf{z}_t))\cdot\hat{\mathbf{e}}_1}{\mathbf{z}_t^i\cdot\hat{\mathbf{e}}_3}.\end{aligned}\tag{5.52}$$

Fix i. First choose φ such that $\varphi(\mathbf{z}_t^i)=1$, $\varphi(\mathbf{z}_t^i)=0$ for all $j\neq i$ and φ constant in a neighbourhood of $\mathbf{z}_t^k$ for all k. This gives an ODE for m^i. Then choosing φ to be a constant in a neighbourhood of $\mathbf{z}_t^j$ for all $j\neq i$ implies that $\nabla\varphi=0$ in a neighbourhood of $\mathbf{z}_t^j$ and taking φ such that $\nabla\varphi(\mathbf{y})=\mathbf{y}$ in a neighbourhood of $\mathbf{z}_t^i$ then gives an ODE for $\mathbf{z}^i$. The evolution of the i-th particle, for $i\in\{1,\dots,N\}$, is governed by the coupled ordinary differential equations:

$$\boxed{\begin{cases}\dot{\mathbf{z}}_t^i=J\mathbf{w}^i(t),\\ \dot{m}_t^i=-m_t^iS^i(t),\end{cases}}\tag{5.53}$$

where

$$\mathbf{w}^i(t)=\begin{pmatrix}(\mathbf{C}^i(\mathbf{z}_t)-\mathbf{z}_t^i)\cdot\hat{\mathbf{e}}_1\\ \frac{c_p\theta_0}{g}E_I(\mathbf{z}_t)\end{pmatrix},$$

$$S^i(t)=\frac{sg}{f_{\mathrm{cor}}\theta_0}\frac{(\mathbf{z}_t^i-\mathbf{C}^i(\mathbf{z}_t))\cdot\hat{\mathbf{e}}_1}{\mathbf{z}_t^i\cdot\hat{\mathbf{e}}_3}.$$

The ODE system (5.53) differs from the the one derived in the incompressible case (Eq. (2.23)) in that compressibility causes the mass of each individual cell to change in time, while the overall mass remains constant. The numerical simulation of the solutions of this ODE system will constitute the first step towards a full 3D discretisation scheme for the compressible semi-geostrophic system.

Chapter 6

Conclusion

This thesis has developed a unified and powerful framework for the analysis and simulation of the semi-geostrophic equations, built upon the geometric foundations of semi-discrete optimal transport. By constructing the first fully 3D, energy-conserving numerical scheme for the incompressible system and establishing a foundational existence theory for the more complex compressible case, this work has pushed the boundaries of both computational and theoretical atmospheric science. The rigorous validation of the framework's geometric preconditions for physically crucial rectangular domains ensures that these theoretical advances are not merely abstract, but are directly relevant to practical modelling. The research culminates in the derivation of a novel 2D compressible model in geostrophic coordinates, which completes the cycle of inquiry from computation to theory and back again, laying the groundwork for the next generation of simulations. The profound interplay between the analytical power of optimal transport theory and the physical complexity of mathematical meteorology, as demonstrated throughout this work, opens up a rich landscape of future research, promising deeper insights into the dynamics of our atmosphere.

6.1 Future Research Directions and Open Problems

The contributions of this thesis, illuminate a landscape of compelling open questions that define a clear research program for the future. These avenues for inquiry can be organized into three principal domains: enhancing the physical realism of the SG model, strengthening the underlying numerical and analytical framework, and addressing fundamental theoretical questions at the intersection of optimal transport and fluid dynamics.

6.1.1 Enhancing the Physical Realism of the SG Model

The current model, in line with much of the theoretical literature, makes several idealizing assumptions. Future work should aim to incorporate more complex physics to bring the model closer to operational atmospheric science. A primary extension is the introduction of viscosity, particularly in a vertical boundary layer near the Earth's surface where frictional effects are dominant. This set of equations is known as the Geo-Triptic Equations (see [19]). The strictly decreasing nature of this system's energy in the presence of dissipation suggests that a gradient flow formulation might be a natural and powerful framework for tackling this problem.

Another critical extension is the treatment of a variable Coriolis force. While a key advantage of the SG equations over the quasi-geostrophic system is their validity for a non-constant Coriolis parameter, this thesis has assumed it to be constant for analytical tractability. Incorporating a variable Coriolis force is physically necessary to model flows spanning significant latitudinal ranges, but poses a major challenge in geostrophic coordinates, where the coordinate transformation itself depends on this parameter. Some work in this direction has been done by [62].

Finally, given the inherently chaotic and unpredictable nature of weather, developing a physically meaningful stochastic formulation of the SG equations is an interesting conceptual challenge. It is unclear where stochasticity should be introduced, in the particle dynamics, the transport map, or elsewhere, to represent unresolved sub-grid scale processes or uncertainties in initial data. Successfully addressing these challenges would represent a significant step in transitioning the semi-discrete optimal transport framework from a powerful theoretical and diagnostic tool into a potential component of next-generation predictive models.

6.1.2 Strengthening the Numerical and Analytical Framework

Another avenue for future research stems from a crucial dichotomy observed in the numerical experiments of Chapter 2. While the scheme demonstrates exceptional global energy conservation, long-term simulations exhibit a degradation in accuracy, especially after the formation of sharp fronts, when compared to high-resolution reference solutions. This raises the fundamental question: can a bespoke time-stepping scheme be developed to address this?

The particle ODE system's evolution is dictated by the centroid map, a highly non-local right-hand side whose regularity properties shift dramatically as particle configurations evolve and fronts steepen. Standard ODE solvers are ill-equipped to handle this behaviour. The chal-

lenge, therefore, is to investigate the possibility of designing a custom integrator that preserves the geometric structure of the flow not just in space, but also in time. If such a scheme can be formulated, the next step would be its implementation and testing to validate its efficacy in maintaining long-term accuracy. However, the possibility that no such structure-preserving temporal scheme exists must also be considered.

Another significant open question on the numerical front is the development of a stability condition analogous to the Courant–Friedrichs–Lewy (CFL) condition for grid-based methods. For this particle-based scheme, which couples a standard ODE solver with an Optimal Transport (OT) solver, there is currently no theoretical framework that dictates the relationship between the number of particles (the spatial resolution) and the maximum allowable timestep size for the ODE solver. Establishing an "OT particle CFL" condition would be a major step forward, providing a rigorous guideline for ensuring the stability and convergence of the simulations. This would involve a deep analysis of how errors from the OT solver and the ODE integrator interact and propagate, a challenging task given the complex, non-local nature of the centroid map.

On a more fundamental level, a rigorous numerical convergence result for the semi-discrete scheme remains a major open problem. While convergence has been established for fully discrete, entropy-regularized methods (see [12]), a similar proof for the semi-discrete case is elusive and sought after. The semi-discrete method exists in a challenging middle ground between the continuous and the discrete. This hybrid nature is the source of its power, yielding exact weak solutions for any number of particles, but also the source of its analytical difficulty. A convergence proof would require controlling the approximation error in the limit as the number of particles tends to infinity, a process where the geometric complexity of the underlying Laguerre tessellation can become immense. These problems highlight the frontier of numerical analysis for optimal transport-based methods, and solving them would provide the ultimate validation of the method's reliability.

6.1.3 Fundamental Questions in Optimal Transport and Fluid Dynamics

Several deep theoretical questions remain at the heart of the SG system. The uniqueness of weak solutions to the governing PDE is a major open problem in the field, with significant implications for the predictability of the system.

A related challenge lies in the rigorous validation of the simulations. The first step, a

significant open problem in its own right, is to formally define the full physical velocity field from the semi-discrete particle system. The motion of the cell centroids provides a natural candidate for this construction. However, it remains to be proven that a velocity field derived from these centroids constitutes a valid solution to the governing PDE in the original physical coordinates.

Building on this, a separate but related goal is to validate the physical accuracy of the simulations by demonstrating that the system maintains geostrophic balance. To do so, one must first have a valid definition of the full velocity field in order to measure any deviations from it. With that established, a powerful avenue for validating the simulation's quality would be to show that the ageostrophic component of the flow, the part deviating from the geostrophic ideal, remains appropriately small.

Finally, the theoretical framework, particularly for the existence proof in Chapter 3, relies on placing particles in distinct horizontal planes to prevent collisions. Proving that particles do not collide even if they lie in the same plane would remove this technical restriction and immediately extend the existence and regularity results to 2D cases. These problems are deeply interconnected. Proving particle non-collision is a question about the regularity of the Lagrangian flow map defined by the particle ODEs. Understanding this flow is a prerequisite for rigorously defining the physical velocity field. And the uniqueness of the PDE solution is intimately tied to the stability and regularity properties of these Lagrangian paths.

Bibliography

[1] L. Ambrosio, M. Colombo, G. De Philippis, and A. Figalli. Existence of Eulerian solutions to the semi-geostrophic equations in physical space: The 2-dimensional periodic case. *Communications in Partial Differential Equations*, 37(12):2209–2227, 2012.

[2] L. Ambrosio, M. Colombo, G. De Philippis, and A. Figalli. A global existence result for the semigeostrophic equations in three dimensional convex domains. *Discrete & Continuous Dynamical Systems - A*, 34(4):1251–1268, 2014.

[3] L. Ambrosio, N. Fusco, and D. Pallara. *Functions of Bounded Variation and Free Discontinuity Problems*. Oxford, 2000.

[4] L. Ambrosio and W. Gangbo. Hamiltonian ODEs in the Wasserstein space of probability measures. *Communications on Pure and Applied Mathematics*, 61(1):18–53, 2008.

[5] J.-D. Benamou and Y. Brenier. Weak existence for the semi-geostrophic equations formulated as a coupled Monge–Ampère transport problem. *SIAM Journal on Applied Mathematics*, 58(5):1450–1461, 1998.

[6] J.-D. Benamou, C. Cotter, and H. Malamut. Entropic optimal transport solutions of the semigeostrophic equations. *Journal of Computational Physics*, 500:112745, 2024.

[7] V. Bjerknes. Das problem der wettervorhersage, betrachtet vom standpunkte der mechanik und der physik. *Meteorologische Zeitschrift*, 21:1–7, 1904.

[8] D. P. Bourne, C. P. Egan, B. Pelloni, and M. Wilkinson. Semi-discrete optimal transport methods for the semi-geostrophic equations. *Calculus of Variations and Partial Differential Equations*, 61(1):39, 2022.

[9] D. P. Bourne, B. Schmitzer, and B. Wirth. Semi-discrete unbalanced optimal transport and quantization. *arXiv preprint arXiv:1808.01962*, 2024.

[10] Y. Brenier. Polar factorization and monotone rearrangement of vector-valued functions. *Communications on Pure and Applied Mathematics*, 44(4):375–417, 1991.

[11] F. Cagnetti, M. G. Mora, and M. Morini. A second order minimality condition for the Mumford-Shah functional. *Calculus of Variations and Partial Differential Equations*, 33:37–74, 2008.

[12] G. Carlier and H. Malamut. Well-posedness and convergence of entropic approximation of semi-geostrophic equations, 2024.

[13] J. Charney. *On the Scale of Atmospheric Motions*. Geofysiske Publikasjoner. Cammeremeyer, 1948.

[14] J. G. Charney. The dynamics of long waves in a baroclinic westerly current. *Journal of Atmospheric Sciences*, 4(5):136 – 162, 1947.

[15] J. G. Charney. On a physical basis for numerical prediction of large-scale motions in the atmosphere. *Journal of Atmospheric Sciences*, 6(6):372 – 385, 1949.

[16] J. G. CHARNEY, R. FJÖRTOFT, and J. Von NEUMANN. Numerical integration of the barotropic vorticity equation. *Tellus*, 2(4):237–254, 1950.

[17] C. J. Cotter and D. D. Holm. A variational formulation of vertical slice models. *Proceedings of the Royal Society A: Mathematical, Physical and Engineering Sciences*, 469(2155):20120678, 7 2013.

[18] M. J. P. Cullen. The Use of Semigeostrophic Theory to Diagnose the Behaviour of an Atmospheric GCM. *Fluids*, 3(4):72, 2018.

[19] M. J. P. Cullen. *The Mathematics Of Large-scale Atmosphere And Ocean*. World Scientific Pub Co Inc, 2021.

[20] M. J. P. Cullen and M. Feldman. Lagrangian solutions of semi-geostrophic equations in physical space. *SIAM Journal on Mathematical Analysis*, 37(5):1371–1395, 2006.

[21] M. J. P. Cullen and W. Gangbo. A variational approach for the 2-dimensional semi-geostrophic shallow water equations. *Archive for Rational Mechanics and Analysis*, 156(3):241–273, 2001.

[22] M. J. P. Cullen, W. Gangbo, and G. Pisante. The semi-geostrophic equations discretized in reference and dual variables. *Archive for Rational Mechanics and Analysis*, 185(2):341–363, 2007.

[23] M. J. P. Cullen, D. K. Gilbert, and B. Pelloni. Solutions of the fully compressible semi-geostrophic system. *Communications in Partial Differential Equations*, 39(4):591–625, 2014.

[24] M. J. P. Cullen and H. Maroofi. The fully compressible semi-geostrophic system from meteorology. *Archive for Rational Mechanics and Analysis*, 167(4):309–336, 2003.

[25] M. J. P. Cullen and R. J. Purser. An Extended Lagrangian Theory of Semi-Geostrophic Frontogenesis. *Journal of the Atmospheric Sciences*, 41(9):1477–1497, 5 1984.

[26] H. C. Davies, C. Schär, and H. Wernli. The Palette of Fronts and Cyclones within a Baroclinic Wave Development. *Journal of the Atmospheric Sciences*, 48(14):1666–1689, 7 1991.

[27] F. de Gournay, J. Kahn, and L. Lebrat. Differentiation and regularity of semi-discrete optimal transport with respect to the parameters of the discrete measure. *Numerische Mathematik*, 141(2):429–453, 2019.

[28] E. T. Eady. Long waves and cyclone waves. *Tellus*, 1(3):33–52, 1949.

[29] C. P. Egan, D. P. Bourne, C. J. Cotter, M. J. P. Cullen, B. Pelloni, S. M. Roper, and M. Wilkinson. A new implementation of the geometric method for solving the Eady slice equations. *Journal of Computational Physics*, 469:111542, 2022.

[30] A. Eliassen. *The Quasi-static Equations of Motion with Pressure as Independent Variable.* Grøndahl, 1949.

[31] L. C. Evans and R. F. Gariepy. *Measure Theory and Fine Properties of Functions, Revised Edition.* Chapman & Hall, 2015.

[32] J. Faria. On the existence and weak stability of solutions to the compressible semi-geostrophic equations. *Journal of Mathematical Analysis and Applications*, 406(2):447–463, 2013.

[33] M. Feldman and A. Tudorascu. On Lagrangian solutions for the semi-geostrophic system with singular initial data. *SIAM Journal on Mathematical Analysis*, 45(3):1616–1640, 2013.

[34] M. Feldman and A. Tudorascu. On the semi-geostrophic system in physical space with general initial data. *Archive for Rational Mechanics and Analysis*, 218(1):527–551, 2015.

[35] M. Feldman and A. Tudorascu. Lagrangian solutions for the semi-geostrophic shallow water system in physical space with general initial data. *St. Petersburg Mathematical Journal*, 27(3):547–568, 2016.

[36] M. Feldman and A. Tudorascu. The semi-geostrophic system: Weak-strong uniqueness under uniform convexity. *Calculus of Variations and Partial Differential Equations*, 56(6):158, 2017.

[37] J. Feydy, T. Séjourné, F.-X. Vialard, S.-i. Amari, A. Trouve, and G. Peyré. Interpolating between optimal transport and mmd using sinkhorn divergences. In *The 22nd International Conference on Artificial Intelligence and Statistics*, pages 2681–2690, 2019.

[38] M. C. L. Filho and H. J. N. Lopes. Existence of a weak solution for the semi-geostrophic equation with integrable initial data. *Proceedings of the Royal Society of Edinburgh: Section A Mathematics*, 132(2):329–339, 2002.

[39] G. Friesecke. *Optimal Transport: A Comprehensive Introduction to Modeling, Analysis, Simulation, Applications*. Society for Industrial and Applied Mathematics, Philadelphia, PA, 2024.

[40] T. O. Gallouët and Q. Mérigot. A Lagrangian scheme à la Brenier for the incompressible Euler equations. *Foundations of Computational Mathematics*, 18(4):835–865, 2018.

[41] T. O. Gallouët, Q. Mérigot, and A. Natale. Convergence of a Lagrangian discretization for barotropic fluids and porous media flow. *SIAM Journal on Mathematical Analysis*, 54(3):2990–3018, 2022.

[42] B. J. Hoskins. The geostrophic momentum approximation and the semi-geostrophic equations. *Journal of the Atmospheric Sciences*, 32(2):233–242, 1975.

[43] B. J. Hoskins and N. V. West. Baroclinic Waves and Frontogenesis. Part II: Uniform Potential Vorticity Jet Flows-Cold and Warm Fronts. *Journal of the Atmospheric Sciences*, 36(9):1663–1680, 9 1979.

[44] E. Kalnay. *Atmospheric Modeling, Data Assimilation and Predictability*. Cambridge University Press, 2002.

[45] L. Kantorovich. On the translocation of masses. *Dokl. Akad. Nauk. USSR (N.S.)*, 37(7-8):227–229, 1942.

[46] J. Kitagawa, Q. Mérigot, and B. Thibert. Convergence of a Newton algorithm for semi-discrete optimal transport. *Journal of the European Mathematical Society*, 21(9):2603–2651, 2019.

[47] B. Kloeckner. Approximation by finitely supported measures. *ESAIM: Control, Optimisation and Calculus of Variations*, 18(2):343–359, 7 2012.

[48] T. Lavier. A semi-discrete optimal transport scheme for the 3d incompressible semi-geostrophic equations. *arXiv preprint arXiv:2411.00575*, 2024.

[49] T. Lavier. *Semi-Discrete Optimal Transport Techniques for the Compressible Semi-Geostrophic Equations*. PhD thesis, Heriot-Watt University, to appear.

[50] H. Leclerc and Q. Mérigot. Pysdot, 2024. Available at: https://github.com/sd-ot/pysdot.

[51] H. Leclerc, Q. Mérigot, F. Santambrogio, and F. Stra. Lagrangian discretization of crowd motion and linear diffusion. *SIAM Journal on Numerical Analysis*, 58(4):2093–2118, 2020.

[52] G. Loeper. A fully nonlinear version of the incompressible Euler equations: The semi-geostrophic system. *SIAM Journal on Mathematical Analysis*, 38(3):795–823, 2006.

[53] Q. Mérigot and B. Thibert. Optimal transport: discretization and algorithms. In A. Bonito and R. H. Nochetto, editors, *Handbook of Numerical Analysis*, pages 133–212. Elsevier, 2021.

[54] Q. Mérigot and B. Thibert. Optimal transport: discretization and algorithms. In A. Bonito and R. H. Nochetto, editors, *Handbook of Numerical Analysis*, volume 22, pages 133–212. Elsevier, 2021.

[55] J. Meyron. Initialization Procedures for Discrete and Semi-Discrete Optimal Transport. *Computer-Aided Design*, 115:13–22, 10 2019.

[56] G. Monge. *Mémoire sur la théorie des déblais et des remblais*. De l'Imprimerie Royale, 1781.

[57] G. Peyré and M. Cuturi. Computational optimal transport. *Foundations and Trends in Machine Learning*, 11(5-6):355–607, 2019.

[58] L. F. Richardson. *Weather prediction by numerical process*. Cambridge University Press, 1922.

[59] F. Santambrogio. *Optimal Transport for Applied Mathematicians*, volume 87. Springer International Publishing, Cham, 2015.

[60] C. Sarrazin. Lagrangian discretization of variational mean field games. *SIAM Journal on Control and Optimization*, 60(3):1365–1392, 2022.

[61] C. Schär and H. Wernli. Structure and evolution of an isolated semi-geostrophic cyclone. *Quarterly Journal of the Royal Meteorological Society*, 119(509):57–90, 1 1993.

[62] L. Silini. Local existence of smooth solutions for the semigeostrophic equations on curved domains. *SIAM Journal on Mathematical Analysis*, 55(6):6554–6579, 2023.

[63] C. Villani. *Topics in optimal transportation*. American Mathematical Society, 2003.

[64] C. Villani. *Optimal Transport: Old and NewA vertical slice frontogenesis test case for compressible nonhydrostatic dynamical cores of atmospheric models*. Springer, 2009.

[65] A. R. Visram, C. J. Cotter, and M. J. P. Cullen. A framework for evaluating model error using asymptotic convergence in the Eady model. *Quarterly Journal of the Royal Meteorological Society*, 140(682):1629–1639, 2014.

[66] H. Wernli, R. Fehlmann, and D. Lüthi. The Effect of Barotropic Shear on Upper-Level Induced Cyclogenesis: Semigeostrophic and Primitive Equation Numerical Simulations. *Journal of the Atmospheric Sciences*, 55(11):2080–2094, 6 1998.

[67] H. Yamazaki and C. J. Cotter. A vertical slice frontogenesis test case for compressible nonhydrostatic dynamical cores of atmospheric models. *arXiv preprint arXiv:2501.09752*, 2025.

[68] H. Yamazaki, J. Shipton, M. J. P. Cullen, L. Mitchell, and C. J. Cotter. Vertical slice modelling of nonlinear Eady waves using a compatible finite element method. *Journal of Computational Physics*, 343:130–149, 8 2017.